NAVAL FACILITIES ENGINEERING SERVICE CENTER
Port Hueneme, California 93043-4370

Technical Report TR-2069-SHR

DESIGN CRITERIA FOR EARTHQUAKE HAZARD MITIGATION OF NAVY PIERS AND WHARVES

by

J. M. Ferritto

March 1997

REPORT DOCUMENTATION PAGE

Form Approved
OMB No. 0704-018

1. AGENCY USE ONLY (Leave blank)

2. REPORT DATE
March 1997

3. REPORT TYPE AND DATES COVERED
Final; October 1995 to March 1997

4. TITLE AND SUBTITLE
DESIGN CRITERIA FOR EARTHQUAKE HAZARD MITIGATION OF NAVY PIERS AND WHARVES

5. FUNDING NUMBERS

6. AUTHOR(S)
J. M. Ferritto

7. PERFORMING ORGANIZATION NAME(S) AND ADDRESSE(S)
Naval Facilities Engineering Service Center
1100 23rd Avenue
Port Hueneme, CA 93043-4370

8. PERFORMING ORGANIZATION REPORT NUMBER
TR-2069-SHR

9. SPONSORING/MONITORING AGENCY NAME(S) AND ADDRESSES
Naval Facilities Engineering Command
Code 15
1510 Gilbert Street
Norfolk, VA 23511-2699

10. SPONSORING/MONITORING AGENCY REPORT NUMBER

11. SUPPLEMENTARY NOTES

12a. DISTRIBUTION/AVAILABILITY STATEMENT
Approved for public release; distribution is unlimited.

12b. DISTRIBUTION CODE

13. ABSTRACT *(Maximum 200 words)*

This report develops seismic criteria for Navy wharves and piers. The report is composed of two sections: the design criteria is presented first and is then followed by an extensive supporting technology. The criteria gives performance requirements, design earthquakes, and required structural response. The supporting technology cites the behavior of waterfront structures in previous earthquakes and reviews applicable codes. A discussion of the structural dynamics of piles is presented developing the concepts of curvature and ductility, which are the essence of the criteria. A discussion of soil properties and procedures for computing soil lateral force is given. Pile cap and anchorage techniques are discussed. The supporting technology presents an analysis of a single pile and the analysis of a typical pier for several concepts of achieving lateral force resistance, including seismic isolation of the pier deck. The isolation of the pier deck offers a potential to achieve high levels of lateral force resistance improving the survivability of the pier against the maximum credible earthquake. The criteria presented herein is developed from a compilation of current practice by many agencies combined with state-of-the-art technology for estimation of seismic damage potential.

14. SUBJECT TERMS
Earthquake hazard mitigation, Navy piers, Navy wharves, structural dynamics of piles, waterfront structures, lateral force resistance

15. NUMBER OF PAGES
183

16. PRICE CODE

17. SECURITY CLASSIFICATION OF REPORT	18. SECURITY CLASSIFICATION OF THIS PAGE	19. SECURITY CLASSIFICATION OF ABSTRACT	20. LIMITATION OF ABSTRACT
Unclassified	Unclassified	Unclassified	UL

Executive Summary

This report expands a previous study developing seismic criteria for Navy wharves to include Navy piers. Wharves are structures which are composed of a deck supported by a substructure composed of piles and a dike. The presence of the sloping dike causes the supporting piles to have varying unsupported lengths between the deck and the dike. Generally the row of piles most landward is the shortest and has the majority of the lateral resistance. The relatively short length of these piles makes it relatively easy to achieve required levels of lateral resistance. Piers are structures composed of a deck on free standing piles. Generally pier piles have large unsupported lengths of about 50 feet which makes achieving lateral resistance more difficult. To develop appropriate seismic criteria for piers it is necessary to understand the strength and ductility of piles especially prestressed concrete piles which are most often used. While the pier criteria is expressed in a few numbers relating earthquake return times and ductility limits, it should be recognized that a substantial amount of effort went into developing these numbers as is shown in the Supporting Technology.

The report is composed of two sections; the design criteria is presented first and is then followed by an extensive supporting technology. The criteria gives performance requirements, design earthquakes and required structural response. It is thought that the criteria is well defined, easy to implement, and will achieve a uniform and acceptable level of structure performance. It is thought that the implementation of this criteria will upgrade structure performance but not add appreciably to the construction cost.

The supporting technology cites the behavior of waterfront structures in previous earthquakes and reviews applicable codes. A discussion of the structural dynamics of piles is presented developing the concepts of curvature and ductility which are the essence of the criteria. A discussion of soil properties and procedures for computing soil lateral force is given. Pile cap and anchorage techniques are discussed. The supporting technology presents an analysis of a single pile and the analysis of a typical pier for several concepts of achieving lateral force resistance, including seismic isolation of the pier deck. The isolation of the pier deck offers a potential to achieve high levels of lateral force resistance improving the survivability of the pier against the maximum credible earthquake.

The criteria presented herein is developed from a compilation of current practice by many agencies combined with state-of-the-art technology for estimation of seismic damage potential. It is not a revolutionary step forward but rather an evolution of design. Currently the Navy has used technology contained in DM 1025/1, NAVFAC P355.2 and the AASHTO Code for the design of wharves and piers. The supporting technology shows the design of a pier is a major soil-structure interaction problem and the need for realistic nonlinear representation of soil forces. Prior to this specification we did not have a definition of required pier/wharf performance, nor of the structural response parameters such as ductility to achieve the required level of performance under the assigned load. This specification has developed a cohesive integrated criteria specifying:

1. The required pier performance under expected loads
2. Specification of the expected loads
3. Specification of ductility limits to ensure structural response limits to achieve performance requirements.

The criteria reduces the Level 2 earthquake from the 950-year earthquake specified in NAVFAC P355.2 for essential buildings to the 475-year earthquake ground motion. This is important because we have reduced the ground motion substantially. In the San Diego area, for example, the ground is reduced from 0.6g to 0.4g. But of much more significance we can predict the 475- return time ground motion with greater reliability than the 950-year event. This translates into a significant reduction in the 95 percent confidence bounds on the estimated motion. We have shifted the criteria points into regions where we can predict loads with greater reliability and also predict structural response with greater reliability. This translates into a significantly more predictable system. This was suggested by the reliability analysis performed on a typical Navy wharf as an early part of this effort, Putcha and Ferritto (1995). That work was significant in defining the major areas of uncertainty and shaped the direction for the criteria.

The overall effect on the design, selection of pile sizes and cost of the pier is not expected to be great; however, the assurance in meeting performance goals is thought to be substantially enhanced.

In the application of this criteria to existing construction, it is thought that the objective of a uniform set of performance goals should be maintained across the waterfront. We should examine the structure under the requirements of the criteria. Where we lack adequate capacity in the existing system, it is thought better to strive for the performance goal, develop several candidate upgrade alternatives, and then perform an economic analysis to determine what is the most cost effective solution considering the potential for a damaging earthquake and the existing lateral force system. This approach is preferred over any system which arbitrarily establishes some percentage reduction of a new-construction criteria. Any single reduction coefficient is probably not optimal over a range of structures and is at best arbitrary.

Table of Contents

Table of Contents (continued)

Criteria Document

Criteria For Seismic Design Of Navy Piers and Wharves

Performance Goal

The goal of this criteria is to standardize the seismic design of Navy piers and wharves providing an acceptable uniform level of seismic safety for all waterfront locations. This criteria is intended to produce a level of design in Navy piers and wharves such that there is a high probability the structures will perform at satisfactory levels throughout their design life. Specifically for structures located in areas of high seismicity, such as Uniform Building Code designated Seismic Zones 3 and 4, structures shall be designed:

- To resist earthquakes of moderate size, Level 1, which can be expected to occur one or more times during the life of the structure without structural damage of significance.

- To resist major earthquakes, Level 2, which are considered as infrequent rare events maintaining life safety, precluding total collapse but allowing a measure of controlled inelastic behavior which will require repair.

- To preclude release of hazardous and polluting materials such as with fuel piers.

- To utilize life-cycle cost analysis where necessary. Since piers and wharves are not like high occupancy building structures which can collapse on occupants, loss of life is a less significant design issue. At times the seismic hazard is dominated by a large active fault in close proximity to a proposed wharf location. In such cases the designer shall consider structure life cycle economics in selection of design loading and structural performance criteria. Life cycle cost analysis shall consider initial costs of seismic strengthening and expected facility damage and loss over the expected operational life.

- To consider liquefaction as a major waterfront problem. The designer shall consider liquefaction factors of safety in design of remedial measures of backfill. Rigid adherence to developing fixed factors of safety may not be economically achievable. Assurance of limited deformations shall be given precedence over a factor of safety. The designer shall have the option of using current technology to demonstrate that settlements and lateral deformations are sufficiently limited to insure structural performance and factors of safety lower than limit values may be used.

In general all waterfront construction falls within the category of essential construction. The Navy policy is to minimize downtime for these facilities. Determination of essential construction shall be determined by the user in conjunction with the Naval Facilities Engineering Command Headquarters. Piers and wharves shall be considered essential construction.

Design Earthquakes

The pier or wharf structure shall be designed to resist the loading produced by:

- A Level 1 earthquake with a 50 percent probability of exceedance in 50 years exposure.
- A Level 2 earthquake with a 10 percent probability of exceedance in 50 years exposure.
- Additionally piers and wharves which are part of fueling systems shall be evaluated for an earthquake with a 10 percent probability of exceedance in 100 years exposure.

The determination of the design earthquake shall be performed using techniques described in NFESC TR-2016-SHR or other equivalent procedures.

Structure Response At Design Loading Levels

The response of the structure under the design earthquake levels shall be:

- For a Level 1 earthquake, essentially elastic response is required throughout the structure.
- For a Level 2 earthquake, limited controlled inelastic behavior with maximum ductility factors of

Pier Prestressed Concrete Piles

1.5	Pile moments in ground
3.0	Piles at pile cap
1.5	Batter piles at pile cap

Wharf Prestressed Concrete Piles

2.0	Pile moments in ground
5.0	Piles at pile cap
2.5	Batter piles at pile cap

Steel Piles for both Wharf and Pier

5.0	Vertical piles only
3.0	Vertical and batter piles

Composite Steel and Concrete Piles
for both Wharf and Pier

5.0	Vertical piles only
3.0	Vertical and batter piles

Displacement ductility is related to curvature and is inversely dependent on pile length. Piers have longer piles than wharves and the above ductility limits are intended to reflect that factor. It is intended that Level 2 curvatures be safely less than ultimate curvature. The pier or wharf shall be designed as a ductile moment resisting frame supported by vertical piles reinforced and so connected to the structure as to form an integral part of the ductile moment resisting frame. Use of batter piles as lateral force resistant elements in wharves is prohibited unless special design provisions are made to reliably demonstrate that the batter piles have sufficient strength and ductility at the pile cap to perform under design loading conditions. If batter piles are used, allowable ductilities at the pile cap shown above shall be reduced for the Level 2 earthquake.

For a wharf, design of the under-wharf dike retaining structures as a minimum shall have permanent horizontal deformation of the slope computed by a Newmark analysis and such deformation shall not exceed:

- For a Level 1 earthquake, 4 inches
- For a Level 2 earthquake, 12 inches

Design of sheet pile bulkheads, dikes and retaining structures shall include provisions to resist full liquefaction of the backfill and for expected potential lateral spread deformation. Retaining structures shall be designed using provisions in NCEL Technical Report R-939. Liquefaction and lateral spread shall be computed based on guidance in NCEL Technical Note 1862.

All crane rails shall be supported on piles including the seaward and the landward rail. The crane rails shall be connected horizontally by a continuous deck, beam or other means to control the gage of the rails and prevent spreading. The rails shall be grounded. For corrosion protection, it is advantageous to insulate the reinforcing steel in the piles from that in the deck.

The presence of any potentially liquefiable materials in backfill areas shall be fully analyzed and expected settlements computed. Specific attention shall be paid to the acceptability of the amount of settlements. Under Level 1 earthquakes large deformations resulting in widespread pavement disruption should be avoided where economically feasible.

- For a Level 1 earthquake the Factor of Safety against liquefaction in the backfill should be 1.5 or higher with settlements of about 1 inch or less and lateral deformations of about 3 inches or less.

- For a Level 2 earthquake the Factor of Safety against liquefaction in the backfill should be 1.0 or higher with settlements of about 4 inches or less and lateral deformations of about 6 to 12 inches or less. Where it may not be possible to achieve a Factor of Safety greater than 1.0, a Factor of Safety greater than 0.9 may be considered as long as the computed deformation state is shown to have limited controlled settlements and lateral spread equivalent to the values stated.

Piers and wharves containing fueling systems shall be evaluated for an earthquake with a 10 percent probability of exceedance in 100 years exposure to insure that a spill of hazardous material is precluded. This may be accomplished by providing containment systems should there be breaks in fuel containment system element or by strengthening these elements.

- Preclude release of hazardous and polluting materials for an earthquake with a 10 percent probability of exceedance in 100 years exposure.

Existing Construction

Seismic reviews of existing waterfront construction directed by requirements of the Naval Facilities Engineering Command shall utilize the above criteria for new construction as the target requirement for upgrade. The requirement for evaluation of the seismic resistance and possible upgrade is triggered when the loading on the structure changes such as when the mission of the structure is changed or when the structure requires major repairs or modifications to meet operational needs. When it is shown to be impossible or uneconomical to achieve new construction levels of performance, an economic life cycle cost analysis shall be performed to determine the most cost effective level of seismic design upgrade. Various alternative upgrade levels shall be considered ranging from the existing condition to the maximum achievable. Each alternative shall be examined to determine the cost of the upgrade, the cost of expected earthquake damage over the life of the structure and the impact of the damage on life safety, operational requirements, and damage to the environment. The choice of upgrade level shall be made by the design team based on a cost effective strategy consistent with requirements of life safety, operational needs and protection of the environment.

1996 AASHTO Requirements And This Criteria

The DM 1025/1 calls for use of the AASHTO Code for guidance. That requirement is maintained subject to changes contained in this criteria. The AASHTO Code specifies that the structure shall be elastic under small to moderate earthquakes and that "exposure to

shaking from large earthquakes should not cause collapse of all or part of the bridge. Where possible damage that does occur should be readily detectable and accessible for inspection and repair." This criteria follows the same guidance but is more definitive in establishing specific earthquake levels and more definitive response criteria. This criteria is designed to insure piers are repairable under the Level 2 earthquake. Further piers are to be classified as AASHTO Category I structures as essential. Division 1A of the AASHTO Code Section 3.2 presents acceleration maps. For pier projects site specific seismicity studies are to be performed in lieu of the maps. Because waterfront soils generally fall in the worst category of site response, as part of the site study, local site response shall be analyzed using as a minimum 1-dimensional wave propagation techniques to determine local site amplification. Soil response described in AASHTO Section 3.6 shall be based on the local site response analysis in lieu of the specified equations.

AASHTO Section 3.9 prescribes for the combination of orthogonal seismic force components. Section 4 describes analysis requirements and Sections 4.5 and 4.6 describe the multimode response spectra and time history analysis procedures. Since piers depend heavily upon the nonlinear soil structure interaction of piles and soil, nonlinear time history procedures are strongly recommended for the analysis of a pier. Only AASHTO procedures 3 and 4 are to be used for pier analysis. Since the response of the pier under Level 2 earthquakes is expected to be nonlinear use of Section 3.9 provisions for combination of orthogonal components are only approximate. To account for the orthogonal effects of seismic load components, a full 3-dimensional pier model is recommended to directly allow for inclusion of all the earthquake components. Actual earthquake records of orthogonal components can be used to represent the seismic loading. Typically one of the components is at a reduced acceleration level compared to the primary component. Vertical acceleration may be included as a loading component but is not required. Use of vertical component acceleration may not be used to reduce the lateral response.

Provisions of AASHTO Chapters 5,6 and 7 shall be applicable to piers including combination of load components with changes in earthquake loading required to meet this criteria.

Life Cycle Cost Analysis

Life cycle cost analysis shall be performed using the provisions in NAVFAC P355.2 Chapter 7 and the guidance in NCEL Technical Notes N 1640 and N 1671.

Supporting Technology

For

Criteria For Seismic Design

Of Navy Piers and Wharves

Introduction

The current potential for interruption to fleet-support operations is probably greater from seismic hazards than hostile combat. The waterfront location on soft marginal soils makes the Navy especially vulnerable. The entire Pacific rim is at risk covering all PACFLT locations. Additionally parts of the East Coast and Europe have the potential for large earthquakes. The Navy has lost over $275 million in damage from the 1989 Loma Prieta and 1993 Guam earthquakes. Executive Order 12699 and 12941 mandate that the federal government develop appropriate technology for safe facility design and evaluate the current vulnerability of government facilities. Seventy five percent of the Navy's piers and wharves are over 50 years old and represent $5 billion in assets. There are over $0.7 billion in noted deficiencies with 84 projects in the C3/C4 categories. Piles are a common element to much of the waterfront construction and recent experience has shown them vulnerable to damage. It is very difficult to inspect and repair damage which occurs to piles underground or under water; therefore, it is desirable to design piles to limit damage under the range of possible earthquakes. For the design earthquake which is expected to occur one or more times during the life of the structure, the piles should be undamaged. For the upper bound earthquake which is a rare event, the structure must sustain limited controlled damage; under such conditions it is desirable that the seismic energy be dissipated by ductile yielding at plastic hinge regions. A recent NFESC report, Ferritto and Putcha (1995), developed criteria for Navy wharves. This report expands on that information and extends the guidelines for the design to include piers. The major concentration of this report will be on pier piles. There are other elements of significance in the seismic design such as deck design, sheet piles and bulkheads. Sheet piles and bulkheads should be coordinated with MIL-HDBK 1007/3 "Soil Dynamics".

Military Handbook 1025/1 is the current guide for design of piers and wharves. It states that all piers and wharves in seismically active areas be designed to resist earthquake forces in accordance with AASHTO Standard Specifications for Bridge Dynamics. The AASHTO code will be discussed in the following section. As an alternative to the AASHTO code a procedure developed in 1976 using the elastic computer program SAPIER is allowed, Tudor/PMP (1976). The criteria developed herein is suggested to be added to the Military Handbook 1025/1. It will have the effect of prescription of more specific performance expectations and a definition of more controlled structure response. The proposed criteria replaces national maps of seismic motion with site specific ground motion levels which are representative of local site conditions. Arbitrary categories of construction are eliminated. More exacting nonlinear behavior is determined by replacing elastic techniques with procedures which can capture structure yielding, formation of plastic hinges and nonlinear soil-pile load-deflection response. The criteria represents an evolutionary update resulting from the increased knowledge of soil-structure behavior and the advent of increased desk-top computer resources.

General Waterfront Damage Mechanisms

Werner and Hung (1982) gives an excellent compilation of case studies mostly recounting Japanese experiences from the 1920's to 1980. They conclude that "By far the most significant source of earthquake-induced damage to port and harbor facilities has been porewater pressure buildup... which has led to excessive lateral pressures applied to quay walls and bulkheads." They cite the 1964 Niigata and 1964 Alaska earthquake where "porewater pressures buildup has resulted in complete destruction of entire port and harbor areas" They note that direct effects of earthquake induced vibrations on waterfront structures is minimal and overshadowed by liquefaction induced damage. Failure of bulkhead anchorage systems is a common significant damage inducing mechanism. Liquefaction also causes damage to piles. The Anchorage City Dock was a reinforced concrete structure supported on pipe pile with diameters from 16 to 42 inches. Some of the piles were batter piles and filled with concrete. The piles were supported on clay which consolidated and settled 4 feet. This movement resulted in deck displacements from 8 to 17 inches buckling the batter piles (Tudor/PMP, 1976) Experience from Niigata and Alaska suggests that piles deform with the soil. In the 1970 Peru earthquake, magnitude 7.8, the Sogesa Wharf suffered severe damage when the inboard piles restrained by the dike structure could not tolerate high displacements, Tudor/PMP (1976).

Table 1 is in part developed from the Werner and Hung (1982) case studies. They correctly show the vulnerability of batter piles as would be observed seven years later in the Port of Oakland. Gazetas and Dakoulas (1991) evaluate numerous waterfront case histories including the performance of sheetpile bulkheads in which the major failures have resulted from large-scale liquefaction in the backfill or supporting base. Frequently the anchored bulkhead damage takes the form of excessive outward movement and tilt caused by excessive movement of the anchor. They show that Japanese code procedures are inadequate because the accelerations values are often exceeded and the vertical component is omitted, they neglect ground motion amplification, and they do not take into account lateral soil spreading caused by a loss of stiffness. They note limitations in traditional pseudostatic sheetpile procedures to properly define the location of the active sliding surface. They develop an empirical seismic design chart based on the observed case histories. Other works of significance include Swanson (1996) which summarizes observed damage in the Kobe earthquake, Harn and Malick (1992) which gives design guidance, and Erickson and Fotinos (1995) which summarizes various code requirements.

The 1978 magnitude 7.4 earthquake Miyagi-Ken-Oki earthquake caused severe damage to gravity quay walls, piers and sheet pile bulkheads. The Sendai Port area has a soil profile composed of a sand layer 3 to 20 meters thick underlain by layers of medium coarse sand and silty loam. Dense sand and bedrock underlie the silty loam layer. Two nearby bulkheads serve as a comparison study, Figure 1. A seismic lateral coefficient of 0.1 g was used in the design. Bulkhead No. 4 was anchored with vertical H-beam. The area behind this bulkhead experienced cracking and settlement.. Bulkhead No. 5 was constructed in a similar manner except that it used batter piles to restrain the anchor. This bulkhead withstood the earthquake without damage. Note as shown in Figure 1 the near

surface soil behind Bulkhead No. 4 had lower blowcounts which when combined with reduced anchorage could have caused the increased lateral spread and associated damage.

Damage To Waterfront Structures Having Piles

The 1989 Loma Prieta Earthquake caused major port damage to the Port Of Oakland, Table 1. Soil liquefaction caused damage to the terminal facilities much of which is filled land composed of loose dumped or hydraulically placed sand underlain by soft normally consolidated Bay Mud. There were four areas damaged: the 7th Street Terminal, the Matson Terminal, the APL Terminal and the Howard Terminal. All of these terminals had pile supported wharves typically represented by Figure 2. The piles extended through the rock dike which served as containment for the fill composed of fine dredged sands and silty sands. The most severe damage occurred at the 7th Street Terminal where liquefaction of the fill resulted in settlements and lateral soil spreading, cracking the pavement over a wide area. Maximum settlements of the paved yard area were up to a 12 inches. The inboard crane rail was supported on the fill directly which settled; the outboard crane rail was supported on the wharf piles and did not settle. As a result of this differential movement the cranes were inoperable. Damage occurred to the tops of the batter piles, Figure 2, through shear, compression, and tension. The vertical piles were largely undamaged with a few exceptions. The stiff batter piles absorbed much of the loading among the other more flexible elements. Seed et al. (1990) suggests "the mode of failure was predominantly tensile failure driven by outward thrust of the fill, suggesting that liquefaction and associated spreading were important factors". As a result of this damage the port of Oakland is replacing all the 7th Street Terminal batter piles with vertical piles designed to resist lateral forces. The pile-wharf deck is being extended inboard to provide support for the crane rails. The Howard Terminal and the APL Terminal which had vertical or near vertical piles instead of batter piles did not sustain pile damage although liquefaction caused comparable settlements in the filled areas. Both crane rails were also pile supported.

On August 8, 1993 a magnitude 8.1 earthquake occurred offshore 50 miles from Guam and caused over $125 million in damages to Naval facilities on Guam, Table 1. Nearly all of Guam is firm soil or rock except for the region containing the Navy port which had soft soil composed of natural alluvium and artificial fill. It is estimated the peak horizontal ground accelerations were about 0.25g. Liquefaction was a major problem and lateral spreading of 1 to 2 feet was observed at wharf areas. It also resulted in settlements, backfill collapse and bulkhead movements. Buried water and power lines were fractured. Sheet piles failed in shear and deadman anchors pulled out. Batter piles failed in shear at the pile cap. Other Navy damage consisted of fuel tank leaks, sloughing of a dam, damage to masonry housing units and major damage to the power plant which supplied 20 percent of the island's power capacity.

On August 17 1995, the Hyogo-ken Nambu (Great Hanshin Kobe) earthquake, Japanese magnitude 7.2 (about 6.9 moment magnitude), occurred in Kobe Japan. This

event produced major damage to Japan's second busiest port. Liquefaction was a major contributor to the extent of the damage producing typical subsidence of a half meter. Piles were used extensively in this area. They were designed to account for the negative skin friction and additional ground improvement was also performed. Structures on such piles performed well even though major subsidence occurred in surrounding areas. Other structures not on piles suffered differential settlement and tilting and significant damage. Liquefaction caused up to 3 meters of lateral spread displacement, sunk quay walls, broke utility lines, and shut down 179 out of 186 berths at the port. It was responsible for major damage to crane foundations. Hydraulic fill behind concrete caisson perimeter walls fill liquefied causing the caissons to move outward rotating up to 3 degrees and settling from 0.7 to 3.0 meters. The caissons were designed for a lateral coefficient of 0.1g. A seismic coefficient of 0.2g was normally specified for dockside cranes. Peak accelerations of 0.8g in the NS direction, 0.6g in the EW direction and 0.3g vertical were noted from accelerograph recordings. The event had a duration of about 20 seconds. The outboard crane rails which were supported on the caisson also spread outward, Figure 3. The middle crane rails which were supported on piles did not move. The inboard crane rails settled between 1 and 2 meters. The increase in distance between crane rails resulting from lateral spreading was from 1 to 5 meters. Both old and new caisson construction faired equally poorly. The resulting deformation disabled all the dockside container cranes collapsing one and shutting down all port operations. Damage is attributed to liquefaction since structures supported on pile suffered much less damage, Liftech (1995). It should be noted that caissons designed for 0.25g sustained lower levels of damage.

Pile designs must be checked for the location of the maximum moment, generally at the pile cap. The second highest point is within the support soil. Damage below the soil line cannot be seen and easily repaired; thus, consideration of this must be included in the design. POLA provides for decreased ductility for wharf pile sections below the soil line. It is important to note that the pile curvatures are controlled by the stiffness of the supporting soil. Soil movement may be concentrated at interfaces between stiff and soft soils causing local increases in curvature, overstressing the pile. Soil layers and their associated stiffness must be accurately modeled in a pile analysis.

During the 1995 earthquake in Kobe Japan damage occurred to precast concrete piles on Port Island, Matso, K. (1995). Typically the failure mode consisted of anchor reinforcing bars pulling out of the pile caps producing separation between the piles and the pile cap. The Hanshin Expressway which collapsed was an elevated roadway supported on a series of single concrete pier. The failure of the pier was associated with failure of the transverse shear reinforcement and premature termination of longitudinal reinforcement. This reinforcement consisted of perimeter ties lapped at the ends and was spaced 30 cm on center. The inadequate shear reinforcement resulted in non-ductile behavior. Additionally gas-pressure weld splices of reinforcing bars failed; this technique is no longer used.

Most pile failures are associated with liquefaction of soil which can result in buckling of the pile, loss of pile friction capacity, or development of pile cracking and hinging. Hinging may be at the cap location or at an interface between soil layers of

differing lateral stiffness, Figure 4. Meyerson et al. (1992) present a state-of-the-art approach for evaluating pile buckling capacity for conditions of liquefaction of a soil layer and also determining allowable lateral deformation capacity. Most buckling occurs when the zone of liquefaction extends to the surface with the water table at the surface producing a large unsupported length. An axial transition load exists such that at less than that load the pile will not buckle.. Typically the transition load is at one-fourth to one-third of the ultimate bearing capacity. Flexible piles will tend to try to conform with soil movement and will have large curvatures at the interface between liquefied and non-liquefied material. Meyerson et al. present dimensionless curves relating pile lateral displacement capacity before formation of a hinge as a function of pile characteristic length. Yoshida and Hamada report on 2 case studies of piles beneath buildings which were damaged by liquefaction during the 1964 Niigata Earthquake. The first building, Building A, was a three story reinforced concrete building and is shown in Figure 5. The piles in this case were end bearing piles. The piles exhibited tensile cracks and concrete crushing. Pile number 2 exhibited a total disintegration of concrete probably from a lack of adequate confining steel. The second building designated as Building S is also a three story reinforced concrete building and is shown in Figure 6. The piles in this case were friction piles. All piles in both buildings were damaged by the lateral deformation associated with the liquefaction. Generally pier piles will develop hinges first at the pile cap; however this may not be the case for wharves having piles with much shorter freestanding lengths.

Priestley et al. (1992) contains an extensive report on the causes of bridge damage much of which is relevant to piers. In discussing damage to existing older bridges they note " All deficiencies tend to be a natural consequence of the elastic design philosophy almost uniformly adopted for seismic design of bridges prior to 1970, and still used in some countries notably Japan." Seismic deflections were underestimated in part by use of gross rather than cracked member stiffness. Seismic design forces were low and the ratio of seismic to static loads was incorrect resulting in erroneous moment patterns. Points of contraflexure were mislocated resulting in premature termination of reinforcement. Adjacent frames of bridges experienced out-of-phase-motion, with displacements often exceeding member supports. Soft soils amplified motion and liquefaction caused loss of pile support. Pounding of bridge members can impart high impact forces. Column longitudinal reinforcement was often lap-spliced immediately above the foundation with an inadequate development length of 20 bar diameters. " Displacement ductility factors as high as $\mu = 6$ to 8 may be needed in some cases. At ductility levels of 2-3, concrete compression strains in the plastic hinge regions exceed the unconfined strain capacity and spalling of the cover concrete occurs. Unless the core concrete is well confined by closely spaced transverse hoops or spirals, the crushing rapidly extends into the core, the longitudinal reinforcement buckles, and rapid strength degradation occurs.." Cap beam failures were attributed to low shear capacity, early cutoff of negative top beam reinforcement, and insufficient anchorage of large diameter cap reinforcement in the column. Development lengths of 3 to 5 feet for #18 bars was shown to be inadequate in the Loma Prieta earthquake resulting in large flexural cap beam cracks. Rupture of #18 bars bent on a 18-inch radius. "Problems can be expected for columns with longitudinal

reinforcement anchorage provided by 90 degree hooks bent away from the column axis, creating an unfavorable tension field in the joint region.. ... Current analysis indicates that considerable amount of vertical and horizontal shear reinforcement is required in the joint region, but are commonly omitted in older designs.

Japanese research, Kubo, 1969 and Hayashi, 1974 reports that piles move with the soil during elastic portions of motion. Locations of potential failure occur at the point of sharpest curvature in the pile top, at just below the mud line, and at a depth in the soil profile at high curvature. Piles tend to move with the soil such that the region of maximum displacement curvature in the soil field controls the pile response. Batter piles exert large reactions on the pier structure which may have detrimental effect on the pile cap. The pier should be structurally separated from the abutment to provide isolation. Tudor/PMP (1976) report that piers tend to have a narrow range of natural periods with good damping properties. They note that it is common practice to assign the total lateral force demand to the batter piles. For simple analysis the pier deck mass can be based on the deck and half the mass of the supporting piles. An added mass factor for the mass of the displaced water can be included. A pile preliminary design in high seismicity regions for gravity and earthquake loads can be made based on Tudor/PMP (1976):

$$M_u = 1.5\ E\ I_p / R$$

where

Mu	Required ultimate moment (k ft)
E	Pile modulus of elasticity (k /sq ft)
I_p	Pile moment of inertia (ft^4)
R	Radius of curvature from soil response (ft)
R = 100	for very soft fill, soft clay, loose sand
R = 250	for soft stiff clay, medium dense sand
R = 250	for Medium to dense gravel or dense sand

This suggests design curvatures in the range of 0.01 rad/ft to 0.004 rad /ft or 0.0008 rad/in to 0.00033 rad/in based on the soil stiffness and the pile tracking expected soil displacement.. It is believed that these values are probably too low and will result in substantial plastic pile behavior, cracking, and loss of prestress.

The approximate depth of pile support, d, in feet is given by:

$$d = \sqrt[4]{\frac{4EI}{k_s D}}$$

where

k_s	Coefficient of subgrade reaction (k/ft^3)
k_s = 2	for very soft fill, soft clay

k_s	= 20	for soft moderately stiff clay, loose sand
k_s	= 200	for Medium to dense stiff clay, dense sand or gravel
D		Width or pile diameter (ft)

Tudor/PMP (1976) note for prestressed piles steel dowels extending into the cap can be used for bending resistance and ductility.

AASHTO Standard Specification For Highway Bridges

This is a national code and as such divides the US into regions based on levels of expected ground motion. A map is provided which shows peak horizontal rock accelerations with a 90 percent probability of not being exceeded in 50 years which is a nominal 500 year return time event. Two categories of bridge structure are defined, essential bridges which are expected to function after a design earthquake and other bridges which are designed for near elastic response at moderate events and for limited damage at the maximum credible event. Four categories A through D are defined to treat importance and variation in seismic acceleration potential. A and B are low threat level requirements while D is highest representing an essential structure in the highest exposure zone. The 1996 AASHTO Code implements changes to update the code and bring it into agreement with recent changes developed by the Applied Technology Council and NEHRP. Four new site profiles are defined and serve to define site amplification. Equations are given to compute the elastic seismic response coefficient. A map of the United States gives the acceleration coefficient based on a 10 percent exceedance probability in 50 years.

Elastic earthquake lateral forces are determined based on the map accelerations and site soil factor. Component response modification factors are used to reduce the elastic forces for substructure elements while connections of superstructure to abutment and expansion joints are increased. The modification factors are analogous to ductility factors. It is assumed that columns will yield when subjected to forces from the design ground motion but that the connection will be able to resist the deformations with little damage. Wall piers have minimal ductility and an R value of 2 was assigned. Well designed columns in a multi-column bent have good ductility. A value of 5 was assigned to them. Single columns lack redundancy, thus a value of 3 was assigned. For C and D bridges the connections are designed for the maximum forces that can be developed by plastic hinging in the columns. The probability of elastic force levels not being exceeded in 50 years is in the range of 80 to 90 percent. Procedures are given to calculate displacements. Modal response techniques are used in the analysis of response. The 1996 Code allows for time history analysis, It is suggested that a factor of safety against liquefaction be 1.5 for important bridges. Guidance is given for pile design.

Concrete Piles

Reinforced concrete has been used as one of the major construction materials at the waterfront. Figure 7 is an axial force - moment interaction diagram of a reinforced concrete section. Note the figure does not consider section buckling. Point 1 illustrates a section entirely under a concentric compression load without moment. The strain field is uniform across the section and at the ultimate state is ε'_{cu} . Point 2 illustrates a combination of axial load and moment caused in this case by the load having an eccentricity. The amount of eccentricity in this case is set so as to produce a case of zero strain on the tension (bottom) face and maximum ε_{cu} strain on the compressive (top) face. Point 3 represents the point of maximum moment capacity and a balanced design such that the steel reinforcing is at yield point strain and the concrete is at maximum strain. Point 4 is the case of pure bending without axial load; the concrete is at maximum strain and the steel has yielded. This is a typical beam bending case. Point 5 is a case of axial load in tension and is controlled by the steel capacity. The tensile capacity of concrete is neglected in estimating strength. The concrete sections shown by points 1 and 2 have only compressive strain and the section would not undergo tensile cracking. In this case the section moment of inertia would be computed based on the gross (total) concrete section. The remaining points in Figure 7 show regions of tension. Since concrete is much weaker in tension, cracking would be expected to occur when the tensile stresses in the concrete were exceeded, typically at numerical level equal to about 10 percent of the maximum compressive stress. Cracking is a normal occurrence in concrete members under flexural load. When the concrete cracks the section moment of inertia is reduced; generally the cracked moment of inertia is about half the gross moment of inertia. In a marine environment it is desirous to control the cracking to prevent corrosion of the reinforcing steel. Confining steel is used to increase concrete strength, produce ductility and increase shear strength. An initial prestress force is used in piles as a mechanism for improving concrete performance by keeping the cracks closed. It has been noted that crack widths of 0.007 to 0.009 inches are sufficiently small to preclude deterioration of the reinforcement so an allowable crack width may be approximated at about 0.01 inches. It is not possible to directly equate the crack width to an allowable tensile strain since crack spacing is not known; however, corrosion has not been a problem when reinforcing stress has been restricted to a tension of 17 ksi or less under service loads. At concrete compressive strains below 0.0021 in/in the compression concrete does not evidence damage and crack widths under cyclic load should be acceptable. Occasional larger loads may be sustained without deterioration as long as a permanent offset does not occur and the prestress forces can close the cracks. Reinforcement deterioration is most pronounced in the presence of oxygen such as in a pier pile where the pile is freestanding out of water or in the splash zone. At deep water depths or in soil, the oxygen content is reduced such that pile reinforcement deterioration is less. Large loads causing loss of the concrete cover result in loss of pile capacity and facilitate deterioration; such conditions can be repaired if accessible by jackets around the pile. Loss of concrete cover begins at displacement ductilities of about 2.0, Joen and Park (1990b)

Until recently, piles were designed neglecting the confinement effects of the reinforcing on the concrete. Work by Joen and Park (1990a) shows the significant increase in moment capacity by considering the effect of spiral confinement on the concrete. This work uses the Mander et al (1988) concrete model for confined and unconfined concrete. Typically the ultimate compressive concrete strain of unconfined concrete is about 0.003 for use in computing flexural strength as reported by Priestley et al. (1992). For confined concrete the following may be used, Priestley et al. (1992),

$$\varepsilon_{cu} = 0.004 + (1.4\,\rho_s\,f_{yh}\,\varepsilon_{sm})/f_{cc} \geq 0.005$$

where

- ρ_s effective volume ratio of confining steel
- f_{yh} yield stress of confining steel
- ε_{sm} Strain at peak stress of confining reinforcement, 0.15 for grade 40 and 0.12 for grade 60
- f_{cc} Confined strength of concrete approximated by 1.5 f_c'

Prestressing of concrete piles is a mechanism for improving pile performance. Prestress tendons of steel are placed in tension in a form and anchored. Concrete is then poured in the form. When the concrete has attained sufficient strength the anchorage of the tendons is released and an axial compression is transferred to the pile. Prestressing is a very useful technique to minimize the size of cracks which occur in the concrete as it undergoes flexure. In piles spiral reinforcement is used to confine the concrete and improve shear strength. Pile ends are reinforced to facilitate pile driving forces. Figure 8 illustrates a typical pile which may be square, circular or octagonal. Table 2 gives typical pile axial capacities. The prestressing force acts like an axial compression force acting on the pile and has the effect of lowering the section capacity. This is illustrated in Figure 9. At the end of a pile, absent external anchors, the tendon prestress force is zero at the free edge. The level of prestress force in the end section of a pile depends on its distance from the end of the pile and on bond conditions. The limiting stress in the tendon is a function of a friction bond length and increases with distance from the end of the pile to full development. The transfer length to achieve the effective prestress is given by:

$$l_t = f_{se} * d / 3$$

where

- f_{se} effective prestress in the tendon (3 or 7 wire strand) (ksi)
- d diameter of tendon

The full development length of the maximum stress in the prestressing steel is given by:

$$l_d = (f_{ps} - 2\,f_{se}/3)\,d$$

where

f_{ps} maximum stress in the prestressing steel (ksi).

Since a lack of bond causes the prestressing force to vary from maximum to zero at the pile end, the moment capacity at the pile top end can be reduced over the development length. This is important since the top of the pile is normally a high moment region. The moment capacity at the pile cap depends on the design of the tendon anchorage and can be reduced from full moment capacity of a section having full tendon anchorage.

Sheppard (1983) provides a useful summary of the design of prestressed piles for seismic loads. He reports on several pile tests and then utilizes that data to develop three levels of ductility demand. Where loading is light such that the applied moment is less than 20 percent of ultimate and the applied axial load is less than 30 percent of ultimate spiral steel volumetric ratios greater than 0.003 can produce curvatures of 0.0003 /in . For earthquake loading volumetric ratios greater than 0.014 are required. This level of spiral reinforcement can produce maximum curvatures of 0.0007. Severe earthquakes require volumetric ratios of 0.021 to achieve maximum curvatures of 0.001. To achieve ductile behavior during cyclic loading especially in the areas of plastic hinging, a minimum volumetric ratio of spiral confining reinforcement is required. The following is recommended by Joen and Park (1990a) and Sheppard (1983):

$$\rho_s = 0.45\left[\frac{A_g}{A_c} - 1\right]\frac{f'_c}{f_{yh}}\left\{0.5 + \frac{1.25}{\phi}\left(\frac{P_e}{f'_c A_g} + \frac{f_{cp}}{f'_c}\right)\right\}$$

or

$$\rho_s = 0.12\frac{f'_c}{f_{yh}}\left\{0.5 + \frac{1.25}{\phi}\left(\frac{P_e}{f'_c A_g} + \frac{f_{cp}}{f'_c}\right)\right\}$$

which ever is greater

where

A_c area of concrete core of pile cross section measured to outside of spiral
A_g gross area of pile cross section
f'_c concrete cylinder compressive strength
f_{cp} compressive stress in concrete from prestress
f_{yh} yield strength of spiral steel
P_e external compressive load on pile
ϕ strength reduction factor
ρ_s volume of spiral steel to volume of concrete core measured to outside of spiral

The axial load of the pile consisting of external load plus prestress should be less than 70 percent of the pile gross concrete strength. In the zone of the plastic hinge, the pitch of the spiral based on test data by Joen and Park (1990b) should not be more than 4 times the tendon steel diameter. The 1982 New Zealand code has additional limitations for the spiral pitch to be less than one-fifth of the pile diameter, or six times the longitudinal steel diameter, or 7.9 inches, whichever is less. Outside the plastic hinge zone the pitch may be double that of the plastic hinge zone. Use of high strength steel with 125 to 150 ksi yield can minimize the amount of spiral reinforcement and facilitate concrete placement; however such materials must exhibit large yield plateaus and strain capacity before rupture and not be brittle. The 1982 New Zealand code which first recognized the importance of spiral confinement, limited the yield strength of the spiral to 73 ksi. Additional research may be needed in this area. Banerjee et al. (1987) reviews seismic performance of prestressed piles. He notes that spiral volumetric steel reinforcing ratio of 0.0035 results in maximum curvatures of 0.0003 rad/in which is inadequate for high seismic motion. Values of 2 percent reinforcing ratio are required to provide high curvature under severe seismic regions. They noted hollow piles burst inward and should be avoided under all conditions. "Pile performance is influenced most strongly by the amount of spiral steel, axial load and the embedment conditions. .. The curvature demand reduces significantly with increasing pile size. Since the curvature capacity is also believed to reduce with increasing pile size, both effects should be considered in choosing piles for a specific site." Rotational fixity at the pile cap can produce high curvature and shear. The curvatures are larger in soft soil and are especially severe at the interface between layers where significantly different soil modulii exist.

Joen and Park (1990 b) state " A well designed pile can continue to carry significant moment and vertical load after loss of the concrete cover at large deformations in the post-elastic range... because the confinement of the concrete core provided by the spiral enhances the strength and ductility of the core. They also state that the presence of nonprestressed longitudinal reinforcement in prestressed concrete piles is not essential to the satisfactory performance of the piles. The authors compare moment capacity calculations using an unconfined concrete strength model and a confined concrete strength model. They conclude that for a series of 17 piles tested, the unconfined concrete model under predicted pile strength by a factor of 1.12 to 2.39. Use of a confined concrete strength model is shown to be more accurate and is recommended for Navy use. Of equal significance, they note in tests of pile caps that the strength of a pile may be reduced at the ends by the development length and should be included as a moment capacity reduction factor at pile ends.

An important measure of pile capacity is the moment curvature relationship. As a measure of section capacity, it is determined by dividing the concrete outer fiber (compressive face) strain by the depth to the neutral axis. Curvature capacity is a measure of pile ductility. Joen and Park (1990a) report that a large increase in flexural strength and curvature ductility factor is attributed to confinement. "The flexural strength increase is particularly high at large axial load levels, due to the greater dependence of the flexural strength on the contribution from the compressive force in the concrete at large axial

loads.....to obtain a more uniform available curvature ductility factor, more spiral reinforcement should be provided at high axial load levels, and less at low axial load levels."

Curvature demand or the amount of curvature imposed by the pile loading is based on the distribution of moment along the pile and is related to the bending moment equation as a function of distance along the pile divided by the product of the modulus of elasticity times the moment of inertia.

$$\phi = M(x) \; / \; EI$$

The adequacy of a pile design can be made by comparing pile curvature capacity to pile curvature demand. The curvature ductility demand can be expressed as μ_ϕ

$$\mu_\phi = \frac{\phi_{max}}{\phi_y}$$

For sections with reinforcement located on the tension and compressive extremities which yield prior to concrete crushing the actual moment curvature relation may be approximated by a bilinear representation and a clear yield point is evident as illustrated in Figure 10a. In other cases where the moment-curvature displays a curved relationship, as illustrated in Figure 10b, the yield point may be represented by some offset such as 40 percent of maximum moment. Moment capacity would be expected to increase if strain hardening of reinforcement occurred. For analysis of Navy concrete piles, the computer program BIAX developed by Wallace and Moehle (1989) under an NSF grant may be used to calculate pile axial force - moment interaction diagrams and pile moment - curvature diagrams. Figure 11 is an axial force -moment interaction diagram for a typical 24-inch octagonal pile whose moment curvature diagram is shown in Figure 10a. Figure 10b is moment curvature diagram for an 18-inch square fender pile tested at NFESC, Warren (1989). Figure 12 illustrates the construction of an equivalent bilinear ductility approximation based on equal areas under the moment-curvature diagram. If the geometry of the structural element, elastic deflected shape, and support conditions are defined the internal curvature can be related to the external displacement as illustrated for an example in Figure 13.

$$\Delta = \frac{1}{\phi} - \sqrt{\frac{1}{\phi^2} - L^2}$$

Two lines in Figure 14 after Priestley et al. (1992) illustrate a beam column with elastic limit deformation and with the formation of a plastic hinge. The elastic deflection can be related to the corresponding elastic curvature:

$$\Delta_y = \phi_y L^2/3$$

Once the ultimate capacity has been reached, a plastic hinge forms in the section and the hinge rotates at a constant moment. The amount of hinge rotation, θ_p, is related to the length of the hinge, L_p and the portion of curvature associated with the plastic hinge, ϕ_p:

$$\theta_p = L_p * \phi_p$$

The length of the plastic hinge in constant moment elements such as columns or piles is approximately proportional to the diameter of the pile or column. When a hinge is formed, the total deformation, Δ, is composed of the elastic deformation, Δ_y, and the plastic deformation, Δ_p, caused by the plastic hinge rotation.

$$\Delta_{max} = \Delta_y, + \Delta_p$$

For small deformations, the plastic deflection, Δ_p can be approximated by multiplying the hinge rotation times the clear length of the member, (L - L_p/ 2)

$$\Delta_p = \phi_p * (L - L_p/2)$$

The displacement ductility can be expressed as

$$\mu_\Delta = \frac{\Delta_{max}}{\Delta_y}$$

$$\mu_\Delta = \frac{\Delta_y + \Delta_p}{\Delta_y} = 1 + \frac{\Delta_p}{\Delta_y}$$

$$\mu_\Delta = 1 + 3(\mu_\phi - 1)\frac{L_p}{L}(1 - 0.5\frac{L_p}{L})$$

This equation gives a means of relating displacement ductility with curvature ductility. Priestley et al. (1992) note " The flexural ductility capacity of existing members can be expressed either in terms of the section curvature ductility factors, or of displacement ductility factors. Although the later is more convenient in terms of structural assessment in

that it frequently compares rather closely to the force reduction factor relating elastic response level to design or provided strength. The structural ductility factor relates to the structure as a whole. Individual member ductility factors can differ widely from the global factor, and may bear little resemblance to the force reduction factor resulting from an elastic demand/capacity ratio. ... Overall structure ductility should be assessed at the center of seismic force. "

The above relation for μ_Δ and μ_ϕ is based on a elasto - plastic representation of force shown in Figures 15a and b. Note that M_y corresponds to the moment at which the tensile reinforcing steel reaches a yield strain. The M_u corresponds to the peak moment capacity at ultimate concrete compression strain. M_n is equivalent elasto-plastic maximum moment. The equivalent elasto-plastic yield curvature must be extrapolated

$$\phi_y = \frac{M_n}{M_y} \phi_y'$$

Figure 15c is a plot of the above ductility displacement - curvature ductility relationship and illustrates the effect of the L_p / L ratio. There are limiting values of curvature ductility beyond which pile performance is unacceptable and unreliable. Thus these limits translate into displacement ductility limits which are seen to vary with the L_p / L ratio. Pile displacement ductility criteria must reflect this factor. In development and implementation of a general criteria for piles, the application will control the allowable ductility. A wharf with short piles will permit higher allowable displacement ductilities than a pier with long piles.

Priestly et al. (1992) report that the shear strength of rectangular sections can be estimated by:

$$V_n = v_c A_e + A_v f_y (d/s) \text{ Cot } (\theta) + 0.2 P$$

and the shear strength of circular sections can be estimated by:

$$V_n = v_c A_e + (\pi/2) A_s f_y (D'/s) \text{ Cot } (\theta) + 0.2 P$$

where

v_c	Concrete shear strength
A_e	Area confined concrete
A_v	Area shear steel reinforcement
A_s	Area spiral steel reinforcement
fy	Steel yield stress
d	Bar spacing
D'	Spiral diameter
s	Bar spacing or spiral pitch

P Axial load
θ Inclination angle of crack

The value of v_c can be determined from a graph and is related to ductility, Priestley et al. (1992), Figure 16.

The initial estimate of a pile's properties represents the first cycle of loading. Under an earthquake a number of cycles of loading occur. The pile's properties degrade with cycling. Figure 17 is pile tested by Warren (1989) which illustrates this concept. One model which has been used to represent this degradation is the modified Takeda model. The extended Takeda model modifies the unloading stiffness K_u by a factor α times the extent of the post elastic loading R_p. A second factor, β, determines the reloading stiffness and the extent of degradation Figure 18 illustrates the concept.

Calculation of Earthquake Demand On Piles

The previous section explained how the pile capacities are computed. Figure 19 conceptually illustrates a pile under lateral load and shows static deflection, slope, moment shear and soil reaction. The earthquake loading places a performance demand on the piles which can be expressed in terms of moment-curvature or moment-deflection. To calculate the response of the piles a model of the structure mass and stiffness must be developed. The model of the pile must include the nonlinear soil force resisting lateral motion which varies along the pile depth. The engineer has several options.

One option is to use the peak horizontal acceleration times the mass of the structure on the pile or pile group as an applied lateral force. The computer program CBEAMC solves the general beam-column with nonlinear supports problem. The pile is divided into a series of vertical 2-dimensional line elements with elastic beam bending elements and the soil is represented by a series of nonlinear springs. The solution gives moments, shears, deflections and rotations at each node point. This approach has limitations. The model evaluates a single pile and does not permit consideration of the superstructure. The pile is modeled elastically and the extent of pile yielding can only be estimated.

A second option is the use of general purpose finite element programs to perform static, response spectra or time history analyses. Elastic solutions are not recommended because accurate modeling of the soil resisting pile deflection requires a nonlinear relationship. Elastic response from modal analysis does not have validity since the mode shapes, periods and effective damping are altered by plastic hinge formation.

The best option is a nonlinear finite element analysis. The DRAIN2DX/ DRAIN3DX programs were developed under a grant from the NSF. These are general purpose 2 and 3-dimensional finite element programs with nonlinear beam-column elements whose strength is described by a moment-force diagram. The programs have

provisions for use of the extended Takeda degrading stiffness model so the pile strength can be modeled accurately under cyclic loading. A bilinear spring element can be used to represent the soil resistance. The pier superstructure can be modeled as well. The location of the concrete elements and the amount of strain experienced determines whether the element will be in a cracked state with reduced section properties or an uncracked state with uncracked section properties based on the moment of inertia of the total concrete cross-section. The earthquake loading is input as a time history and the time step integration procedure used for the solution. The program computes nodal moments, shears, deflections and rotations for each time step. Before a time series solution is performed it is suggested that a lateral force be applied in increasing steps as a "pushover" analysis. This will give a picture of the location of the structure's first yield point, the yield pattern, and the collapse mechanism. From this picture of the structure the engineer can focus on the structure's weak points for detailed study.

The DRAIN2DX program allows the beam column elements to yield only at the element ends in concentrated plastic hinges. These hinges yield under constant moment. Total plastic rotation is shown for each element end and a code is shown indicating yielding. It should be recognized that a two-dimensional representation is only an approximation. Factors such as pile group interaction, pile-wave interaction, radial damping are not considered. Evaluation of element hinge capacities can be made by use of the above derived equations resulting in:

$$\theta_p = L_p * \phi_p$$

where the plastic hinge rotation, θ_p, comes directly from the analysis results and L_p is the length of the plastic hinge. The element curvature can be determined. The element displacement ductility can now be calculated where L is the length from the hinge to the point of contraflexure.

$$\mu_\Delta = 1 + 3(\mu_\phi - 1)\frac{L_p}{L}(1 - 0.5\frac{L_p}{L})$$

Characterization Of Soil Forces Acting On Piles

Novak (1991) gives a state-of the-art paper on pile dynamics in which he discusses causes of damage to piles such as liquefaction and earth movement. He discusses theoretical studies which develop dynamic soil-pile interaction; he shows that there is a cylindrical boundary zone around a pile which undergoes nonlinear behavior. Pile soil separation is possible under lateral load, Figure 20. The length of the pile separation, L_s, is a function of the lateral deformation:

$$L_s / d = 260\ \Delta/d$$

where

Δ the amount of lateral deformation , $0.001 \leq \Delta/d \leq 0.005$
d Pile diameter

Wolf and Weber (1986) show the difference in horizontal stiffness and damping for alternative modeling assumptions. Figure 21a shows a linear model with soil tension. Figure 21b allows soil separation which is seen to reduce damping. Figure 21c allows soil separation and slipping of the pile in the soil which reduces both horizontal stiffness and damping. Large displacements require nonlinear representation of the soil around the pile. To account for gapping, slippage and friction lumped mass finite element models evolved as the most often used approach. Soil resistance deflection relationships known as p-y curves were developed. Figure 22 is a typical p-y curve. To account for pile separation the soil reaction displacement curve shown in Figure 23 has been used. Figure 24 shows cyclic loading p-y curves for sand and clay.

Yoshida and Hamada (1991) report on the Japanese Highway Bridge Code which establishes the subgrade modulus reaction k for use with piles:

$$k = 0.2 * 28N * D^{-0.35} \ (kgf/cm^3)$$

where

D the diameter of the pile in cm
N Japanese penetration test N value of blowcounts

The spring constant is found by multiplying the diameter of the pile times k times the pile length between springs.

Martin and Lam (1995) present a recent state-of-the-art summary of the design of pile foundations. They show that a nonlinear soil model is required to capture the lateral behavior of a pile. A Winkler Spring Beam-Column representation with nonlinear springs is shown to be an acceptable method for computing pile behavior to lateral loads. They have reviewed procedures for computing the required soil load-deformation relationship to characterize the spring properties and found the American Petroleum Institute (1994) procedure to be the accepted common practice. This procedure is found in a recent recommended practice and is approved by the American National Standards Institute.

The origin of the API equation for sand evolved from work by Reese, Cox, and Koop (1974) who established a set of equations based on the forces associated deformation of a soil wedge and the lateral deformation of a rigid cylinder into soil. They established the early shape of the soil load deflection p-y curve based on the soil subgrade modulus. The procedure was modified by Bogard and Matlock (1980) principally as a simplification by consolidation of terms. The shape of the p-y curve was finally based on work by Parker and Reese (1970). O'Niell and Murtcheson (1983) wrote an excellent summary of the development of the procedure for constructing p-y curves and performed

a comparison study showing the API equation as having least cumulative error in comparison with experimental data from full scale pile tests, although one must consider that this is still a very approximate procedure.

The American Petroleum Institute (1994) recommended practice for offshore platforms gives guidance in determining p-y curves. That information is reported verbatim in the following sections:

> **Lateral Bearing Capacity for Soft Clay.** For static lateral loads the ultimate unit lateral bearing capacity of soft clay p_u has been found to vary between 8c and 12c except at shallow depths where failure occurs in a different mode due to minimum overburden pressure. Cyclic loads cause deterioration of lateral bearing capacity below that for static loads. In the absence of more definitive criteria, the following is recommended. The value of p_u increases from 3c to 9c as X increases from 0 to X_R according to:
>
> $$p_u = 3c + \gamma' X + J c X / D \qquad (1)$$
>
> and
>
> $$p_u = 9 c \text{ for } X \geq X_R \qquad (2)$$
>
> where:
>
> p_u ultimate resistance, in stress units
> c undrained shear strength of undisturbed clay soil samples, in stress units
> D pile diameter
> γ' buoyant unit weight of soil, in weight density units
> J dimensionless empirical constant with values ranging from 0.25 to 0.5 having been determined by field testing. A value of 0.5 is appropriate for Gulf of Mexico clays.
> X depth below soil surface
> X_R depth below soil surface to bottom of reduced resistance zone. For a condition of constant strength with depth, Equations 1 and 2 are solved simultaneously to give:
>
> $$X_R = 6D / ((\gamma' D / c) + J)$$
>
> Where the strength varies with depth, Equations 1 and 2 may be solved by plotting the two equations, i.e., p_u vs. depth. The point of first intersection of two equations is taken to be X_R. These empirical relationships may not apply where strength variations are erratic. In general, minimum values of X_R should be about 2.5 pile diameters.

Lateral soil resistance-deflection relationships for piles in soft clay are generally nonlinear, Figure 25. The p-y curves for the short-term static load case may be generated from the following table:

p/p_u	y/y_c
0.00	0.0
0.50	1.0
0.72	3.0
1.00	8.0
1.00	∞

where:

p actual lateral resistance, in stress units
y actual lateral deflection
y_c $2.5\ \varepsilon_c D$
ε_c strain which occurs at one-half the maximum stress on laboratory undrained compression tests of undisturbed soil samples

For the case where equilibrium has been reached under cyclic loading, the p-y curves may be generated from the following table:

$X>X_R$		$X<X_R$	
p/p_u	y/y_c	p/p_u	y/y_c
0.5	1.0	0.5	1.0
0.72	3.0	0.72	3.0
0.72	∞	$0.72X/X_R$	15.0
		$0.72X/X_R$	∞

Lateral Bearing Capacity for Stiff Clay. For static lateral loads, the ultimate bearing capacity, p_u, of stiff clay ($c > 96$ kPa or 1 Tsf) as for soft clay would vary between 8c and 12c. Due to rapid deterioration under cyclic loadings, the ultimate static resistance should be reduced for cyclic design considerations. While stiff clays also have nonlinear stress-strain relationships, they are generally more brittle than soft clays. In developing stress-strain curves and subsequent p-y curves for cyclic loads, consideration should be given to the possible rapid deterioration of load capacity at large deflections for stiff clays.

Lateral Bearing Capacity for Sand. The ultimate lateral bearing capacity for sand has been found to vary from a value at shallow depths determined by Equation 3 to a value at deep depths determined by Equation 4. At a given depth the equation giving the smallest value of Pu should be used as the ultimate bearing capacity.

$$P_{us} = (C_1X + C_2D)\,\gamma'X \qquad (3)$$

$$P_{ud} = C_3\,D\ \gamma'\ X \qquad (4)$$

where

Pu ultimate resistance (force/unit length) (s=shallow, d=deep)
γ' buoyant soil weight, in weight density units
X depth
ϕ' angle of internal friction in sand
C1 Coefficient determined from Figure 26 as a function of ϕ'
C2 Coefficient determined from Figure 26 as a function of ϕ'
C3 Coefficient determined from Figure 26 as a function of ϕ'
D average pile diameter from surface to depth

The lateral soil resistance-deflection (p-y) relationship for sand is also nonlinear and in the absence of more definitive information may be approximated at any specific depth X, by the following expression.

$$P = A\, p_u \tanh [\, (k\, X\, y\,)/(A\, p_u)] \qquad (5)$$

where

A factor to account for cyclic or static loading continued.

$A = 0.9$ for cyclic loading.

$A = (3.0 - 0.8X/D) \geq 0.9$ for static loading.

p_u ultimate bearing capacity at depth X in units of force per unit length
k initial modulus of subgrade reaction in force per volume units. Determine from Figure 27 function of angle of internal friction.
y lateral deflection
X depth

Pile group. Consideration should be given to the effects of closely spaced adjacent piles on the load and deflection characteristics of the pile group. Generally, for pile spacing less than eight diameters, group effects may have to be evaluated.

For piles embedded in clays. the group capacity may be less than a single isolated pile capacity multiplied by the number of piles in the group; conversely, for piles embedded in sands, the group capacity may be higher than the sum of the capacities of the isolated piles. The group settlement in either clay or sand would normally be larger than that of a single pile subjected to the average pile load of the pile group.

For piles with the same pile head fixity conditions and embedded in either cohesive or cohesionless soils, the pile group would normally experience greater lateral deflection than that of a single pile under the average pile load of the corresponding group. The major factors influencing the group deflections and load distribution among the piles are the pile spacing, the ratio of pile penetration to the diameter, the pile flexibility relative to the soil, the dimensions of the group, and the variations in the shear strength and stiffness modulus of the soil with depth.

It has been noted that piles spaced 5 pile diameters apart do not exhibit a significant group effect.

Soil Properties

The soil properties which influence the pile lateral deflection and are required for definition of a spring model are as follows:

Cohesionless Soils

γ' buoyant soil weight, in weight density units

ϕ' angle of internal friction in sand

Cohesive Soils

ε_c strain which occurs at one-half the maximum stress on laboratory undrained compression tests of undisturbed soil samples

γ' buoyant unit weight of soil, in weight density units

c undrained shear strength of undisturbed clay soil samples, in stress units

J dimensionless empirical constant with values ranging from 0.25 to 0.5 having been determined by field testing. A value of 0.5 is appropriate for Gulf of Mexico clays.

The following soil properties are taken from the NCEL Handbook for Marine Geotechnical Engineering (1985).

Properties for Cohesionless Soil

Type	Standard Penetration Blow Count, N	ϕ (Degrees)	Relative Density, D_r (%)	Effective Unit Weight, γ_b (lb/cu ft)
Very Loose to loose	<10	28-30	0-35	45-55
Medium Dense	10-30	30-36	35-65	55-65
Dense	30-50	35-42	65-85	60-70
Very Dense	50 +	40-45	85-100	60-70

Properties of Cohesive Soils

Type	Undrained Shear Strength, (Lb/sq in)	Strain at 50% maximum stress ε_c	Effective Unit Weight, γ_b (lb/cu ft)
Unconsolidated clays	0.35-1.0	2	20-25
Normally consolidated soils at depth z , inches.	1.0 + 0.0033z	2-1	25-50
Overconsolidated soils based on consistency:			
medium stiff	3.5-7	1.0	50-65
stiff	7-14	0.7	50-65
very stiff	14-28	0.5	50-65
hard	over 28	0.4	50-65

Values of ε_c can be estimated from the following table when other data is not available:

Shear Strength lb/sq ft	ε_c %
250-500	2.0
500-1000	1.0
1000-2000	0.7
2000-4000	0.5
4000-8000	0.4

Figures 28 and 29 show the variation of cohesionless soil effective friction angle as a function of blow count and the variation of cohesive soil strain at 50 percent of maximum stress as a function of shear strength.

Figures 30 and 31 give the buoyant unit weight and friction angle as a function of depth (Forrest, 1996). The values shown are intended to represent the range of maximum and minimum values found at a waterfront site, and as such to be the bounds to be used in analysis of pile moments and displacements. The middle line in Figures 30 and 31 represents what is thought to be a frequently occurring typical value. Figures 32, 33 and 34 present undrained shear strength, strain at half the maximum stress, and buoyant

weight as a function of depth for cohesive soil. Again the data shown is intended to represent the range of maximum and minimum values found at the waterfront.

Significance of Soil on Pile Moment

Figure 35 is taken from a Japanese Waterfront Handbook and gives a closed form solution for maximum moment in the pile at the top of the pile and in the soil as a function of geometry and soil elastic subgrade modulus. This derivation assumes a constant subgrade modulus with depth and is a non-yielding elastic solution. Figure 36 shows the variation in pile top moment with subgrade modulus and Figure 37 shows the variation in maximum pile moment at depth in the soil. As can be seen the soil modulus has effect on the pile top moment at the lower range of subgrade modulus and lesser effect as it increases. There is a much lesser effect on the pile moment at depth in the soil. There is a major difference between the lateral resistance afforded by cohesionless soils compared to cohesive soils. This suggests that the pile moments may be significantly influenced by the type of restraining soil.

The shorefront soil conditions are spatially variable based on geologic process of deposition. Near surface materials of the seafloor are influenced by tidal sediment transport. Figure 38. is shows boring logs from a portion of the near shore region of the Naval Air Station, North Island, California. The numbers in the figure are blowcounts and are noted to vary laterally and with depth evidencing a range of medium dense to very dense material. The soil types noted in the figure are common at the waterfront and are as follows:

SP Poorly graded sands or gravely sands, little or no fines

SM Silty sands and sand-silt mixtures

ML Inorganic silts and very fine sands, silty or clayey fine sands or clayey silts

CL Inorganic clays of low to medium plasticity, gravely clays, sandy clays, silty clays, lean clays

Figure 39 shows the variation in blowcount for four borings near the piers at Naval Weapons Station, Earl New Jersey. Figure 40 shows the same data showing the spread in the data which is typical of blowcount data. The composition of the seafloor varies horizontally and vertically in both density and composition. The presence of layers of sands and clays may be noted; however these layers vary with depth and may not be evidenced in all boring hole logs. Conservative engineering design practice establishes a set of lower bound soil strength parameters which can be used uniformly throughout the design and have a high assurance of being met across the site.

Soil - Pile Model

Figure 41 shows a finite element model in which a 24 inch diameter prestressed concrete pile is represented by bilinear beam elements and the soil is represented by bilinear spring connectivity elements. The soil is assumed to be a cohesionless material whose friction angle varies with depth as shown in Figure 31 and whose effective unit weight varies with depth as shown in Figure 30. Using the API equations for cohesive and cohesionless soils results in the soil yield strength shown in Figure 42 expressed as pounds per inch of pile length for the given pile diameter. Figure 43 gives the soil spring stiffness.

The top of the pile was restrained against rotation and an increasing lateral force was applied to the top of the pile. The results of the analysis show the pile initially yields at the pile cap; a second hinge forms in the soil at a lateral load of about 18 kips at which time a collapse mechanism occurs. The actual collapse load is a function of the soil type:

Soil Type	Collapse Load, Kips
Stiff clay	19.5
Upper bound of sand	18.5
Sand	18
Lower bound of sand	17
Soft clay	14.5

The pile deflection and moment at a lateral load of 10 kips are shown in Figures 44 and 45. The pile deflection and moment just prior to collapse are shown in Figures 46 and 47. Figures 44 through 47 show the range of results for the full range of soil properties. The above data represents what is believed to be a maximum spread in possible soil properties. It can be seen that for the geometry studied the maximum moment occurs at the pile cap. The location of the second hinge occurs in the pile at a depth of less than a third of the pile embedment. For stiffer soils, the location of the maximum moment of pile in soil is within the top 10 feet. Very soft soils lower the location of the pile maximum moment within the soil embedment zone; however its magnitude tends to remain constant. The magnitude of the moment in the pile at the pile cap increases as the soil stiffness decreases.

The study was repeated for the case of a 10-inch square prestressed concrete pile having four 1/2-inch tendons. The soil properties were the same adjusted for the pile width. The results show the same typical deflected shape pattern and moment diagram, Figures 48 and 49. The maximum moment for this geometry is at the top of the pile at the pile cap.

Typical Site Case

The data shown in Figure 39 is based on boring logs from the Carrier Dock Extension project at Naval Air Station, North Island in the San Diego area. This site is typical of West coast cohesionless sites. The four boring logs containing Standard Penetration data shown in Figure 39 were used to estimate buoyant density and friction angle properties as a function of depth. The soil profile for each boring formed the basis for establishing the pile-soil model parameters shown in Figure 41. A horizontal load of 10 kips was applied to the top of the pile at the pile cap. Figures 50 and 51 show the results of the four analyses. The results show that even though there is substantial variation in blowcount data with depth between the profiles, the pile response is relatively the same. There is about 10 percent variation in pile cap displacement. Appendix A presents a comparison of lateral load test data and comparisons with p-y curves computed using the API equations.

Pile Analysis

To study the behavior of a pile under cyclic loading the DRAIN2DX program was used to analyze a single 24-inch diameter octagonal prestressed pile whose properties are shown in Figure 10a and Figure 11. Figure 52 shows the finite element model of the beam-column elements excluding soil spring elements. The pile was modeled as a bilinear elasto plastic material defined by the axial force-moment interaction diagram in Figure 11. Attached to each node was an inelastic nodal connectivity element with bilinear stiffness and gaping representing the soil restraint around the pile. For the first analysis the soil degraded stiffness was reduced to one-third of the initial stiffness which precludes large yielding and represents a stiff condition. The pile was restrained against rotation at the top and a lumped mass was used to represent the pier deck.

A static horizontal force was applied to the top of the pile in what is termed " a push-over analysis". Figure 53 shows the pile moments with depth for three load levels and Figure 54 shows pile deflection with depth. Figure 55 gives displacement of the top of the pile. The pile developed its first plastic hinge at the top, Node 1 Element 1, at a load of 130 kips. A second hinge developed at Node 9 Elements 8 and 9 at a load of 210 kips. This inelastic behavior spread upward to Node 8, Elements 7 and 8, where a third hinge occurred at about 260 kips. Figure 56 gives the element net deflection determined by subtracting the horizontal lower node displacement from the upper node displacement. Figure 57 gives the plastic hinge rotation at the ends of each element sustaining inelastic behavior. The locations of the hinges and hinge sequence are also shown.

The following illustrates the computation of ductility. The table summarizes the plastic hinge rotation from the pushover analysis using DRAIN2DX.

Plastic Hinge Rotation

	Element 1		Element 7		Element 8		Element 9	
P kips	Node 1	Node 2	Node 7	Node 8	Node 8	Node 9	Node 9	Node 10
130	yields							
210	.01024					yields	yields	
260	.02960			yields	yields	.00701	.00934	
300	.04912			.00854	.01294	.00701	.00934	

For the example pile from the moment curvature figure $\phi_y = 0.00025$

For the pile in the example $L_p =$ 18 in.

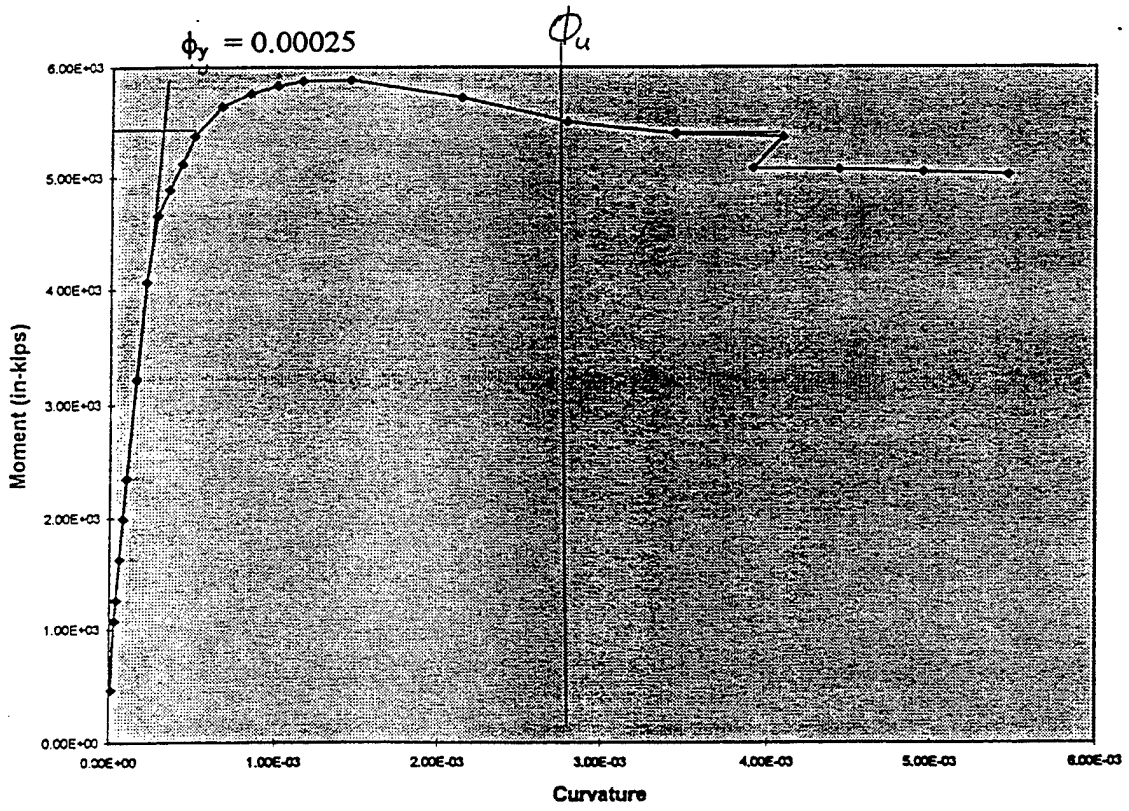

Node 1 Element 1

Load step 26 P = 260 kips

From the DRAIN2DX pushover analysis the plastic hinge rotation $\theta_p = 0.02690$

$$\phi_p = \theta_p / L_p = 0.02690 / 18 = 0.00149$$

$$\mu_\phi = 1 + \phi_p / \phi_y = 1 + (0.00149 / 00025) = 6$$

$$\mu_\Delta = 1 + 3(\mu_\phi - 1)\frac{L_p}{L}(1 - 0.5\frac{L_p}{L})$$

From moment - depth plot for Load Step 26 the distance from the hinge at Node 1 to the point of contraflexure, L = 27 inches See Figure 58.

$$\mu_\Delta = 1 + 3(6 - 1)(18/27)(1 - 0.5(18/27)) = 7.67$$

For Load Step 30 P = 300 kips

From the DRAIN2DX pushover analysis the plastic hinge rotation $\theta_p = 0.04912$

$$\phi_p = \theta_p / L_p = 0.04912 / 18 = 0.00273$$
$$\mu_\phi = 1 + \phi_p / \phi_y = 1 + (0.00273 / 00025) = 12$$

From moment - depth plot for Load Step 30 the distance from the hinge at Node 1 to the point of contraflexure, L = 22 inches

$$\mu_\Delta = 1 + 3(12 - 1)(18/22)(1 - 0.5(18/22)) = 16.95$$

Node 9 Element 8 and Element 9

Load step 26 P = 260 kips

From the DRAIN2DX pushover analysis the plastic hinge rotation is found from summing the rotations for element 8 and element 9, both of which yield at node 9 $\theta_p = 0.01636$

$$\phi_p = \theta_p / L_p = 0.01636/ 18 = 0.000909$$

$$\mu_\phi = 1 + \phi_p / \phi_y = 1 + (0.000909 / 00025) = 4.63$$

$$\mu_\Delta = 1 + 3(\mu_\phi - 1)\frac{L_p}{L}(1 - 0.5\frac{L_p}{L})$$

From moment - depth plot for Load Step 26 the distance from the hinge at Node 9 to the point of contraflexure, L = 69 inches

$$\mu_\Delta = 1 + 3\,(4.63 - 1)(18/69)(1 - .5(18/69)) = 3.47$$

over both elements 8 and 9 node 9

For Load Step 30 P = 300 kips

Elements 8 and 9 at Node 9 yield at P = 210. At P = 260, node 8, elements 7 and 8, yields. At this point the plastic rotation at node 9 remains constant and further increases in loading are carried by increases in rotation at node 8. The yielding at nodes 8 and 9 is viewed as an extension of the second hinge rather than a formation of a third hinge. In so doing an approximation is made to sum all the rotation for nodes 8 and 9 into a lumped approximation. From the DRAIN2DX pushover analysis the plastic hinge rotation θ_p = 0.03784. The distance to L from the hinge to point of contraflexure is decreased to 62.

$$\phi_p = \theta_p / L_p = 0.03784 / 18 = 0.00210$$

$$\mu_\phi = 1 + \phi_p / \phi_y = 1 + (0.00210 / 00025) = 9.4$$

$$\mu_\Delta = 1 + 3\,(9.4 - 1)(18/62)(1 - 0.5(18/62)) = 7.25$$

If a criteria were set that the maximum element displacement ductility could not exceed a value of μ_Δ = 5.0, a value of P around 240 kips causes a μ_Δ = 5.6 at node 1 element 1 based on an L = 29, θ_p = 0.01964, and μ_ϕ = 5.36. So the limiting value would be slightly less than P = 240 with a pile tip deflection of about 2 inches.

The pile was reanalyzed using a bilinear stiffness consisting of the average soil stiffness and a degraded stiffness of .01 times the initial stiffness. This represents a much more realistic soil condition. Figures 59 shows pile moment and Figures 60 and 61 give pile deflection. In this case the pile first yields and develops a hinge at the top at a horizontal load of 110 kips; a second hinge forms at node 9 element 9, at a horizontal load of 170 kips followed immediately by large deformation. Comparing Figure 53 with Figure 59, we can see that the softer soil causes the pile moment diagram to a different shape stressing the pile at greater depth. The contraflexure points are lower. Comparing Figure 55 with Figure 61, we note that the softer soil results in lower load capacity and a flat yield plateau with a well defined failure load point. This illustrates the significant difference in response between an bilinear non-yielding soil response with a yielding soil response. Accurate computation of pile capacity requires capturing the soil load-deflection properties accurately as a function of depth. The Navy has previous developed the computer program SAPIER for the analysis of piers. This program was developed from the elastic finite element analysis program, SAP. It utilizes linear elastic spring stiffness representations of the soil supporting the piles, and as such would be suspect as giving erroneously high pile lateral force capacities.

The pile with yielding soil properties was analyzed dynamically. The fundamental mode shape is shown in Figure 62. A dynamic time step analysis was performed in which the El Centro earthquake record scaled to 0.45g , Figure 63, was applied to the pile model in a horizontal direction. Under the dynamic loading the soil was permitted to cycle in a nonlinear mode with gapping. Figure 64 shows the pile top displacement and Figure 65 shows the pile deflection envelope. Under a peak horizontal acceleration of 0.45 g, the pile reaches ultimate moment intermittently in element 1, nodes 1 and 2, and element 2 node 2. The loading is increased an summarized as:

Absolute Cumulative Maximum Plastic Hinge Rotation

	Element 1, Node 1	Element 2, Node 2	Element 2, Node 2	Element 2 Node 3
0.45g	.000469	.000154	.000047	0
0.68g	.00199	.00109	.000507	0
0.90g	.00463	.00299	.00187	0
1.35g	.0136	.0100	.00755	0.00204

The ultimate capacity of the pile is predicted from the static analysis at an acceleration of;

$$a = \text{Horizontal Failure Load/ Mass} = 170/117 = 1.45g$$

This is a good approximation of the ultimate strength in this case although the amount of yielding is more extensive.

It should be noted that use of DRAIN2DX requires careful preparation of the input data. The program considers yielding to be an event and has a provision to include events within a time step. This is important to convergence of the stiffness. Additionally selection of variable time step to allows the program to reduce the time step to produce convergence and hold error tolerance when yielding occurs. The program has a bilinear connectivity element used to model the soil. If a trilinear representation is desired 2 elements can be used in parallel. The stiffness of the first element is set at the desired reduced stiffness level. The stiffness of the second element is set at the difference between the desired initial stiffness minus the reduced stiffness. When both elements are used their stiffness add together and the desired result is achieved.

Pile - Pile Cap Connections

Joen and Park (1990b) tested 3 types of pile - pile cap connection, all of which performed in an acceptable manner. The first type consists of roughening the upper surface of the pile using a jack hammer to producing 1/8 inch deformations, embedding the pile in the form work for the pile cap and casting the pile cap concrete around the pile, Figure 66. Spiral reinforcement is placed around the exterior of pile. The pile cap reinforcement is designed to withstand the pile moments with a factor of safety. The depth of embedment should exceed the transfer length for development of full prestress. This is

an easy connection to construct and ranked first. Figure 67 shows a second connection procedure in which the concrete at the end of the pile is removed by jack hammering and the exposed steel is used for anchorage in the pile cap. A nut can be inserted in the prestressing tendon for additional anchorage as shown in the detail. This concept is ranked second. Figure 68 illustrates a procedure of using dowel bars inserted in holes drilled and epoxied into the pile. A spiral reinforcement is placed around the longitudinal reinforcing and ends of the rebar in the pile cap have 90 degree bends for anchorage. When this concept was tested, post elastic deformations concentrated to form a wide crack at the pile-pile cap interface restricting plastic hinging. This option was ranked third. All of the concepts provided a ductility of at least 8. Spalling of the concrete cover was observed to commence at a displacement ductility of about 2. It was shown above that the ends of prestressed piles have transition regions where full prestress can not be developed. The code requirements for transition length development are 50 tendon diameters and for development length are 140 diameters. For the first concept, Figure 66, the transition length was contained within the pile cap at which the full prestress force could be developed. It was then assumed that the prestress force increased from the full prestress force to the ultimate stress of the prestressing steel over the next 90 bar diameters (50 + 90 = 140 diameters). These limiting values of tendon stress result in pile moment reductions over these sections. For the second concept, Figure 67, the tendons were not prestressed in the pile cap. Based on the length of tendon in the pile cap a prestress force was determined at the pile-pile cap interface based on the ratio embedment length of the tendon in the cap divided by the 140 tendon diameter times the ultimate strength of the prestress force. The third concept utilized the full reduced tendon stress of the pile but allowed for embedment of the conventional reinforcing dowels Allowance for these reductions in capacity was shown to be the most accurate representation of pile moment curvature and a conservative approach indicating that spiral containment in the cap facilitated development length.

Pier Analysis

A typical pier was selected for study. The pier was 80 feet across and a typical bent is illustrated in Figure 69; such a pier is used for berthing destroyers and cruisers. The 9 piles are 24-inch octagonal prestressed piles discussed in the previous section. The pier was modeled by a 2-dimensional analysis. A static lateral force push over analysis was applied in conjunction with the standard vertical dead and live loads. It was found that the pier resisted 261 kips applied horizontally before collapse began. This is equal to an equivalent static lateral force (acceleration) coefficient of 0.25 g. Yielding of the piles at the deck level with the formation of the first hinge; a second hinge developed at the mud line depth which produced a collapse mechanism. The structure underwent large gradual deformation near failure. The structure was analyzed using the El Centro earthquake record as a dynamic lateral load function. The structure was able to undergo large deflection without the occurrence of a computational instability indicating collapse. As a practical limit, a 10-inch displacement was set as an effective limit. This occurred at a lateral load of about 0.75g.

The pier was modified by the inclusion of 2 24-inch octagonal prestressed concrete batter piles as shown in Figure 70. The extent of restraint provided by the batter piles is a function of soil restraining the piles. Modeling of batter piles involves not only the horizontal py soil resistance but also the tz vertical soil resistance and the amount of q-w end-bearing. These will be discussed in the next section. For this case, the batter piles had a significant stiffening effect on the structure. A static lateral force push over analysis was performed and a lateral force of 648 kips was found to cause collapse which is equivalent to a static lateral force coefficient of 0.63g. As loading increased the batter pile in tension reached its failure capacity first. When this pile failed load was transferred to the remaining batter pile which failed causing failure of all the remaining piles. The structure performed in a brittle manner such that collapse occurred immediately after the first pile failed. This structure was also analyzed using the El Centro earthquake record as a dynamic lateral load function. Collapse occurred at a peak horizontal acceleration of about 0.9g. The structure had substantially reduced lateral displacements compared to the pier without batter piles. Again the onset of batter pile failure resulted in the rapid collapse of the structure and was initiated by exceeding pile tensile limits.

Batter Piles

Previous sections focused on the lateral resistance of vertical; to fully understand the behavior of a batter pile it is necessary to review the axial pile soil skin friction (tz component) and the pile end bearing (qw component). For a vertical pile the axial and end bearing components are also vertical. Figure 71 shows the force components acting on a vertical pile. The spring elements are intended as visual aids to represent the forces acting along the entire length of the pile. ultimate capacity of a vertical pile is given by:

$$Q = f A_s + qA_p$$

where

f	Unit skin friction, tz
A_s	Area side surface of pile
q	Unit end bearing capacity, qw
A_p	Area of end of pile

For cohesive soils the skin friction is

$$f = a\,c$$

where

$$a = 0.5\,\psi^{-0.5} \quad \psi \leq 1.0$$

$$a = 0.5\ \psi^{-0.25} \quad \psi > 1.0$$

and

c	Undrained shear strength
ψ	c/p_o'
p_o'	Effective overburden at point in question

For cohesive soils the end bearing unit stress of piles is:

$$q = 9\ c$$

For cohesionless soils the unit skin friction is:

$$f = K\ p_o'\ \tan\ \delta$$

where

K	dimensionless coefficient of lateral earth pressure, usually = 1
δ	friction angle between the soil and pile

For cohesionless soils the unit end bearing stress is:

$$q = p_o'\ N_q$$

API (1994) gives procedures for computing tz axial force-deflection curves and qw end bearing-deflection curves which define the soil resistance pictured in Figure 71. For comparison consider the following for cohesionless soils:

Lateral	Vertical
$pu/D = (c1\ X + C2\ D)\ \gamma'\ X/D$	$f = K\ p_o' \tan \delta\ D$

for a depth of 10 feet, 18-inch pile diameter

$pu/D \cong (14)\ \gamma'\ X$	$f \cong (.7)\ \gamma'\ X$

For cohesive soils

Lateral	Vertical
$pu \cong 10\ c$	$q \cong 1\ c$

From the above it may be seen that the py lateral resistance is much greater than the tz axial skin friction. For this reason it is logical that most of the lateral resistance of a pile is mobilized in the near surface region of a pile to a depth of 5 to 10 pile diameters. To resist vertical loads without end bearing requires long pile development lengths. End

bearing is a significant component in pile capacity. The magnitude of the end bearing resistance is on the same order as the lateral resistance. The capacity of a pile in tension is much less than in compression and less than in lateral resistance. Having reviewed the fundamentals of vertical pile behavior, it is now possible to discuss batter piles.

Figure 72 illustrates a batter pile based rotation of a vertical pile. For simplicity the forces are kept normal and axial to the pile. Consider as the tz axial resistance of the soil goes to zero the pile would tend to slip out of the ground with minimal axial loading in tension. The modeling of a pile by finite element representation must accurately capture this interaction. In a finite element model it is possible to use spring/truss elements to model the soil resistance. Use of horizontal and vertical springs to model the components of py and tz resistance would introduce a major problem of how to combine these elements. The axial tz acts independent of the normal py and must allow pile slippage. End bearing is an axial component. After a number of trial iterations of various models, the only model recommended for use is one with spring elements axial and normal to the batter pile. Additionally the end bearing must be an axial spring. All py, tz and qw load deflection curves are based on the depth of the element below the ground surface.

A analysis was performed on batter pile with a 1 horizontal to 2 vertical slope driven to a depth of 50 feet and loaded laterally at a height of 3 feet above the ground. The pile was a 24-inch circular pipe pile in medium sand. The soil py and tz curves were calculated at intervals of 1 foot using the equations in API (1994). Normal and axial soil springs were spaced at 1-foot intervals for the first 20 feet and then at 2-foot intervals. The soil springs utilized bilinear material properties. A vertical load of 20 kips was used. The lateral capacity of the batter pile when pulled horizontally in a direction away from the batter was 12 kips compared to 36 kips when pulled horizontally in the direction of the batter. The lateral capacity of an equivalent vertical pile was 20 kips.

From a series of studies of a batter pile it is concluded that the lateral load capacity of the batter pile is dependent upon the vertical load of the pile. When the lateral load acts horizontally opposite to the direction of the batter, a component of this load acts on the pile axially in tension. The vertical load offsets this effect and can increase pile capacity up to a limit. This is generally the direction of lower pile capacity. When the lateral load acts horizontally toward the direction of the batter the vertical load resists the moment caused by the lateral load and reduces deflection.

The vertical distribution of pile soil reaction is a function of pile length. The longer the pile the greater the friction along the pile and the less in end bearing. Since stiffness increases with depth more force is transferred into the soil at deeper depths (assuming pile compression is not significant).

Seismic Isolation of Piers

The concept of isolation of the pier deck was examined by modification of the structural model used in the previous section and shown in Figure 69. The piles were tied together by a horizontal beam. The deck was located above the beam and attached to the beam by a lateral spring of controlled stiffness and a stiff vertical spring. About 85 percent of the mass was assigned to the deck portion with the remaining assigned to the substructure. A series of dynamic analyses showed that the deck could be isolated from the majority of the lateral force. The substructure underwent limited deformation remaining near elastic with only slight plastic behavior. At a lateral acceleration of 0.45g the substructure had a peak displacement of about 6 inches, the deck of about 8 inches, Figure 73. Relative displacements of up to 4 inches occurred, Figure 74. Accelerations in the deck were lower than those of the substructure, Figure 75. The analysis was repeated at twice the loading, 0.9g; Figures 76, 77 and 78 give the results. A combination of substructure strength and isolation spring stiffness can control the amount of displacement. The pier with batter piles shown in Figure 70 was isolated in a similar manner. Results are shown in Figures 79 to 81 for a peak acceleration of 0.45g and in Figures 82 to 84 for a peak acceleration of 0.9g. The fundamental period of response of this stiffer structure is higher that the pier without batter piles. While the substructure displacements are less than the pier without batter piles, the deck displacements are greater causing a higher relative displacement. Deck and substructure accelerations are higher.

The conclusion of this brief study is that it is feasible to isolate a pier with today's technology. One problem area is resisting the lateral fender berthing impact forces. This may be accomplished by separating the fender system from the deck. Figure 85 presents a concept for developing an isolated pier system.

P - Delta Effect

One element of structural analysis should be noted- that of the P - delta effect. This is usually thought of as a secondary effect of the additional moment which is imposed on a column by the axial load acting on a moment arm caused by the deflection of the top of the column. For piers and bridge structures this can be significant. Duan and Cooper, 1995 discuss this extensively and conclude that the effect should be included in seismic analysis. To illustrate the Figure 86 shows the static load deflection diagram for the pier in Figure 69 subject to a static lateral load pattern applied in steps as a push over analysis. The DRAIN2DX program has the provision for the P-delta effect. Note the difference in peak capacities. When the P-delta effect is included the structure sustains an instability under force loading and the solution terminates.

Use of Elastic Response Spectra Techniques

The above section have illustrated the need for nonlinear representation of the soil-pile interface and the p-Δ effects. Use of linear response spectra and force reduction factors in building codes has been common practice. Such techniques should be avoided where possible in pier design to insure the accuracy of the solution. The pier in Figure 69 was analyzed for the El Centro earthquake. It was found that a time history analysis with the earthquake record scaled to 0.38g peak horizontal acceleration produced a $\mu = 1$ condition with threshold yielding at the pile cap. By a nonlinear time history analysis, a $\mu = 3$ condition was found to occur at a peak horizontal acceleration of 0.79g. A linear elastic response spectra analysis was performed using the 5 percent damped El Centro response spectra scaled to 0.38g. The computed displacements were about 3 percent lower that those found from the nonlinear time history analysis. Good agreement would be expected because the structure is responding elastically and the soil springs are at low enough level to be behaving essentially without yield. The spectra was multiplied by the desired ductility level of 3.0 and the structure analyzed for this increased spectra. The computed displacements were about 5 percent lower that those of the nonlinear response spectra. In this case agreement is satisfactory; however the general case can produce results where agreement could be much worse especially where soft soils would undergo more nonlinear behavior. For this reason it is suggested that the nonlinear techniques are preferable and that the linear techniques should be used only with caution. The case analyzed had a fundamental period of the pier of 1.39 seconds which is near the constant velocity portion of the spectra. Results might not have been so favorable had the pier had a shorter period.

Development Of Waterfront Seismic Criteria

The following section contains the proposed criteria in italics. Additional explanation is inserted where needed.

Performance Goal

The goal of this criteria is to standardize the seismic design of Navy piers and wharves providing an acceptable uniform level of seismic safety for all waterfront locations. This criteria is intended to produce a level of design in Navy piers and wharves such that there is a high probability the structures will perform at satisfactory levels throughout their design life. Waterfront structures have been classified as essential structures. Although the criteria focuses on the regions where seismicity is highest such as on the West Coast, it is applicable to other zones as well. *Specifically for structures located in areas of high seismicity, such as Uniform Building Code designated Seismic Zones 3 and 4, structures shall be designed:*

- *To resist earthquakes of moderate size, Level 1, which can be expected to occur one or more times during the life of the structure without structural damage of significance.* This represents a condition of expected repeated loading.

- *To resist major earthquakes, Level 2, which are considered as infrequent rare events maintaining life safety, precluding total collapse but allowing a measure of controlled inelastic behavior which will require repair.* This represents a condition of expected loading to occur at least once during the design life of the structure. In reality most Navy structures end up being used well beyond their design life.

- *To preclude release of hazardous and polluting materials such as with fuel piers.* The intention is to prevent spills on fuel piers. This may be accomplished by installation of cutoff valves, and containment to limit the size of the spill and prevent its spread. It may also be accomplished by increased strengthening of components.

- *To utilize life-cycle cost analysis where necessary. Since piers and wharves are not like high occupancy building structures which can collapse on occupants, loss of life is a less significant design issue. At times the seismic hazard is dominated by a large active fault in close proximity to a proposed wharf location. In such cases the designer shall consider structure life cycle economics in selection of design loading and structural performance criteria. Life cycle cost analysis shall consider initial costs of seismic strengthening and expected facility damage and loss over the expected operational life.* This section is intended to allow the designer freedom to consider economic analysis of alternative load conditions in the infrequent case where a local fault dominates a site and is capable of very high ground motions. Such a condition requires specialized extensive evaluation of the site hazard.

- *To consider liquefaction as a major waterfront problem. The designer shall consider liquefaction factors of safety in design of remedial measures of backfill. Rigid adherence to developing fixed factors of safety may not be economically achievable.* The intent is place more credence in the expected deformations and consequences of liquefaction which will occur rather than the simple factor of safety. *Assurance of limited deformations shall be given precedence over a factor of safety. The designer shall have the option of using current technology to demonstrate that settlements and lateral deformations are sufficiently limited to insure structural performance and factors of safety lower than limit values may be used.* By current technology, we mean the use of procedures for the computation of vertical and lateral deformations.

In general all waterfront construction falls within the category of essential construction. The Navy policy is to minimize downtime for these facilities. Determination of essential construction shall be determined by the user in conjunction with the Naval Facilities Engineering Command Headquarters. Piers and wharves shall be considered essential construction. Emphasis shall be placed on minimizing downtime and interruption to mission essential functions.

Design Earthquakes

The pier or wharf structure shall be designed to resist the loading produced by:

- *A Level 1 earthquake with a 50 percent probability of exceedance in 50 years exposure.* This is a nominal 475- year return time event ground motion.

- *A Level 2 earthquake with a 10 percent probability of exceedance in 50 years exposure.* This is a nominal 950-year return time event.

- *Additionally piers and wharves which are part of fueling systems shall be evaluated for an earthquake with a 10 percent probability of exceedance in 100 years exposure.*

The determination of the design earthquake shall be performed using techniques described in NFESC TR-2016-SHR or other equivalent procedures.

Structure Response At Design Loading Levels

The response of the structure under the design earthquake levels shall be:

- *For a Level 1 earthquake, essentially elastic response is required throughout the structure.*

- *For a Level 2 earthquake, limited controlled inelastic behavior with maximum ductility factors of*

Pier Prestressed Concrete Piles

1.5	*Pile moments in ground*
3.0	*Piles at pile cap*
1.5	*Batter piles at pile cap*

Wharf Prestressed Concrete Piles

2.0	*Pile moments in ground*
5.0	*Piles at pile cap*
2.5	*Batter piles at pile cap*

Steel Piles for both Wharf and Pier

5.0	*Vertical piles only*
3.0	*Vertical and batter piles*

Composite Steel and Concrete Piles for both Wharf and Pier

5.0	*Vertical piles only*
3.0	*Vertical and batter piles*

As noted from preceding sections the development of the ductility limits was not arbitrary; but rather is based on the recent developments in structural research and current practice. We have considered the effects of batter piles and the high damage observed during recent earthquakes. We also consider for prestressed concrete piles the difficulty of inspecting piles in soil and the potential for corrosion and loss of strength from cracking. For this reason we limit the below ground ductilities. Recall from the sections above that section curvature and displacement ductility are related by 1/L. Thus tall piles in piers have different ductility limits compared with shorter piles in wharves.

Displacement ductility is related to curvature and noted to be inversely dependent on pile length. Piers have longer piles than wharves and the above ductility limits are intended to reflect that factor. It is intended that Level 2 curvatures be safely less than ultimate curvature. The pier or wharf shall be designed as a ductile moment resisting frame supported by vertical piles reinforced and so connected to the structure as to form an integral part of the ductile moment resisting frame. Use of batter piles as lateral force resistant elements in wharves is prohibited unless special design provisions are made to reliably demonstrate that the batter piles have sufficient strength and ductility at the pile cap to perform under design loading conditions. Previous experience has shown batter piles are very stiff and are easily damaged. The intent is to discourage their use for most wharves which can achieve lateral stiffness through vertical piles and other restraints. For the few exceptions which might exist, proof of functionality is required. *If batter piles are used, allowable ductilities at the pile cap shown above shall be reduced for the Level 2 earthquake.*

For a wharf, design of the under-wharf dike retaining structures as a minimum shall have permanent horizontal deformation of the slope computed by a Newmark analysis and such deformation shall not exceed:

- *For a Level 1 earthquake, 4 inches*
- *For a Level 2 earthquake, 12 inches*

Design of sheet pile bulkheads, dikes and retaining structures shall include provisions to resist full liquefaction of the backfill and for expected potential lateral spread deformation. Retaining structures shall be designed using provisions in NCEL Technical Report R-939. Liquefaction and lateral spread shall be computed based on guidance in NCEL Technical Note 1862.

All crane rails shall be supported on piles including the seaward and the landward rail. Refer to Kobe earthquake damage where settlements caused spreading of the crane rails and collapse or buckling of cranes. *The crane rails shall be connected horizontally by a continuous deck, beam or other means to control the gage of the rails and prevent spreading. The rails shall be grounded. For corrosion protection, it is advantageous to insulate the reinforcing steel in the piles from that in the deck.*

The presence of any potentially liquefiable materials in backfill areas shall be fully analyzed and expected settlements computed. Specific attention shall be paid to the acceptability of the amount of settlements. Under Level 1 earthquakes large deformations resulting in widespread pavement disruption should be avoided where economically feasible. This is a condition expected to occur a number of times during the life of the structure. Extensive repairs after each earthquake are not desired.

- *For a Level 1 earthquake the Factor of Safety against liquefaction in the backfill should be 1.5 or higher with settlements of about 1 inch or less and lateral deformations of about 3 inches or less.*

- *For a Level 2 earthquake the Factor of Safety against liquefaction in the backfill should be 1.0 or higher with settlements of about 4 inches or less and lateral deformations of about 6 to 12 inches or less. Where it may not be possible to achieve a Factor of Safety greater than 1.0, a Factor of Safety greater than 0.9 may be considered as long as the computed deformation state is shown to have limited controlled settlements and lateral spread equivalent to the values stated.* The emphasis is on performance rather than factor of safety only.

Piers and wharves containing fueling systems shall be evaluated for an earthquake with a 10 percent probability of exceedance in 100 years exposure to insure that a spill of hazardous material is precluded. This may be accomplished by providing containment systems should there be breaks in fuel containment system element or by strengthening these elements. Additional guidance is contained in the lifeline criteria.

- *Preclude release of hazardous and polluting materials for an earthquake with a 10 percent probability of exceedance in 100 years exposure.*

Existing Construction

Seismic reviews of existing waterfront construction directed by requirements of the Naval Facilities Engineering Command shall utilize the above criteria for new construction as the target requirement for upgrade. The requirement for evaluation of the seismic resistance and possible upgrade is triggered when the loading on the structure changes such as when the mission of the structure is changed or when the structure requires major repairs or modifications to meet operational needs. When it is

shown to be impossible or uneconomical to achieve new construction levels of performance, an economic life cycle cost analysis shall be performed to determine the most cost effective level of seismic design upgrade. Various alternative upgrade levels shall be considered ranging from the existing condition to the maximum achievable. Each alternative shall be examined to determine the cost of the upgrade, the cost of expected earthquake damage over the life of the structure and the impact of the damage on life safety, operational requirements, and damage to the environment. The choice of upgrade level shall be made by the design team based on a cost effective strategy consistent with requirements of life safety, operational needs and protection of the environment.

Use of AASHTO 1996 Code Provisions with This Criteria

The DM 1025/1 calls for use of the AASHTO Code for guidance. That requirement is maintained subject to changes contained in this criteria. The AASHTO Code specifies that the structure shall be elastic under small to moderate earthquakes and that "exposure to shaking from large earthquakes should not cause collapse of all or part of the bridge. Where possible damage that does occur should be readily detectable and accessible for inspection and repair." This criteria follows the same guidance but is more definitive in establishing specific earthquake levels and more definitive response criteria. This criteria is designed to insure piers are repairable under the Level 2 earthquake. Further piers are to be classified as AASHTO Category I structures as essential. Division 1A of the AASHTO Code Section 3.2 presents acceleration maps. For pier projects site specific seismicity studies are to be performed in lieu of the maps. Because waterfront soils generally fall in the worst category of site response, as part of the site study, local site response shall be analyzed using as a minimum 1-dimensional wave propagation techniques to determine local site amplification. Soil response described in AASHTO Section 3.6 shall be based on the local site response analysis in lieu of the specified equations.

AASHTO Section 3.9 prescribes for the combination of orthogonal seismic force components. Section 4 describes analysis requirements and Sections 4.5 and 4.6 describe the multimode response spectra and time history analysis procedures. Since piers depend heavily upon the nonlinear soil structure interaction of piles and soil, nonlinear time history procedures are strongly recommended for the analysis of a pier. Only AASHTO procedures 3 and 4 are to be used for pier analysis. Since the response of the pier under Level 2 earthquakes is expected to be nonlinear use of Section 3.9 provisions for combination of orthogonal components are only approximate. To account for the orthogonal effects of seismic load components, a full 3-dimensional pier model is recommended to directly allow for inclusion of all the earthquake components. Actual earthquake records of orthogonal components can be used to represent the seismic loading. Typically one of the components is at a reduced acceleration level compared to the primary component. Vertical acceleration may be included as a loading component

but is not required. Use of vertical component acceleration may not be used to reduce the lateral response.

Provisions of AASHTO Chapters 5,6 and 7 shall be applicable to piers including combination of load components with changes in earthquake loading required to meet this criteria.

Life Cycle Cost Analysis

Life cycle cost analysis shall be performed using the provisions in NAVFAC P355.2 Chapter 7 and the guidance in NCEL Technical Notes N 1640 and N 1671.

Discussion Of Criteria

The criteria presented above is developed from a compilation of current practice by many agencies combined with state-of-the-art technology for estimation of seismic damage potential. It is not a revolutionary step forward but rather an evolution of design. Currently the Navy has used technology contained in NAVFAC P355.2 manual for the design of wharves and piers. This manual was intended for design of essential buildings and utilizes elastic response spectra techniques. The information presented above shows the design of a pier is a major soil-structure interaction problem and the need for realistic nonlinear representation of soil forces. The NAVFAC P355.2 focuses only on the specification of earthquakes having a 50 percent and 95 percent probability of nonoccurrence in 50 years. Prior to this specification we did not have a definition of required pier/wharf performance, nor of the structural response parameters such as ductility to achieve the required level of performance under the assigned load. This specification has developed a cohesive integrated criteria specifying:

1. The required pier performance under expected loads
2. Specification of the expected loads
3. Specification of ductility limits to ensure structural response limits to achieve performance requirements.

The criteria reduces the Level 2 earthquake from the 950-year earthquake specified in NAVFAC P355.2 to the 475-year earthquake ground motion. This is important because we have reduced the ground motion substantially. In the San Diego area, for example, the ground is reduced from 0.6g to 0.4g. But of much more significance we can predict the 475- return time ground motion with greater reliability than the 950-year event. This translates into a significant reduction in the 95 percent confidence bounds on the estimated motion. We have shifted the criteria points into regions where we can predict loads with greater reliability and also predict structural response with greater reliability. This translates into a significantly more predictable system. This was suggested by the reliability analysis performed on a typical Navy wharf

as an early part of this effort, Putcha and Ferritto (1995). That work was significant in defining the major areas of uncertainty and shaped the direction for the criteria.

The overall effect on the design, selection of pile sizes and cost of the pier is not expected to be great; however, the assurance in meeting performance goals is thought to be substantially enhanced. By lowering the loading we have made it easier to compute with higher reliability. By defining the response to modest levels of ductility, we have reduced the need to compute collapse levels of large nonlinear inelastic deformation which can not be accomplished with high certainty.

In the application of this criteria to existing construction, it is thought that the objective of a uniform set of performance goals should be maintained across the waterfront. We should examine the structure under the requirements of the criteria. Where we lack adequate capacity in the existing system, it is thought better to strive for the performance goal, develop several candidate upgrade alternatives, and then perform an economic analysis to determine what is the most cost effective solution considering the potential for a damaging earthquake and the existing lateral force system. This approach is preferred over any system which arbitrarily establishes some percentage reduction of a new-construction criteria. Any single reduction coefficient is probably not optimal over a range of structures and is at best arbitrary.

References

API (1994) Recommended Practice 2A-LRFD (RP2A-LRFD) "Recommended Practice for Planning, Design and Constructing Fixed Offshore Platforms - Load and resistance Factor Design" July 1993 Approved April 1994

Banerjee S., J. F. Stanton and N. M. Hawkins (1987) "Seismic Performance of Precast Prestressed Concrete Piles", Journal of Structural Engineering, American Society of Civil Engineers Vol. 113, No 2, Feb. 1987

Bogard, D. and H. Matlock, (1980) "Simplified calculation of P-y Curves for Laterally Loaded Piles in Sand" Unpublished report Ertec, April 1980

Duan Lian and Thomas Cooper (1995) "Displacement Ductility Capacity of Reinforced Concrete Columns" Concrete International Nov. 1995

Erickson B and G Fortinos (1995) "Code Recommendations for Waterfront Structures" ASCE Ports 95 Proceedings, Tampa FL

Ferritto, J, NCEL Technical Note N1640, "An Economic Analysis of Earthquake Design Levels", July 1982

Ferritto, J. NCEL Technical Note N 1671, "An Economic Analysis of Earthquake Design Levels For New Construction", July 1983

Ferritto, J, NFESC Technical Report -2016-SHR "Procedures For Computing Site Seismicity, Feb. 1994

Ferritto, J. and C. S. Putcha (1995) NFESC TM "Seismic Reliability Study Of Navy Wharves And Development Of Design Criteria", Port Hueneme CA Feb. 1994

Forrest, J (1996) Personal communication

Gazetas, G and P. Dakoulas, (1991) " Seismic Design Chart For Anchored Bulkheads", Proceedings from the Third Japan-US Workshop on Earthquake Resistant Design Of Lifeline Facilities and Countermeasures For Soil Liquefaction, State University Buffalo, New York Feb. 1991

Harn R and B. Malick (1995) "Proposed Seismic Design Method for Piers and Wharves", ASCE Ports 92 Proceedings, Seattle Wa

Hayashi, S (1974) " A New Method of Evaluating Seismic Stability of Steel Pile Structures", Proceedings of the Fifth World Conference on Earthquake Engineering, Rome

Joen, Pam Hoat and Robert Park (1990a) "Flexural Strength and Ductility Analysis of Spiral Reinforced Prestressed Concrete Piles" PCI Journal, Vol. 35 No 4, July/August 1990

Joen, Pam Hoat and Robert Park (1990b) "Simulated Seismic Load Test on Prestressed Concrete Piles and Pile-Pile Cap Connections" PCI Journal, Vol. 35 No 6, November/December 1990

Kubo, K. (1969) "Vibration Test of a Structure Supported by Pole Foundation" Proceedings of the Fourth World Conference on Earthquake Engineering, Chile

Liftech (1995) "Earthquake Damage Kobe Container Terminals", Liftech Consultants, Oakland CA

Mander J. B., M. J. N. Priestley and R. Park (1988) "Theoretical Stress-strain Model for Confined Concrete" Journal of Structural Engineering, American Society of civil Engineers, Vol. 114, No 8 August 1988 pp. 1805-1826

Novak M (1991) "Piles Under Dynamic Loading", Proceedings Second International Conference on Geotechnical Earthquake Engineering and Soil Dynamics, St. Louis, March 1991

Martin G. R. and I. Po Lam (1995) "State of the Art Paper Seismic Design of Pile Foundations: Structural and Geotechnical Issues" Proceedings Third International Conference on Recent Advances in Geotechnical Earthquake Engineering and Soil Dynamics" April 1995 St. Louis, Missouri

Matso, K. (1995) "Lessons From Kobe", ASCE Civil Engineering April 1995

Meyerson W, T. O'Rourke, and F. Miura (1992) Lateral Spread Effects On reinforced Concrete Pile Foundations", US Japan Workshop On Earthquake Disaster Prevention For Lifeline Systems, Public Works Research Institute, Tsukuba Science City, Japan

O'Niell, M. W. and J. M. Murtcheson (1983) " An Evaluation Of P-y Relationships in Sands", PRAC 82-41-1, University of Houston, Research Report GT DF02-83

Parker, f and L. C. Reese (1970) "Experimental and Analytical Study of the Behavior of Single Piles in Sand Under Lateral and Axial Loading", Research report No. 117-2, Center for Highway Research, The University of Texas, Austin, Texas, Nov, 1970

Priestley, M. J. N., F. Seible, and Y. H. Chai (1992) Design Guidelines For Assessment Retrofit And Repair Of Bridges For Seismic Performance, University of California, San Diego August 1992

Reese, L.C. W. R. Cox and F.D. Koop (1974) " Analysis of laterally Loaded Piles in Sand", Sixth Annual Offshore Technology Conference, Vol. 2 Paper No 2080, Houston, Texas, May 1974.

Sheppard, David (1983) "Seismic Design Of Prestressed Concrete Piling" PCI Journal Vol. 28 No. 2 March/April 1983

Seed R. B. S. E. Dickenson et al. (1990) EERC-90/05 "Preliminary Report On The Principal Geotechnical Aspects Of The October 17, 1989 Loma Prieta Earthquake", University of California, Berkeley CA, April 1990

Standard Specifications for Highway Bridges, American Association of State Highway Officials, Washington DC 16 edition 1996,

Swanson B. (1996) "Observations From Kobe Earthquake and Lessons Learned For Reducing The Seismic Vulnerability Of US Ports" PIANC Bulletin No. 92 Sept. 1966

Tudor/PMP (1976) Seismic Design of Piers, Consulting Report to NAVFAC, August 1976

Wallace John and Jack Moehle, UCB/SEMM-89/12 " BIAX: A computer Program for the Analysis of Reinforced Concrete Sections" University of California, Berkeley CA July 1989

Warren, G. (1989) NCEL Technical Report R-927 Laterally Loaded Partial Prestressed Concrete Piles, Port Hueneme, CA Sept. 1989

Werner, S. D. and S. J. Hung (1982) "Seismic Response Of Port And Harbor Facilities", Agbabian Associates, El Segundo CA Oct. 1982

Wolf, J. P. and B. Weber (1986) " Approximate dynamic stiffness of Embedded Foundation Based On Independent Thin layers With Separation Of Soil" Proceedings 8th European Conference on Earthquake Engineering, Lisbon 1986

Yoshida, N and M. Hamada (1991), Damage to Foundation Piles and Deformation Pattern of Ground Due to Liquefaction-Induced Permanent Ground Deformation", Proceedings 3rd Japan-US Workshop on Earthquake Resistant Design Of Lifeline Facilities and Countermeasures for Soil Liquefaction, National Center for Earthquake Engineering Research, State University of New York, Buffalo, Feb. 1991

TABLE 1. SUMMARY OF EARTHQUAKE-INDUCED DAMAGE TO PORT AND HARBOR FACILITIES

Earthquake			Port	Damage	
Location	Date	Magnitude	Location	Description	Possible Cause(s)
Kanto, Japan	Sep 1 1923	8.2	Yokohama and Yokosuka	Concrete block quay wall: sliding, tilting, and /or collapse with some bearing capacity failure of rubble-stone foundation Steel bridge pier: buckling of pile supports	A C, E
Kitaizu, Japan	Nov 26 1930	7.0	Shimizu	Caisson quay wall (183 m long): tilting, outward sliding (8.3m), and settlement (1.6m) L-Shaped block quay wall (750 m long): outward sliding (4.5 m) and settlement (1.2 m)	A, B, C
Shizuoka, Japan	Jul 11 1935	6.3	Shimizu	Caisson quay wall: outward sliding (5.5 m) and settlement (0.9 m) accompanied by anchor system failure	A, B, C
Tonankai, Japan	Dec 7 1944	8.3	Yokkaichi Nagoya Osaka	Pile supported concrete girder and deck: outward sliding (3.7 m) accompanied by extensive soil sliding Sheet Pile bulkhead with platform: outward bulging (4 m) Steel sheet-pile bulkhead: outward bulging (3 m)	A, B, C,
Nankai, Japan	Dec 21 1946	8.1	Nagoya Yokkaichi Osaka Uno	Sheet-pile bulkhead with platform: outward bulging (4 m) Pile-supported concrete girder and deck: outward sliding (3.7 m) Steel sheet-pile bulkhead: outward bulging (3m) and settlement (0.6 m) Gravity-type concrete block and caisson quay wall: seaward sliding (0.4 m) accompanied by soil sliding	A, B, C,
Tokachi-Oki, Japan	Mar 4 1952	8.1	Kushiro	Concrete caisson quay wall: tilting, outward sliding (6 m), and settlement (1 m)	A, B, C

Earthquake				Damage	
			Port		Possible
Location	Date	Magnitude	Location	Description	Cause(s)
Chile	May 22 1960	8.4	Puerto Montt	Concrete caisson quay walls: overturning and extensive tilting Steel sheet-pile seawall: outward sliding (up to 1 m) and anchor failure Gravity-type concrete seawall: complete overturning and sliding (1.5 m)	A, B, C
			Talcuhuanno	Concrete block quay wall: outward tilting	A, B
Alaska	Mar 27, 1964	8.4	Anchorage	Dock structures: extensive seaward tilting with bowing, buckling, and yielding of pile supports	B, D, E
			Valdez	Entire harbor: destroyed by massive submarine landslide	
			Whittier	Pile-supported piers and docks: buckling, bending, and twisting of steel pile supports	
				Steel sheet-pile bulkhead: extensive bulging	B, D,
			Seward	Major portion of harbor: destroyed by massive submarine landslide	
Niigata, Japan	Jun 16, 1964	7.5	Niigata	Extensive damage due to liquefaction and sliding of soil strata. Summary of damage is as follows: Piers and landing: sliding (up to 5 m), submergence, and tilting Sheet-pile bulkheads: sliding (over 2 m), submergence, settlement (up to 1 m), and tilting. Extensive anchor failure Quay-walls: sea sliding (up to 3 m) settlement (up to 4 m) with extensive anchor failure and wall tilting	A, B, C,

Earthquake			Port	Damage	
Location	Date	Magnitude	Location	Description	Possible Cause(s)
Tokachi-Oki, Japan	May 16, 1968	7.8	Hachinohe	Steel sheet-pile bulkheads: outward sliding (0.9 m), tilting, and settlement, with anchor failure	A
			Aomori	Gravity-type quay wall: sliding and settlement (0.4 m) Gravity-type breakwater: sliding (0.9 m) and pavement settlement (0.9 m)	A
			Hakodate	Steel sheet-pile bulkhead: seaward tilting (0.6 m) and apron settlement (0.3 m) Quay -wall: settlement (0.6 m) and sliding (0.4 m)	A, B,
Nemuro-Hanto-Oki, Japan	Jun 17, 1973	7.4	Hanasaki	Gravity-type quay wall: sliding (1.2 m) and settlement (0.3 m) with corresponding apron settlement (1.2 m) Steel sheet-pile bulkhead: sliding (2 m) and anchor failure Steel sheet-pile bulkhead: relatively minor damage	A, B
			Kiritappu	Gravity-type quay wall: relatively minor damage	
Miyagi-Ken-Oki, Japan	Jun 12, 1978	7.4	Shiogama	Concrete gravity-type quay wall: outward tilting (0.6 m) and apron pavement settlement	
			Ishinomaki	Steel sheet-pile bulkheads: outward sliding (up to 1.2 m) and apron settlement (up to 1 m) Concrete block retaining wall: sliding, tilting, and cracking with corresponding pavement settlement (0.2 m) relative to wall	A, B
			Yuriage	Concrete block gravity quay wall and steel sheet-pile bulkhead: large horizontal displacement (up to 1.2 m)	
			Sendai	Steel sheet-pile bulkheads: cracking and settlement of apron and pavement	

Earthquake			Port	Damage	
Location	Date	Magnitude	Location	Description	Possible Cause(s)
Offshore, Central Chile	Mar 3, 1985	7.8	San Antonio Valparaiso	Concrete block seawall at western extremity of port: collapse of about 60 percent of seawall length, leading to significant tilting of crane structures. Anchored bulkhead: outward movement of 1 m Seawalls at Sites 6 and 7 (at west side of port): about 08.m of soil movement at top of wall, causing movement of crane rails and disruption of crane operations. Seawall at passenger terminal: lateral movement of seawall, settlement of backfill	A, B
Loma Prieta, California	17 Nov 1989	7.1	San Francisco Oakland	Settlement of portions of piers supported by fills (rather than by piles. Significant structural damage to various buildings along waterfront, including clock tower at Ferry Building. May broken water lines, broken batter piles, cracked concrete decks above piers. Damage to container crane. Seventh Street Terminal: Settlement and lateral movement of perimeter dike and sand fill system. Settlement of crane rail, broken piles, punching of piles through deck. Extended closure of terminal. Middle Harbor Terminal: 0.2 m to 0.7 m of subsidence in yard area. Matson Terminal: Separation between pile and bottom of slab, cracking of piles. Wharf stayed in operation but with limited live loads while crane operating.	A, B, E

Earthquake			Port	Damage	
Location	Date	Magnitude	Location	Description	Possible Cause(s)
Loma Prieta, California (Continued)			Oakland	Howard Terminal: Some lateral movement of landside crane rail (although crane remained operational). Good performance of vertical piles designed as ductile frame.	A, B, C
Philippine Islands	16 Jul 1990	7.8	San Fernando	Government Pier no. 1: Significant cracking, buckling, deformation of reinforced concrete pile-supported pier. Extensive cracking of concrete piles, and particularly severe damage to batter piles. Severe cracking of adjacent concrete seawall. Operations suspended Coal Pier: Large permanent seaward displacement caused concrete slab between pier and seawall fall from seat. Dry Bulk Handling Equipment: Collapsed	A, C, E
Guam	Aug 8 1993	8.0	Apra Harbor	Navy Facilities: Partial collapse of wood-framed structure and lateral spreading. Damage to piers founded in dredge backfill. Sheet pile bulkheads and anchor systems moved as much as 0.7 m. Damage to batter piles near pile caps	A, B

Earthquake				Damage	
			Port		Possible
Location	Date	Magnitude	Location	Description	Cause(s)
Northridge	Jan 17 1994	6.8	Los Angeles	Berths 121-126 of American President Lines Terminal: Seaward movement of berths (0.2 m) and settlement and liquefaction of backland fill areas. Settlement if dikes and damage to 171 lb crane rail. Several days of downtime needed for repairs to restore full operations. Newer portions of wharves (with vertical piles designed as ductile as moment frame and 85 ft rock dike) performed well. Older portions of Berth 126 (with vertical and batter piles) experienced some pile damage. Other Terminals: Settlement, lateral spreading, and liquefaction of fills, with come associated damage to older facilities. Utilities: Ruptured water lines, loss of power to some cranes (which interrupted crane operations), and interruption of telephone service (up to several hours).	A, B
			Long Beach	No damage reported	

Legend

A: Large lateral pressure from backfill materials, in the absence of complete liquefaction
B: Liquefaction.
C: Localized Sliding
D: Massive submarine sliding
E: Vibrations of structure

Table 2. Typical pile properties.

Size in.	Core Dia. in.	Section Properties				Allowable Concentric Service Load, Tons			
		Area $in.^2$	Weight plf	Moment of Inertia $in.^4$	Section Modulus $in.^3$	f'_c			
						5000	6000	7000	8000
Square Piles									
10	Solid	100	104	833	167	73	89	106	122
12	Solid	144	150	1728	288	105	129	152	176
14	Solid	196	204	3201	457	143	175	208	240
16	Solid	256	267	5461	683	187	229	271	314
18	Solid	324	338	8748	972	236	290	344	397
20	Solid	400	417	13,333	1333	292	358	424	490
20	11″	305	318	12,615	1262	222	273	323	373
24	Solid	576	600	27,648	2304	420	515	610	705
24	12″	463	482	26,630	2219	338	414	491	567
24	14″	422	439	25,762	2147	308	377	447	517
24	15″	399	415	25,163	2097	291	357	423	488
Octagonal Piles									
10	Solid	83	85	555	111	60	74	88	101
12	Solid	119	125	1134	189	86	106	126	145
14	Solid	162	169	2105	301	118	145	172	198
16	Solid	212	220	3592	449	154	189	224	259
18	Solid	268	280	5705	639	195	240	284	328
20	Solid	331	345	8770	877	241	296	351	405
20	11″	236	245	8050	805	172	211	250	289
22	Solid	401	420	12,837	1167	292	359	425	491
22	13″	268	280	11,440	1040	195	240	283	328
24	Solid	477	495	18,180	1515	348	427	506	584
24	15″	300	315	15,696	1308	219	268	318	368
Round Piles									
36	26″	487	507	60,007	3334	355	436	516	596
48	38″	675	703	158,199	6592	493	604	715	827
54	44″	770	802	233,373	8643	562	689	816	943

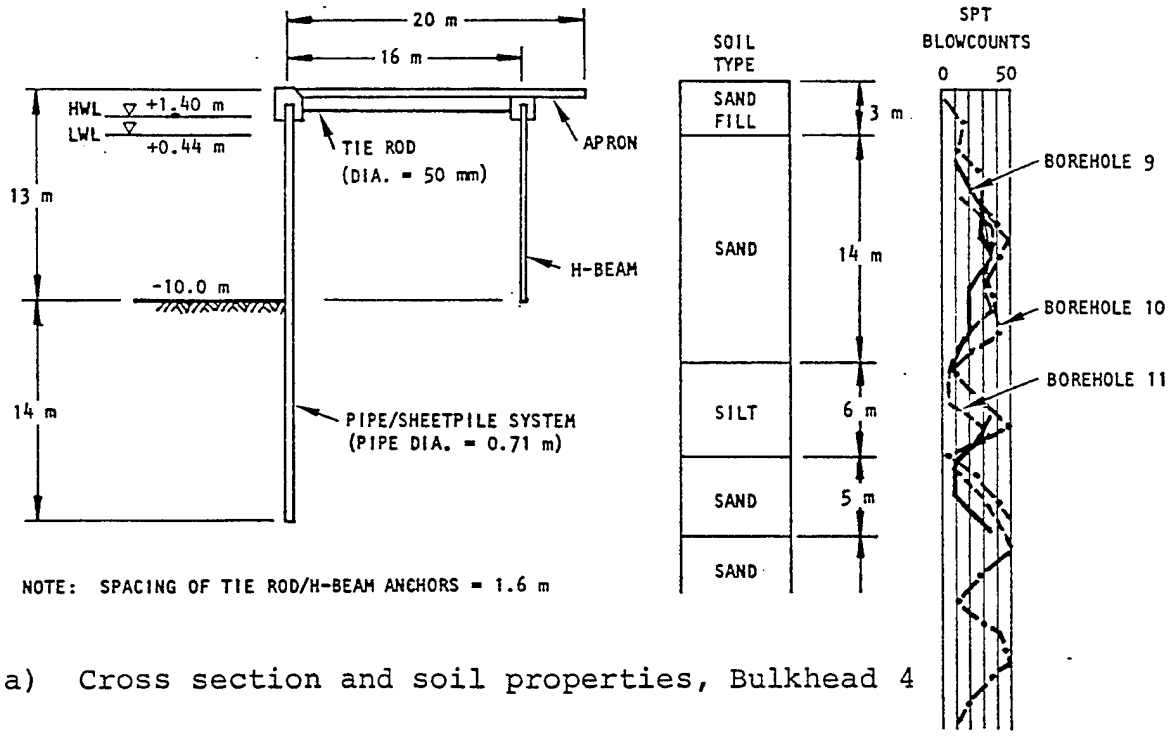

(a) Cross section and soil properties, Bulkhead 4

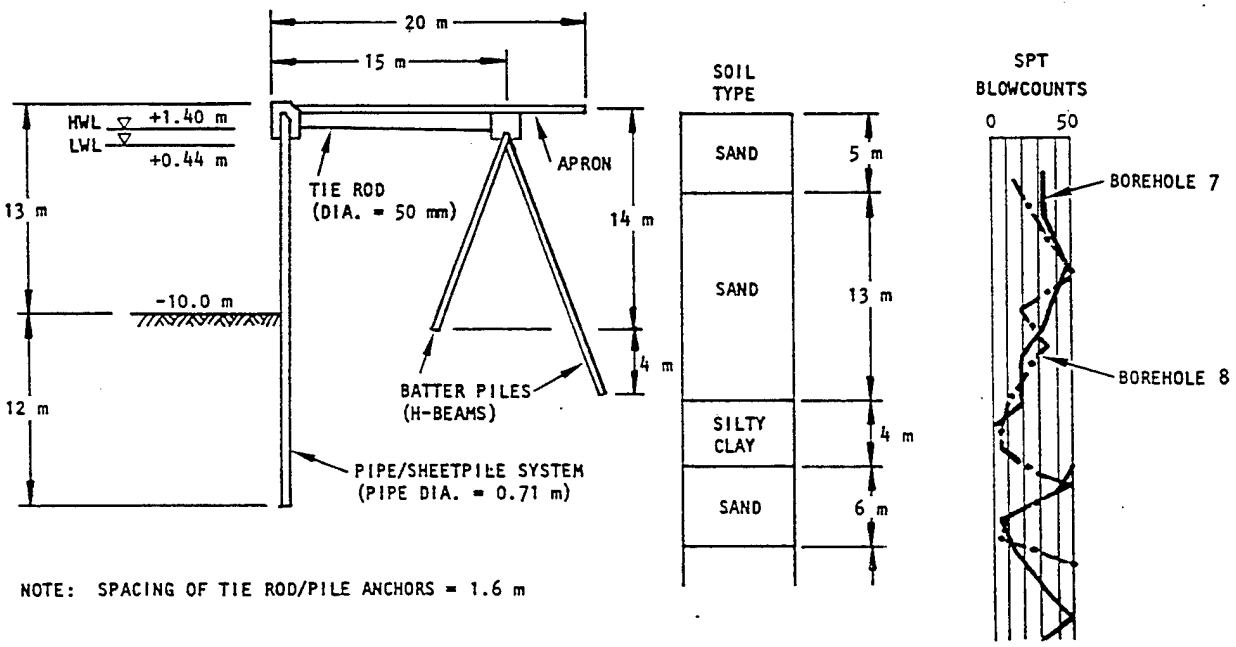

(b) Cross section and soil properties, Bulkhead 5

Figure 1. Bulkheads 4 and 5 at Nakano wharf, Sendai Port.

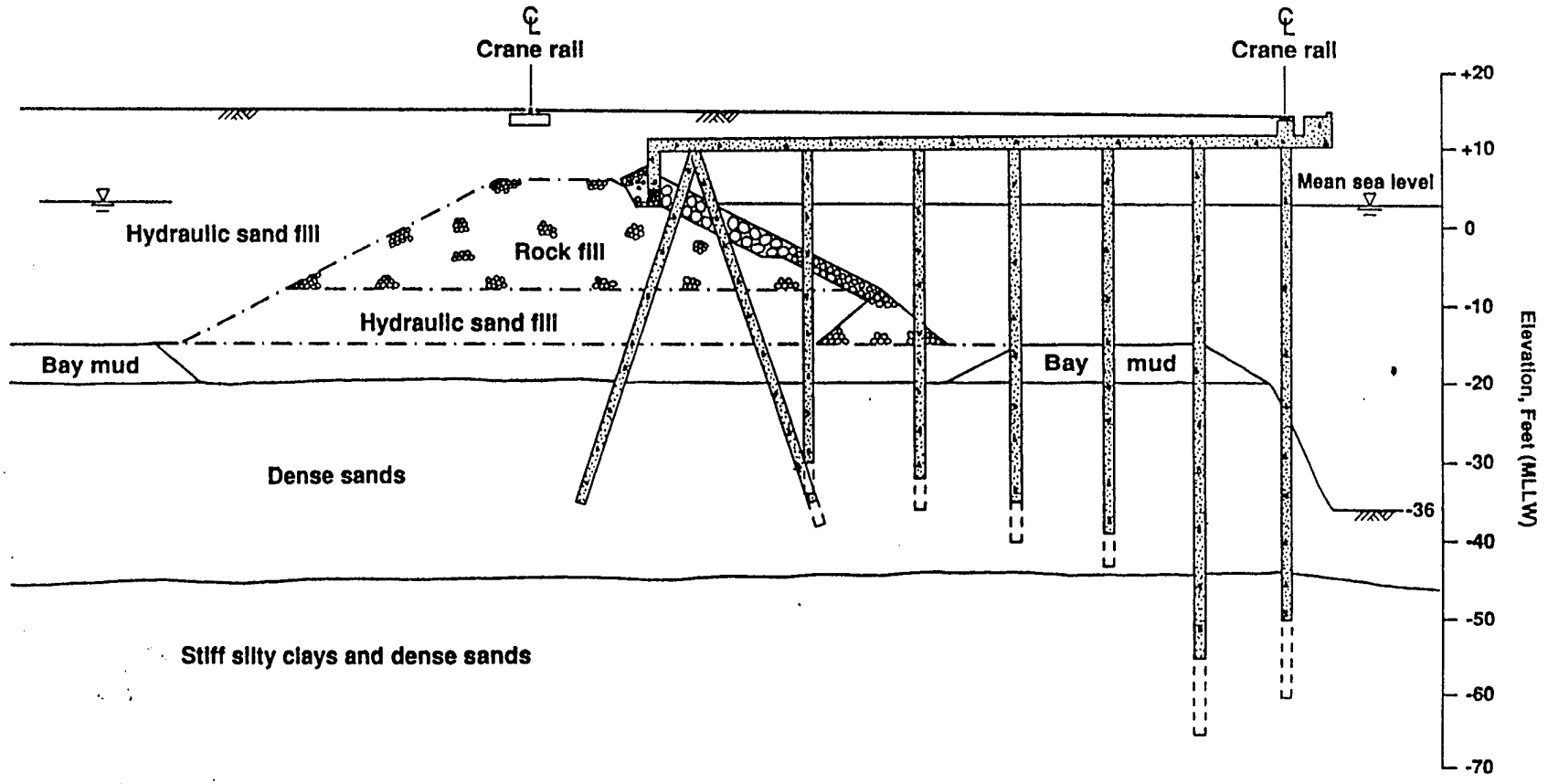

Figure 2. Cross-section 7th St Terminal, Port of Oakland.

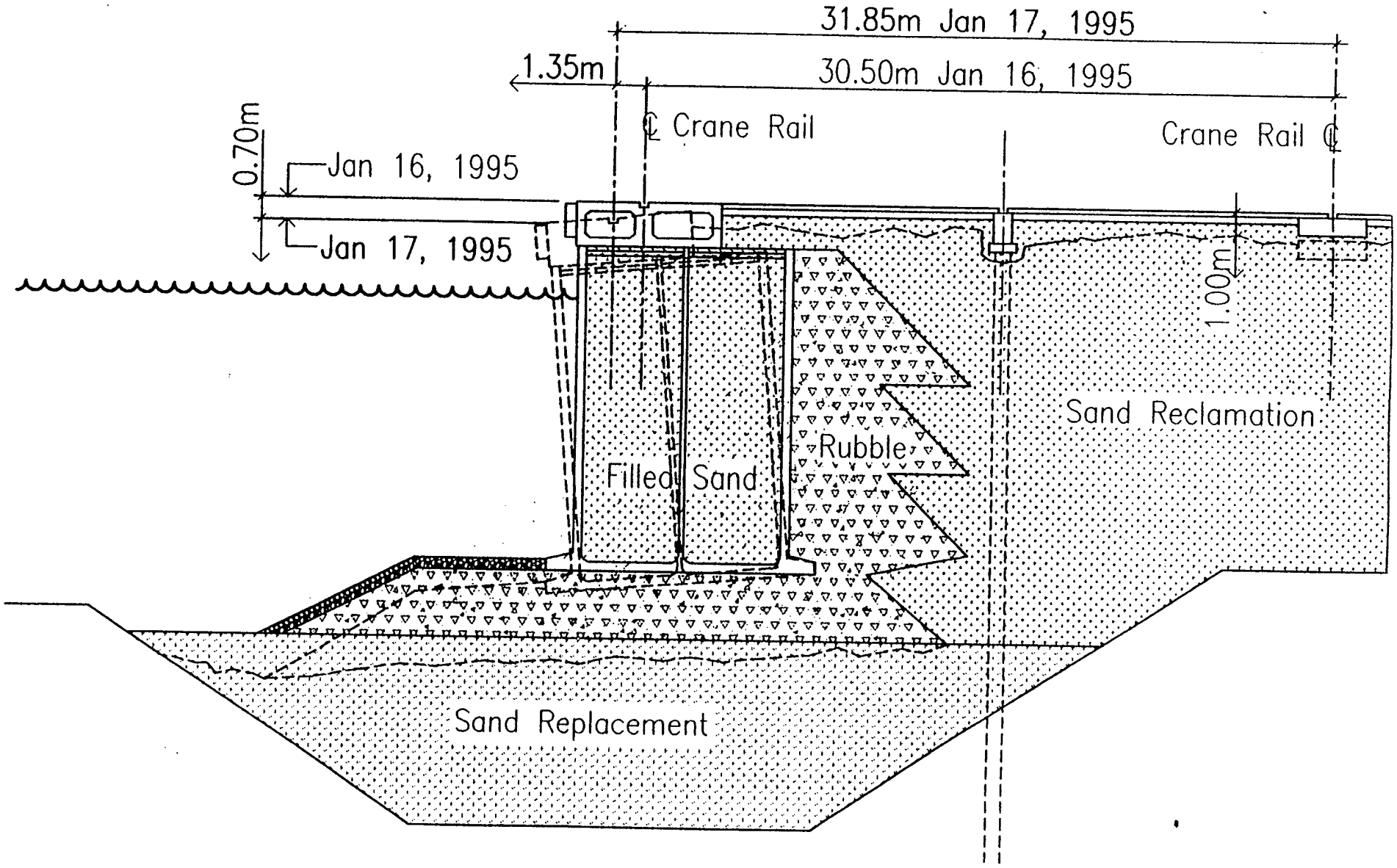

Figure 3. Typical wharf, Kobe Japan.

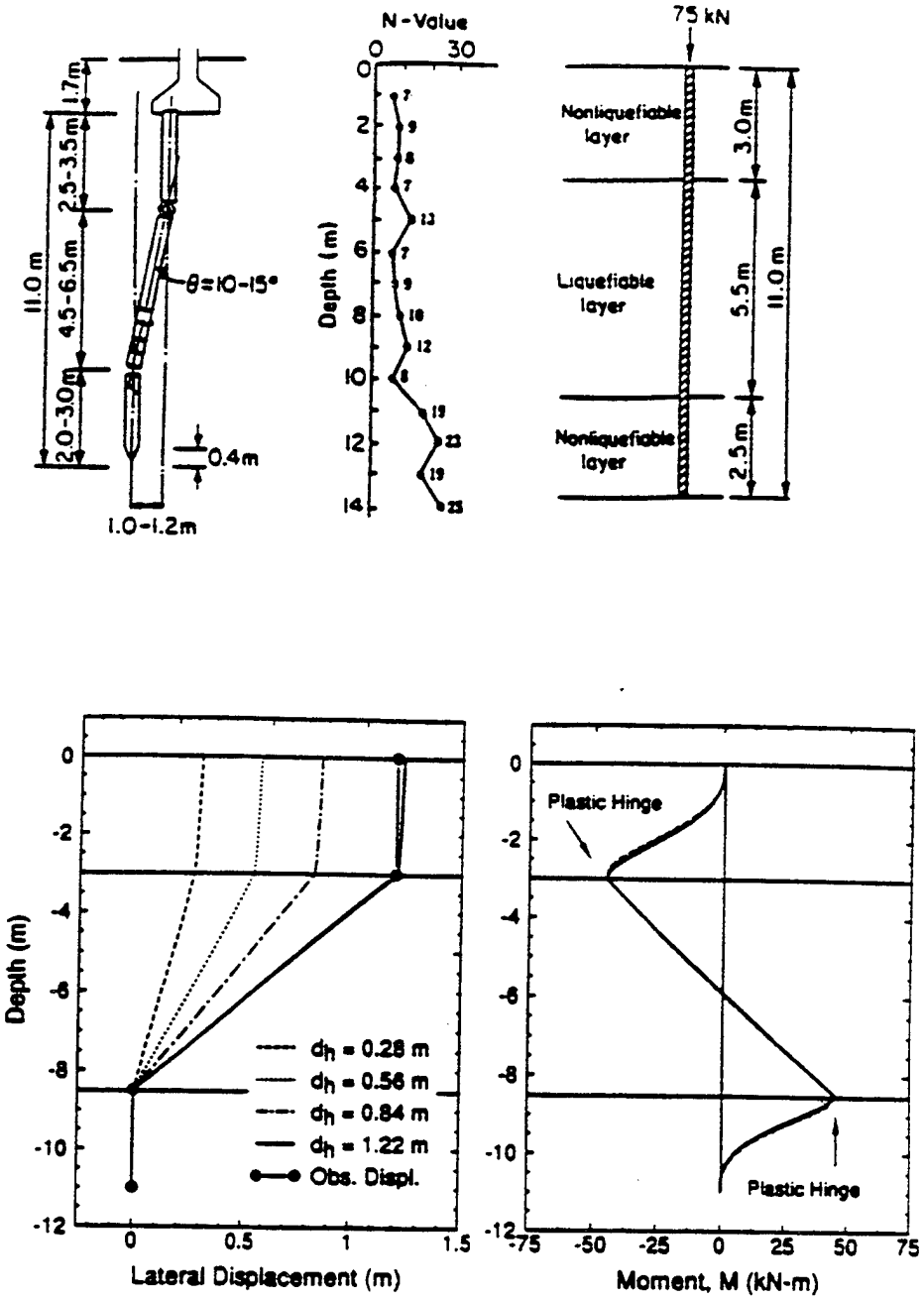

Figure 4. Typical pile damage in liquefaction zone.

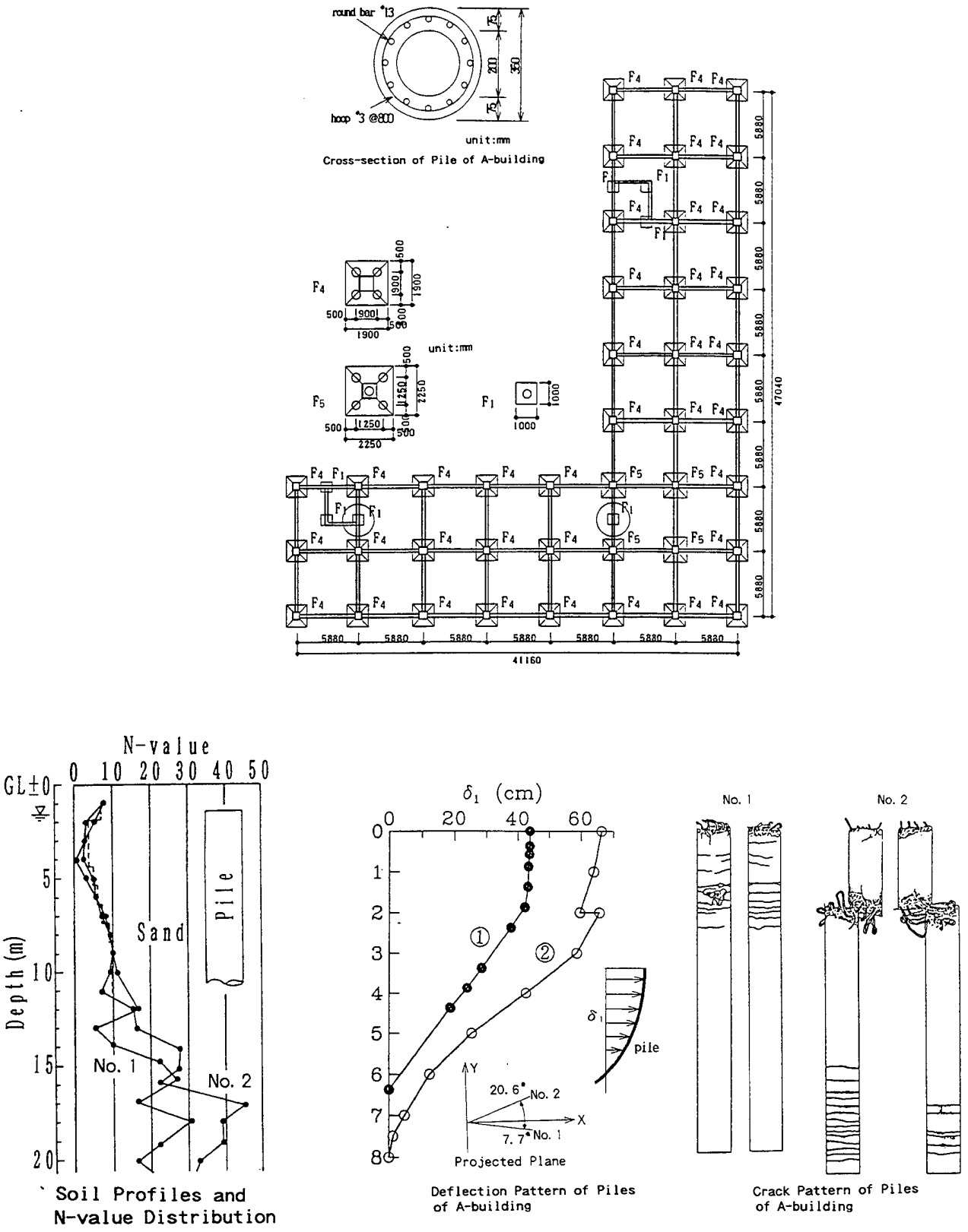

Figure 5. Building A pile damage, Niigata Earthquake.

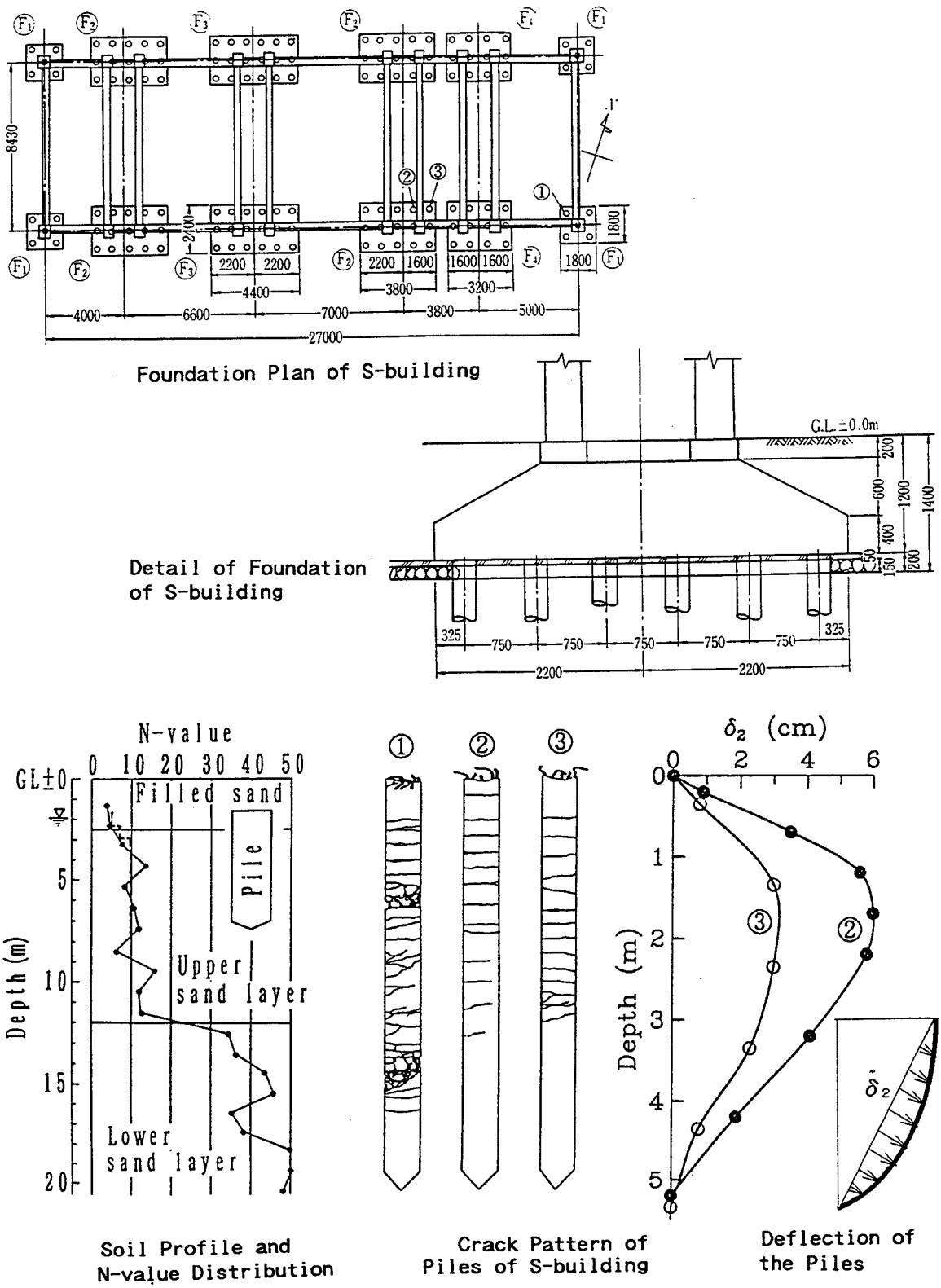

Figure 6. Building S pile damage, Niigata Earthquake.

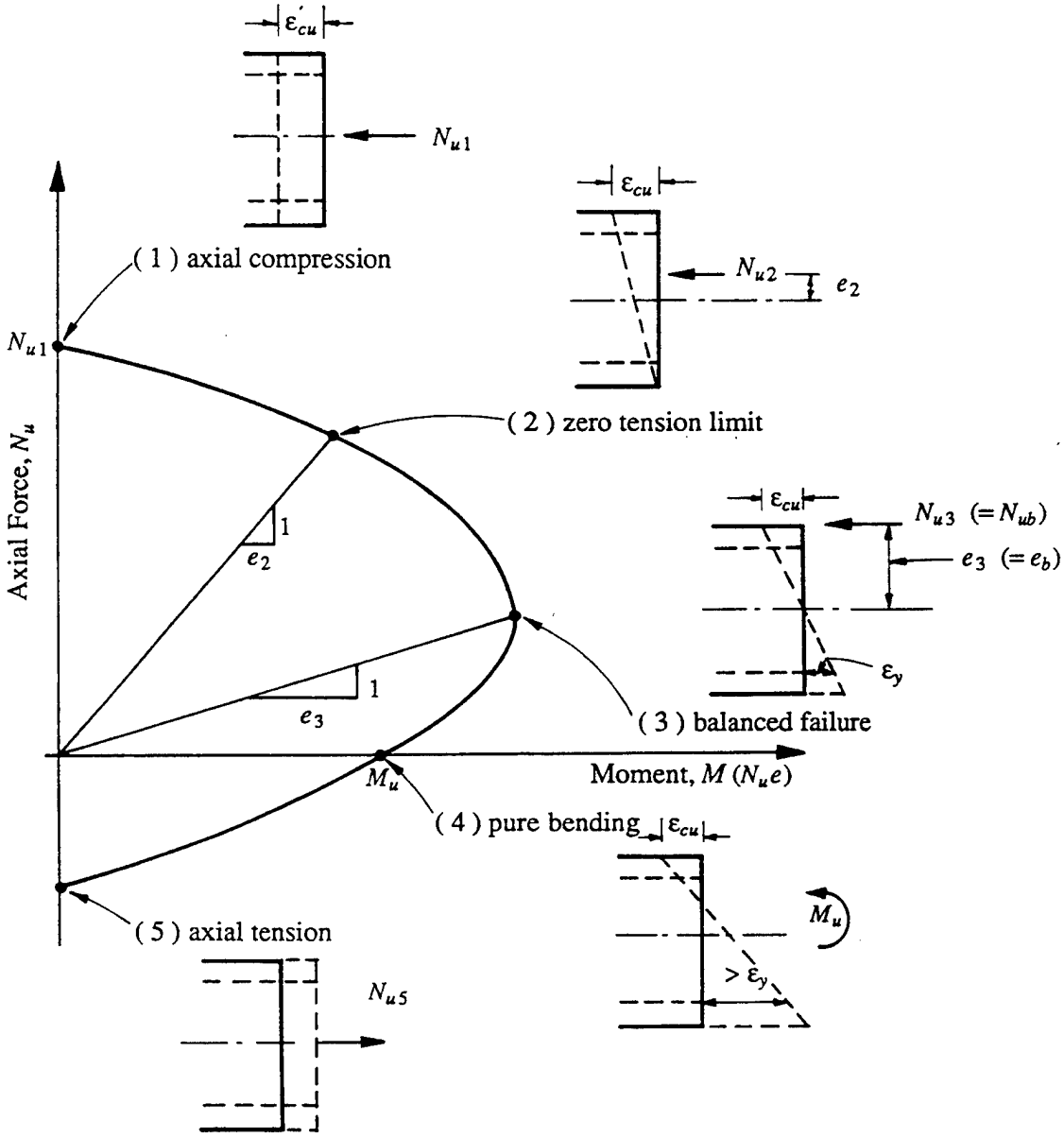

Figure 7. Reinforced concrete axial force-moment diagram.

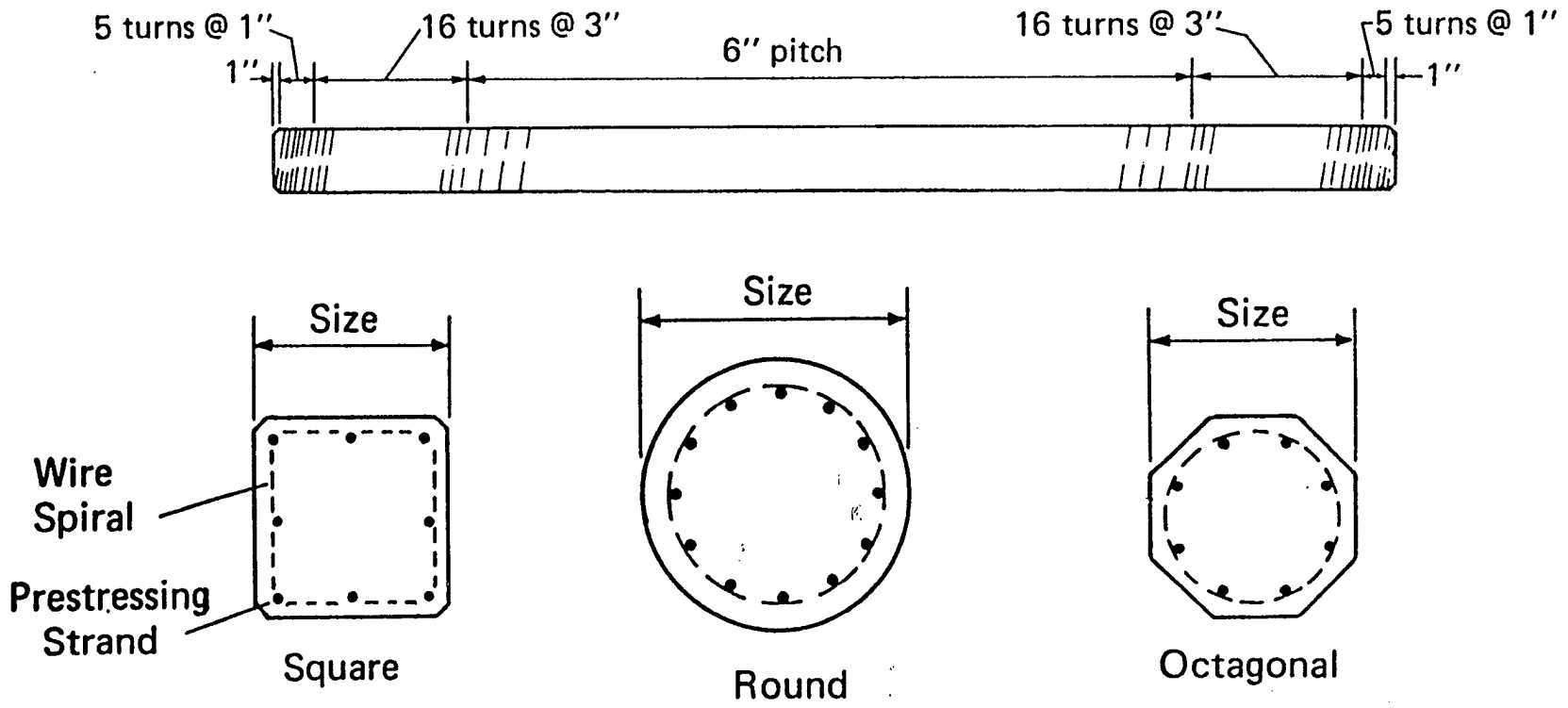

Figure 8. Typical prestressed concrete pile configurations.

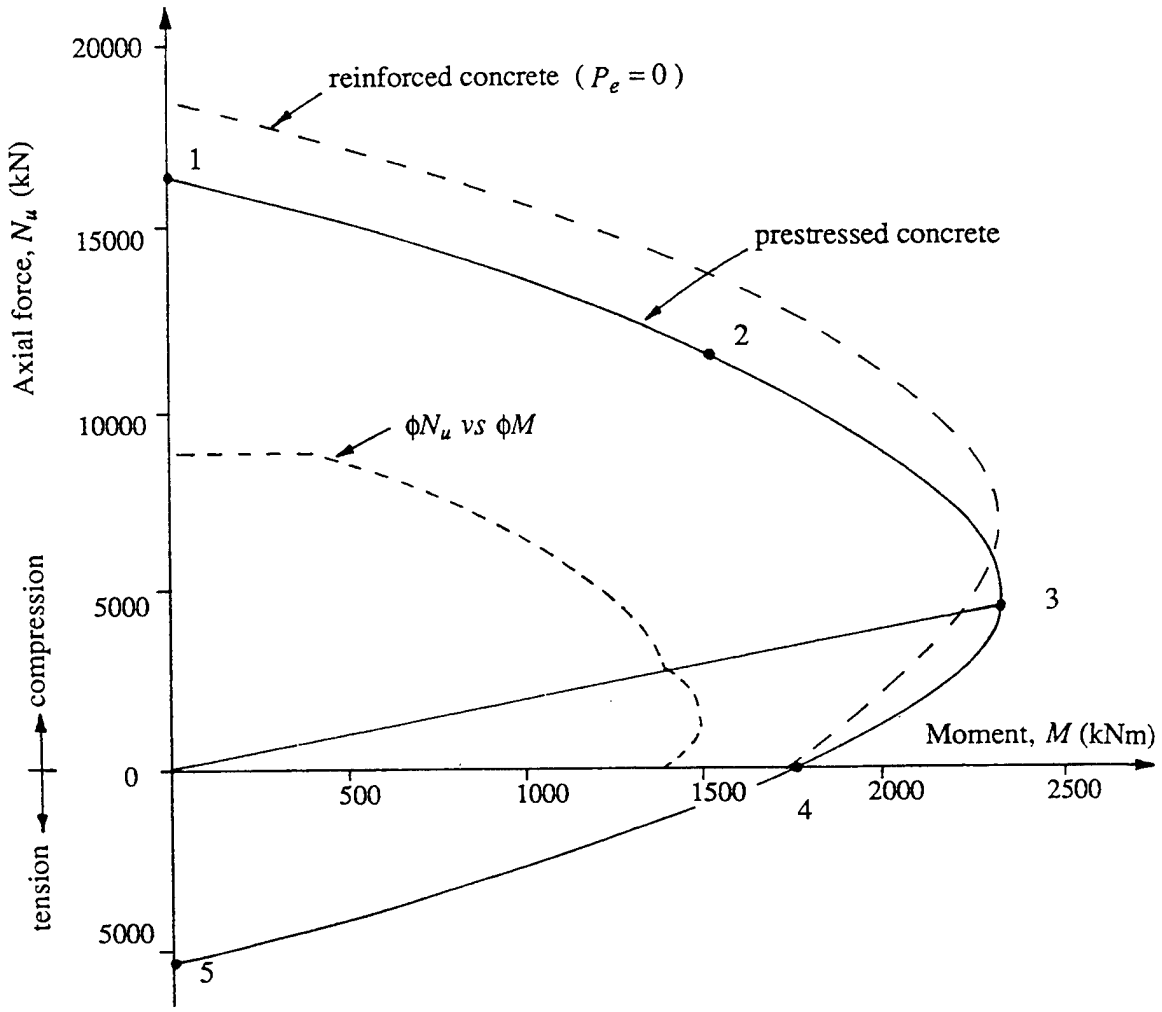

Figure 9. Axial force-moment diagram for prestressed concrete.

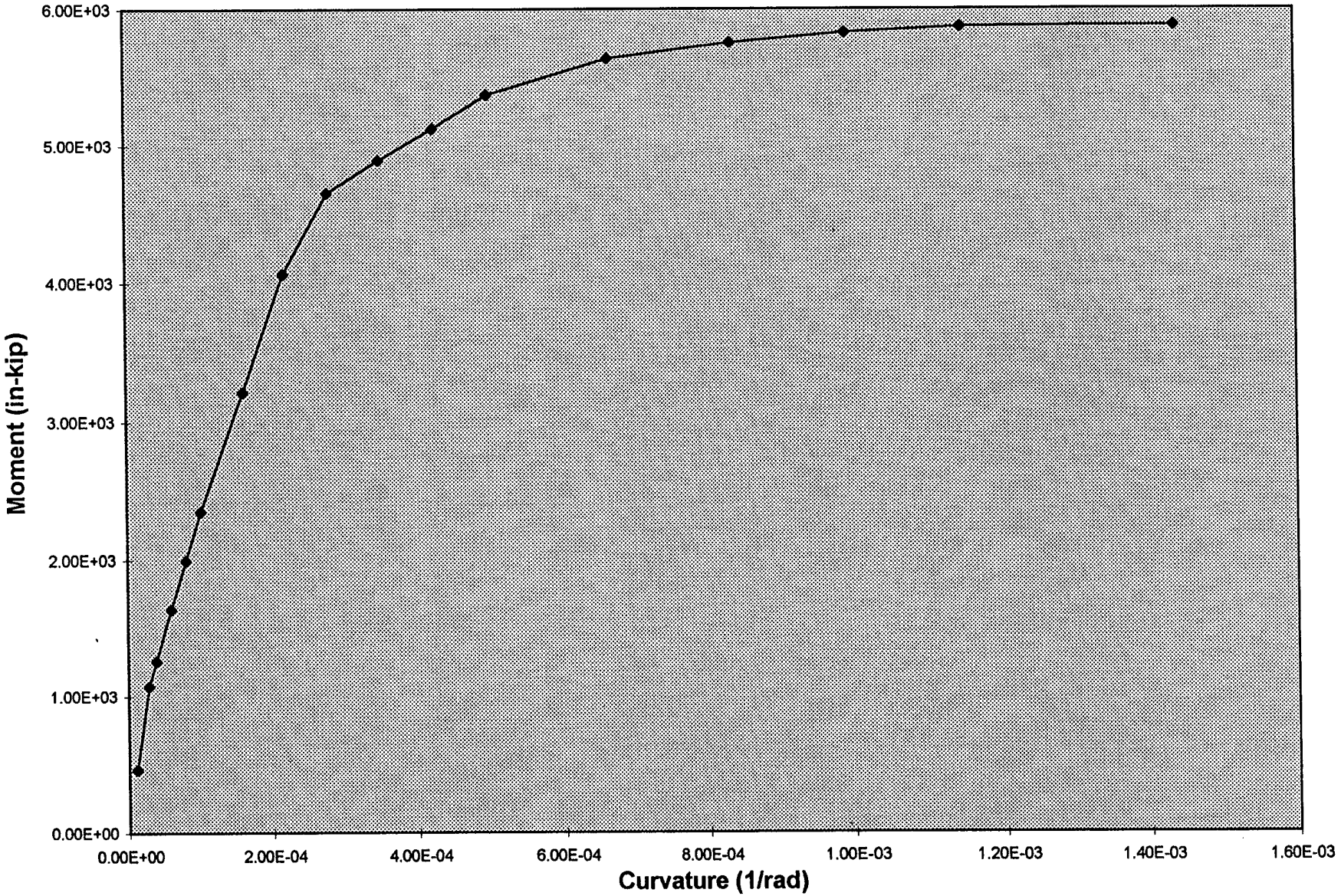

Figure 10a. Typical octagonal pile moment-curvature diagram.

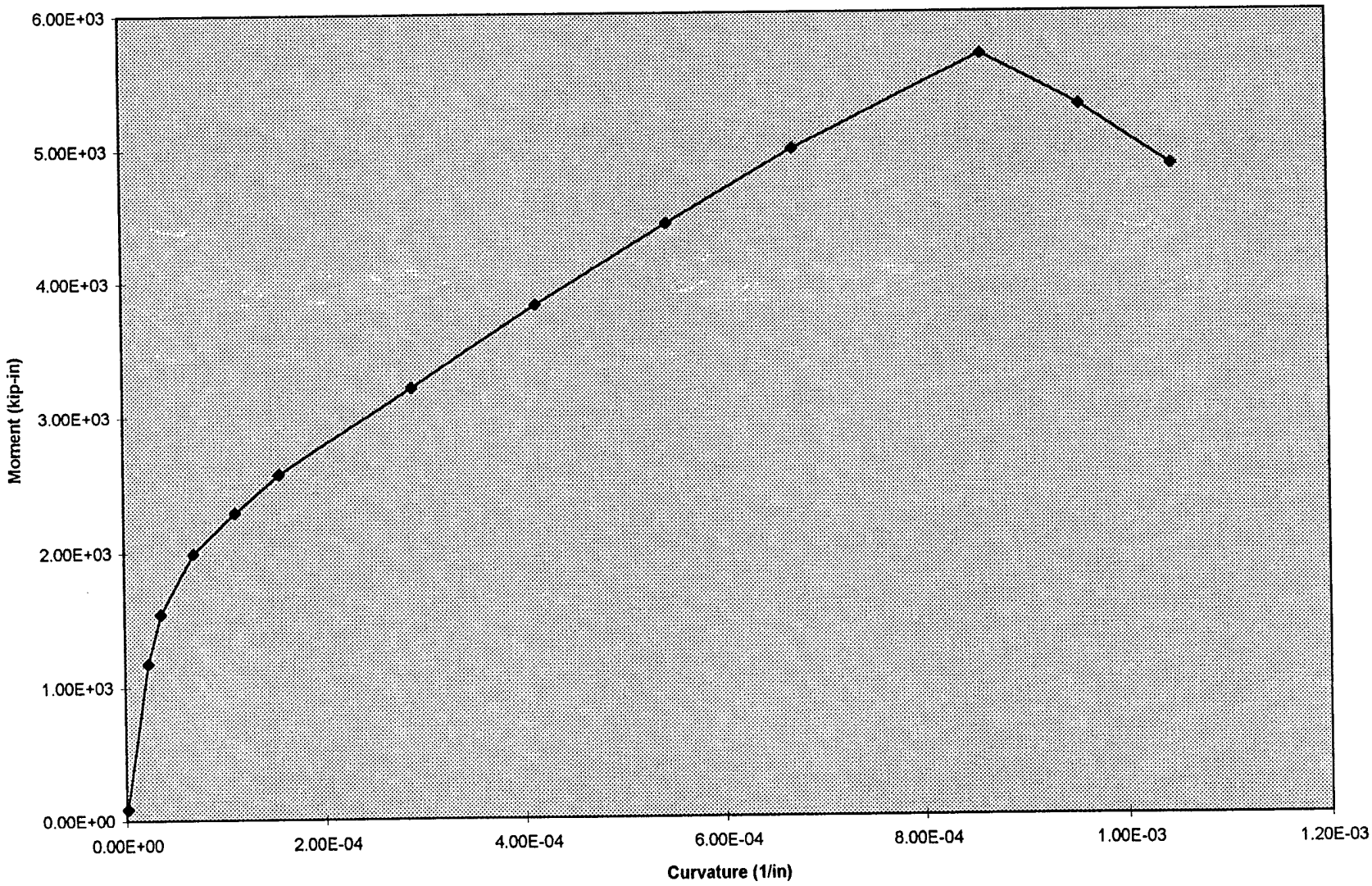

Figure 10b. Moment curvature diagram for pile.

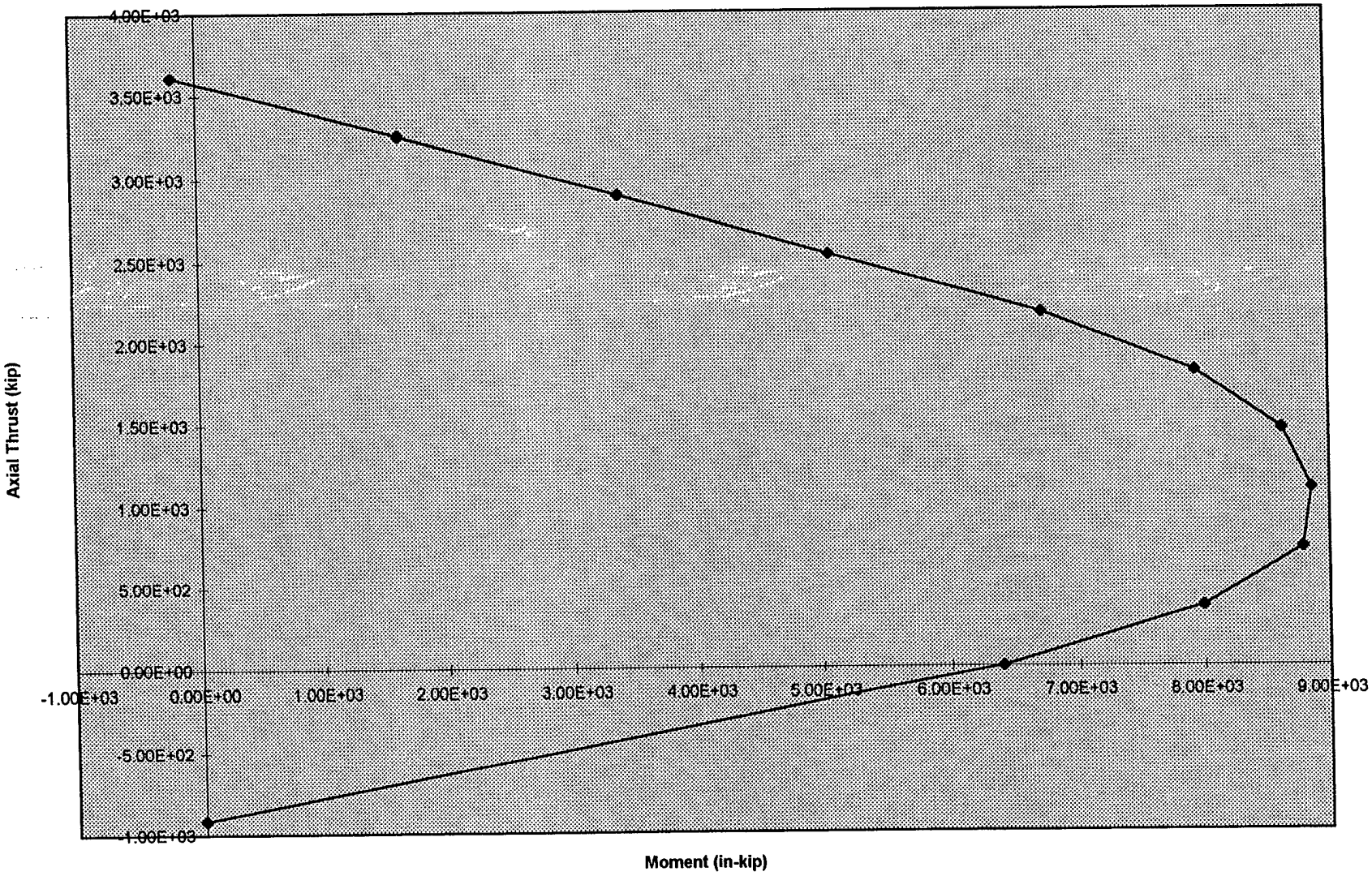

Figure 11. Typical octagonal pile axial force-moment diagram.

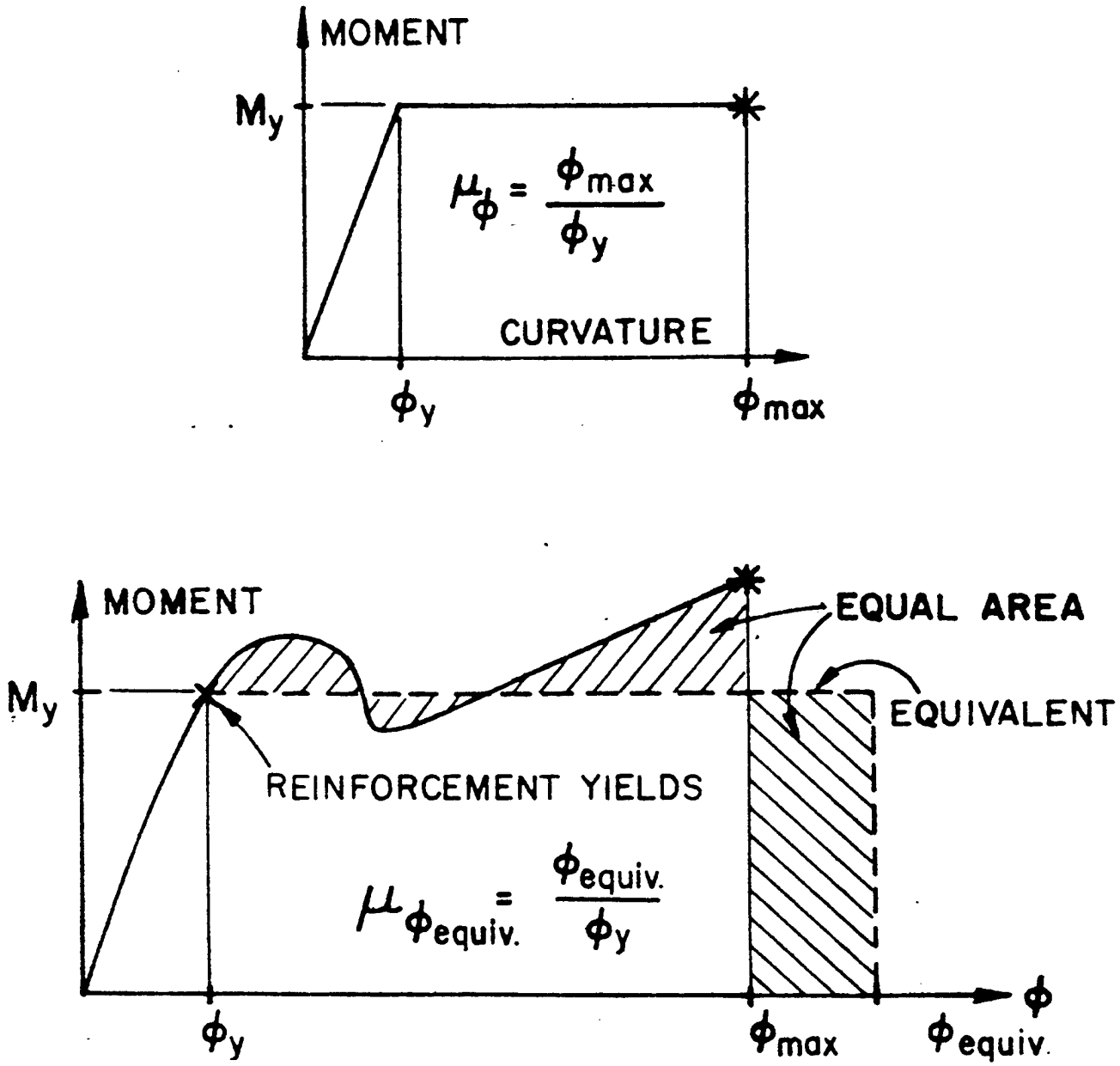

Figure 12. Equivalent ductility.

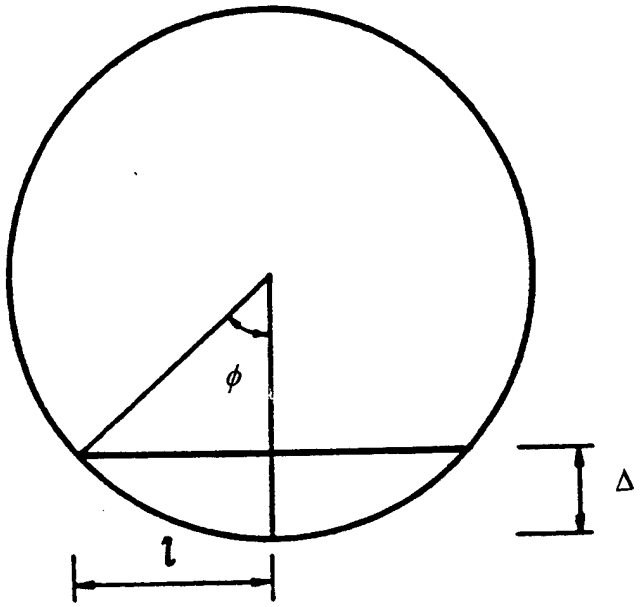

Figure 13. Relation between curvature and displacement.

Note: Represents point of contraflexure in continuous member

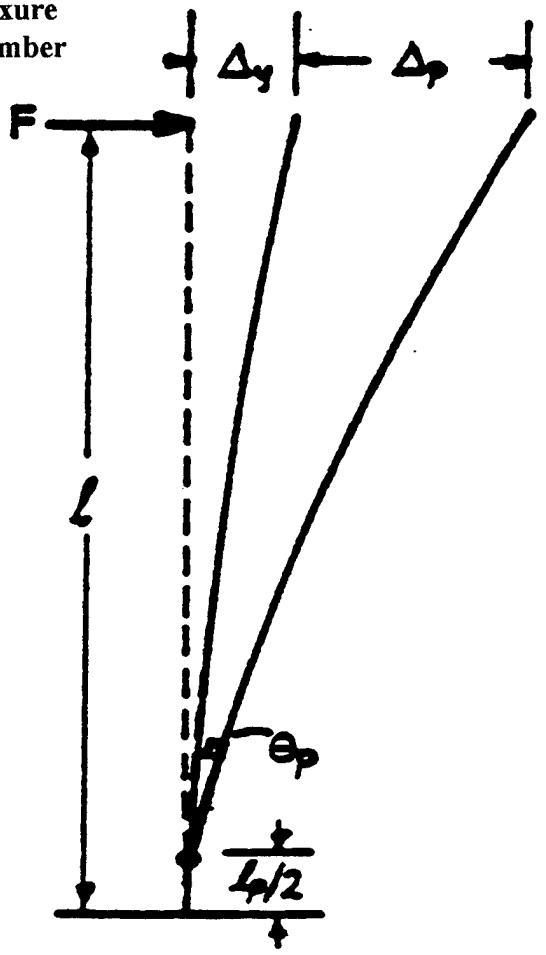

Figure 14. Elastic and plastic deflection.

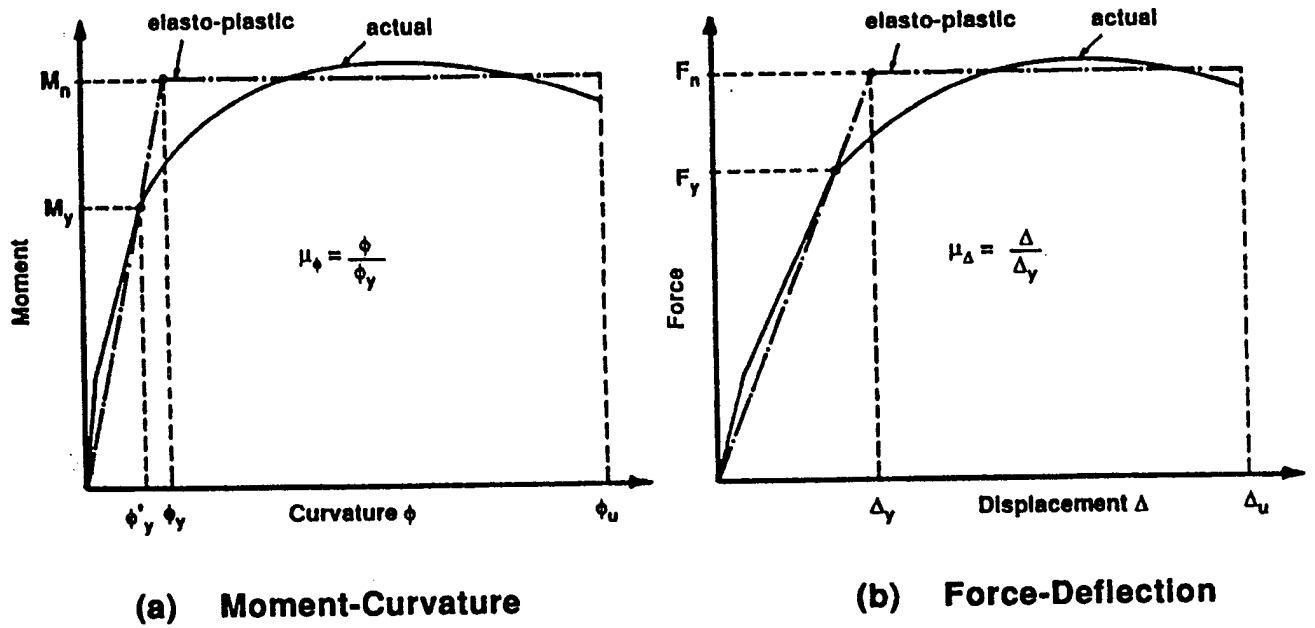

Figure 15. Yield and ultimate curvature.

c. Displacement ductility - curvature ductility relationship.

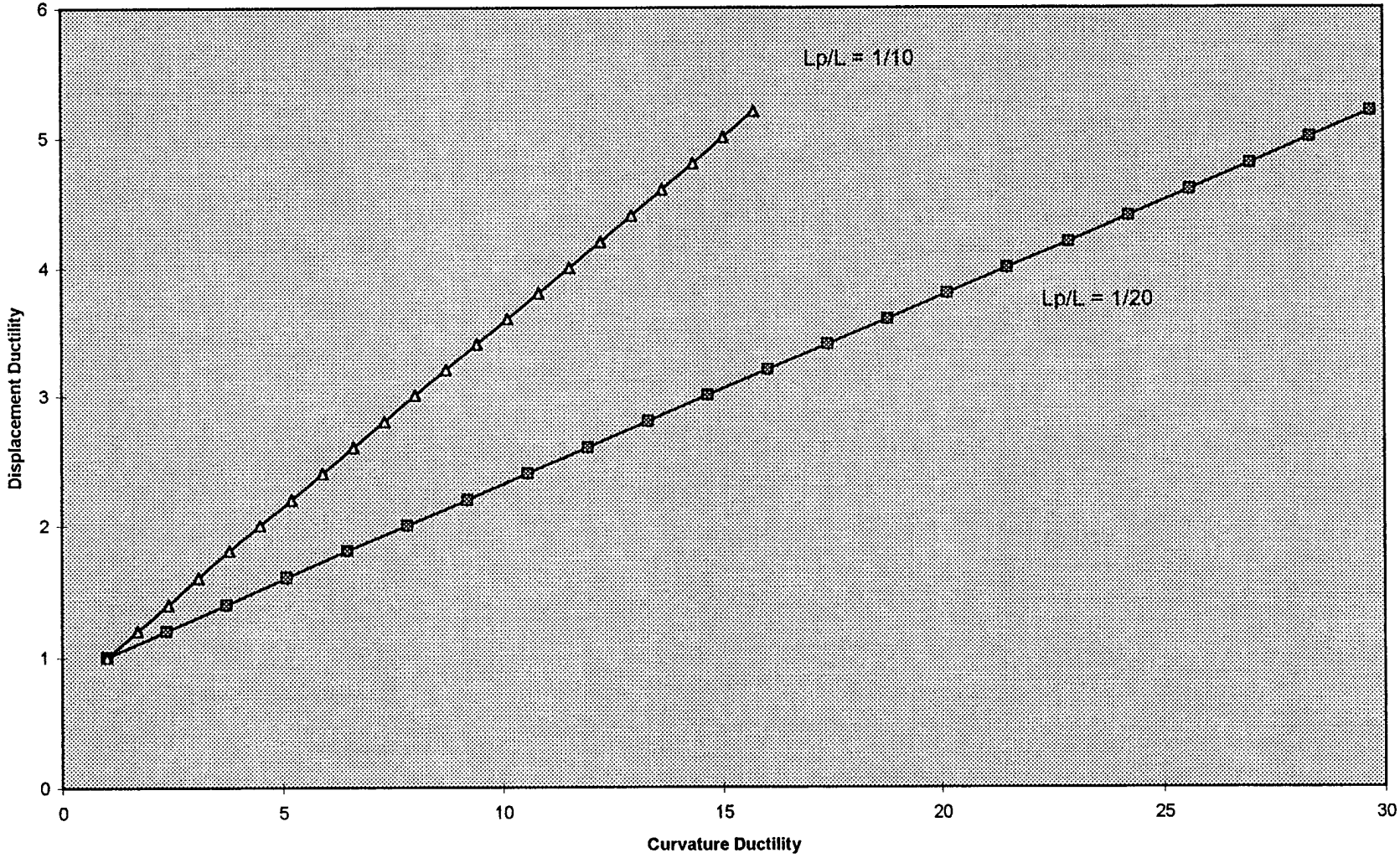

Figure 15. Displacement ductility and ultimate curvature.

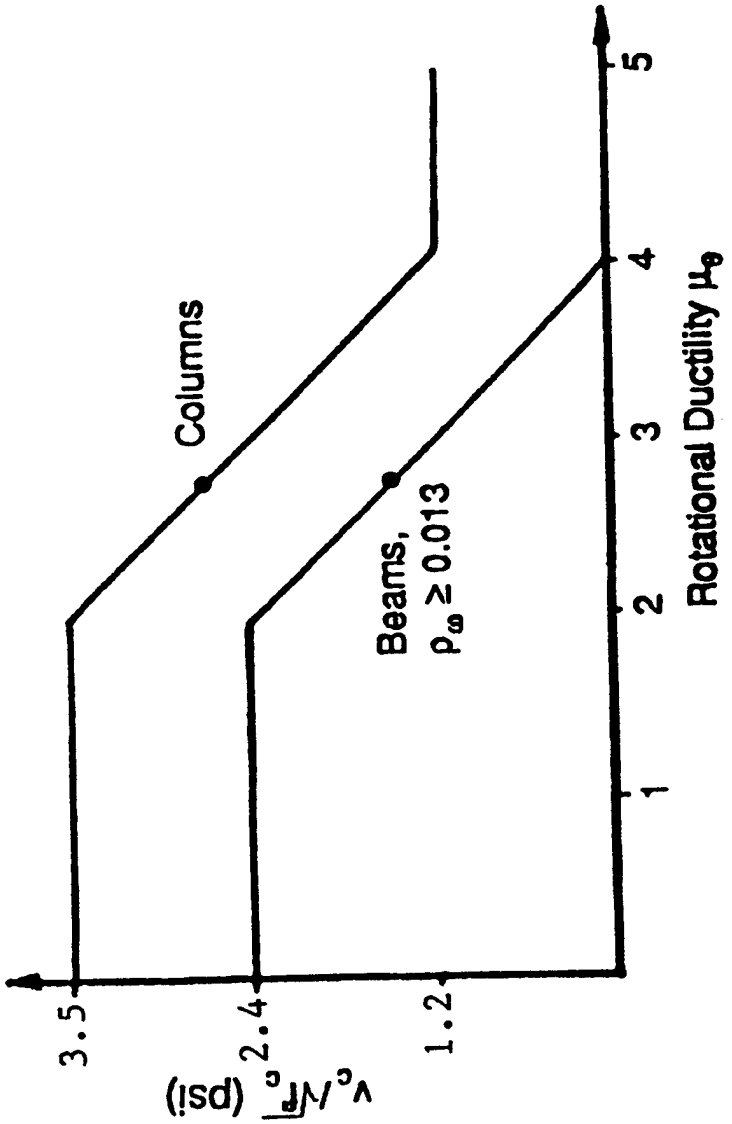

Figure 16. Shear capacity as function of ductility.

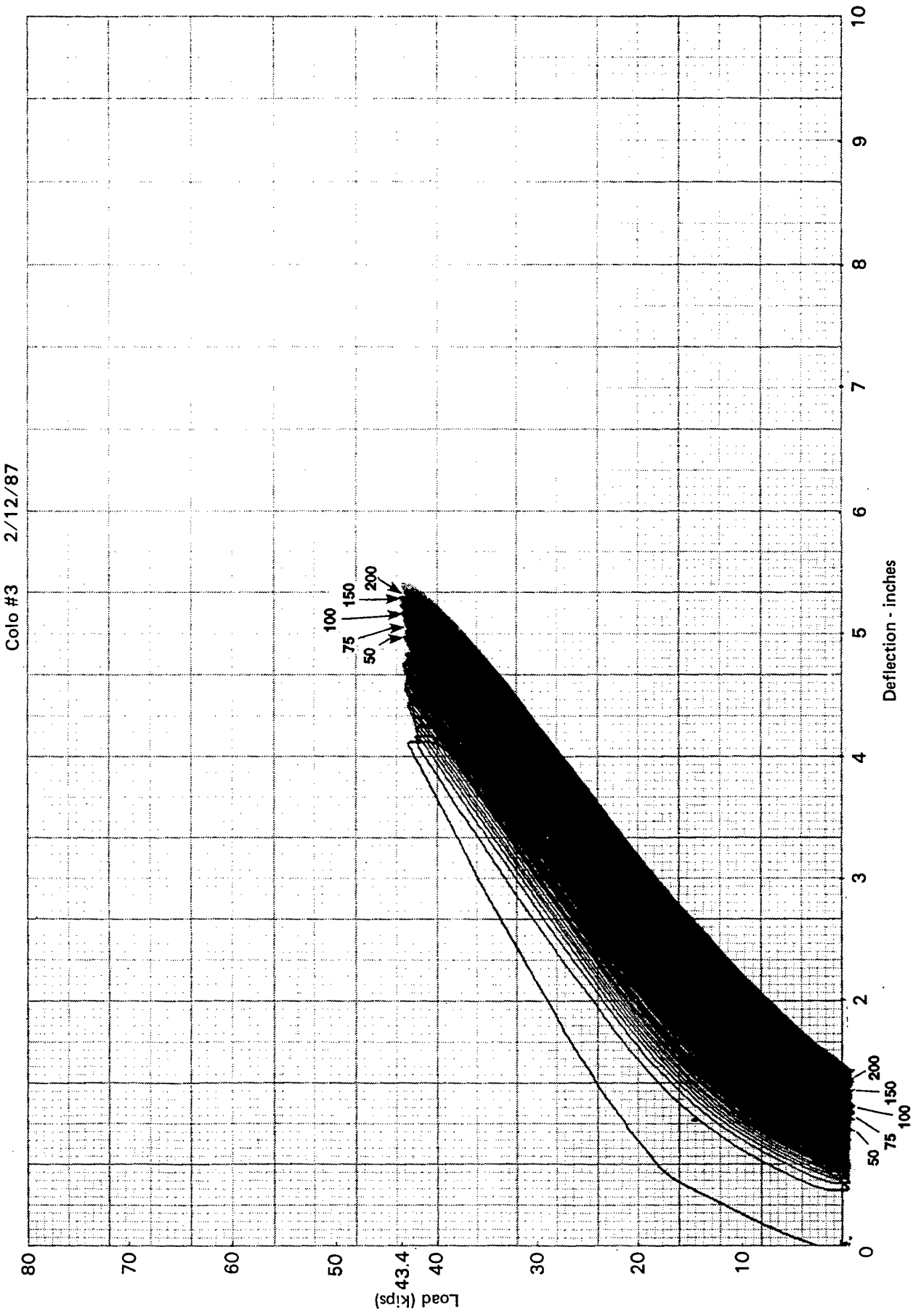

Figure 17. Cyclic pile loading behavior.

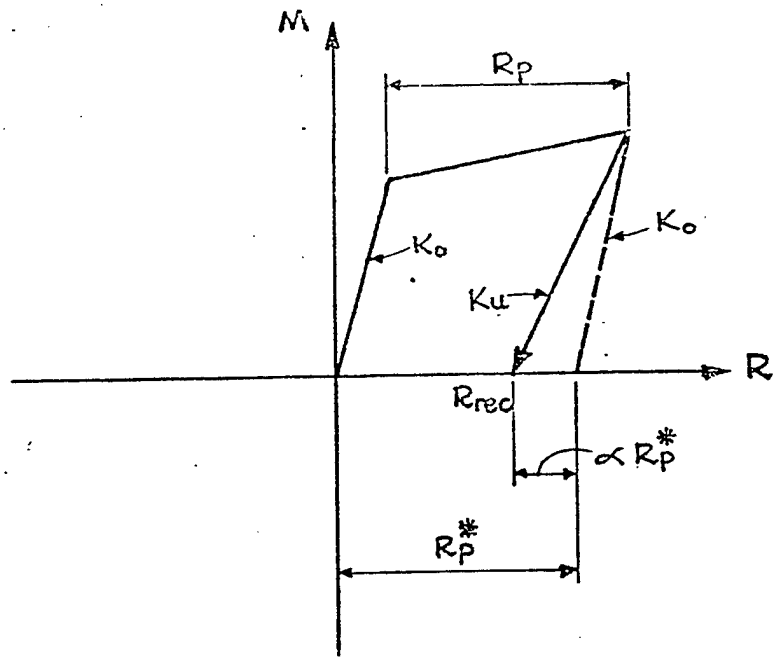

(a) Unloading Stiffness

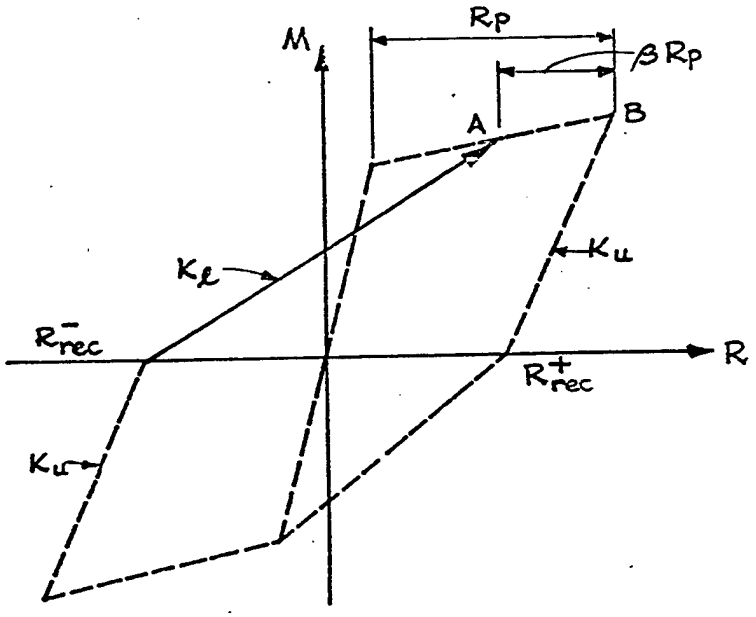

(b) Reloading Stiffness

Figure 18. Modified Takeda model.

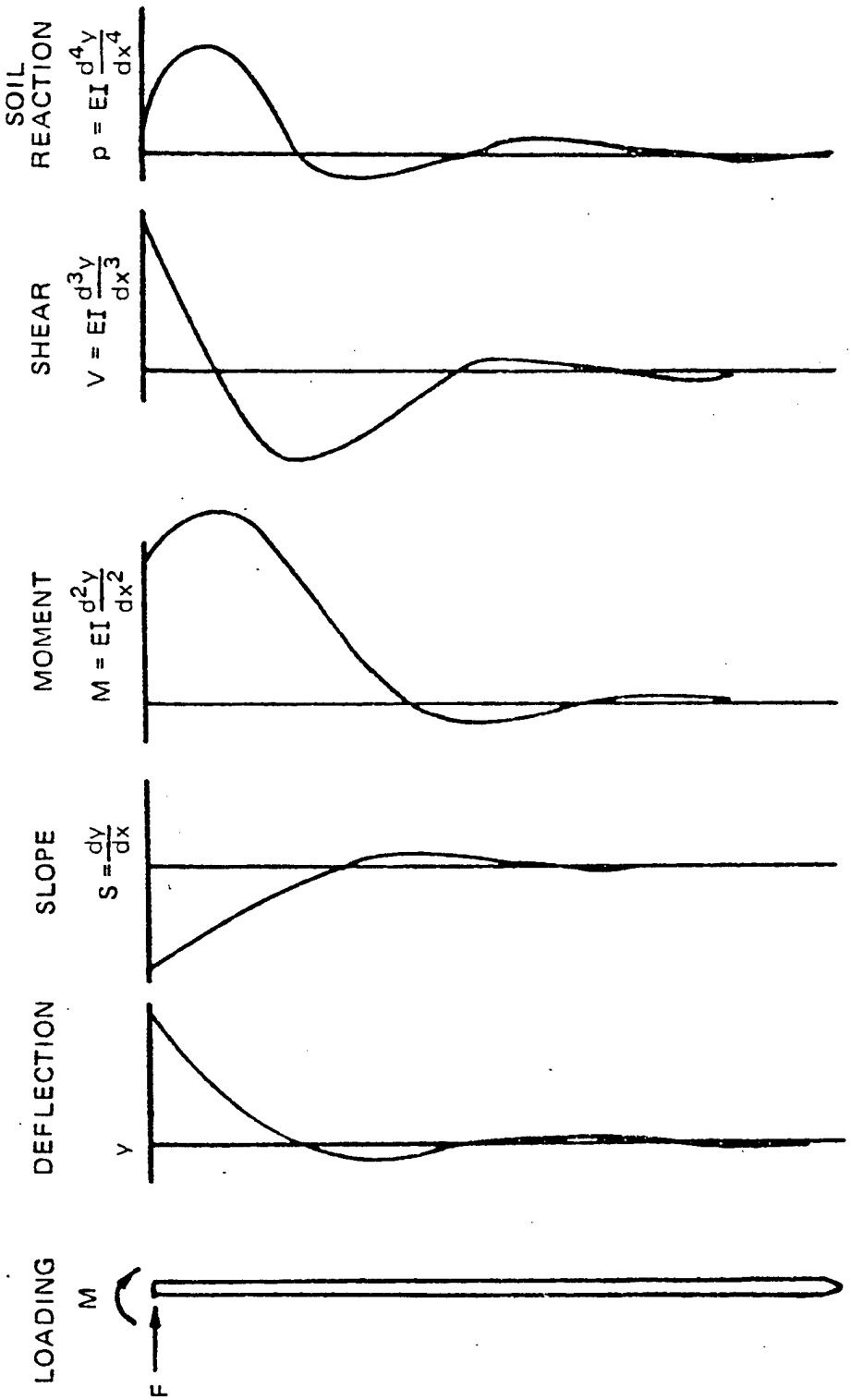

Figure 19. Pile loading diagrams

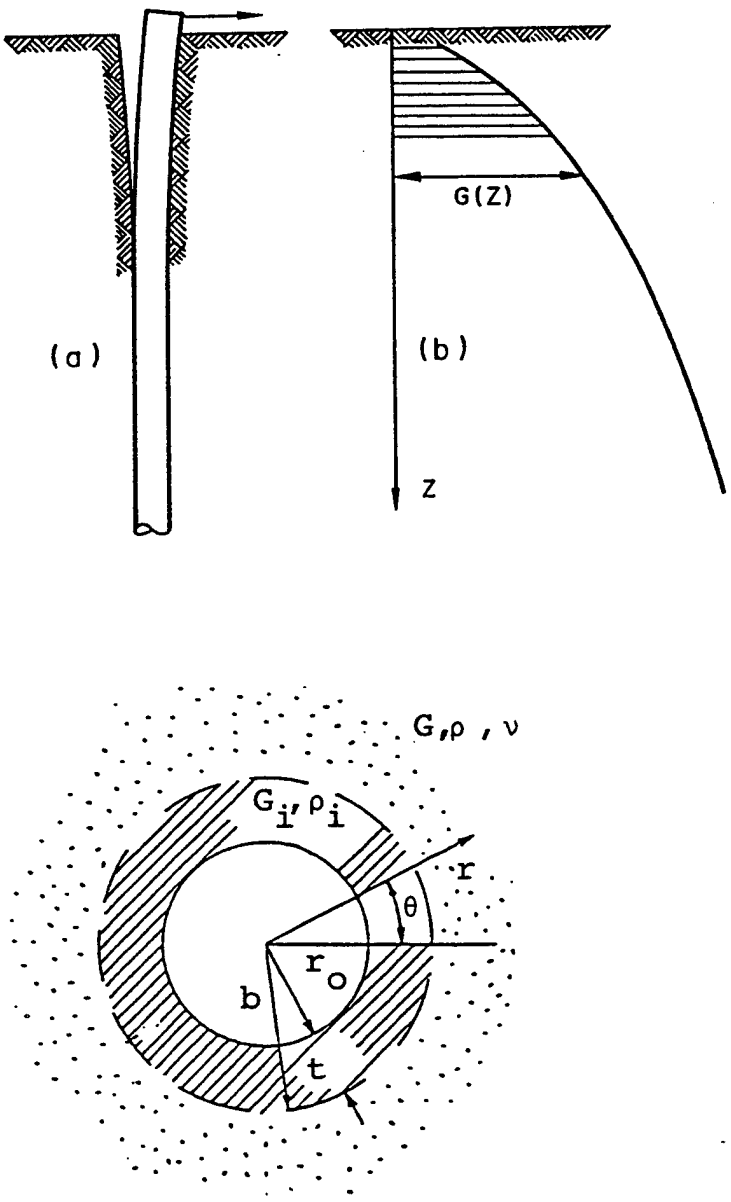

Figure 20. Pile separation and zone of plastic behavior.

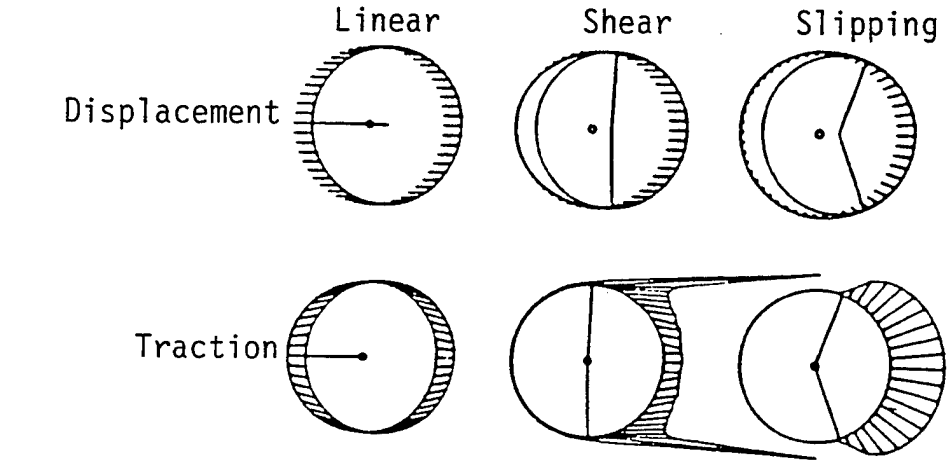

k_h/G	4.28	4.17	2.32
$c_h/R\sqrt{G\rho}$	13.23	6.42	2.60
	(a)	(b)	(c)

Figure 21. Influence of model on behavior.

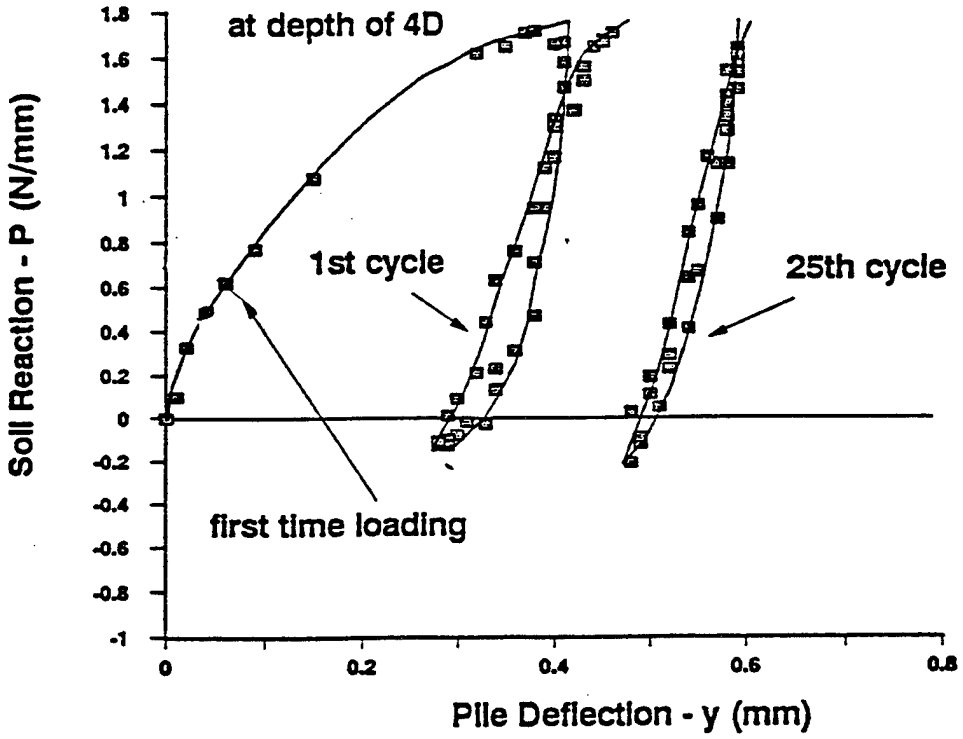

Figure 22. Typical p-y curve.

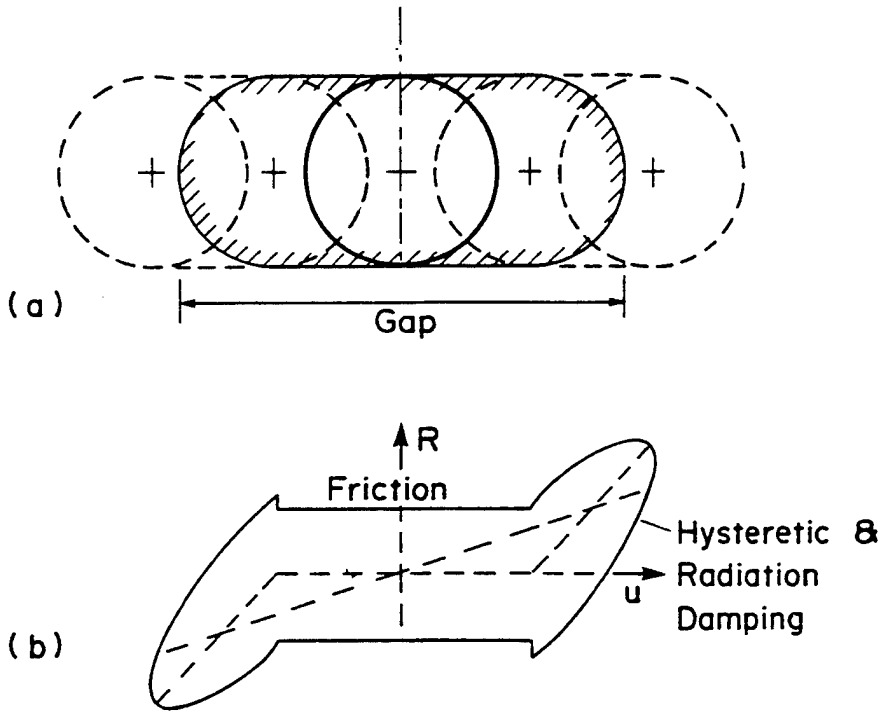

Figure 23. Gapping and hysteretic behavior.

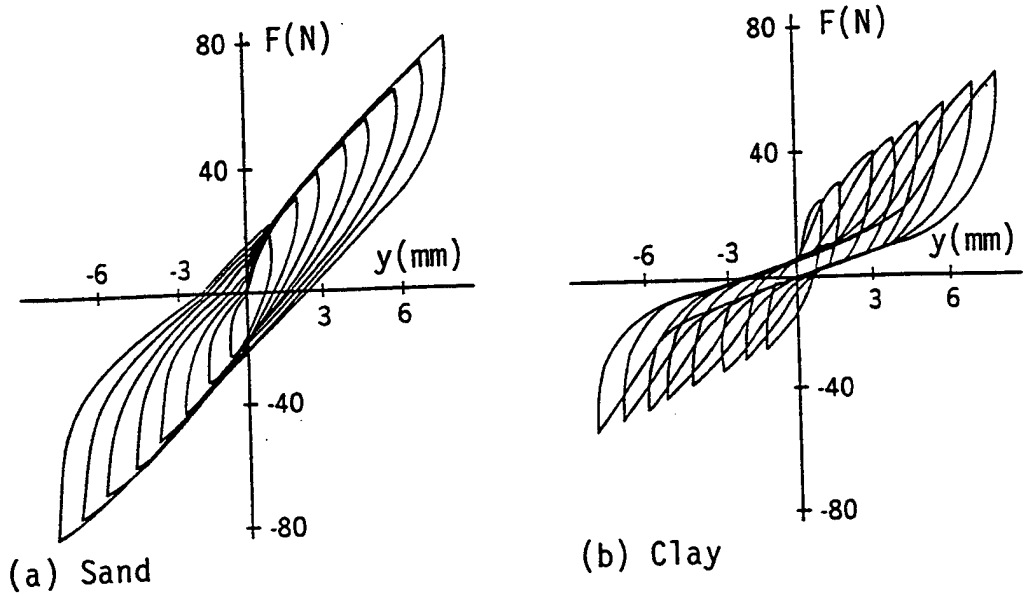

Figure 24. Cyclic behavior for sand and clay.

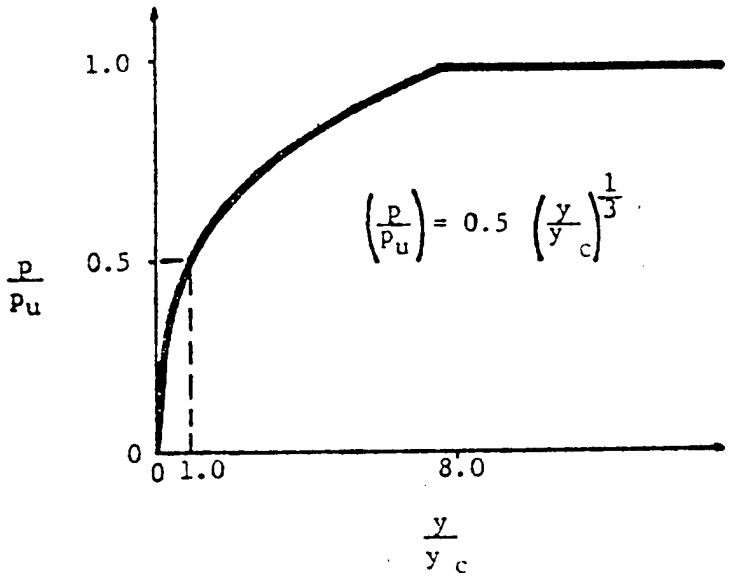

a. Static loading

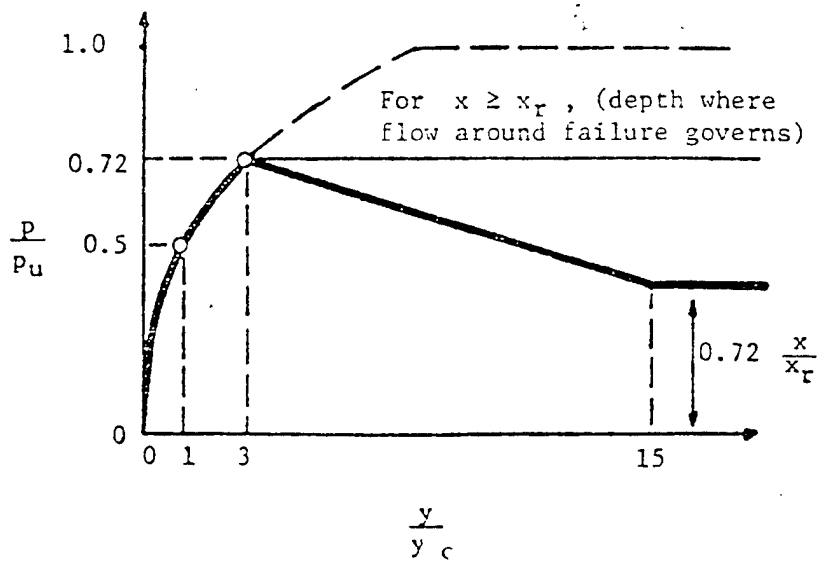

b. Cyclic loading

Figure 25. Shape of p-y curves for soft clay

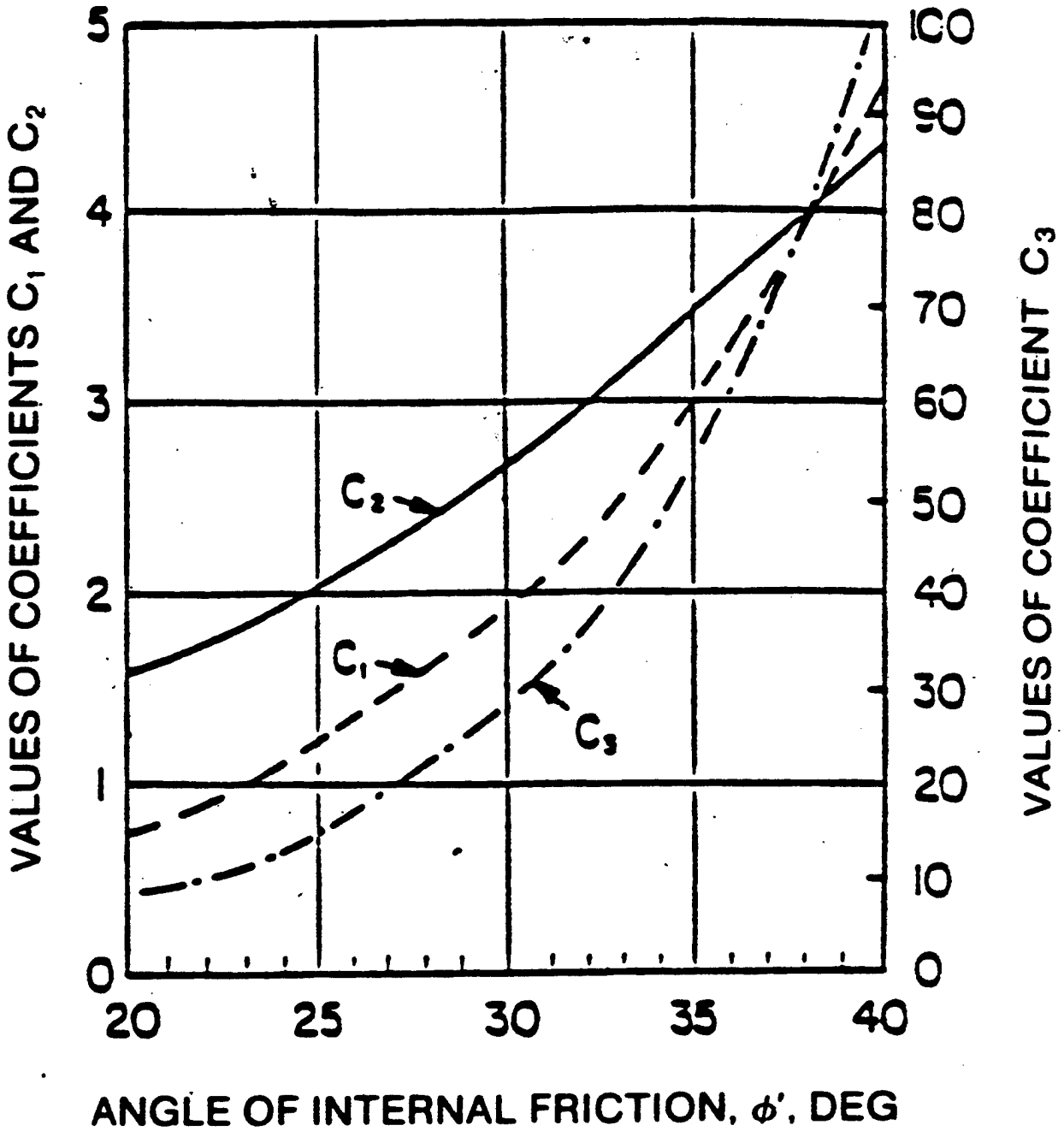

Figure 26. API Coefficients for sand.

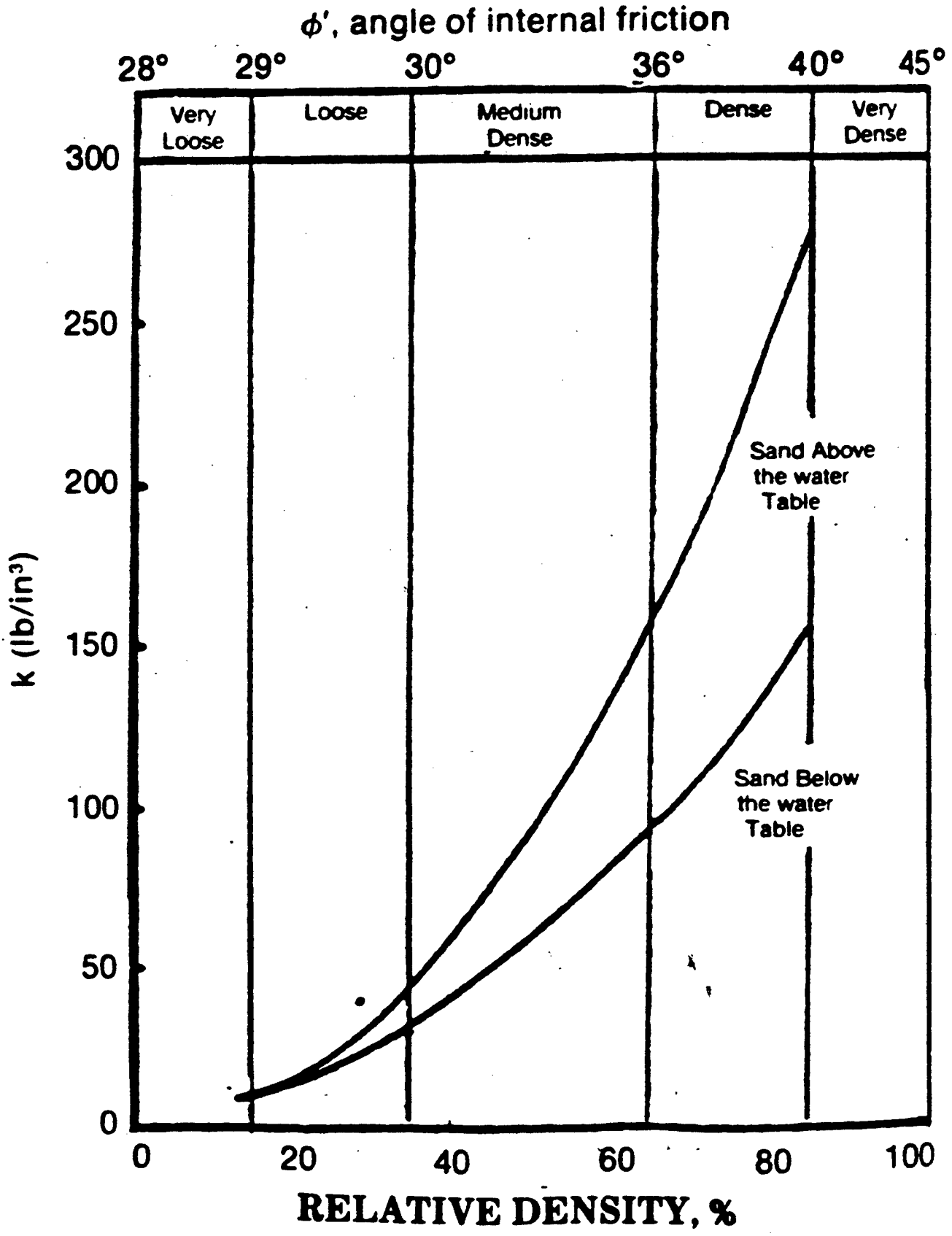

Figure 27. API initial modulus of subgrade reaction.

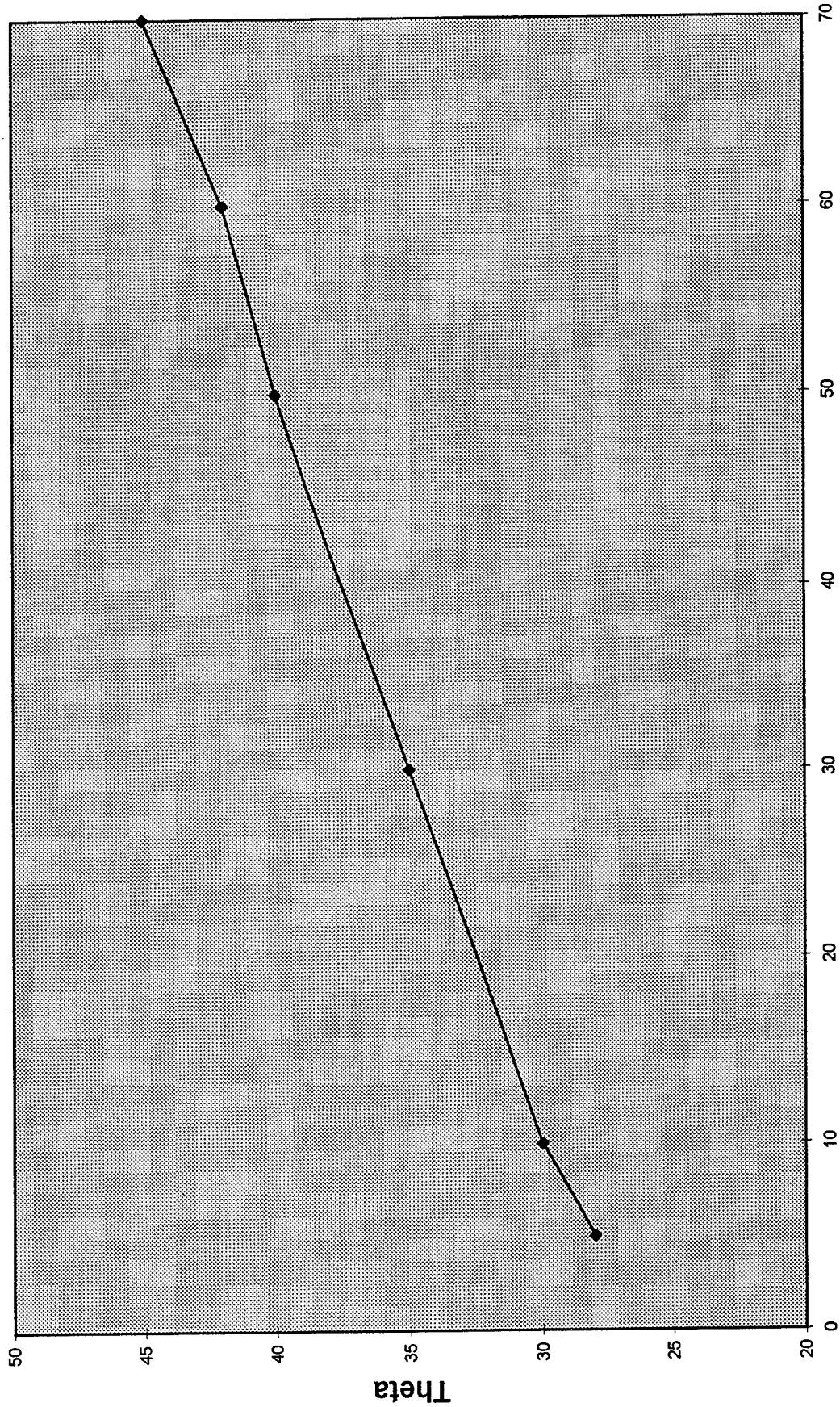

Figure 28. Cohesionless soil friction angle as a function of blow count.

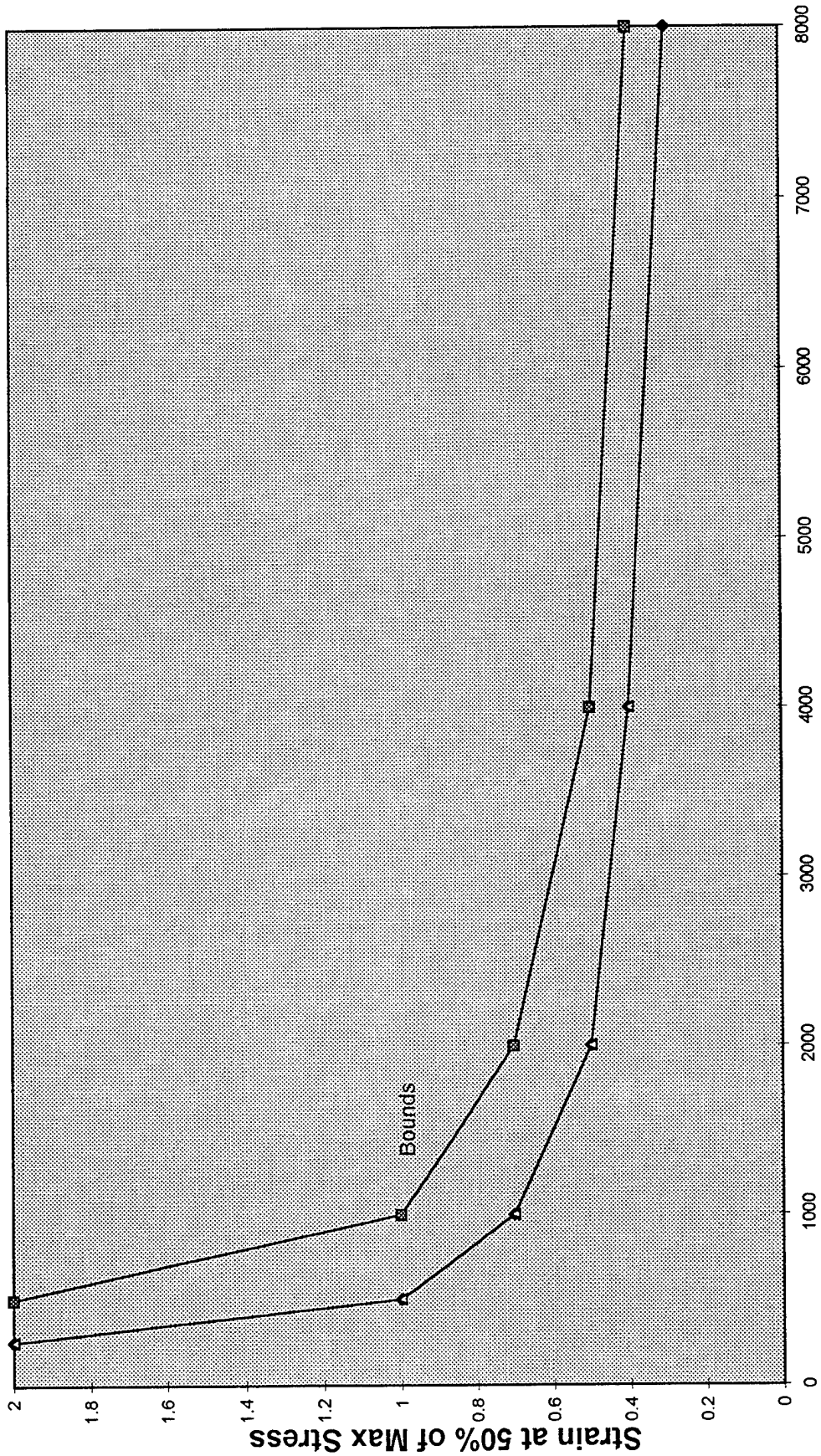

Figure 29. Strain as a function of strength.

Figure 30. Variation of buoyant weight with depth for cohesionless soil.

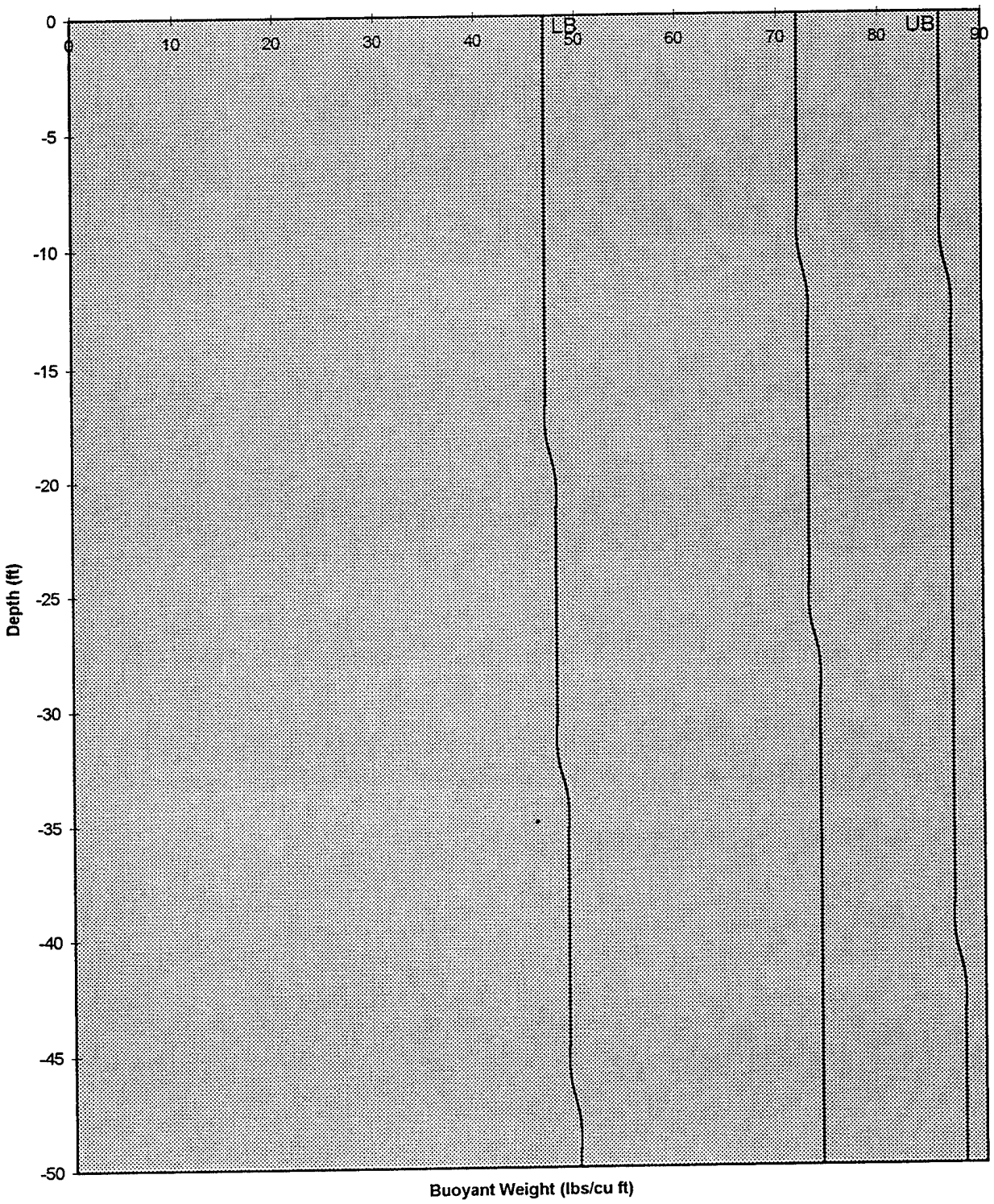

Figure 31. Variation of friction angle with depth for cohesionless soil.

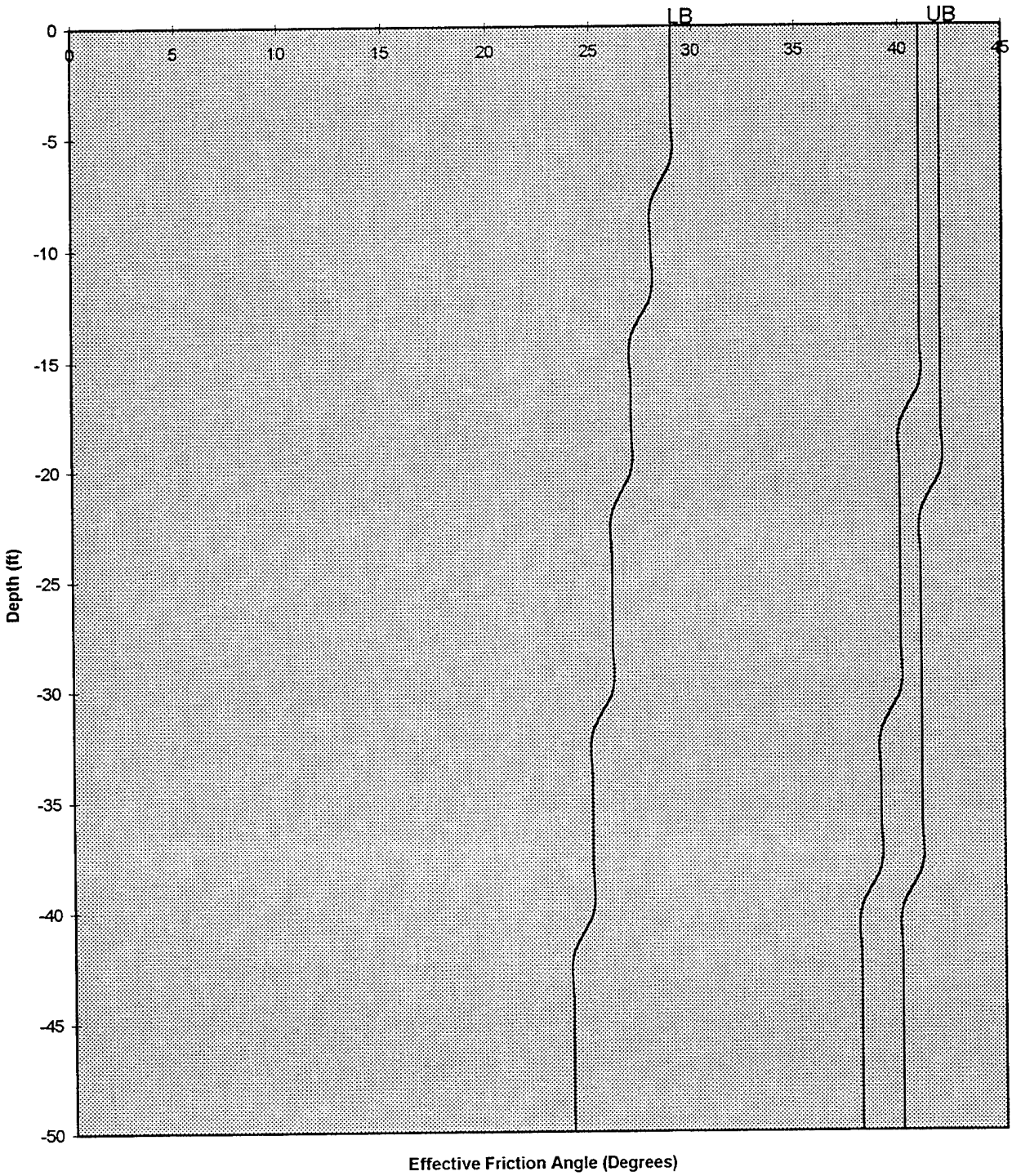

Figure 32. Variation in undrained shear strength for cohesive soil.

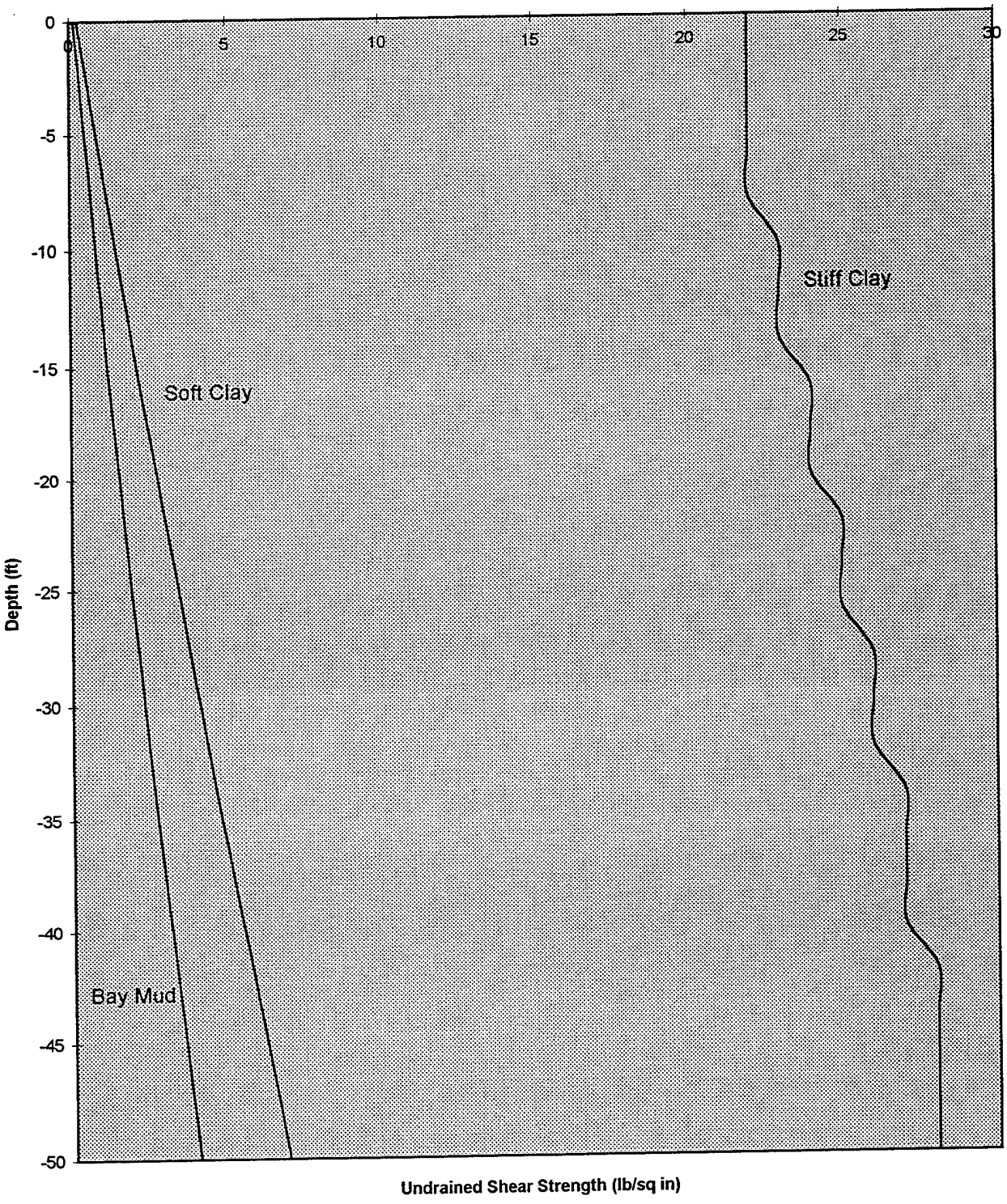

Figure 33. Variation with strain at 50% maximum stress for cohesive soil.

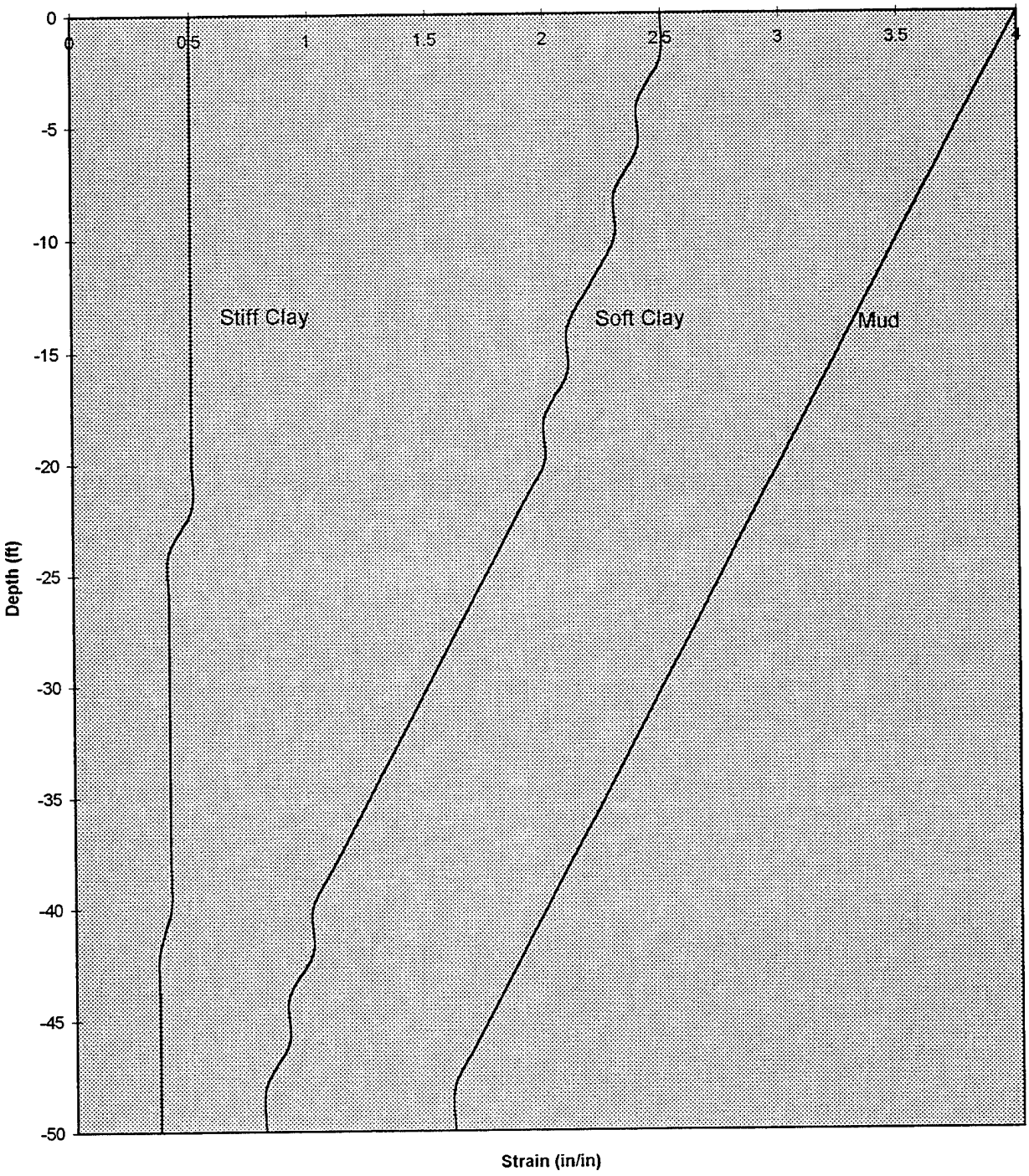

Figure 34. Variation of buoyant weight with depth for cohesive soil.

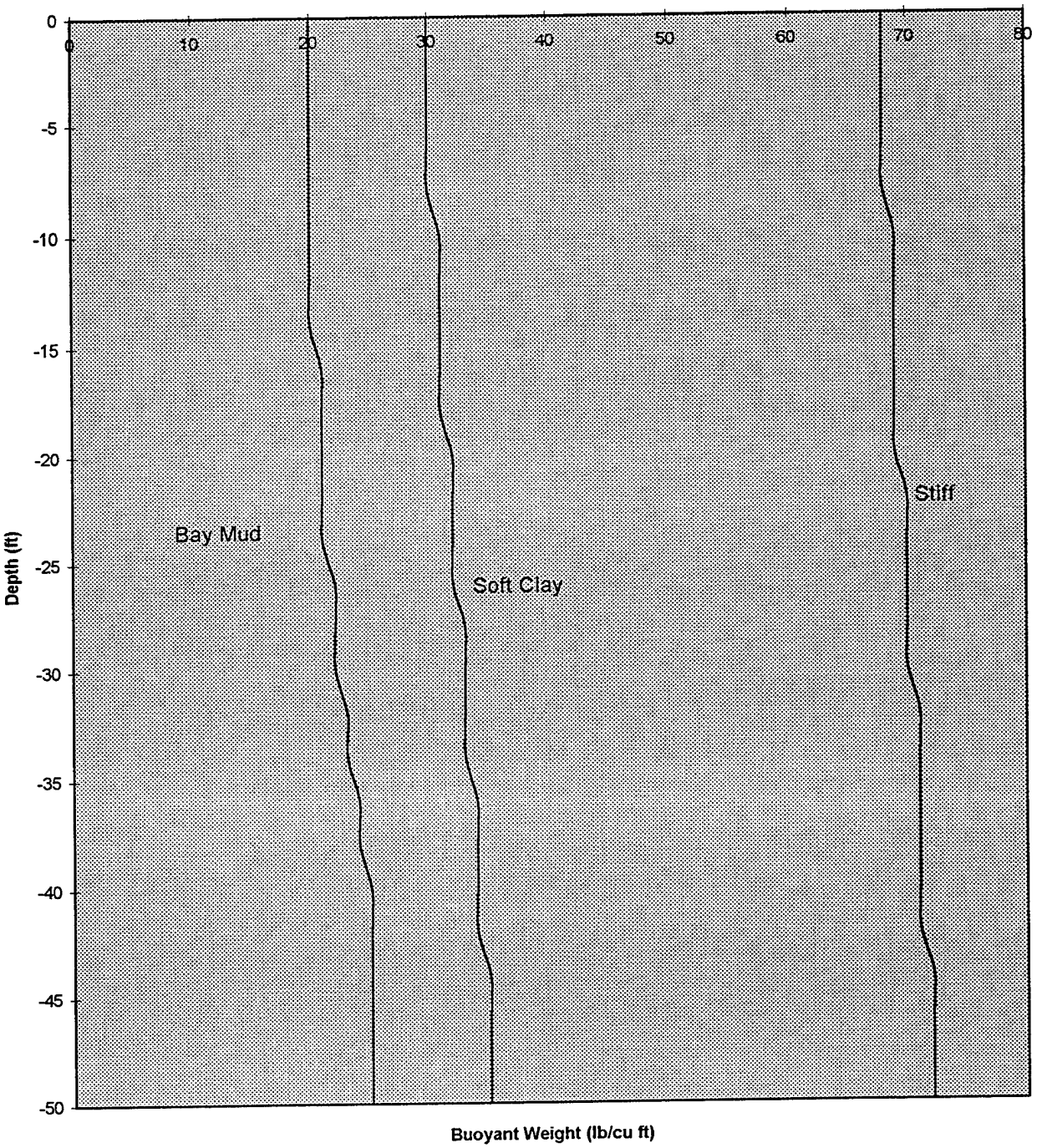

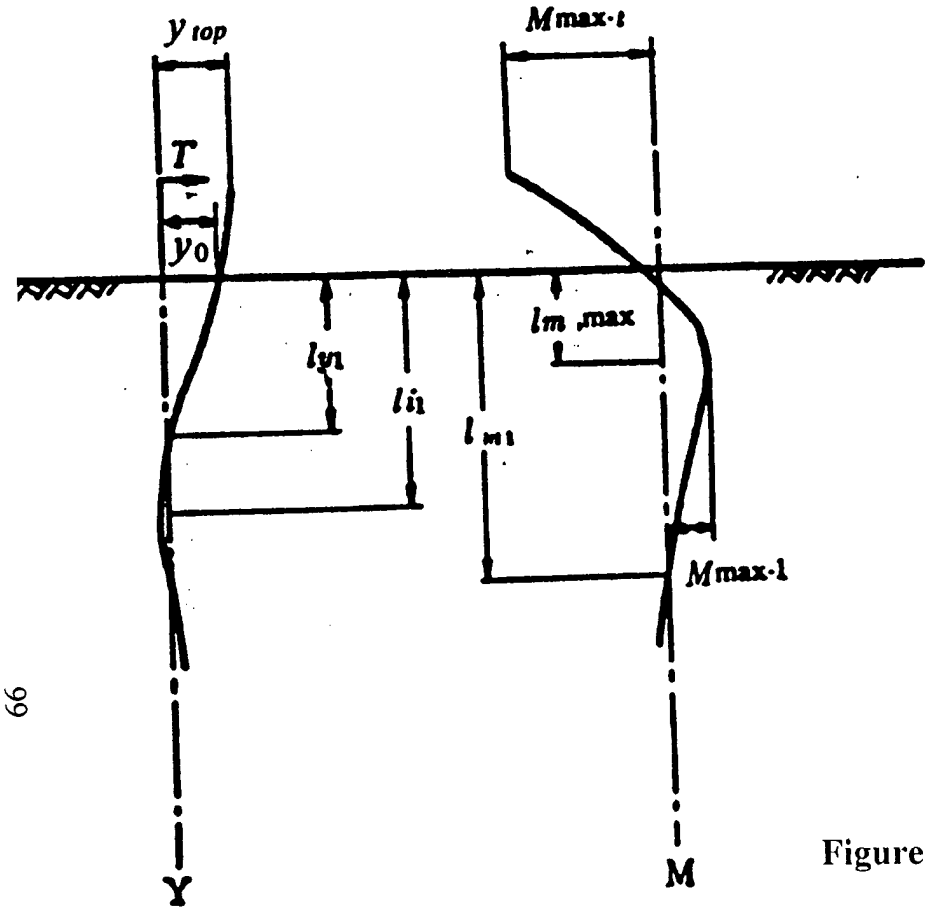

$$
\left.
\begin{aligned}
y_{\text{top}} &= \frac{(1+\beta h)^3 + 2}{12EI\beta^3}\, T \\
y_0 &= \frac{1+\beta h}{4EI\beta^3}\, T
\end{aligned}
\right\}
$$

$$
\left.
\begin{aligned}
M_{\max\text{-}t} &= \frac{(1+\beta h)}{2\beta}\, T \\
M_{\max\text{-}1} &= -h\left\{\frac{\sqrt{1+(\beta h)^2}}{2\beta h}\exp\left(-\tan^{-1}\frac{1}{\beta h}\right)\right\} T
\end{aligned}
\right\}
$$

$$
\left.
\begin{aligned}
l_{y_1} &= \frac{1}{\beta}\tan^{-1}\frac{\beta h + 1}{\beta h - 1} \\
l_{i1} &= \frac{1}{\beta}\tan^{-1}(-\beta h) \\
l_{m_1} &= \frac{1}{\beta}\left(\tan^{-1}\frac{1-\beta h}{1+\beta h} + \pi\right) \\
l_{m,\max} &= \frac{1}{\beta}\tan^{-1}\frac{1}{\beta h}
\end{aligned}
\right\}
$$

Figure 35. Pile analyzed as beam on elastic foundation.

k_h: Coefficient of lateral subgrade reaction (kgf/cm³)

l_{i1}: Depth of the first zero point of deflection angle for a free-head pile or of the second zero point of deflection angle for a fixed-head pile (cm)

l_{m1}: Depth of the first zero point of bending moment for a free-head pile or of the second zero point of bending moment for a fixed-head pile (cm)

l_{y1}: Depth of the first zero point of displacement (cm)

$l_{m,\max}$: Depth to cause the maximum bending moment (excluding the pile head) (cm)

M_1: Bending moment above the ground (kgf • cm)

M_2: Bending moment in the ground (kgf • cm)

$M_{\max}$: Maximum bending moment of a free-head pile (kgf • cm)

$M_{\max\text{-}t}$: Bending moment of the head of a fixed-head pile (kgf • cm)

$M_{\max\text{-}1}$: Maximum bending moment of a fixed-head pile in the ground (kgf • cm)

T: Horizontal force acting on the pile head (kgf)

y_0: Displacement of a pile at ground surface (cm)

y_{top}: Pile head displacement (cm)

E_s: Subgrade elastic modulus (kgf/cm²)

B: Pile width (or diameter) (cm)

EI: Pile flexural rigidity (kgf • cm²)

β: $\beta = \sqrt[4]{\frac{k_h B}{4EI}}\ (\text{cm}^{-1})$

Figure 36. Variation in pile moment at top of pile as a function of subgrade reaction.

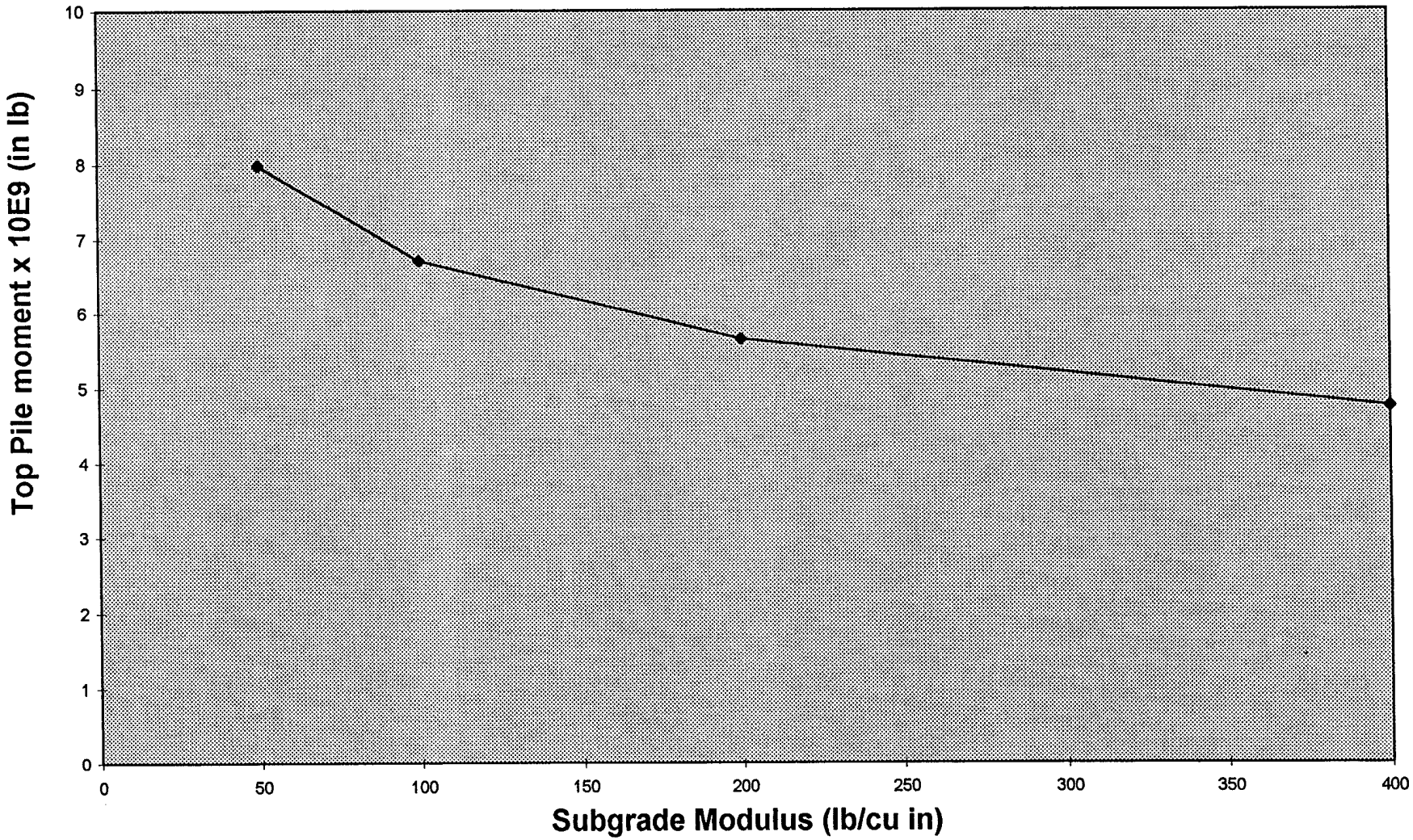

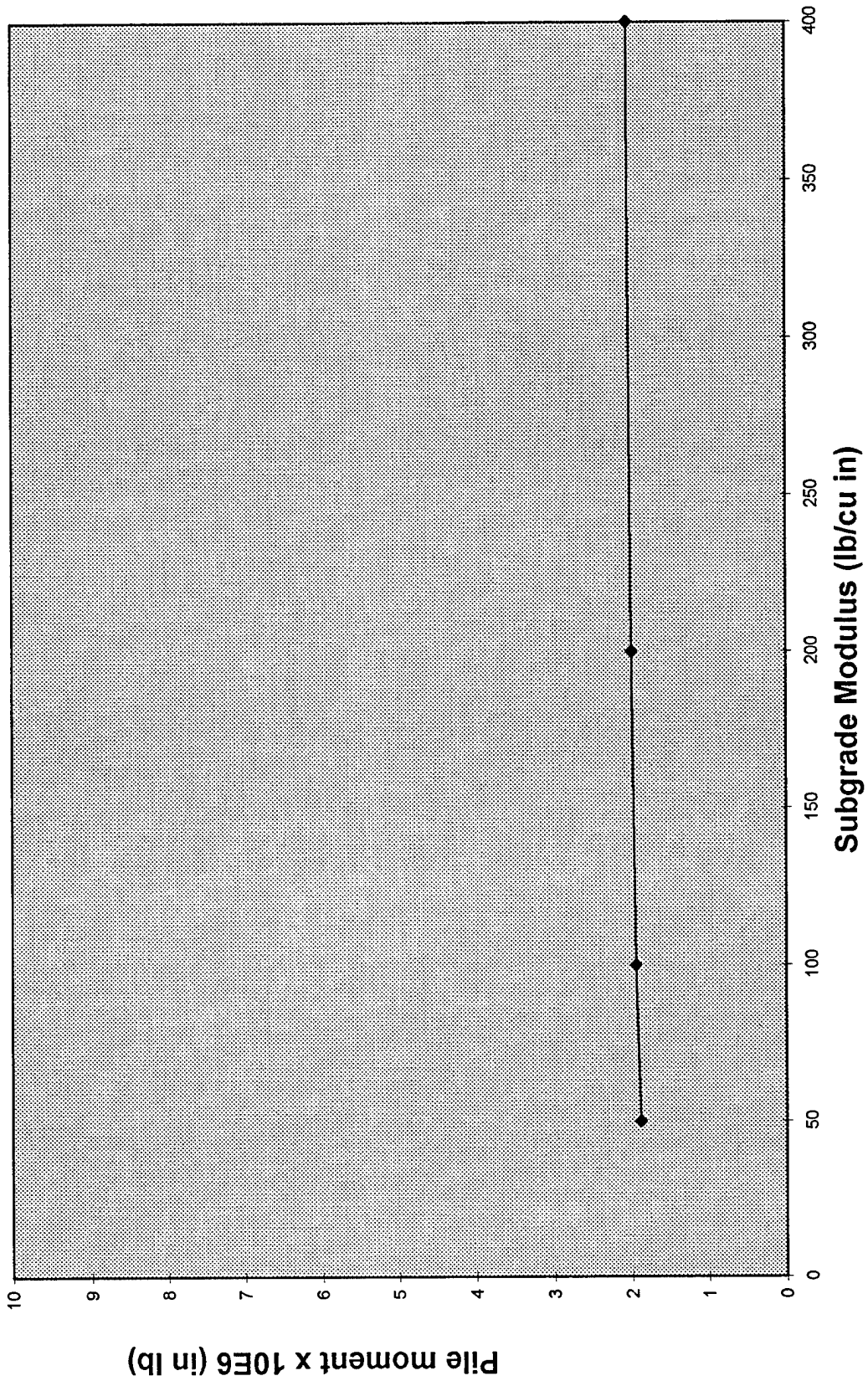

Figure 37. Variation in pile moment in soil as a function of subgrade reaction.

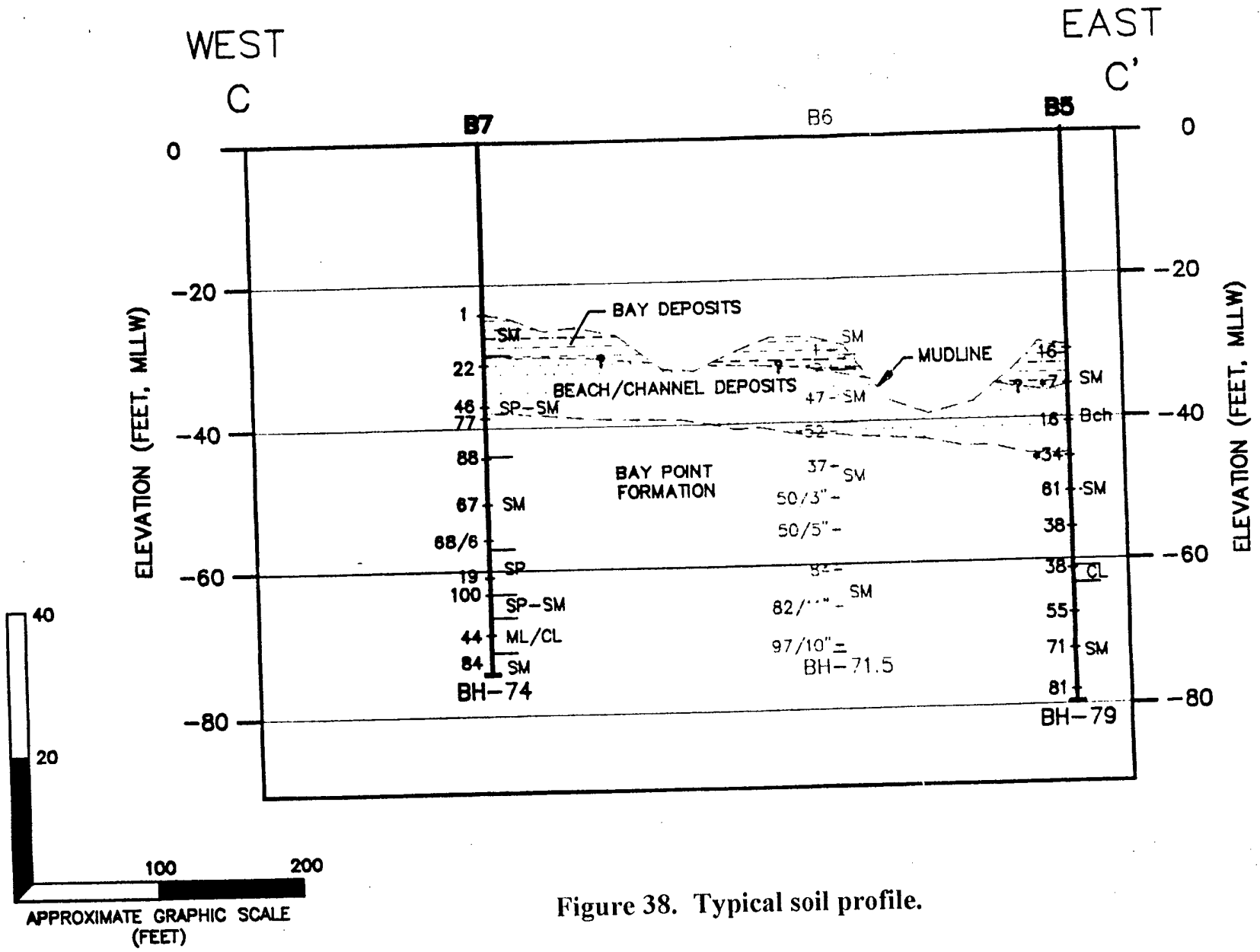

Figure 38. Typical soil profile.

Figure 39. Individual soil boring SPT test data.

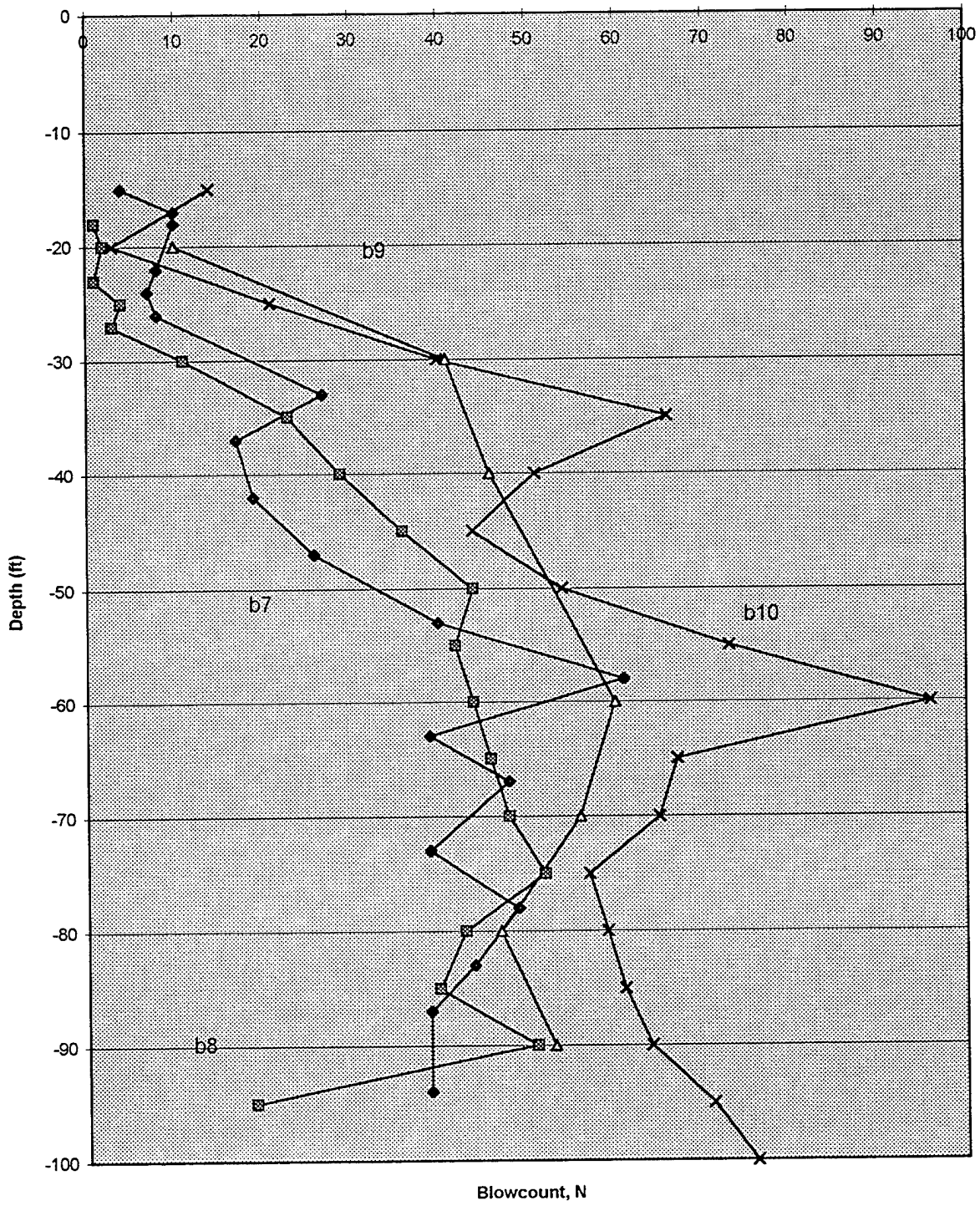

Figure 40. Variation in blowcount with depth.

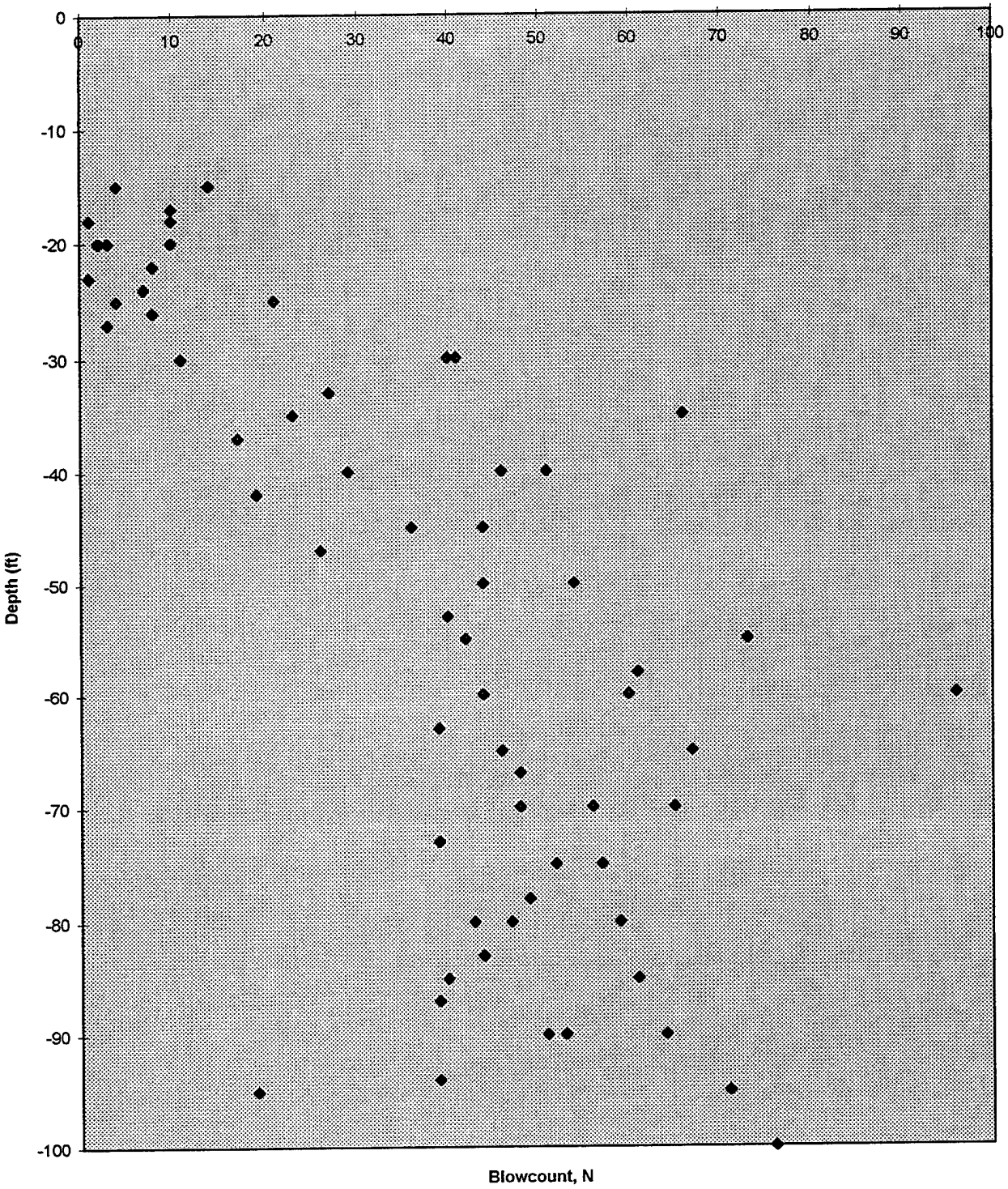

Figure 41. Finite element pile model.

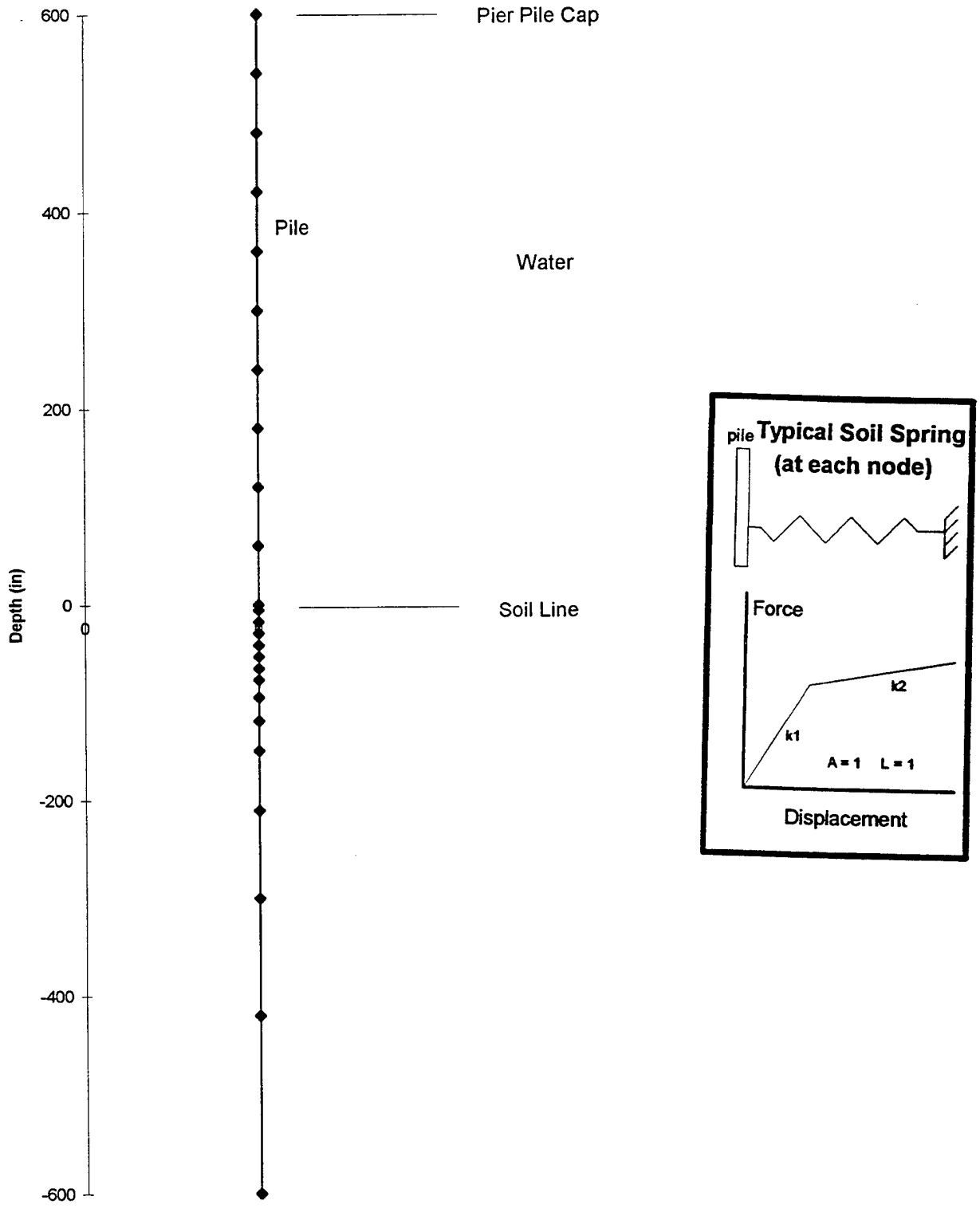

Figure 42. Variation in soil spring yield strength, 24-inch D pile.

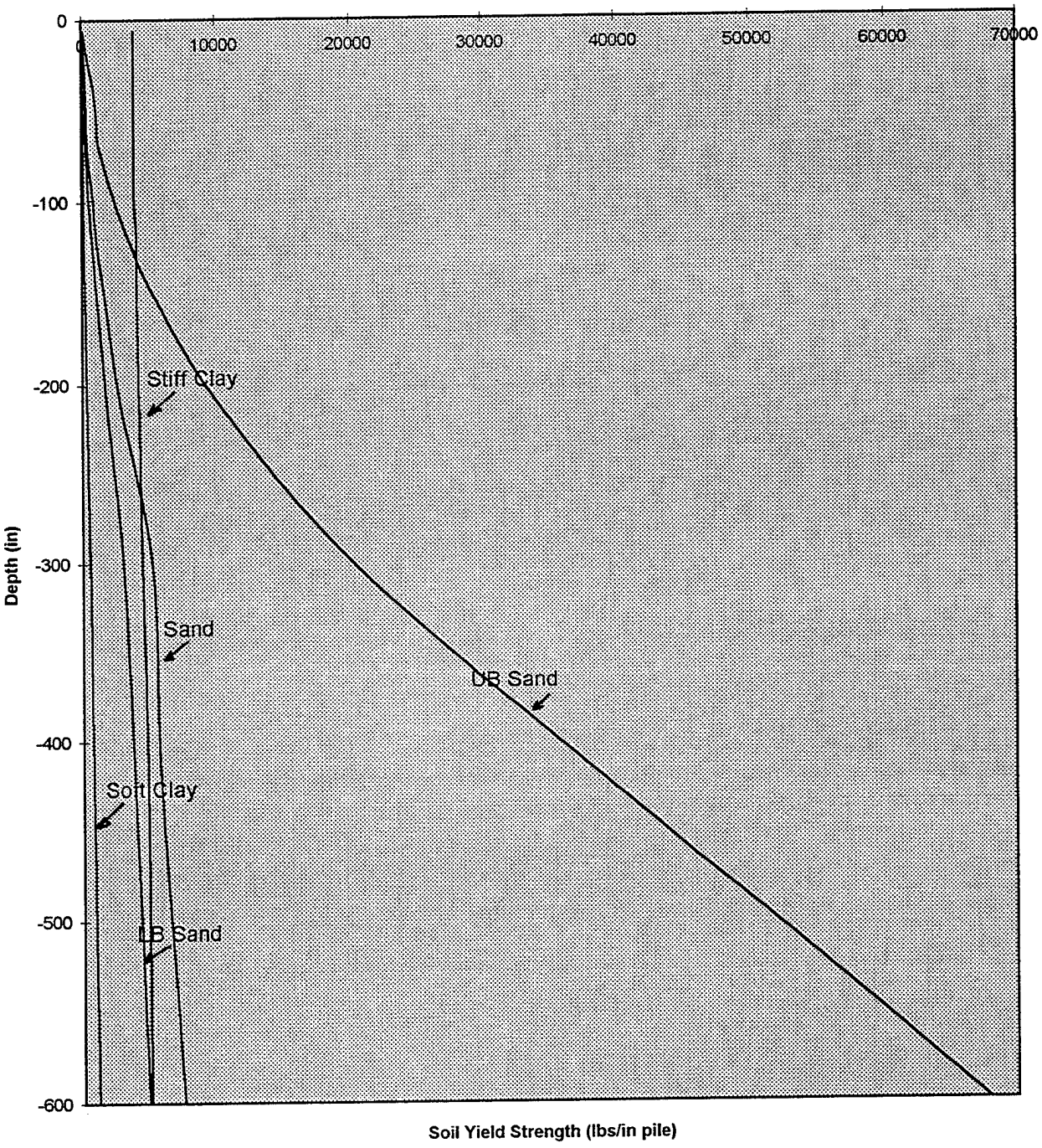

Figure 43. Variation in spring stiffness with depth, 24-inch D pile.

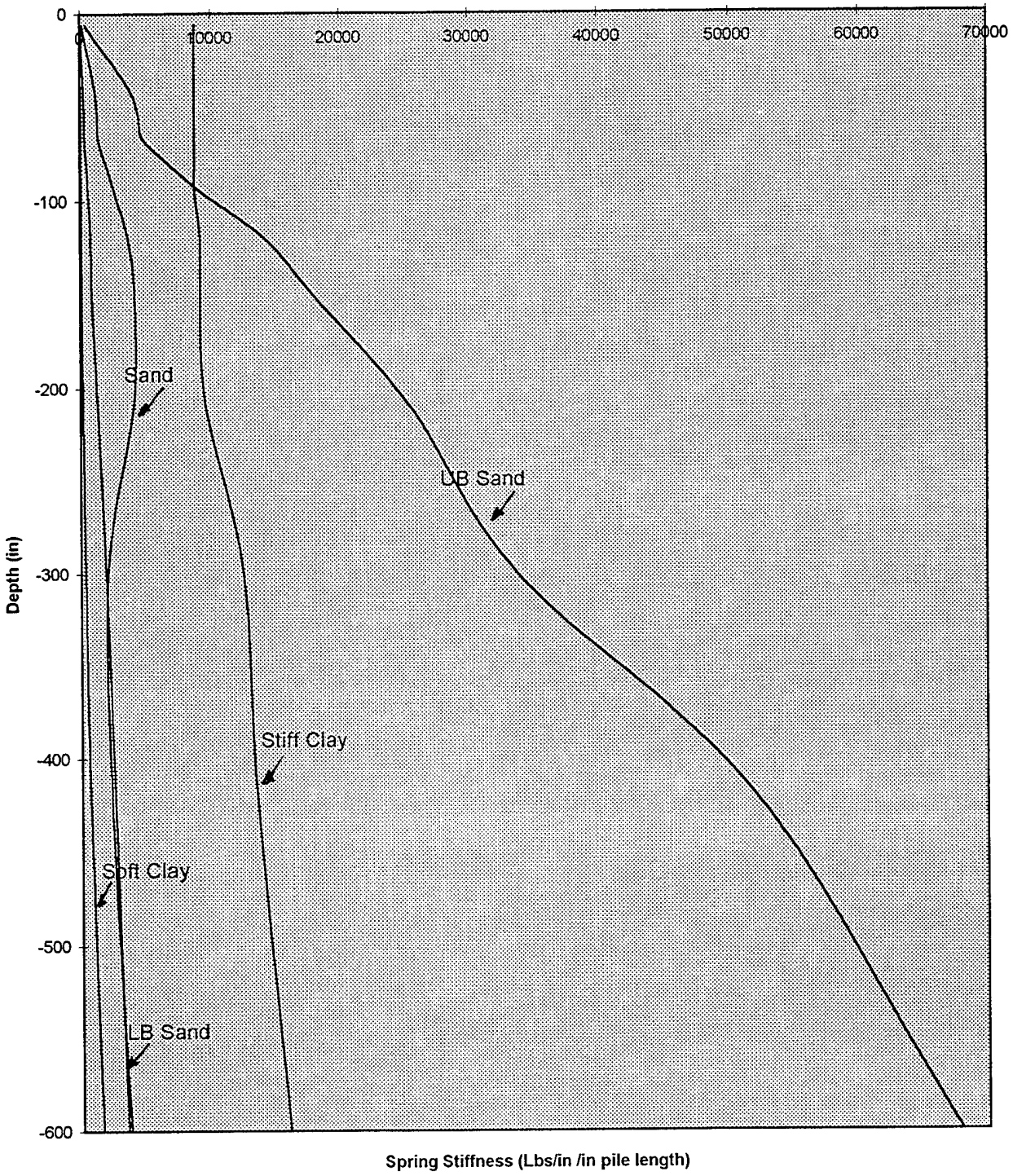

Figure 44. Displacement under 10-kip lateral load.

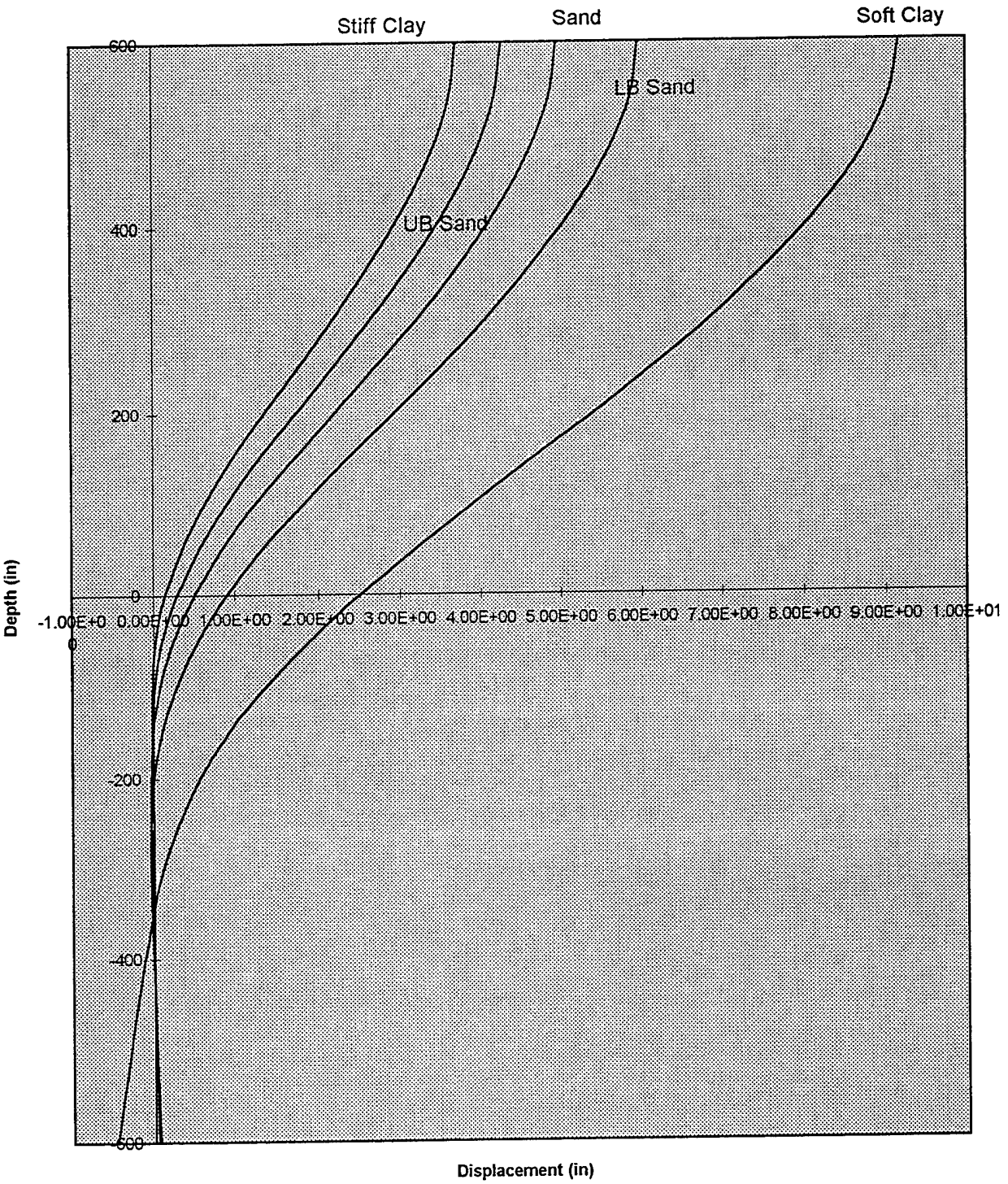

Figure 45. Pile moment at 10 kip lateral load.

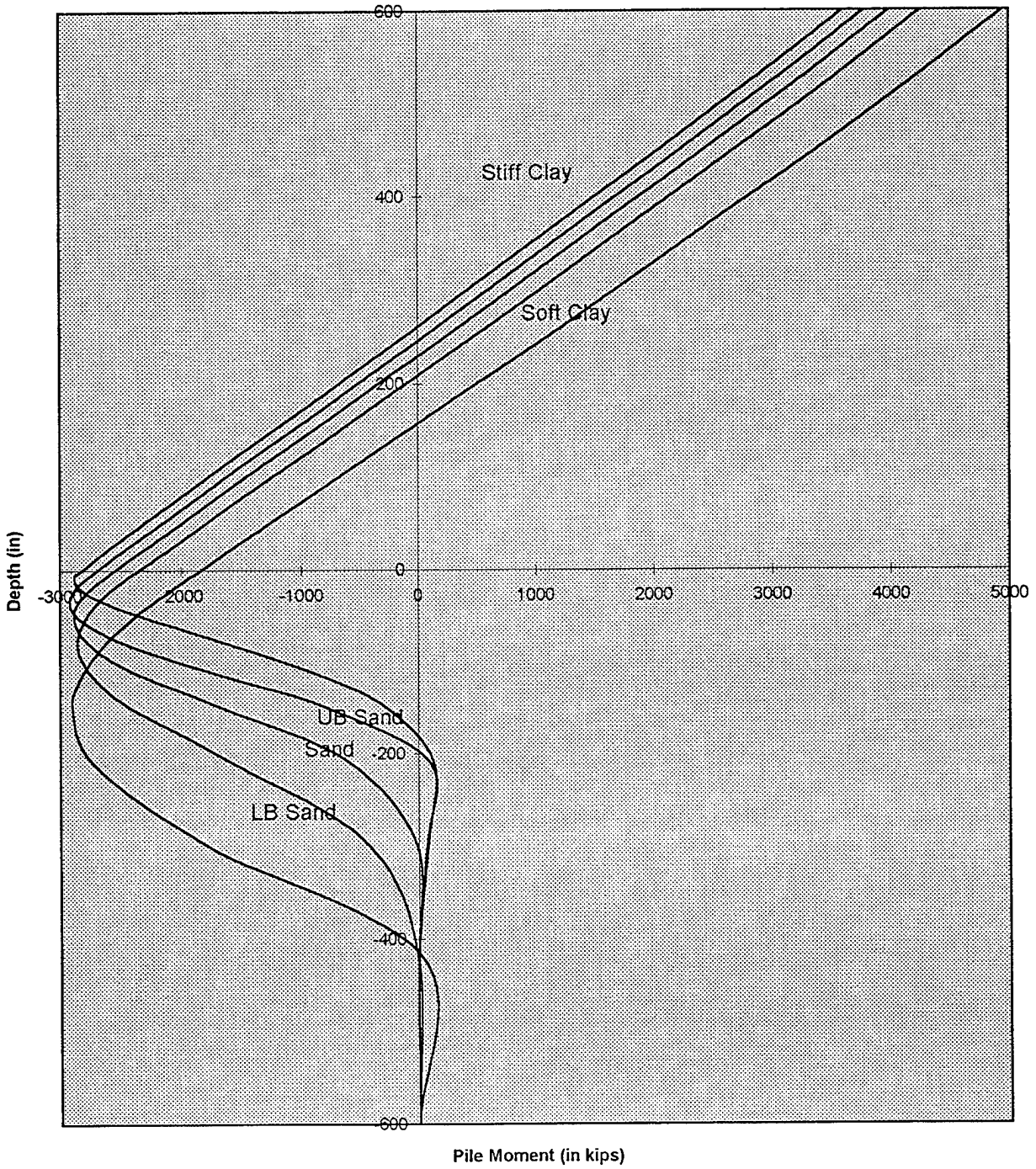

Figure 46. Displacement at collapse lateral load.

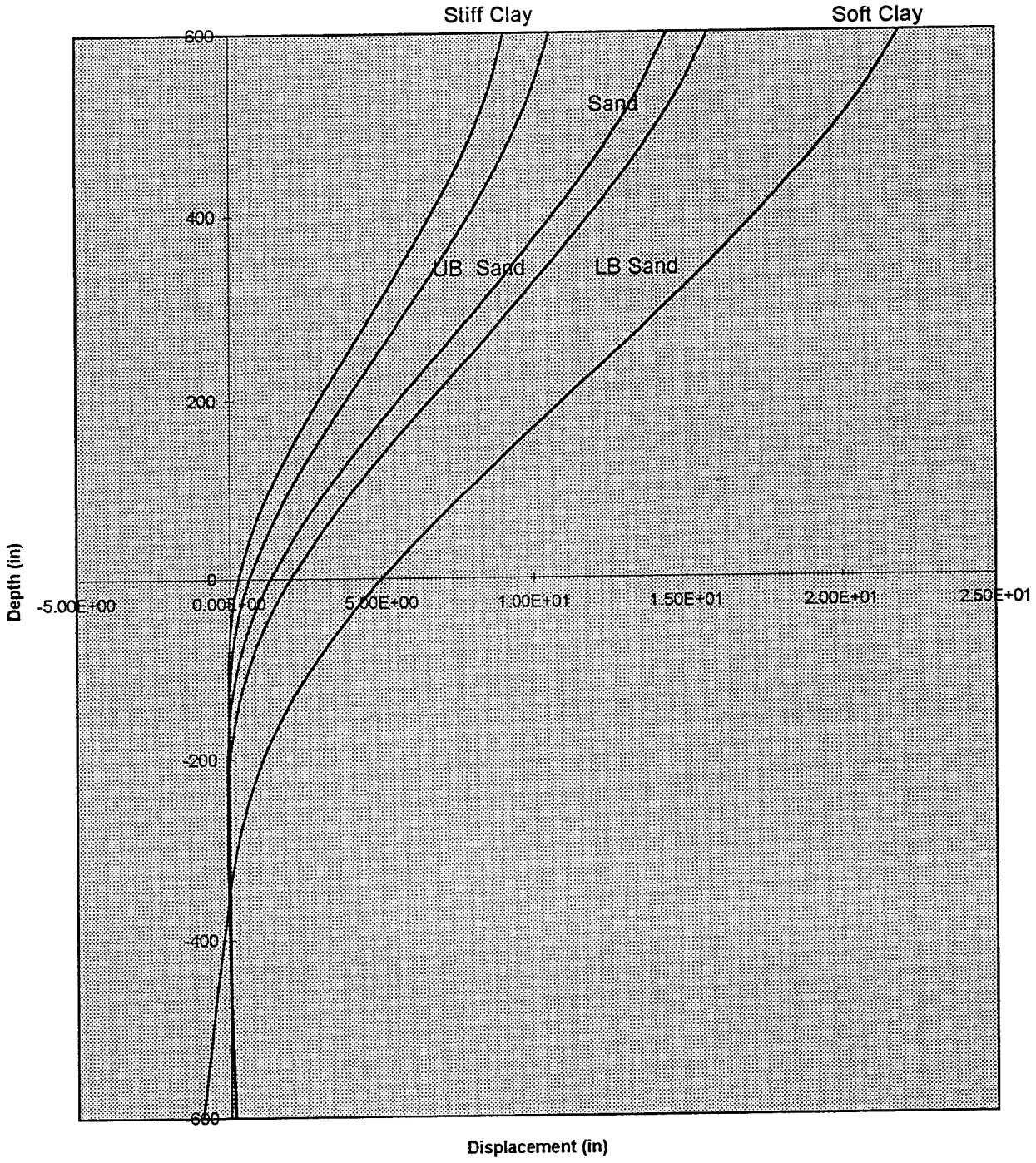

Figure 47. Pile moment at collapse.

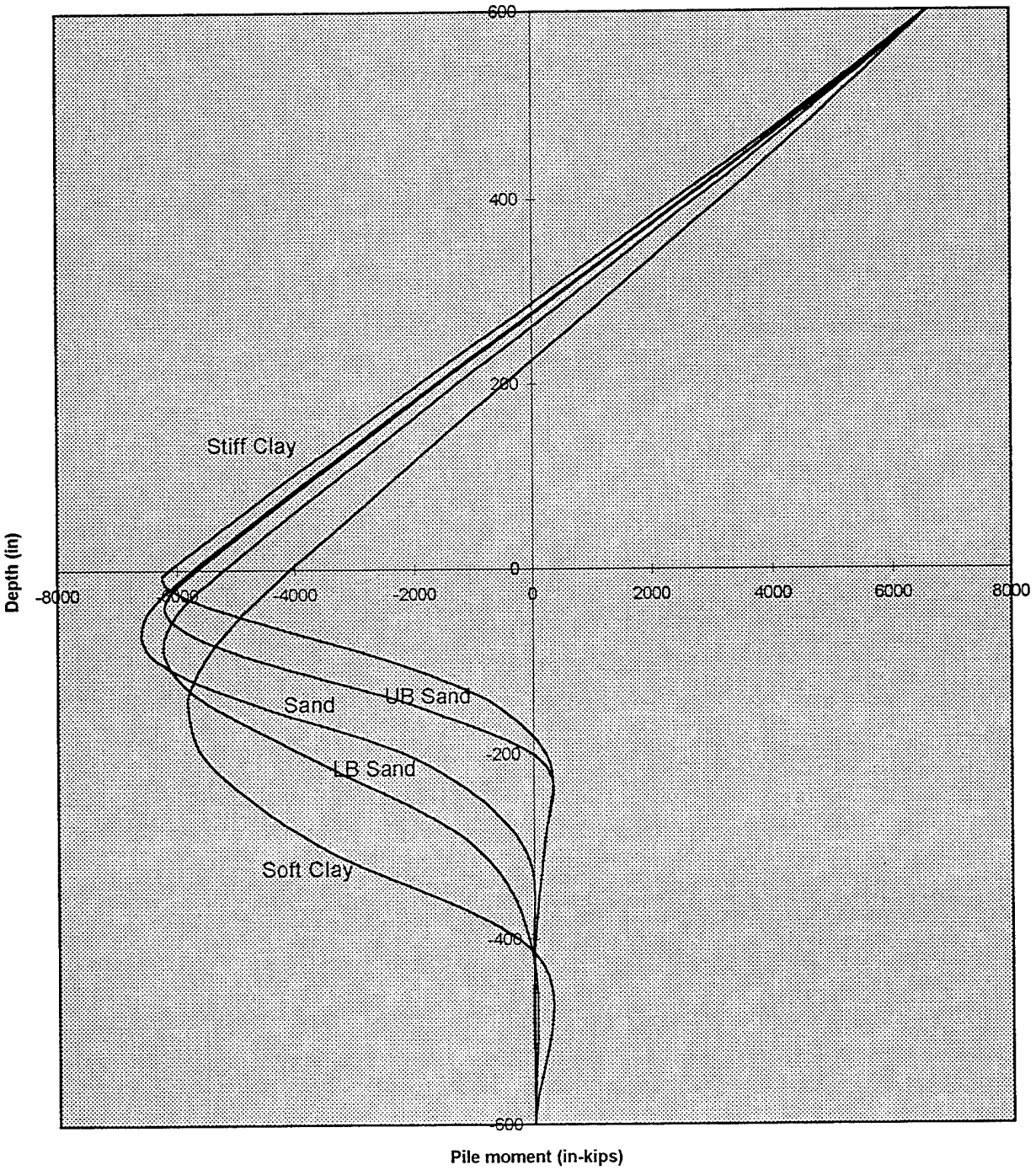

Figure 48. Displacement of 10-inch square pile in medium sand and soft clay.

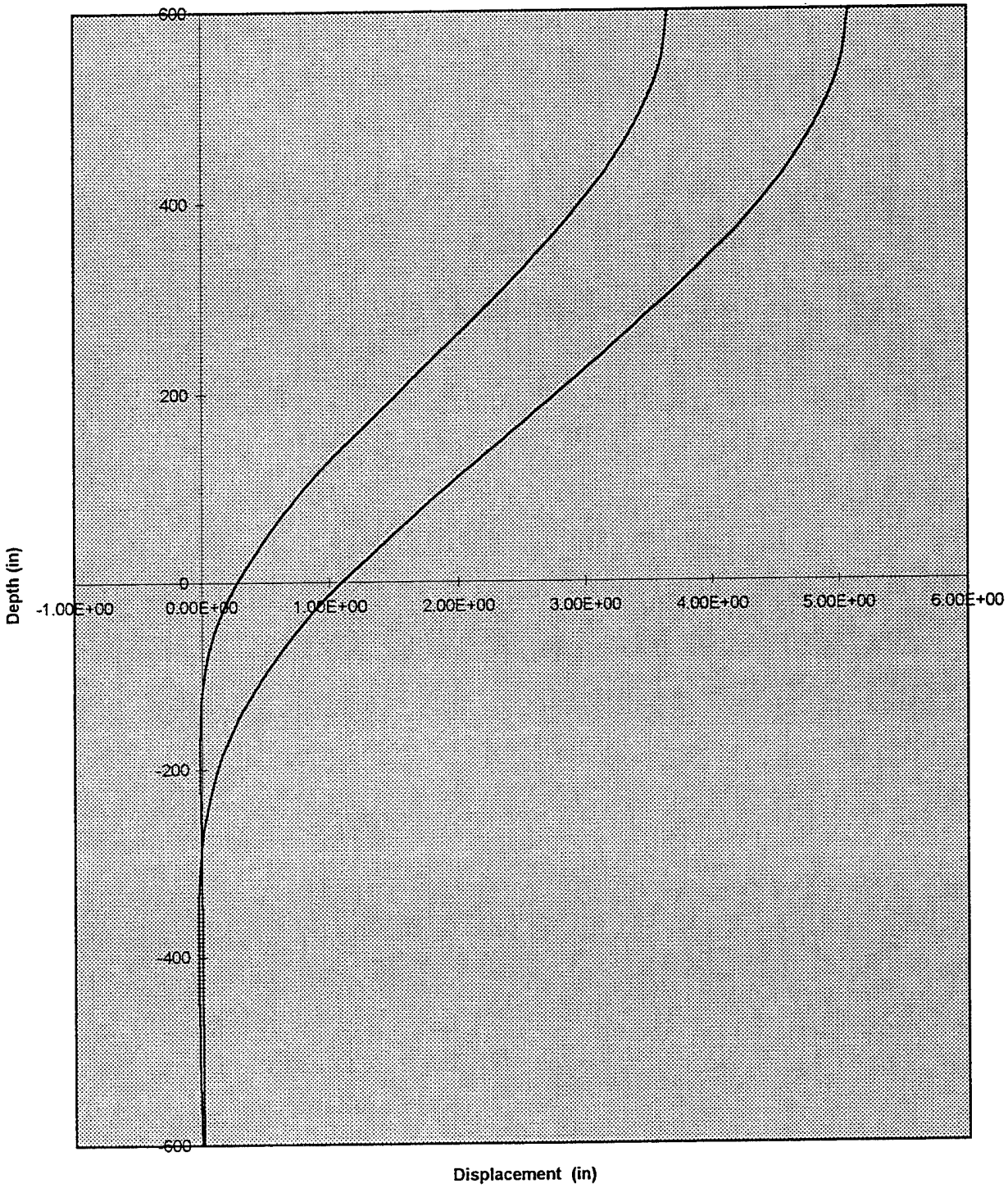

Figure 49. Moment in 10-inch square pile in medium sand and soft clay.

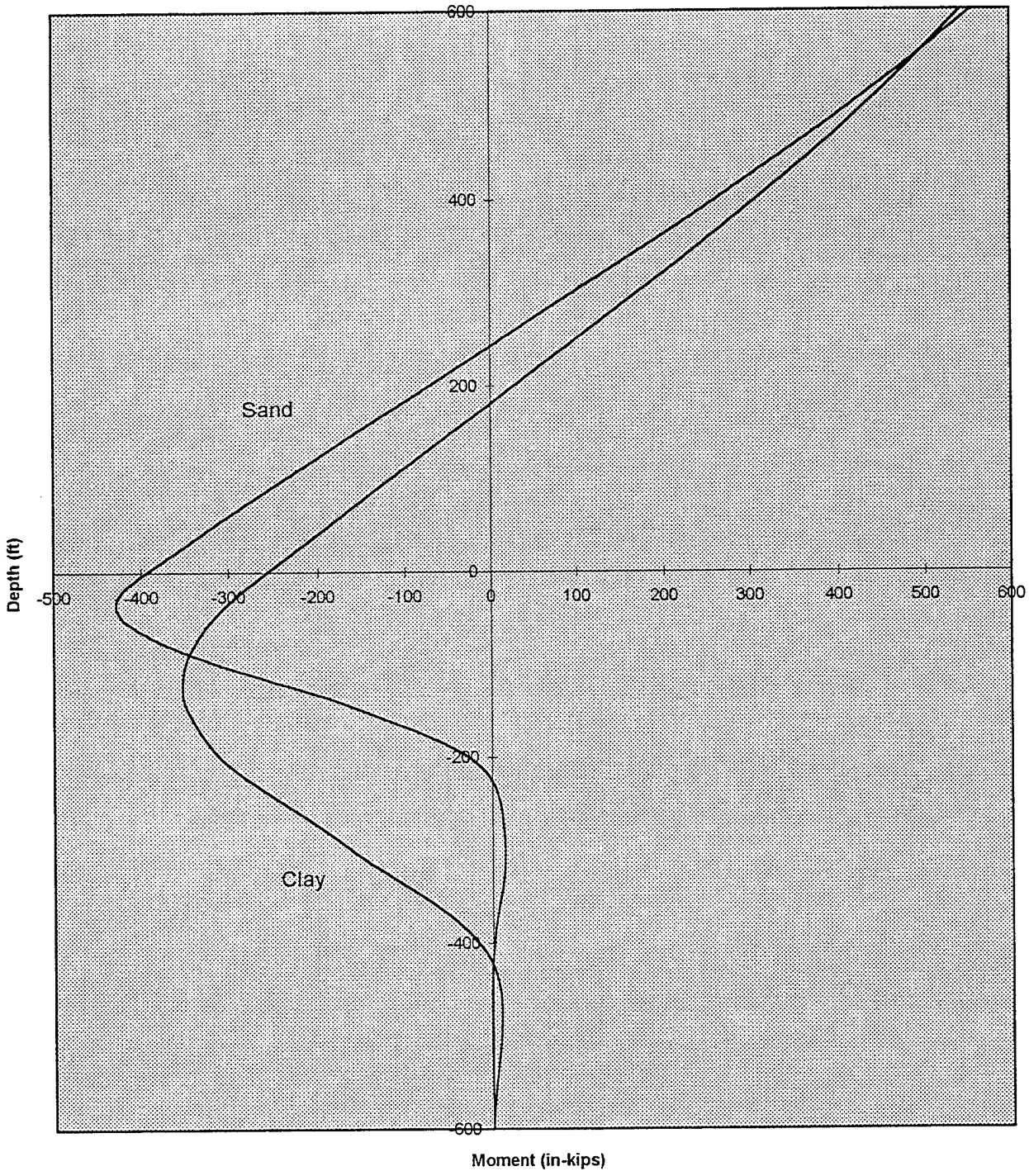

Figure 50. Pile displacement for 4 borings.

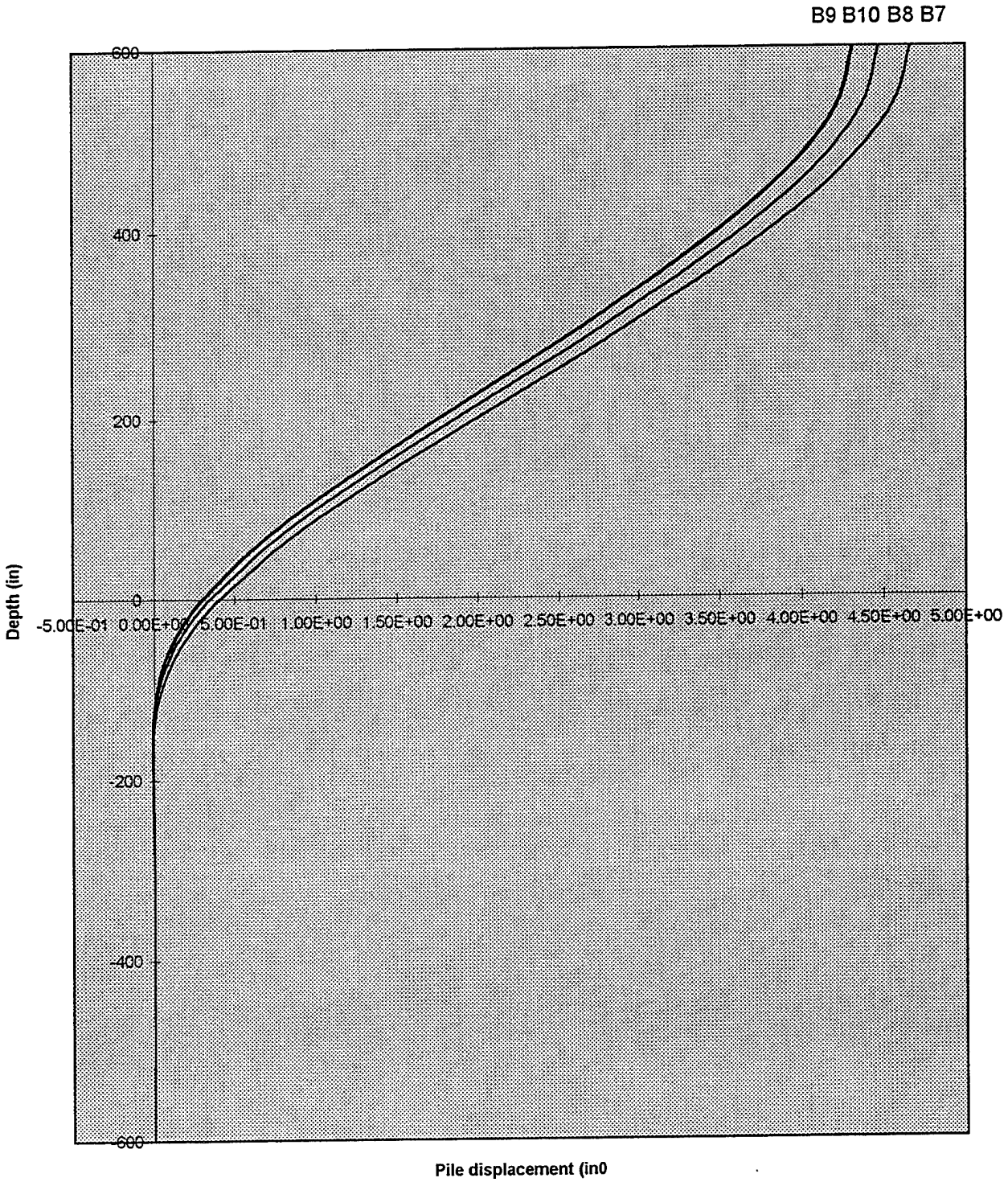

Figure 51. Pile moment for 4 borings.

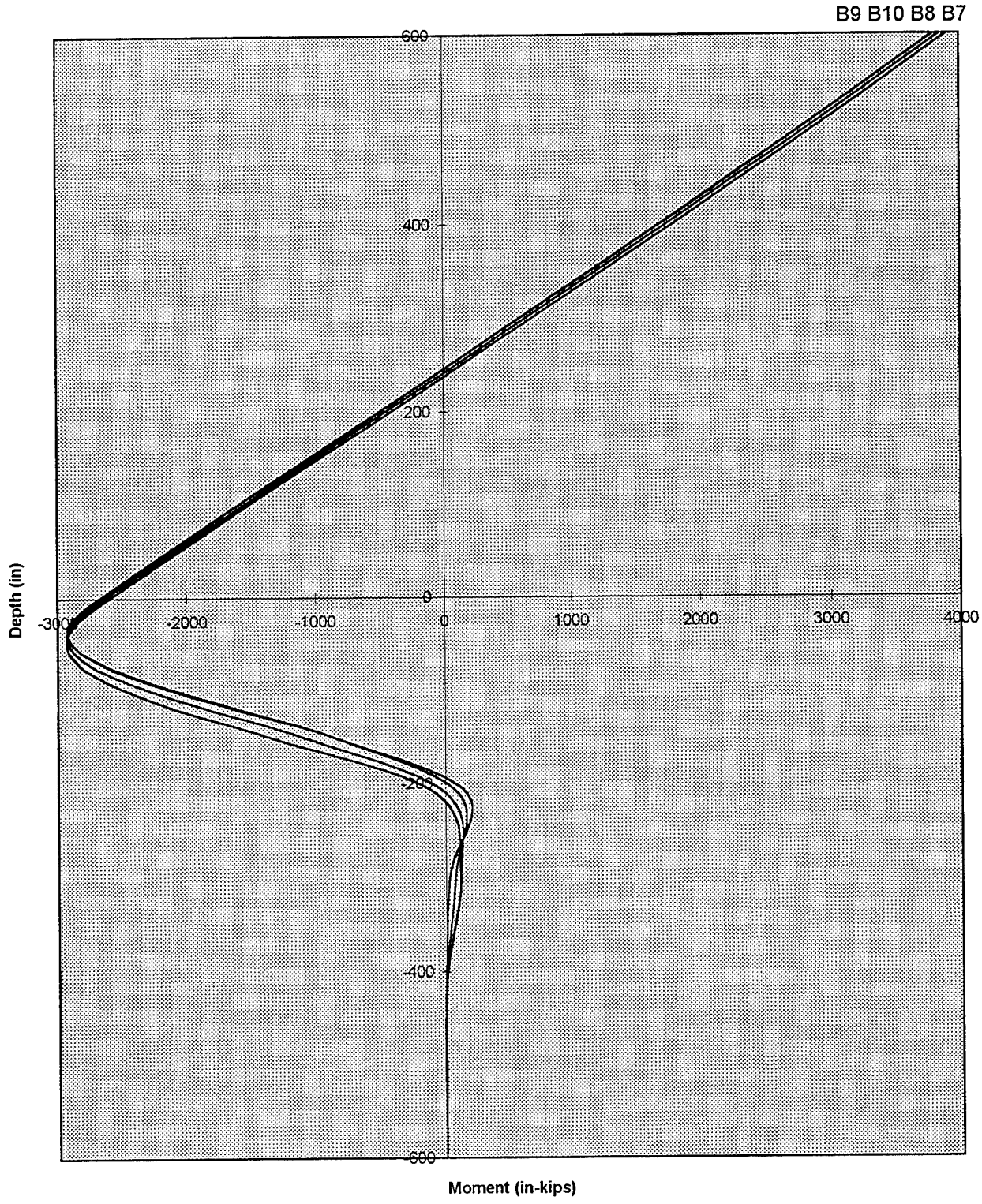

Figure 52. Pile model showing nodes and elements.

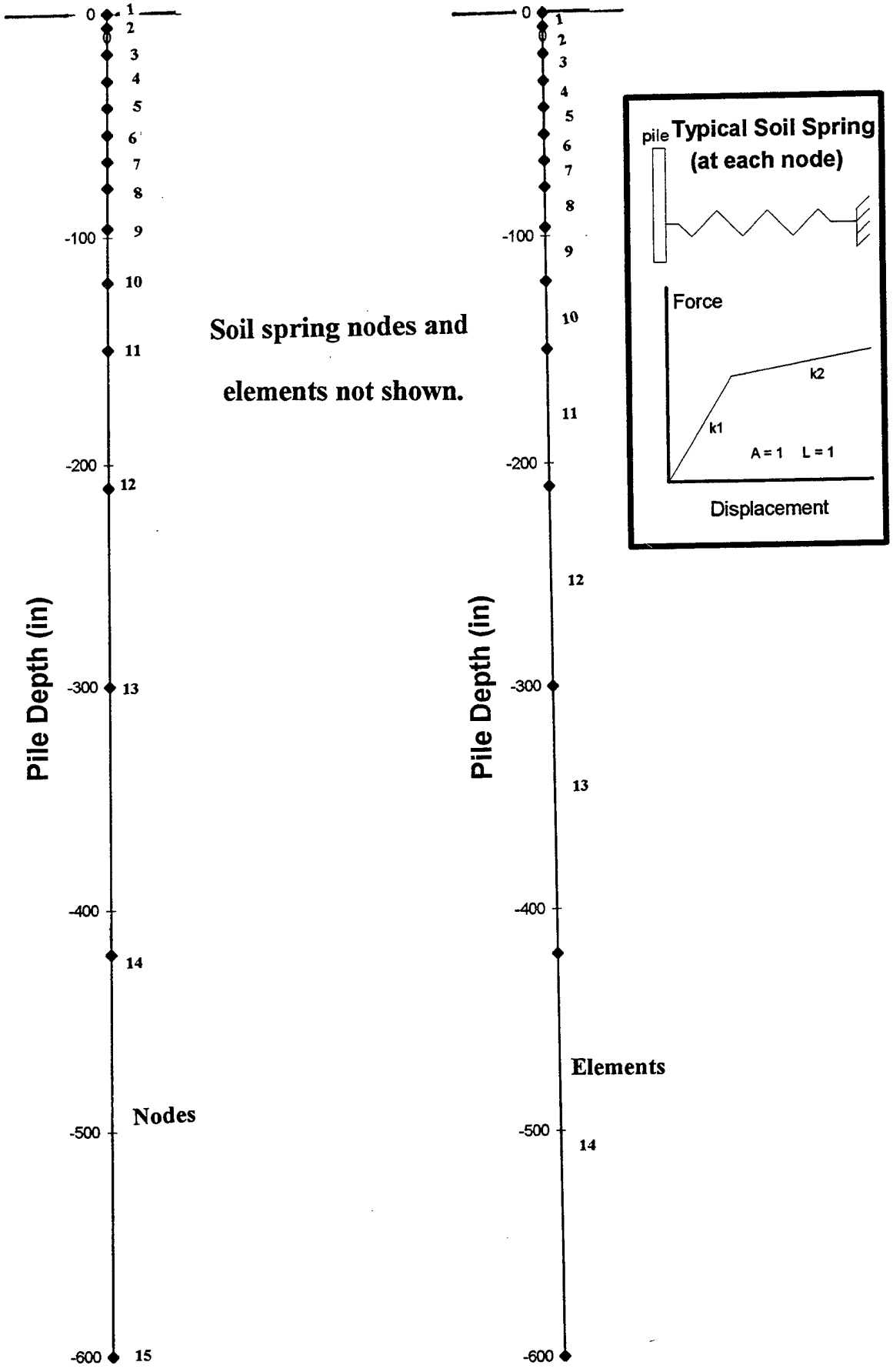

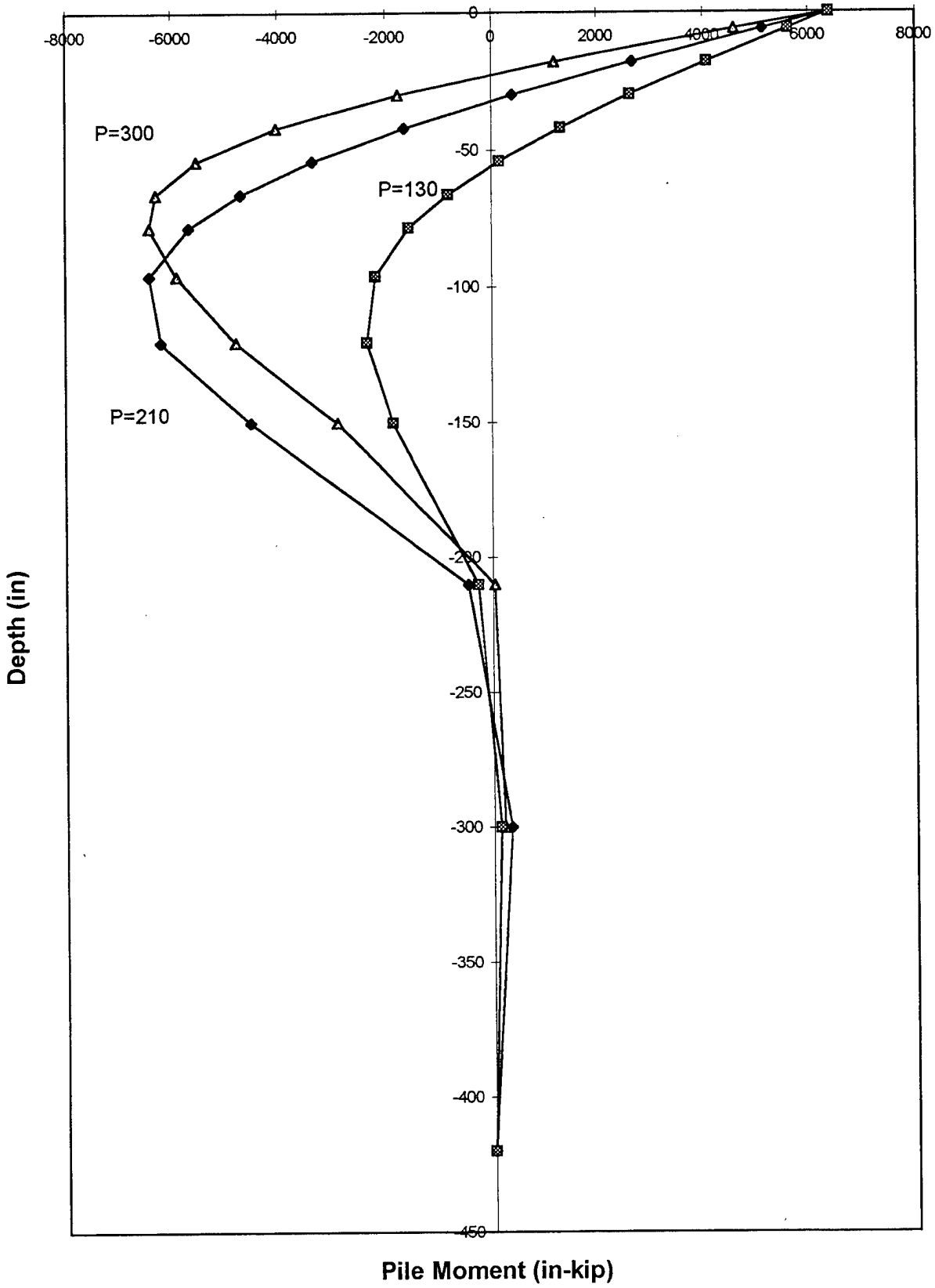

Figure 53. Pile moments at 3 lateral loads.

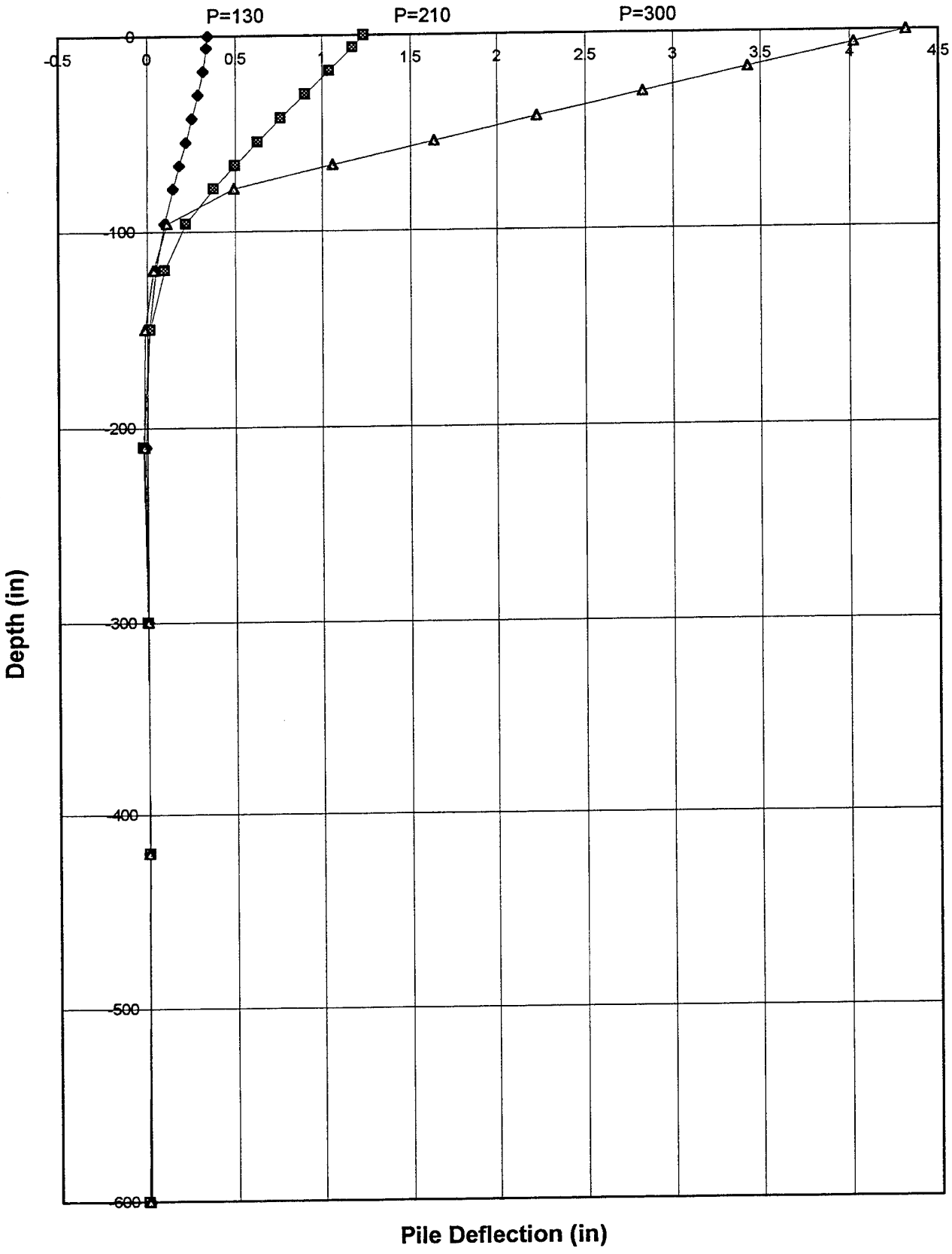

Figure 54. Pile deflection at 3 lateral loads.

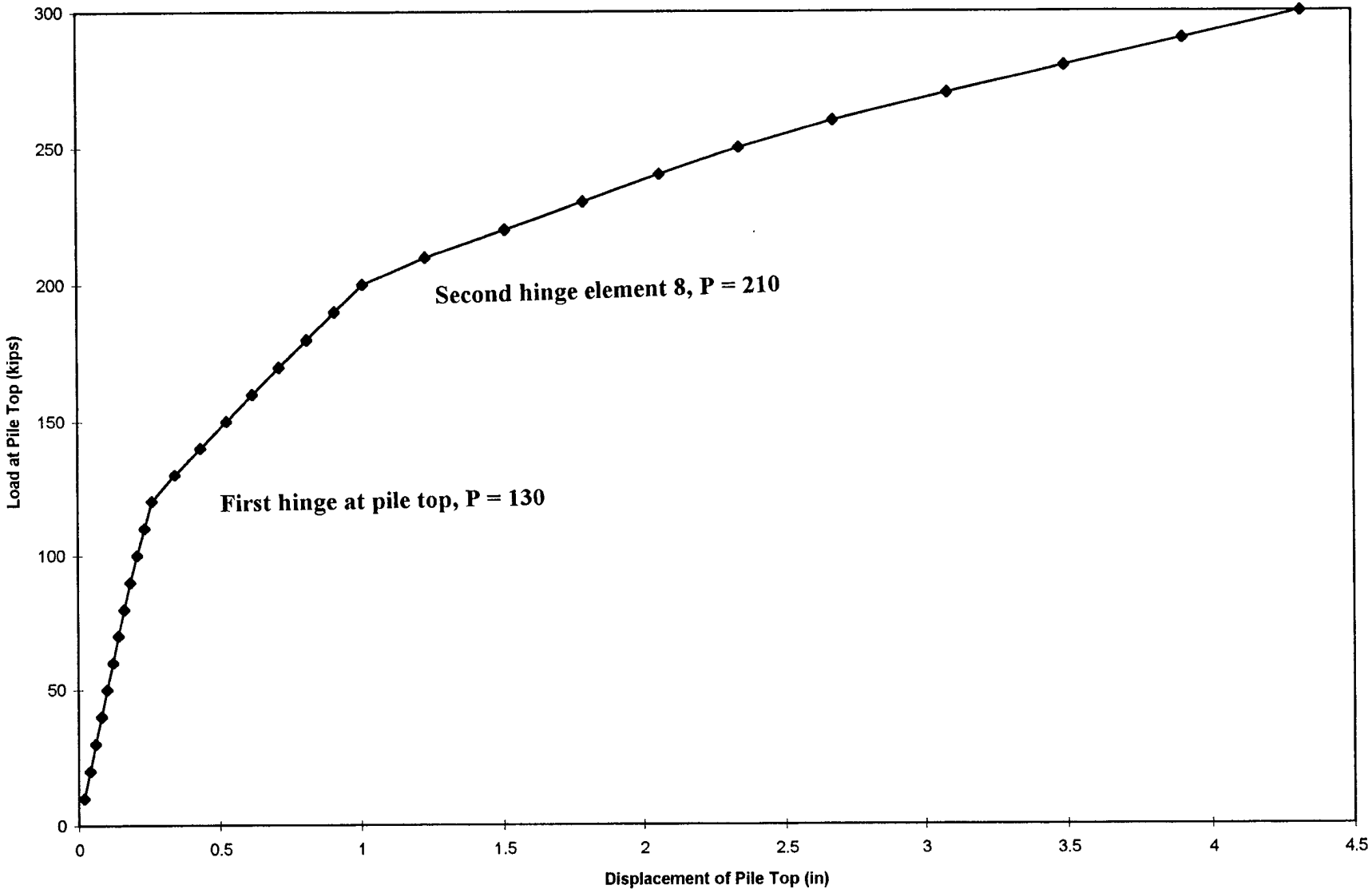

Figure 55. Pile top deflection.

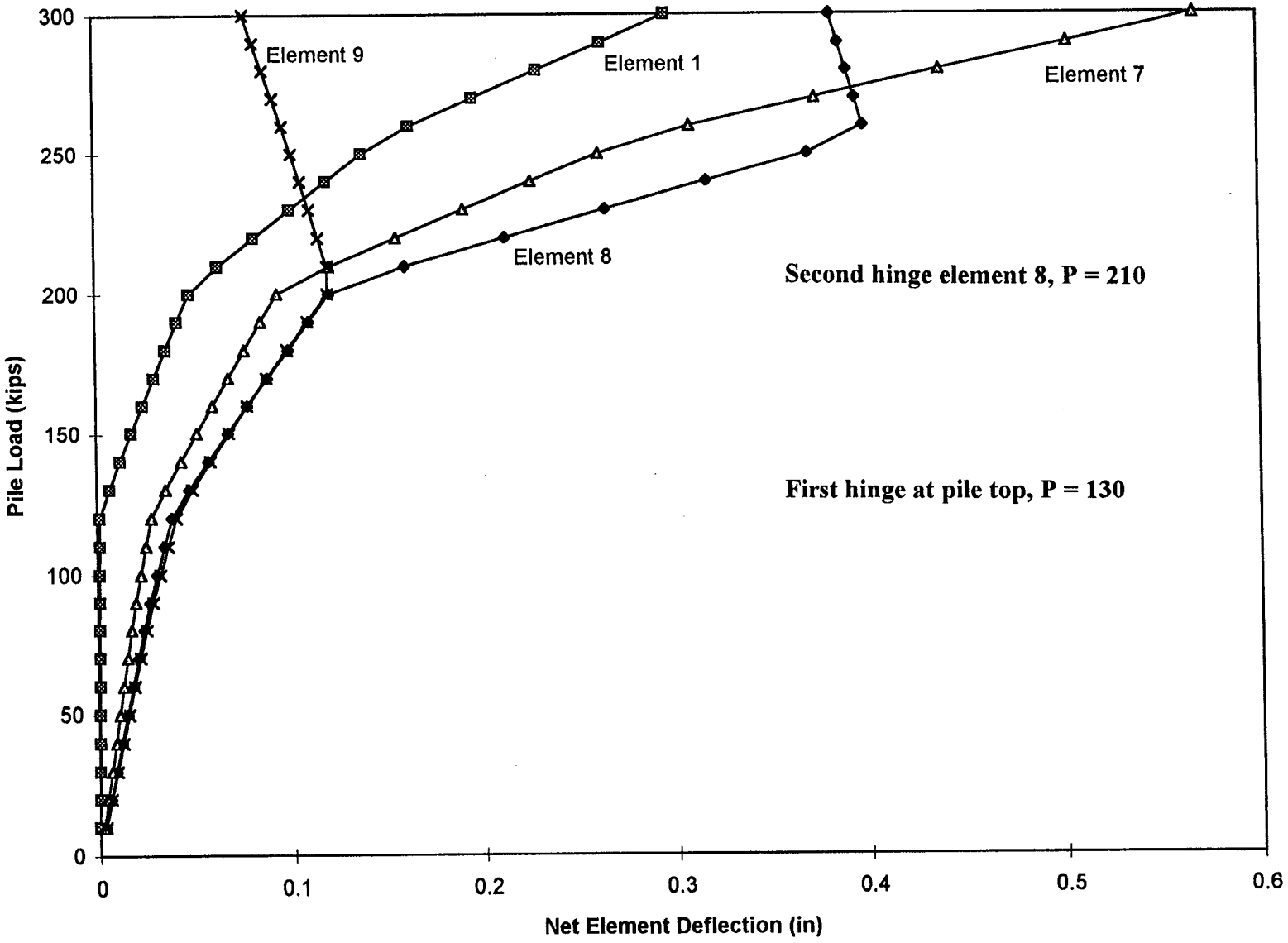

Figure 56. Pile element deflections.

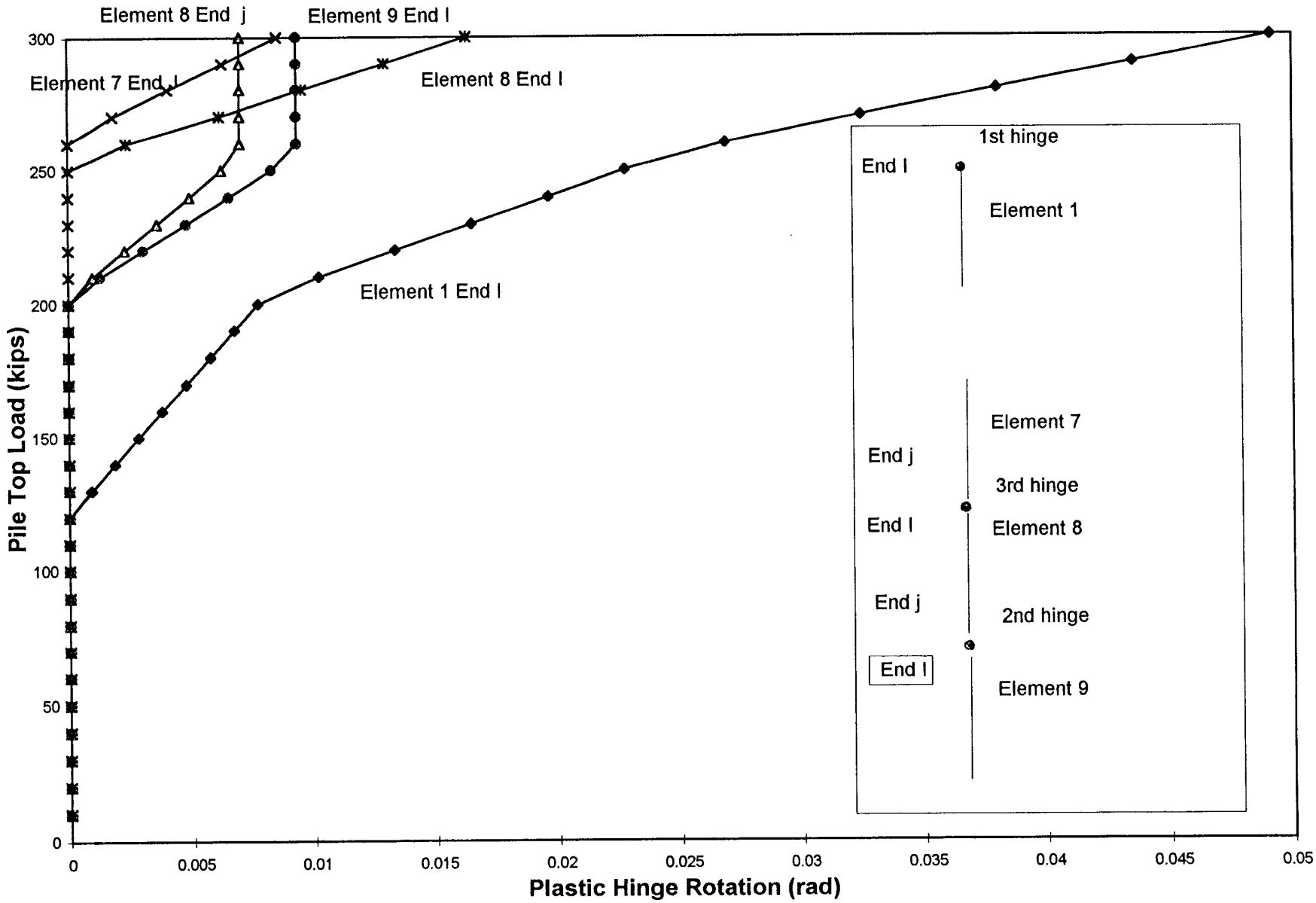

Figure 57. Pile element plastic hinge rotation.

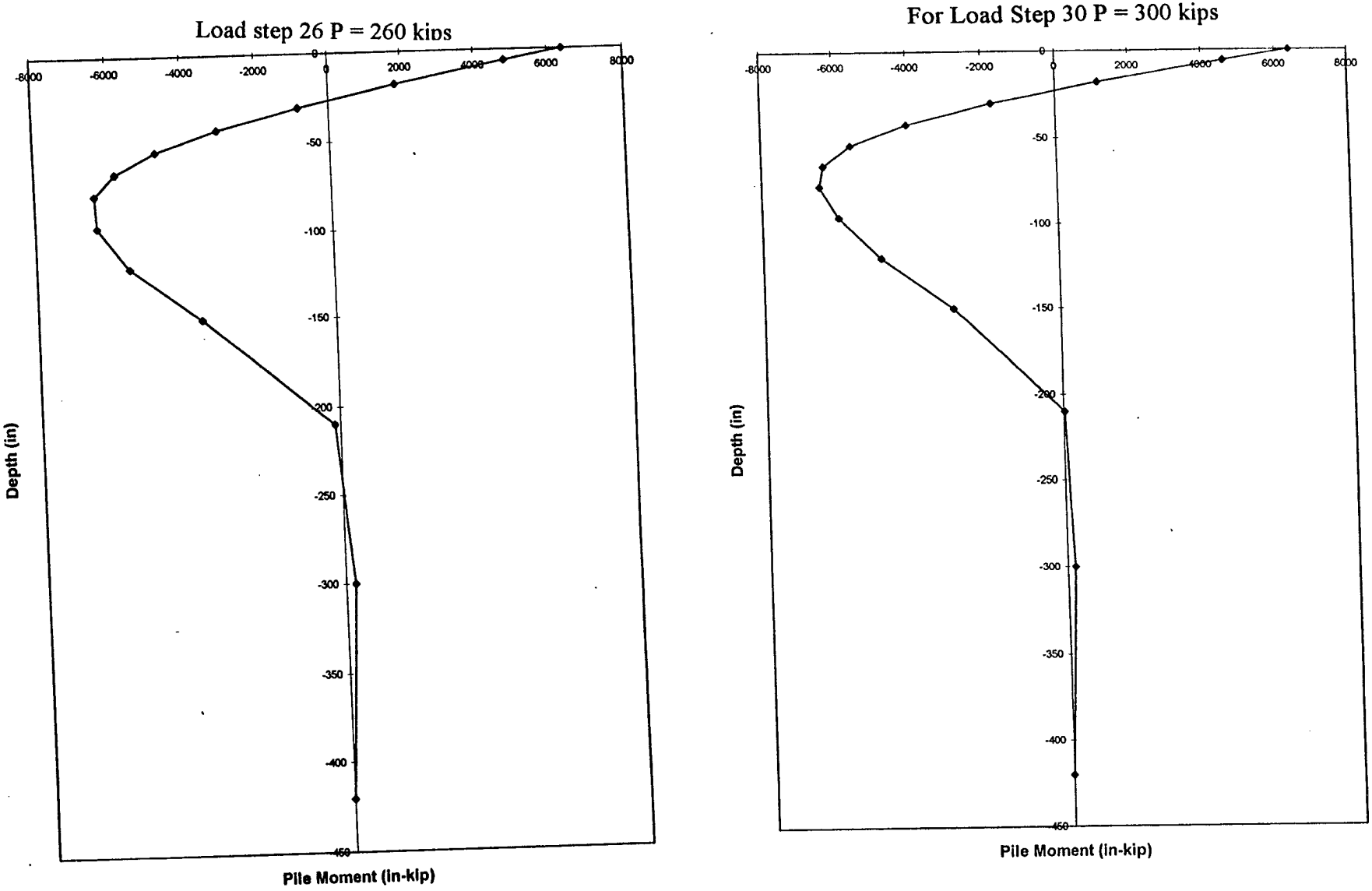

Figure 58. Pile moment and point of contraflexure.

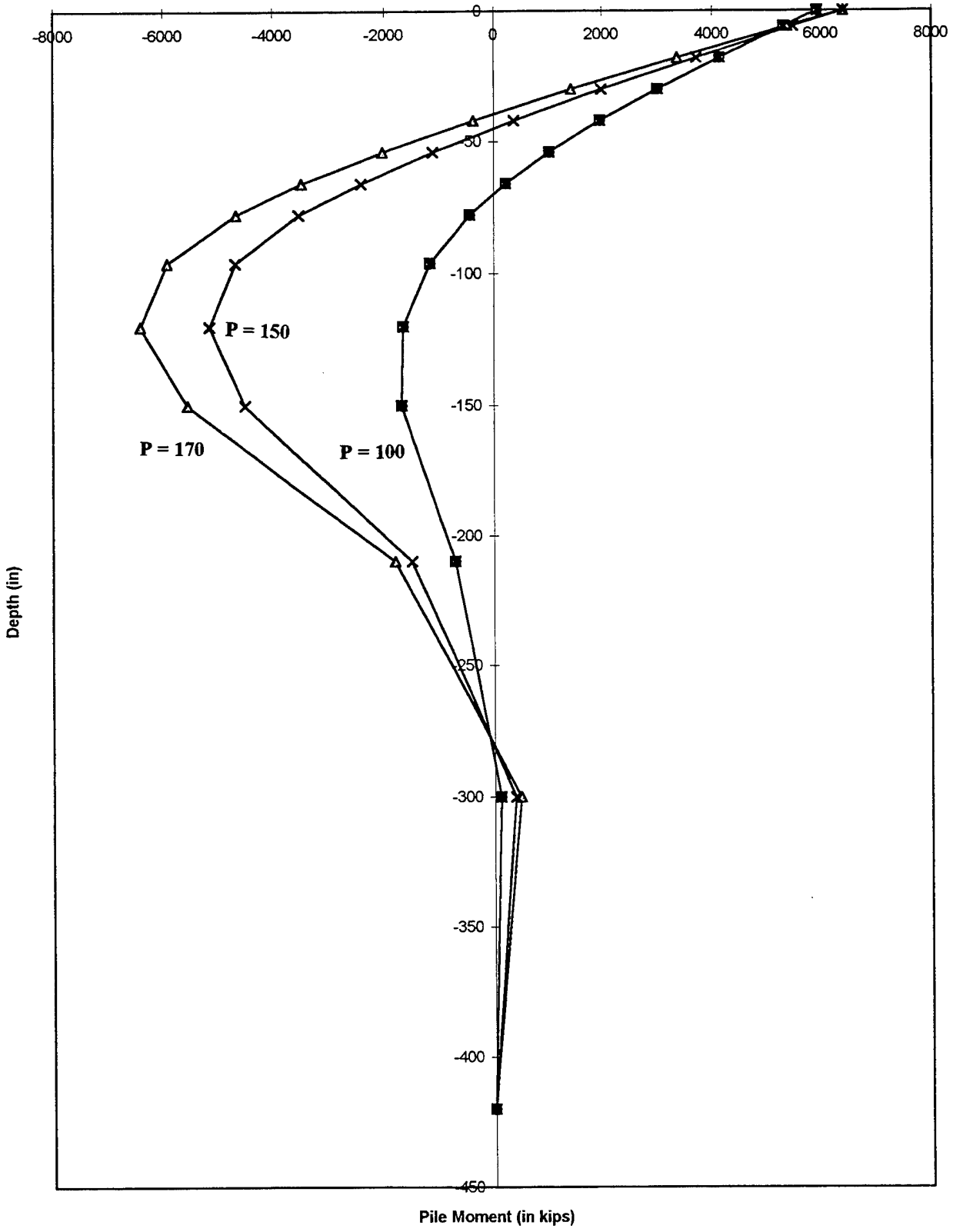

Figure 59. Pile moments at 3 lateral loads.

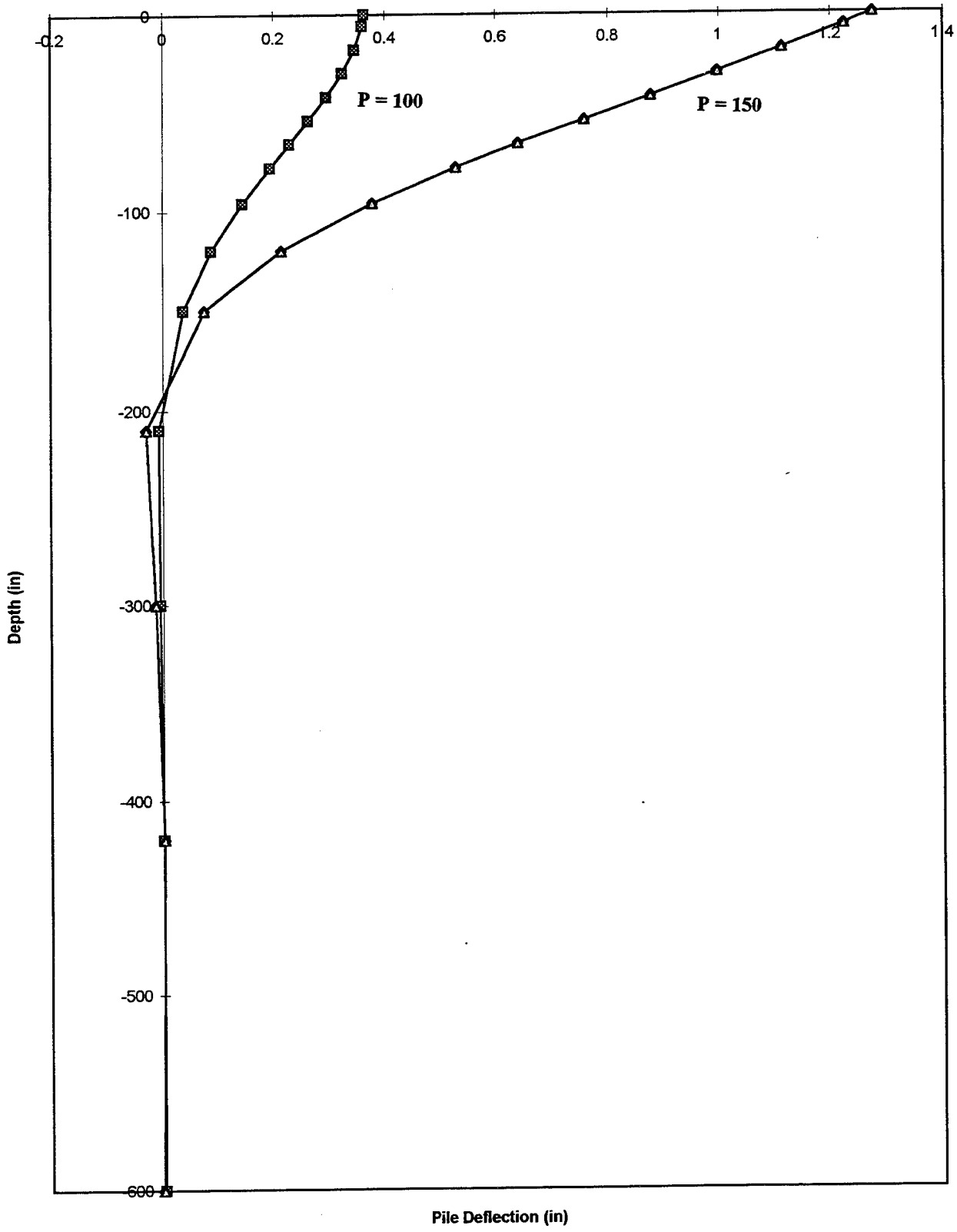

Figure 60. Pile deflection at 2 lateral loads.

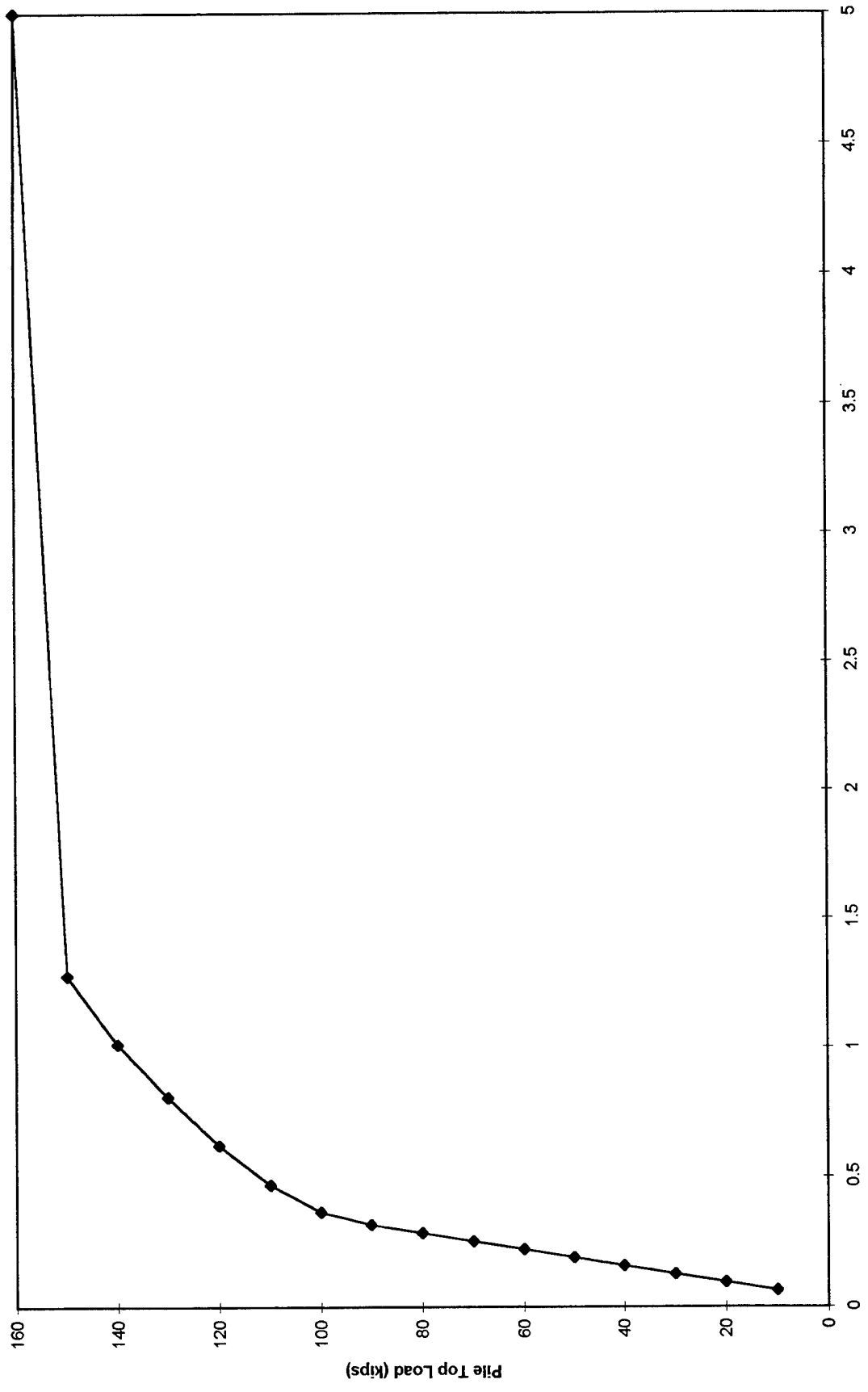

Figure 61. Pile top deflection.

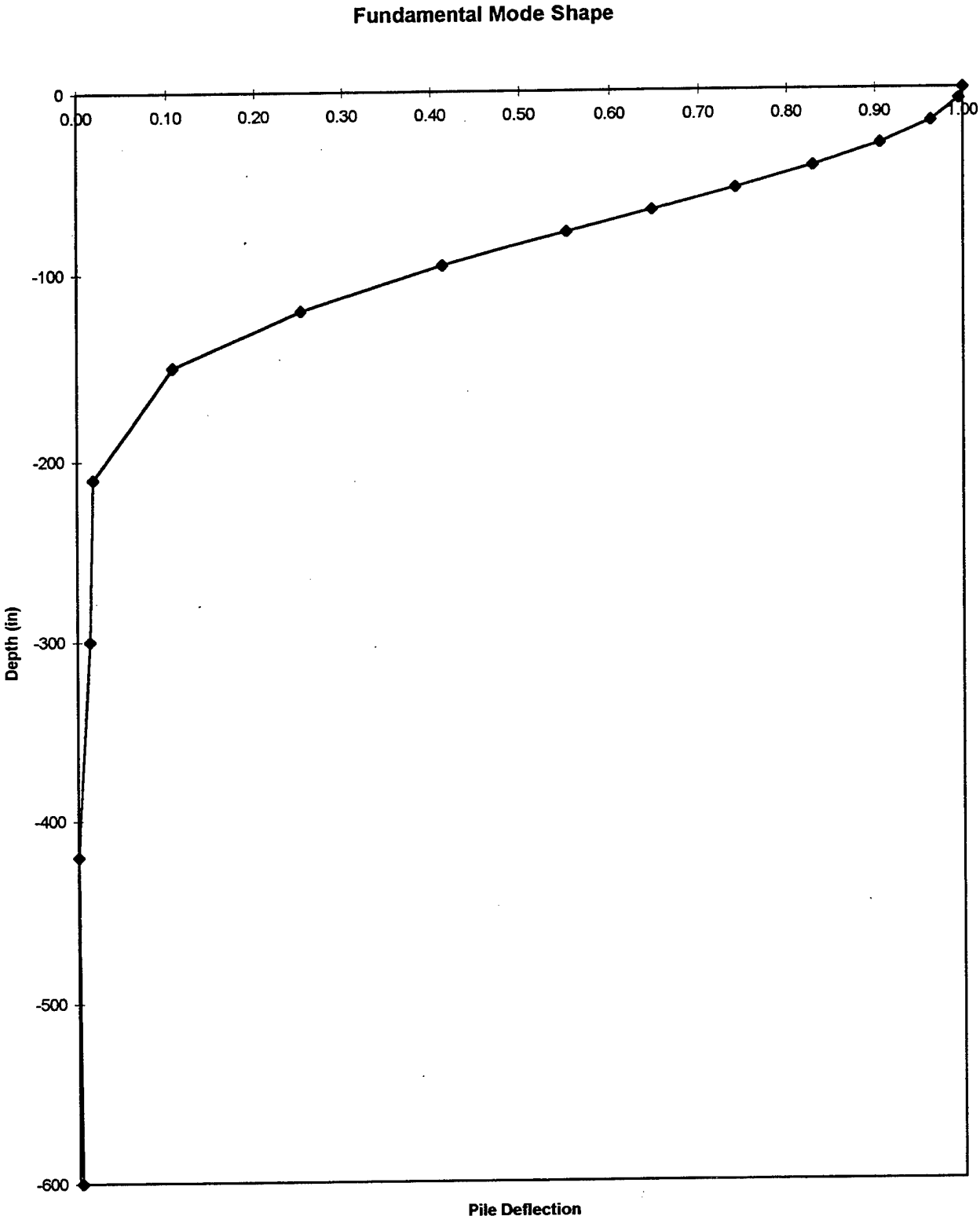

Figure 62. Pile fundamental mode shape.

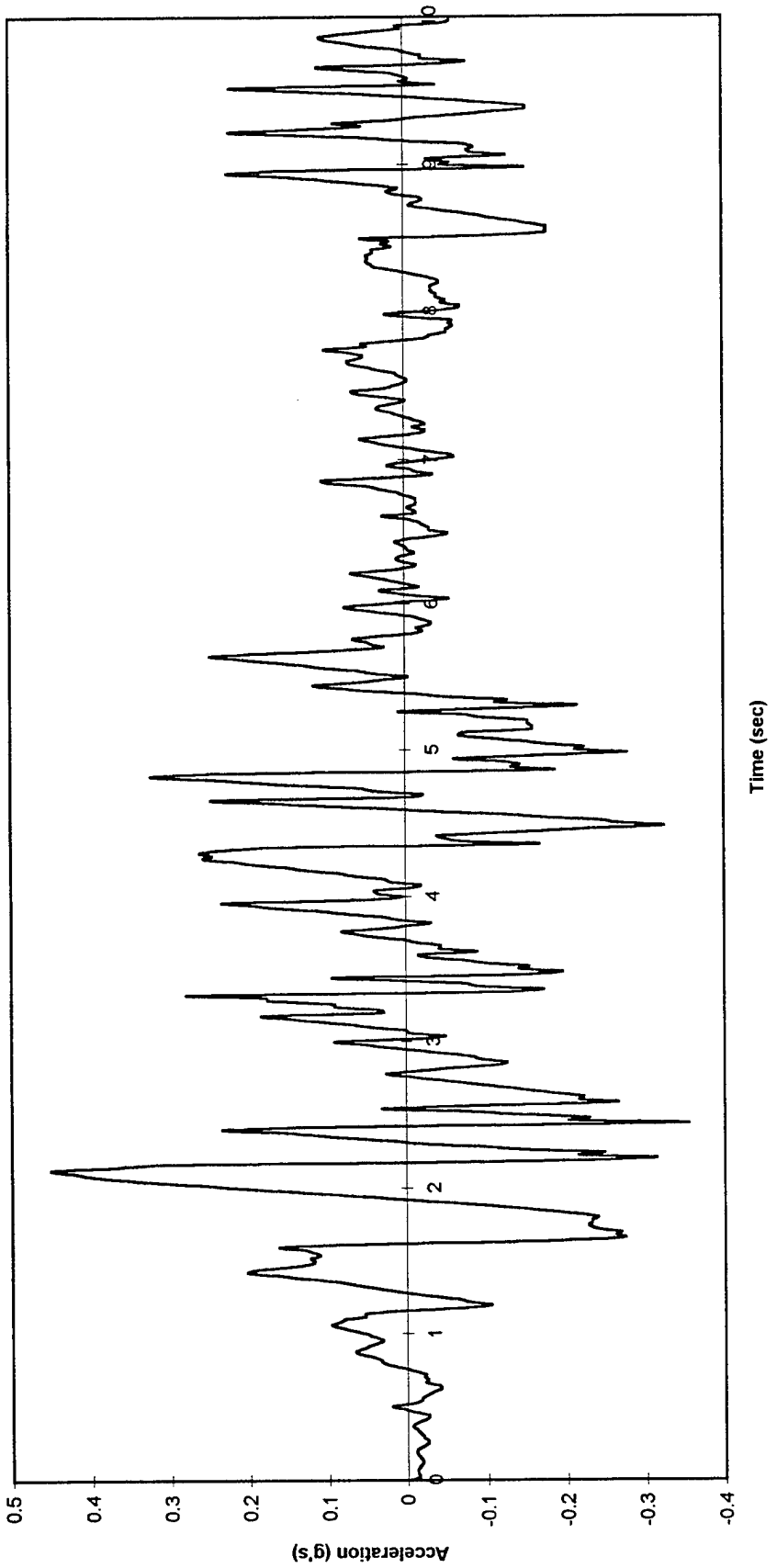

Figure 63. El Centro Acceleration scaled to 0.45g

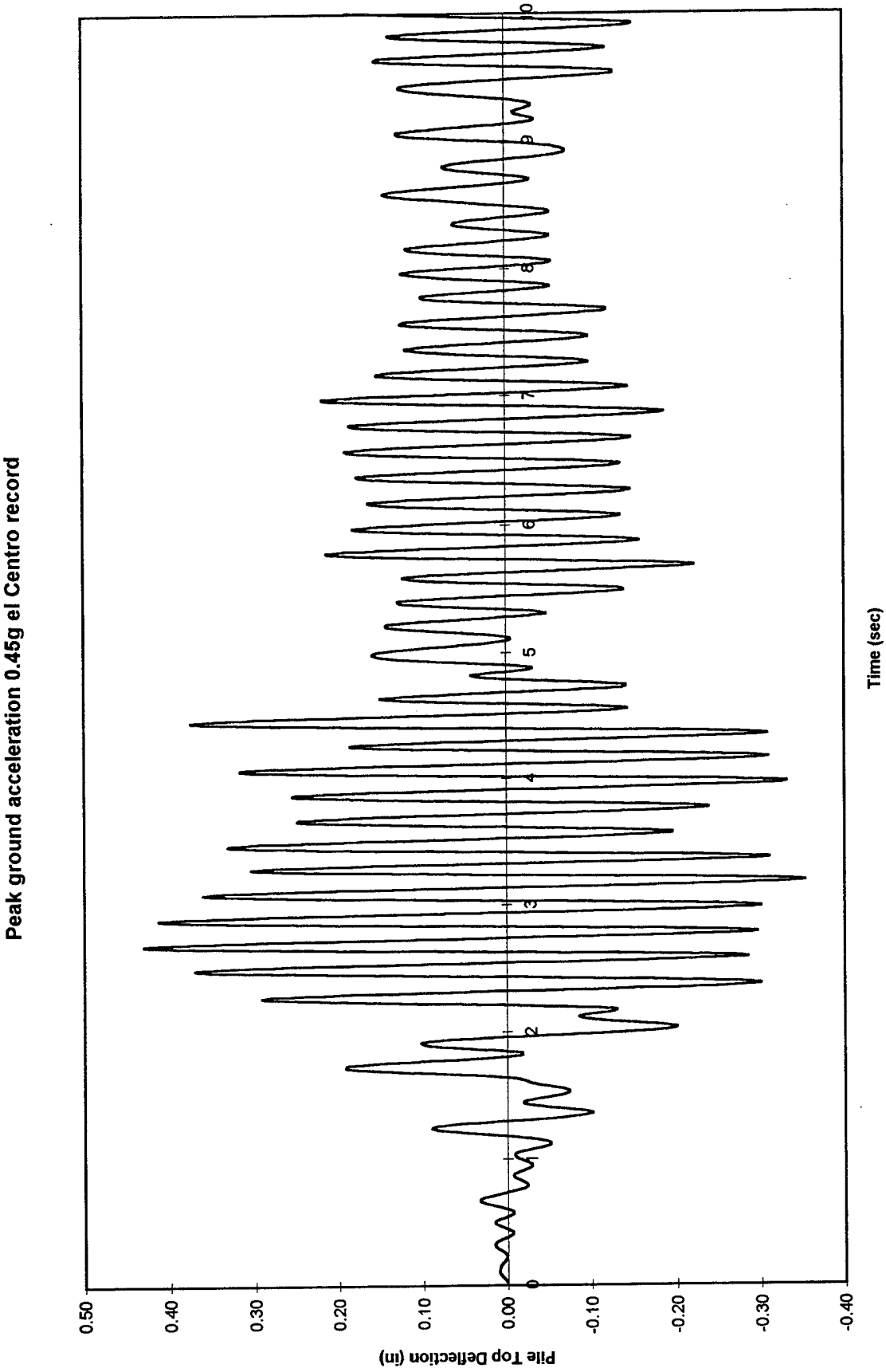

Figure 64. Pile top deflection.

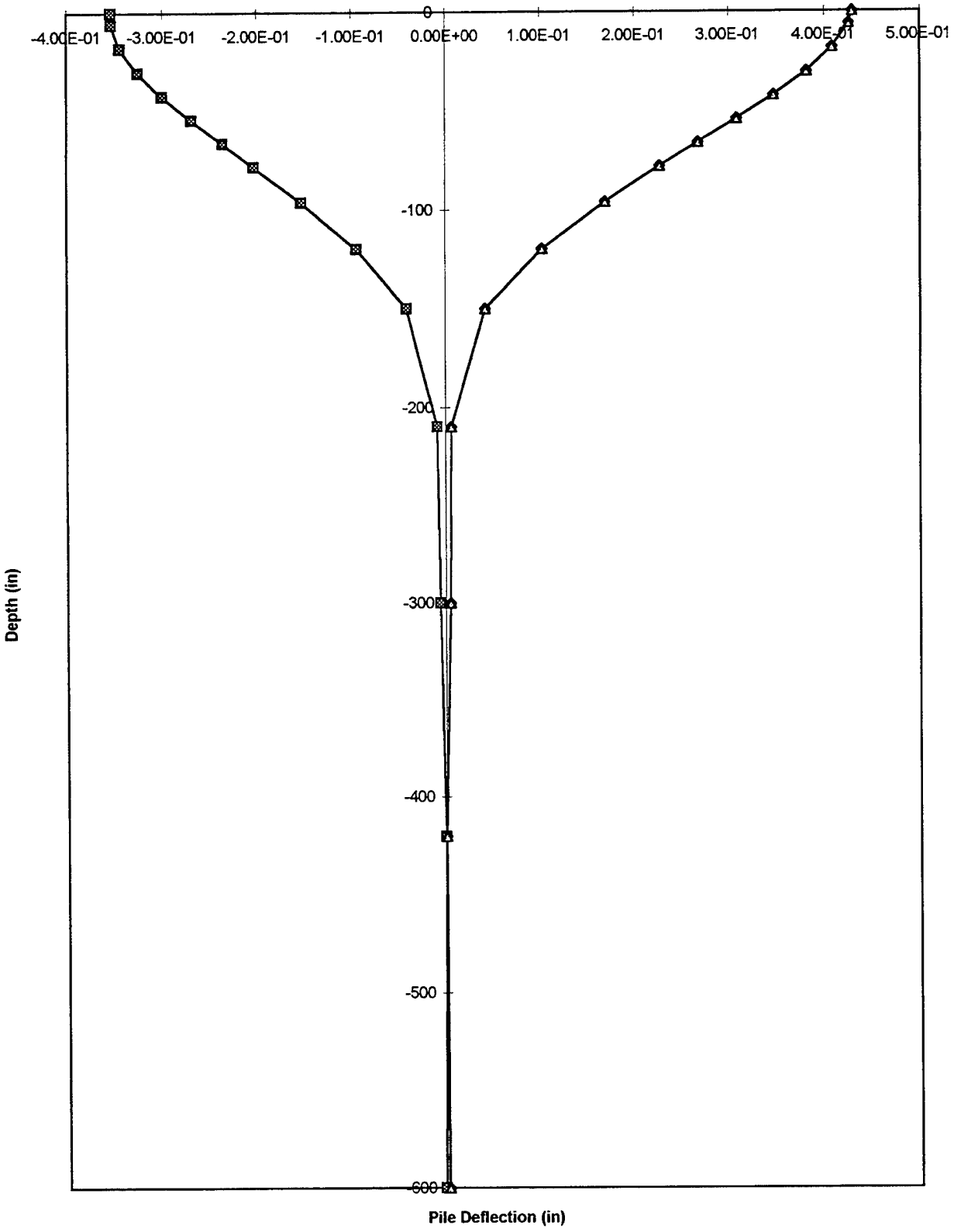

Figure 65. Pile deflection envelope.

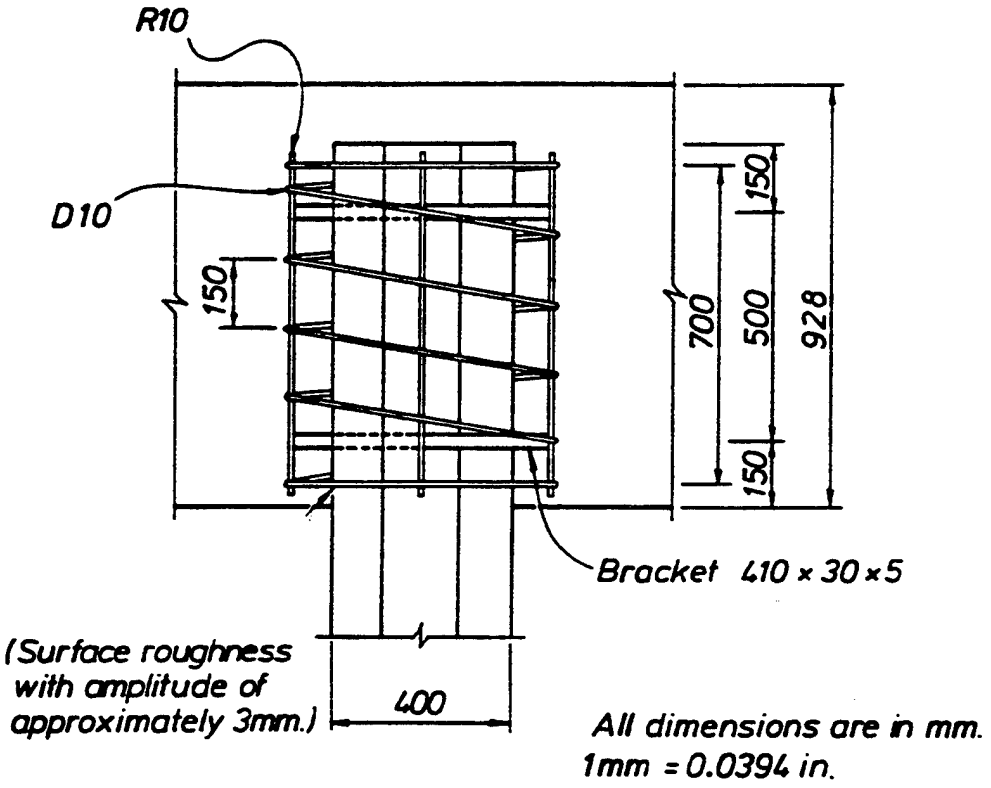

Figure 66. Pile embedment in pile cap.

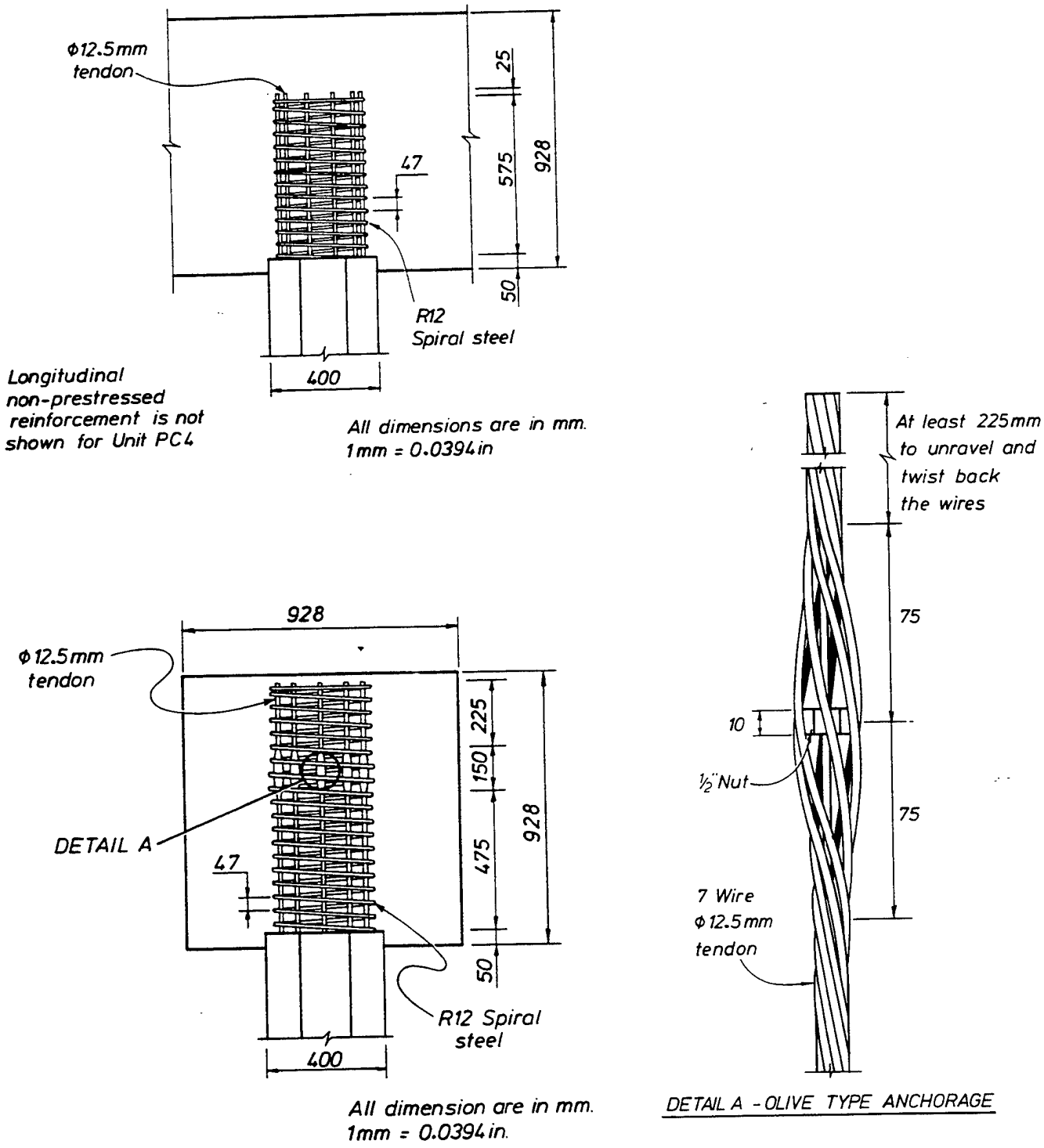

Figure 67. Pile - pile cap connection using pile reinforcement

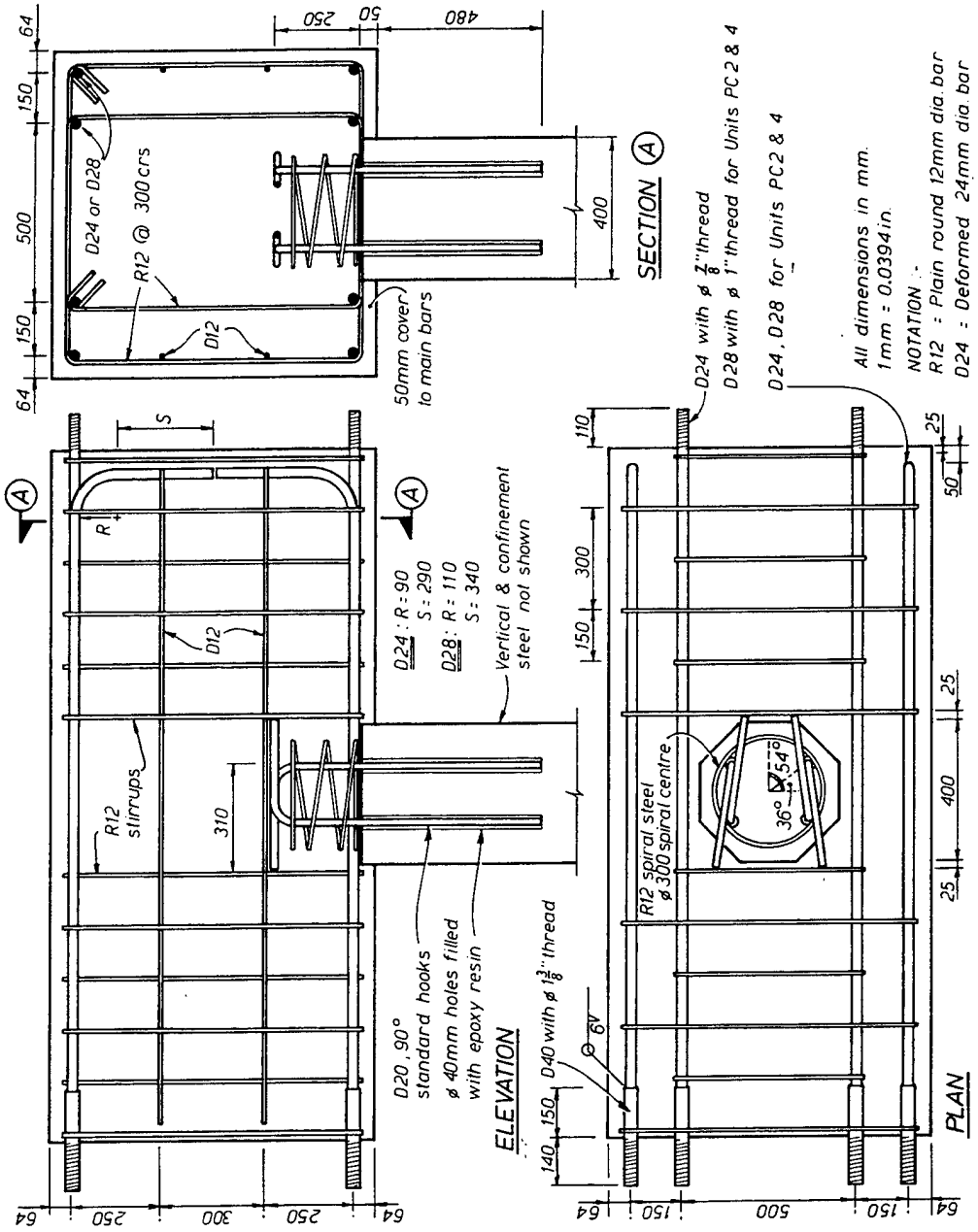

Figure 68. Pile - pile cap conncetion using dowels.

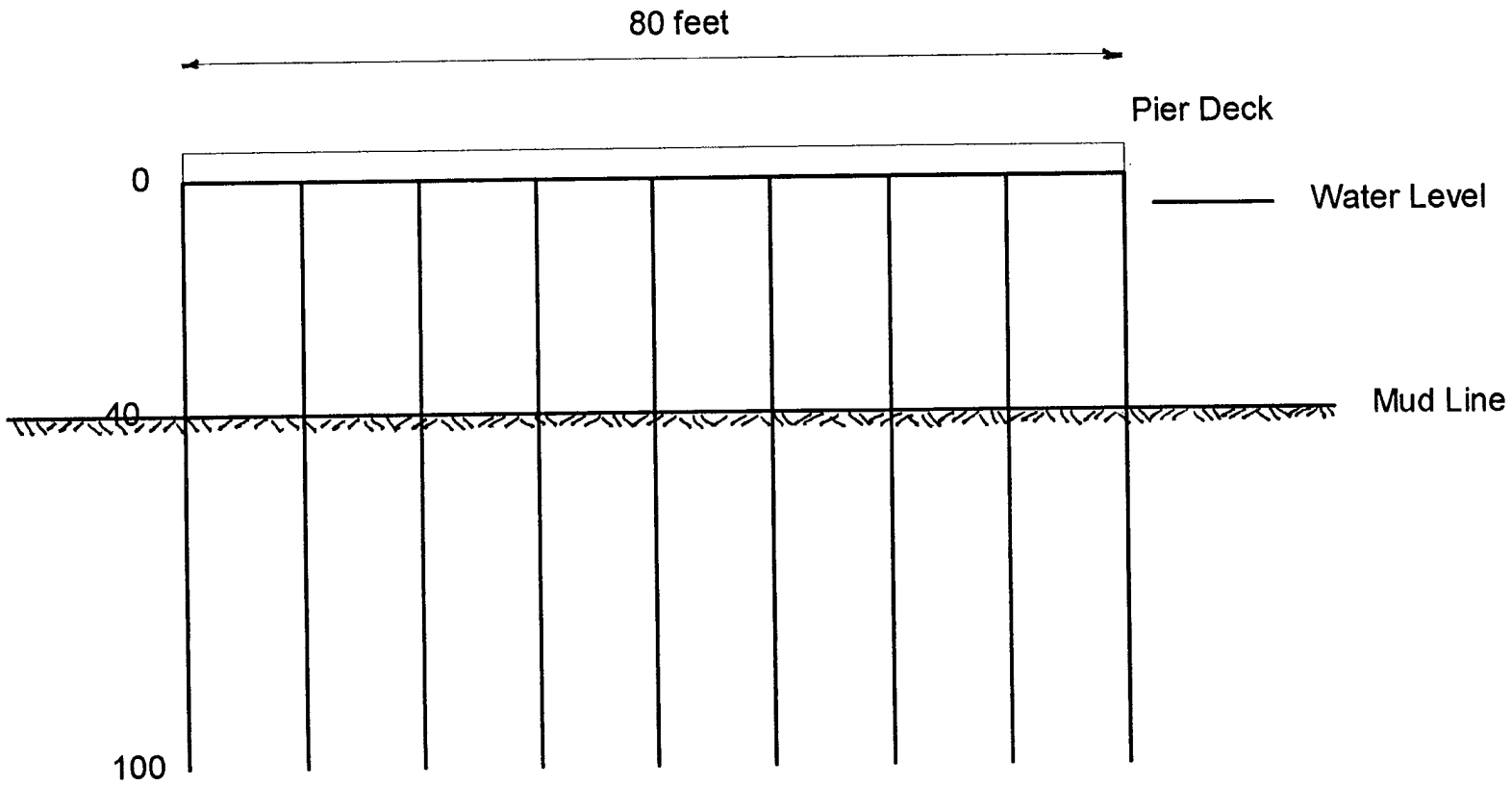

Figure 69. Typical pier used in 2-dimensional analysis.

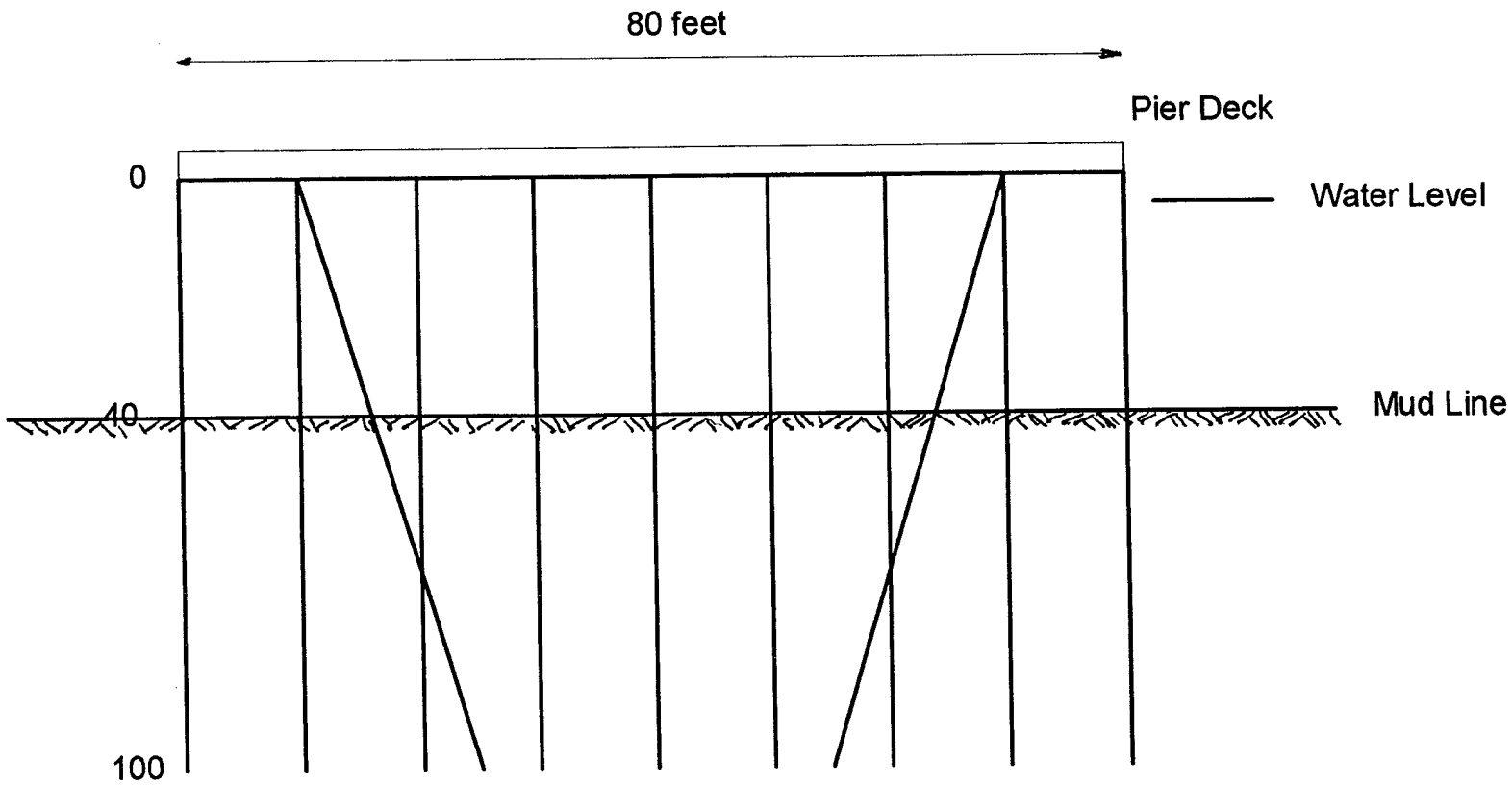

Figure 70. Typical pier with batter piles used in 2-dimensional analysis.

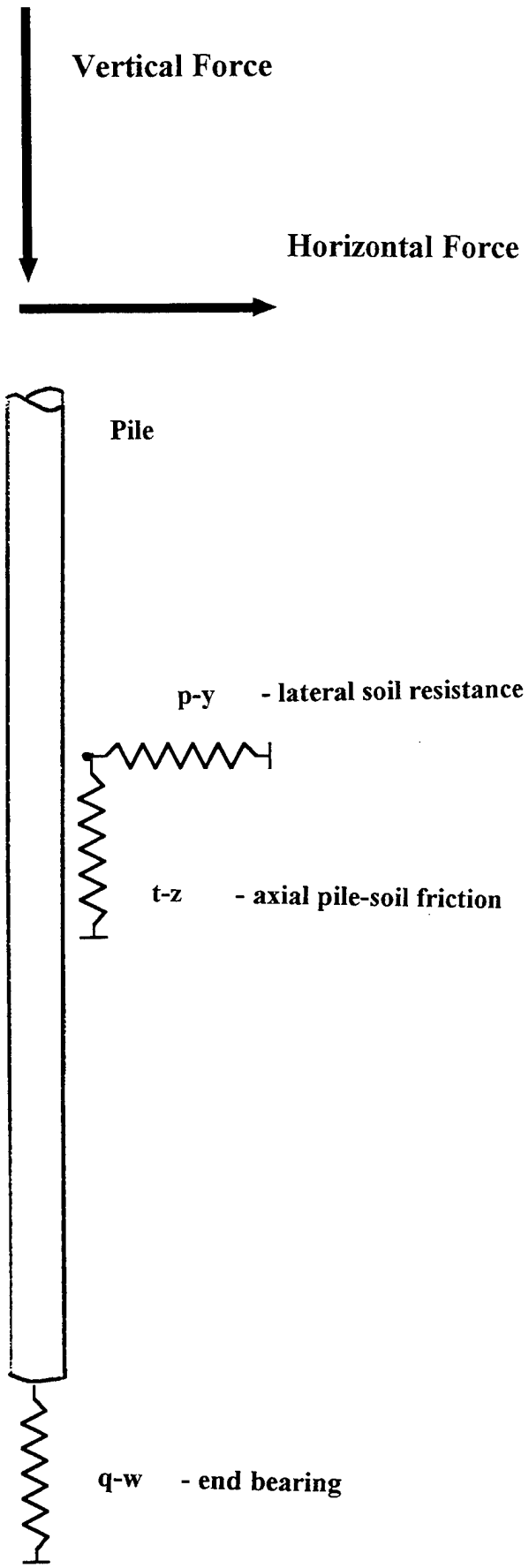

Figure 71 . Vertical pile in soil showing restraints.

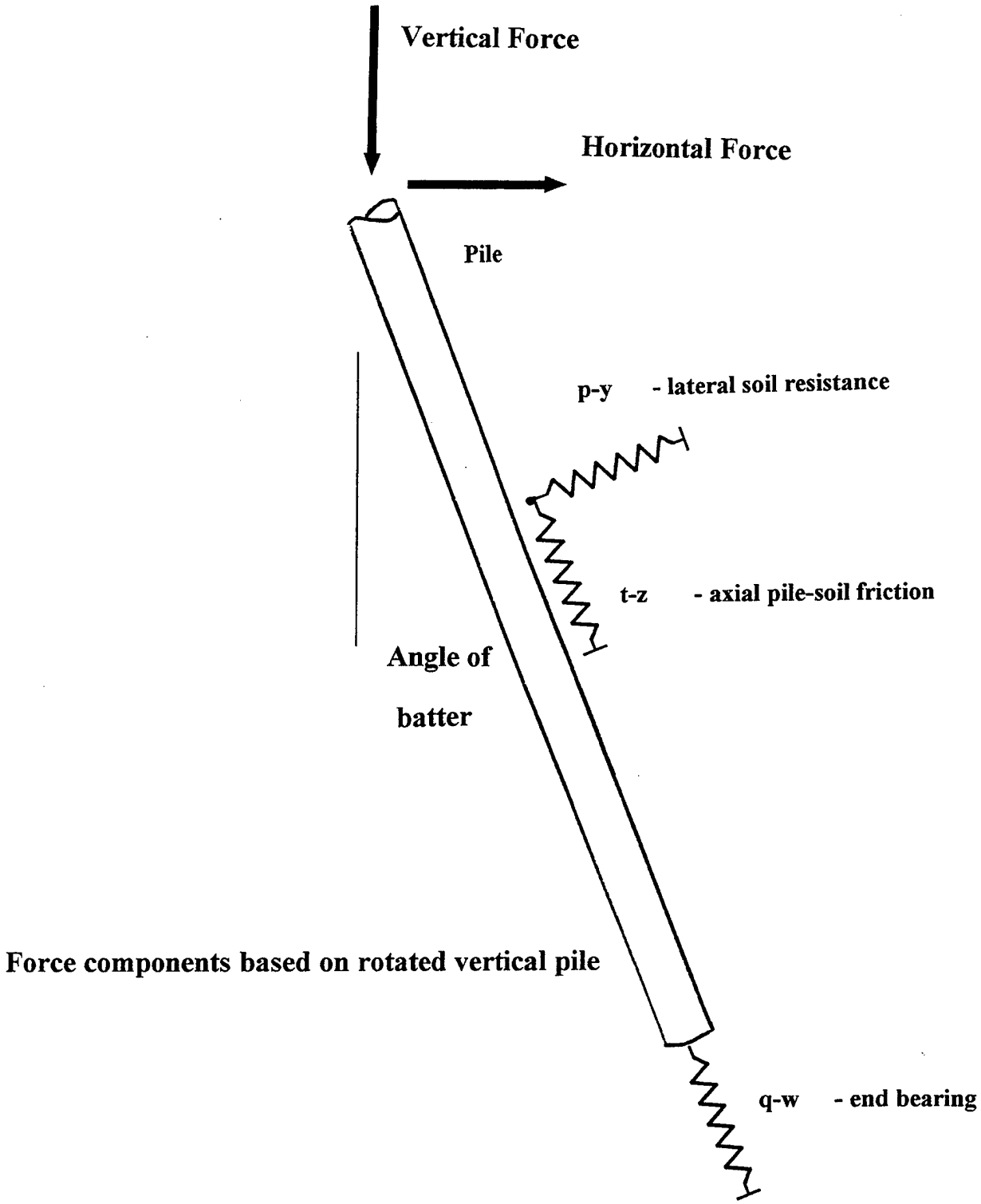

Figure 72 . Batter pile in soil showing restraints.

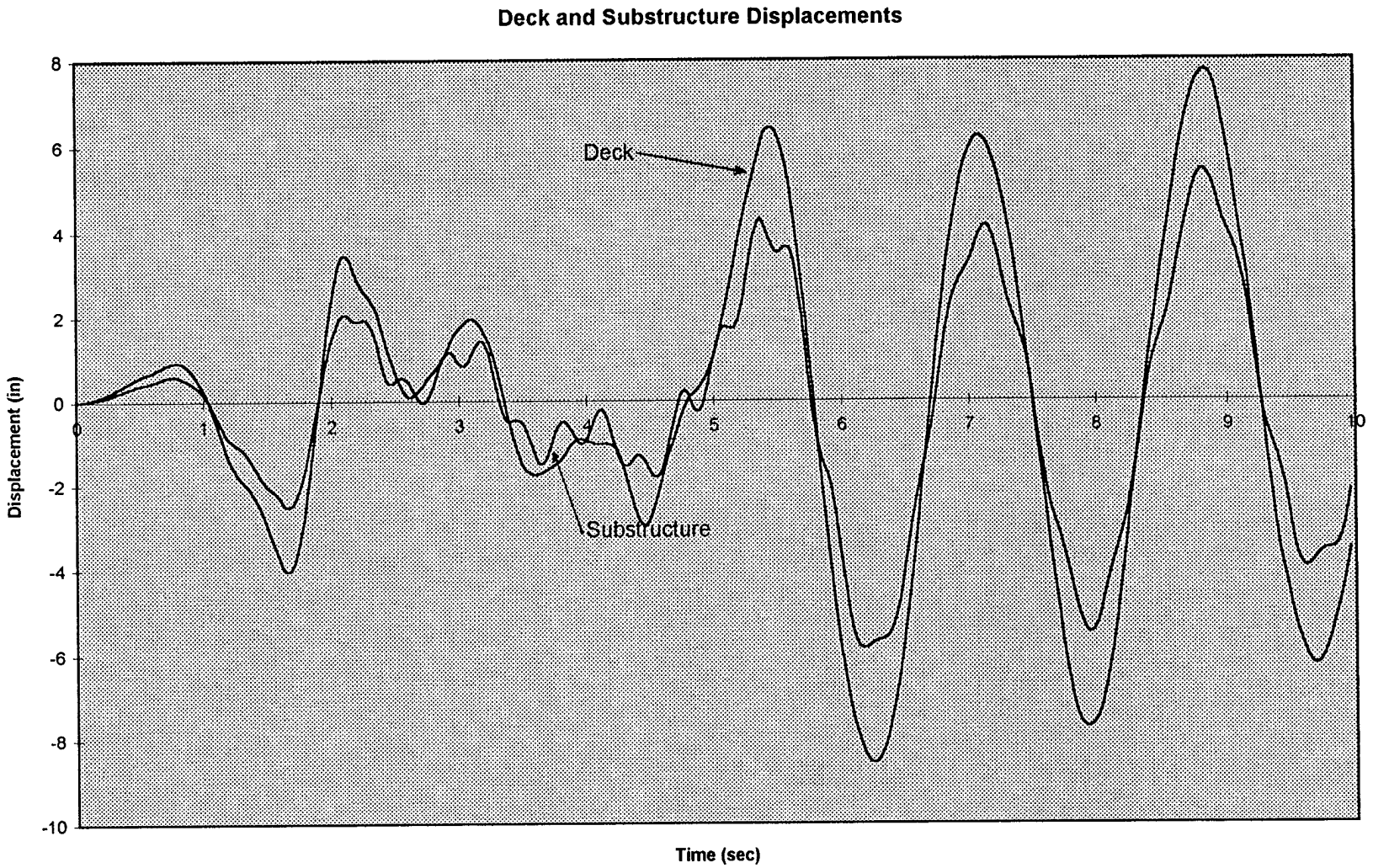

Figure 73. Pier deck and substructure response at 0.45g.

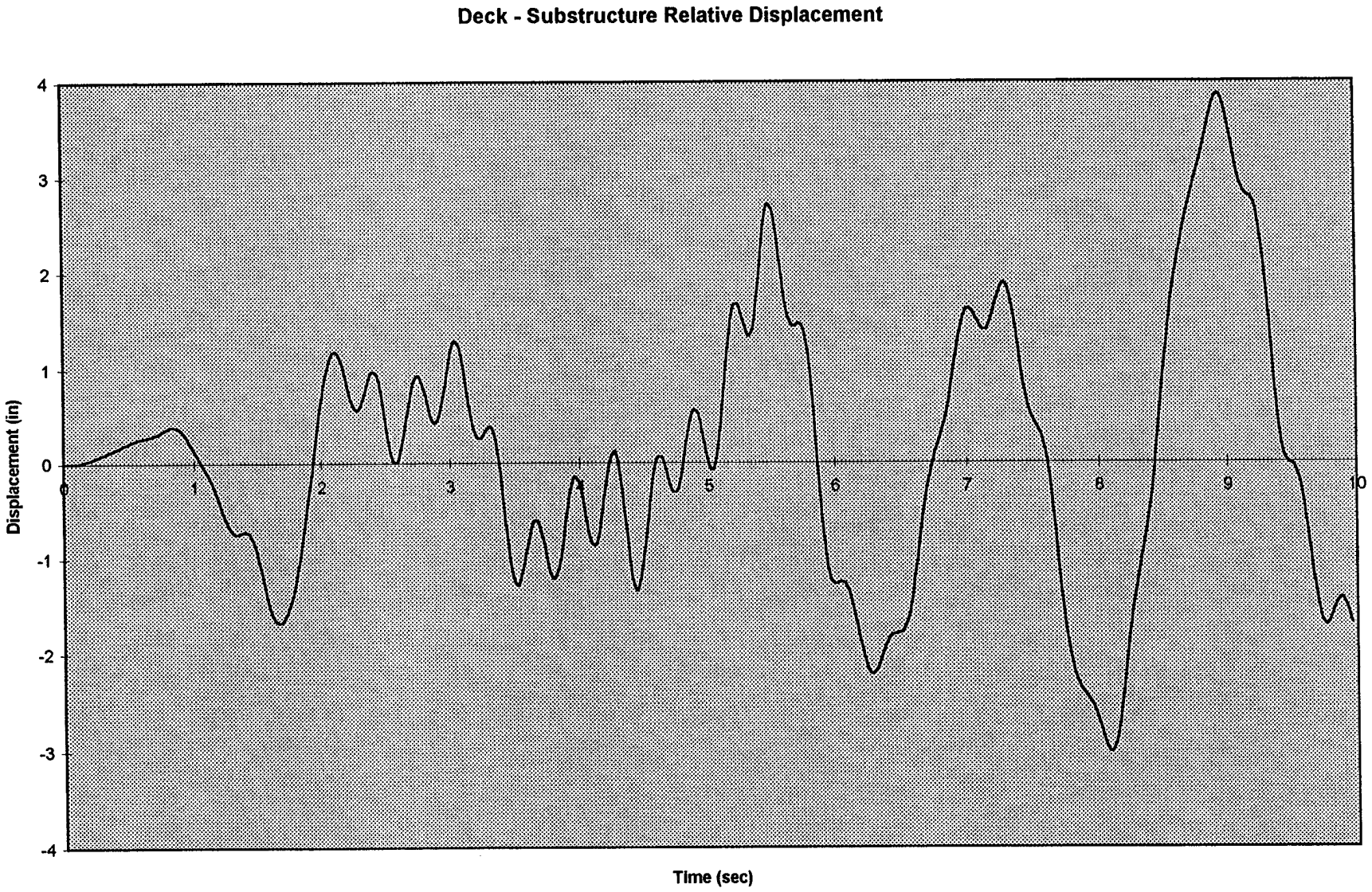

Figure 74. Pier deck and substructure response at 0.45g.

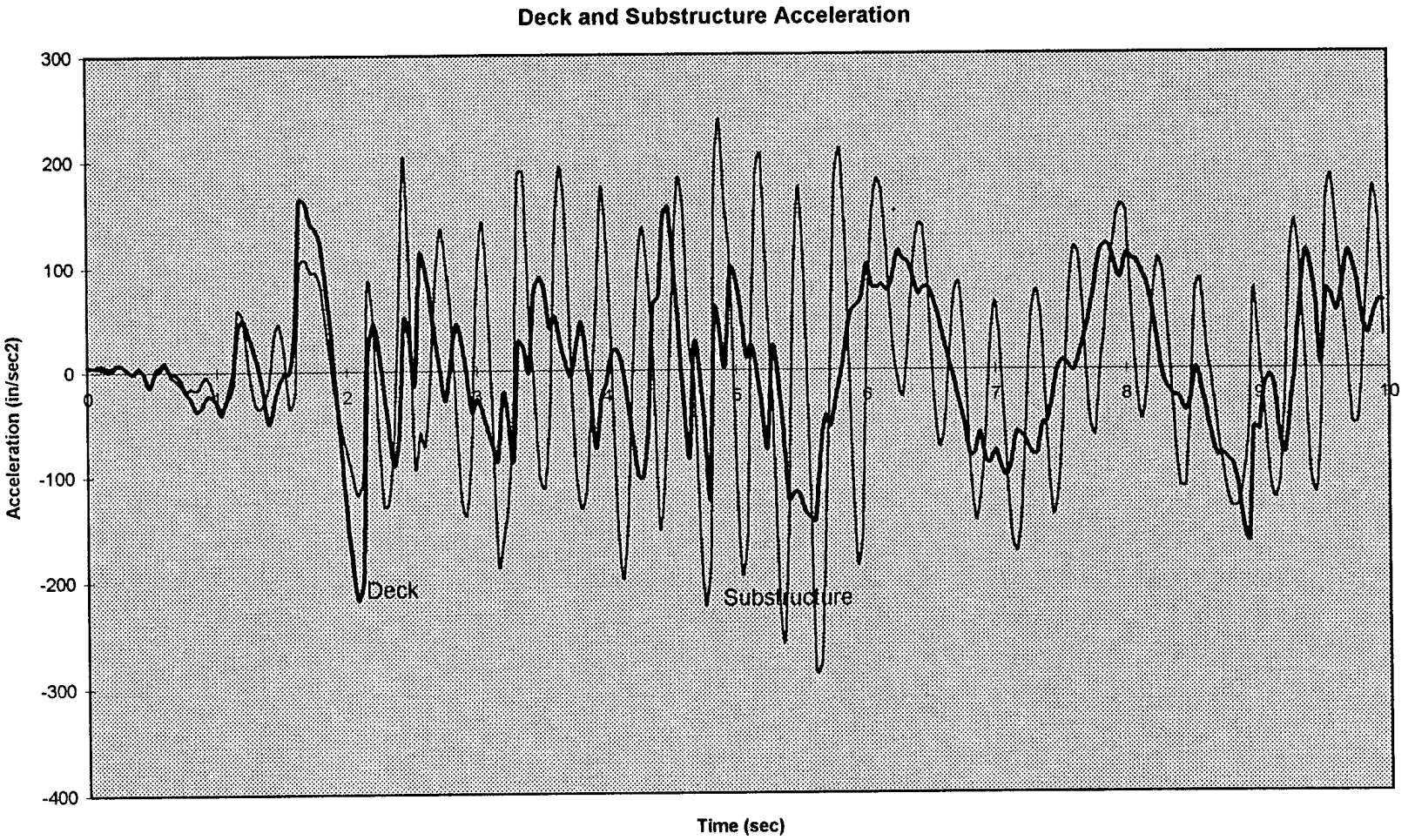

Figure 75. Pier deck and substructure response at 0.45g.

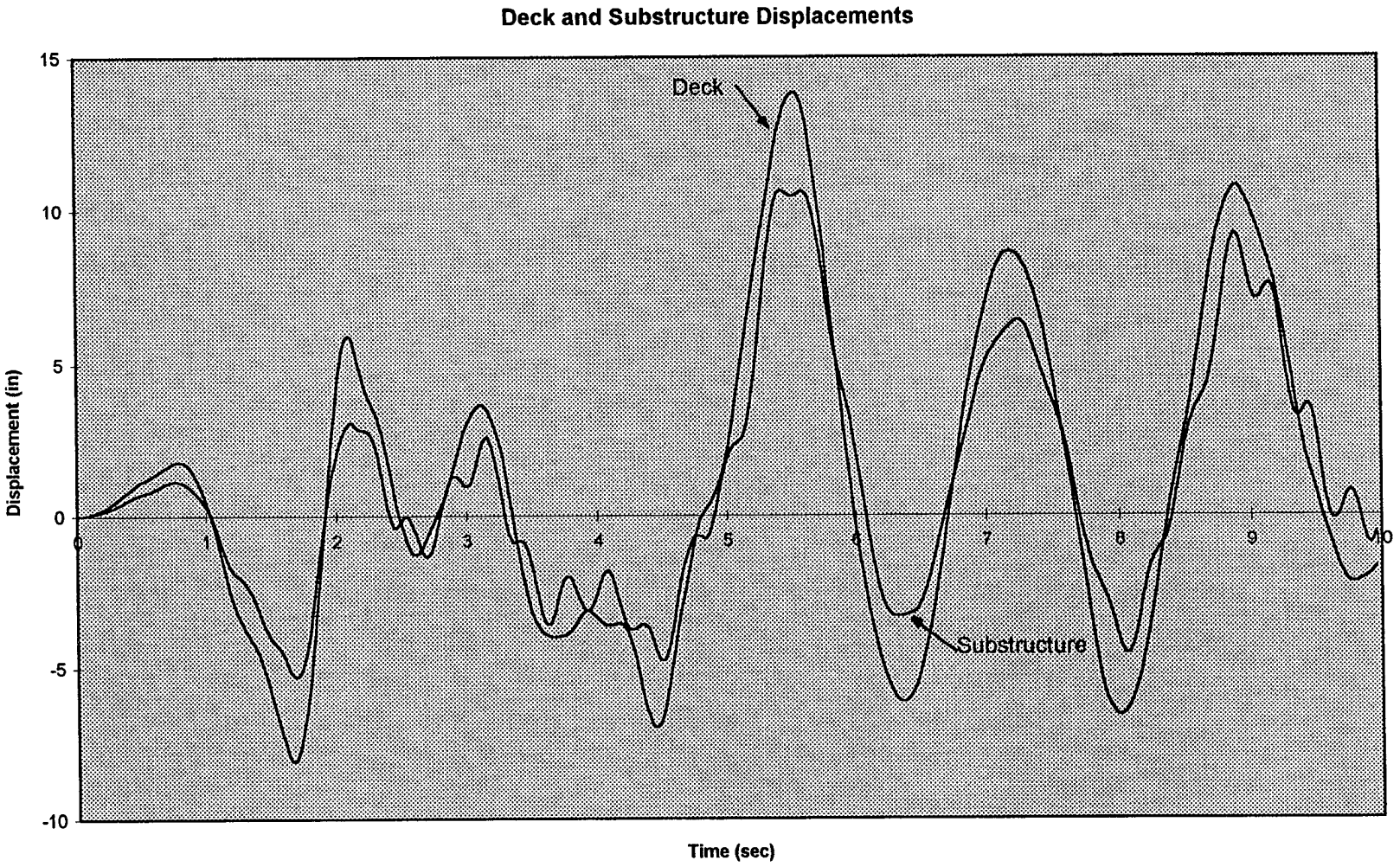

Figure 76. Pier deck and substructure response at 0.9g.

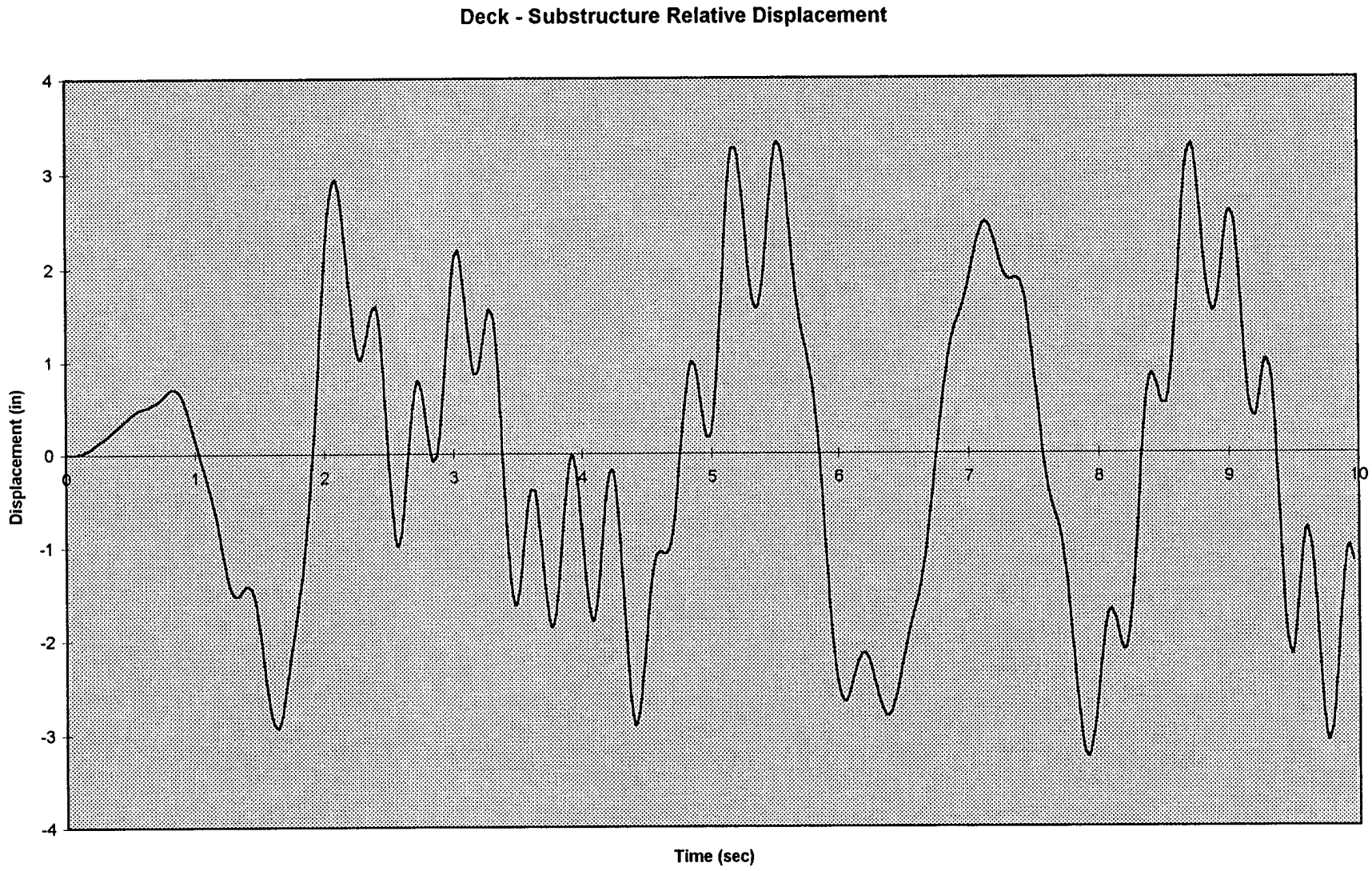

Figure 77. Pier deck and substructure response at 0.9g.

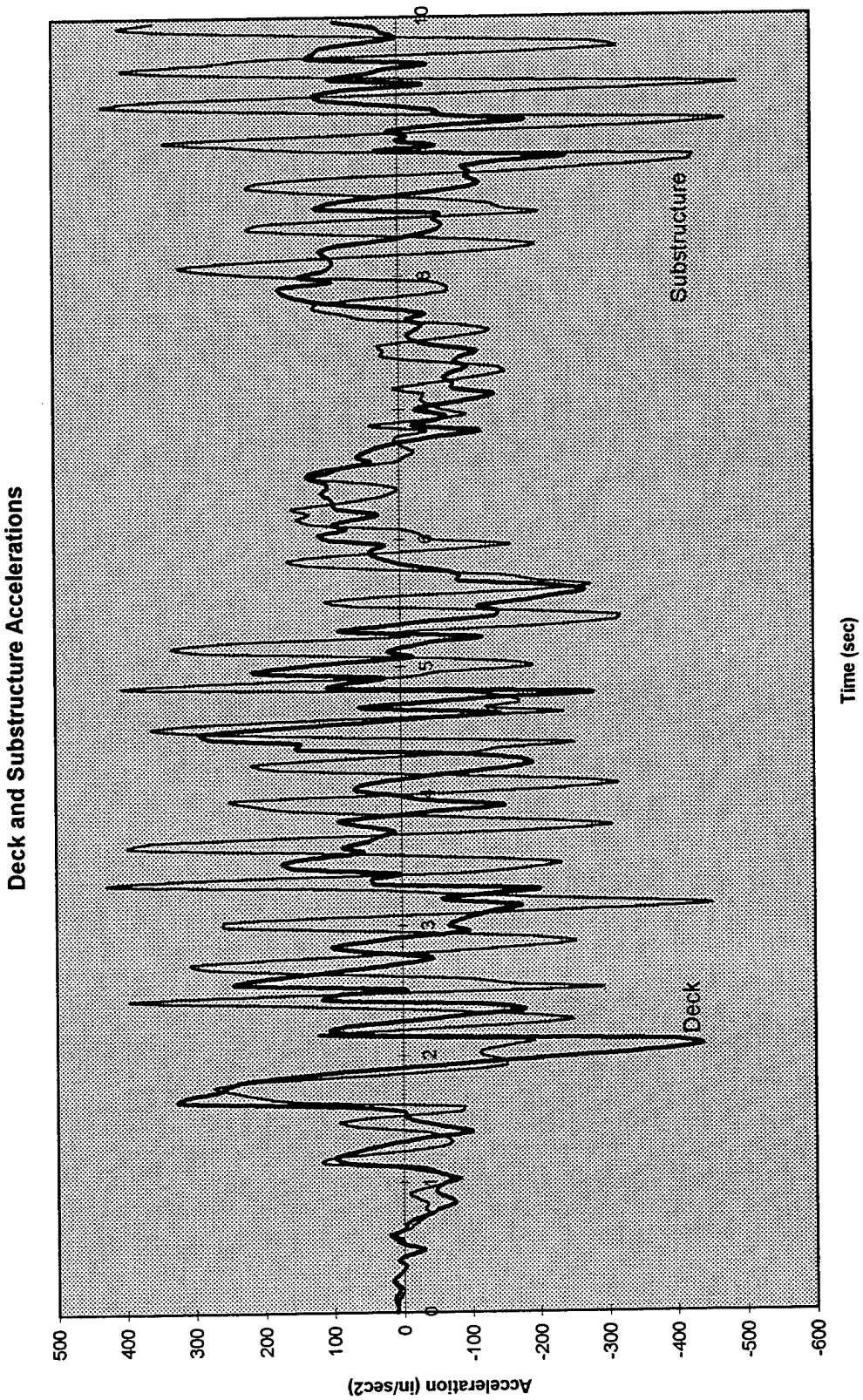

Figure 78. Pier deck and substructure response at 0.9g.

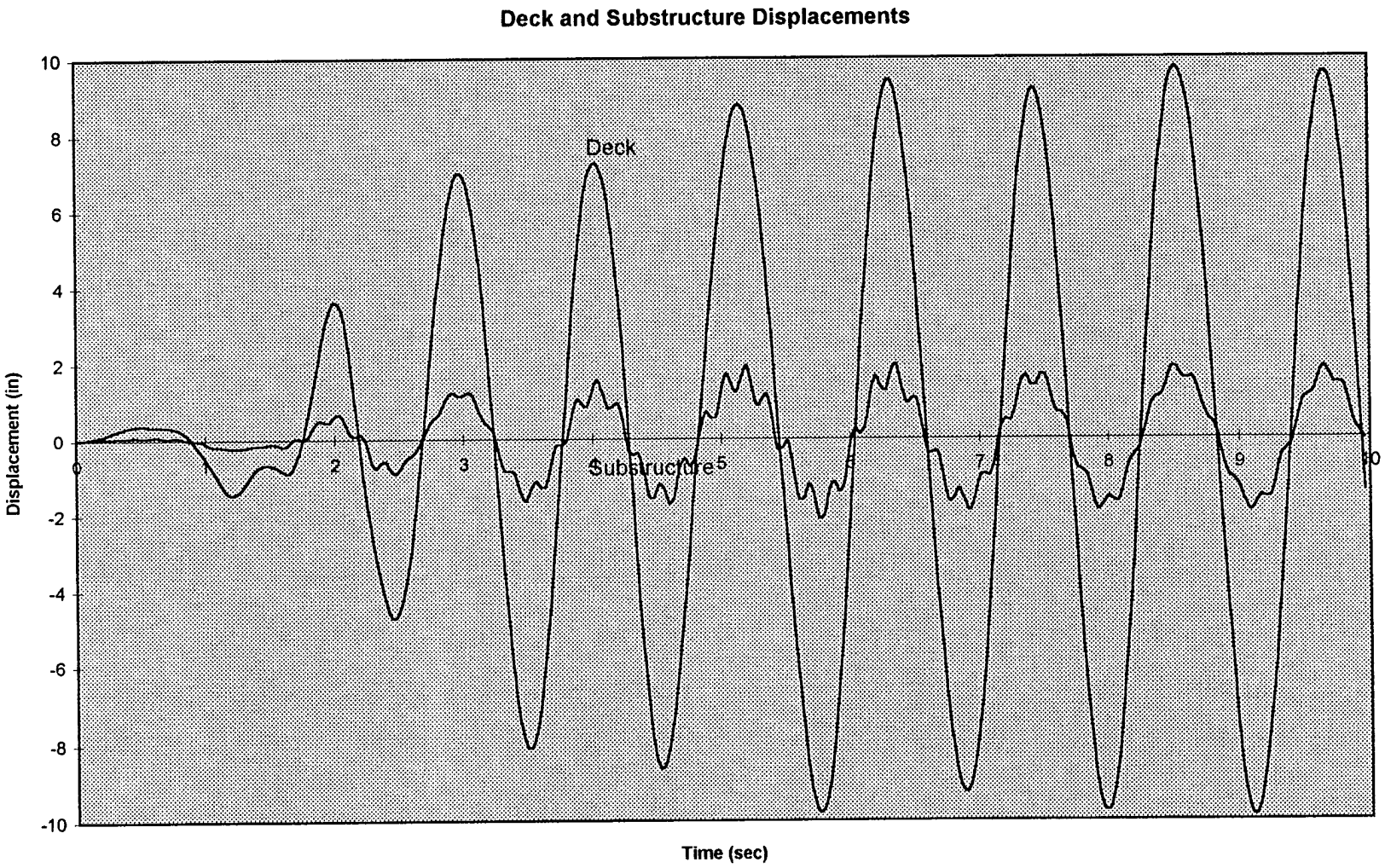

Figure 79. Pier with batter piles deck and substructure response at 0.45g.

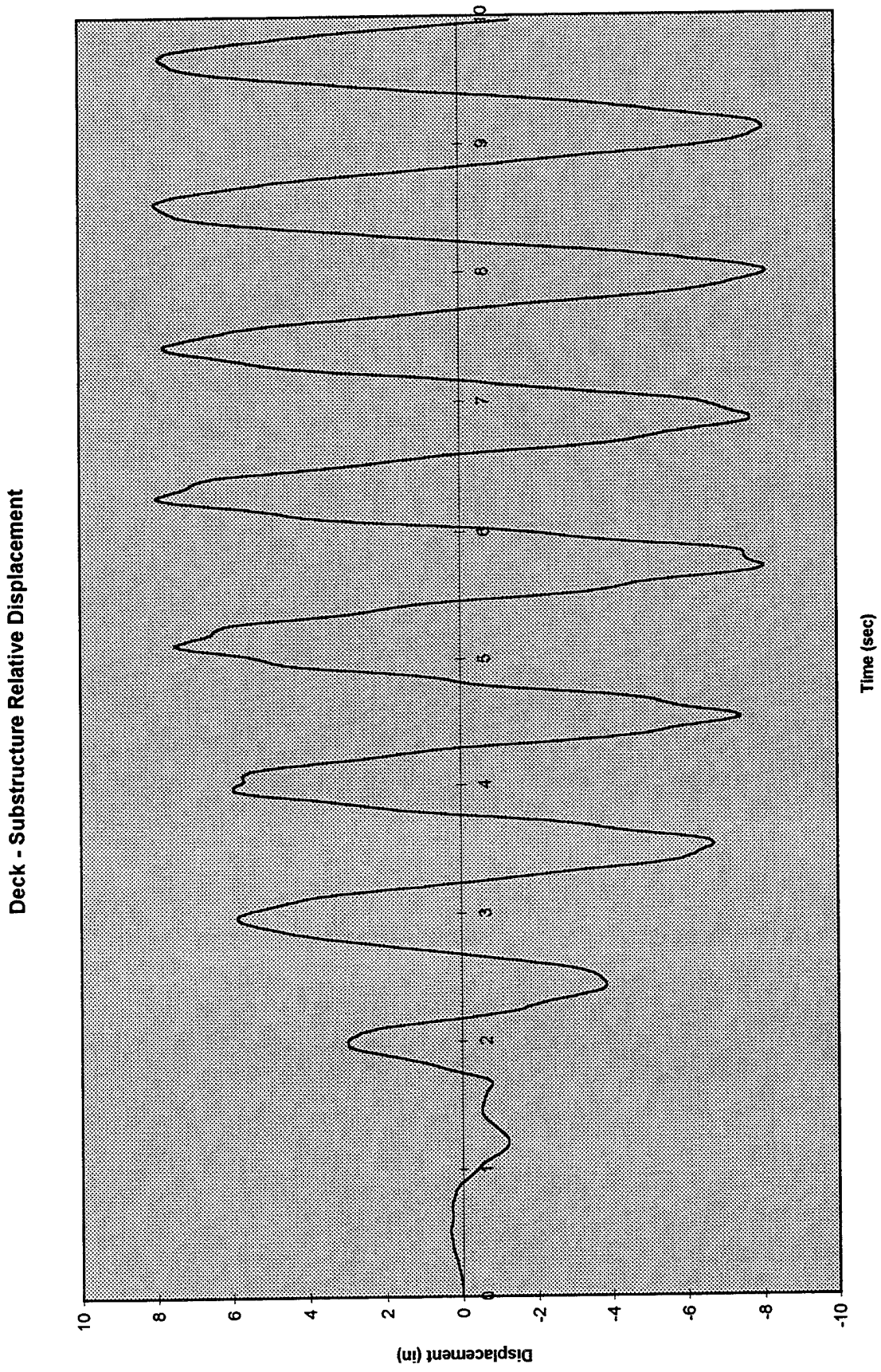

Figure 80. Pier with batter piles deck and substructure response at 0.45g.

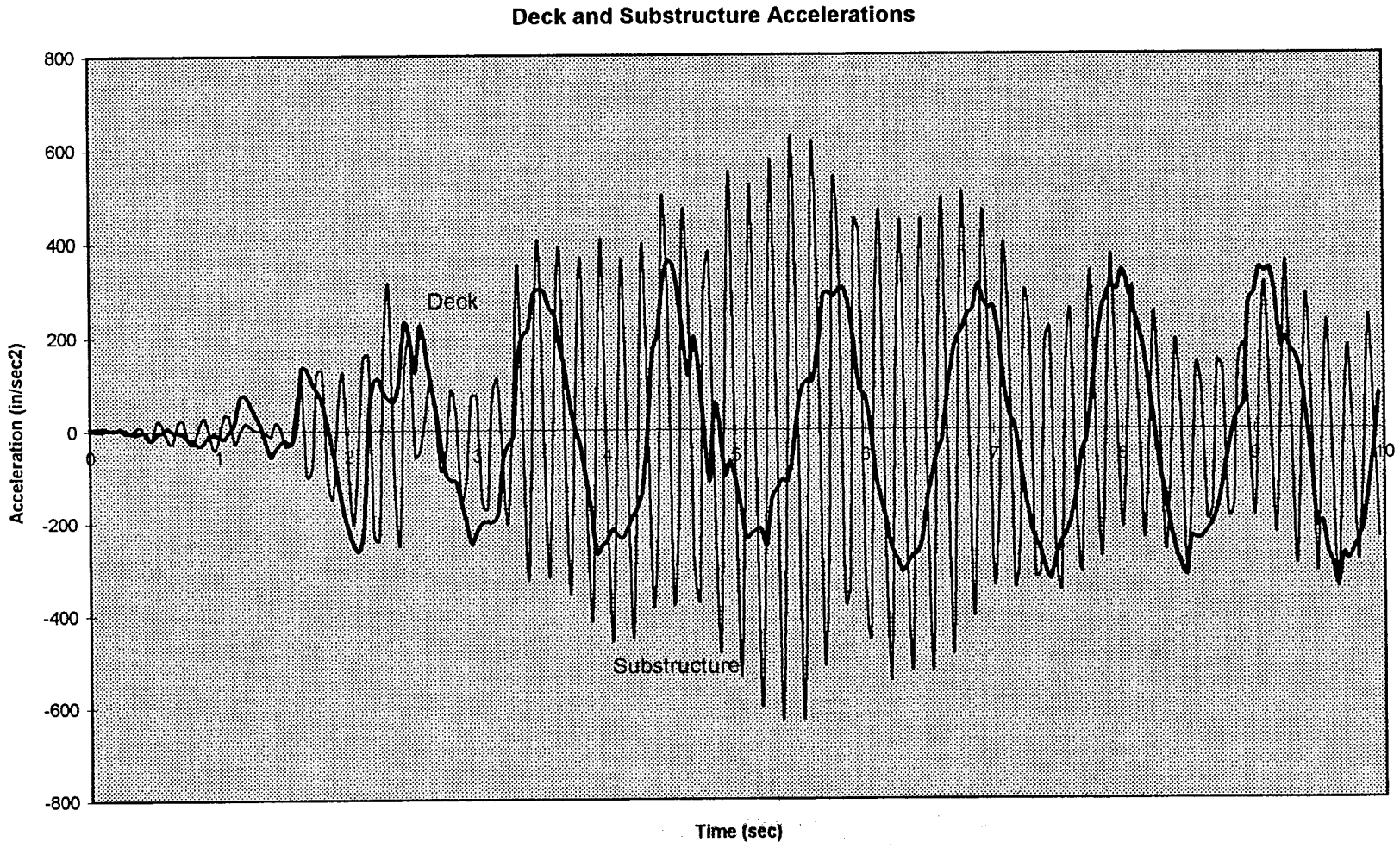

Figure 81 Pier with batter piles deck and substructure response at 0.45g.

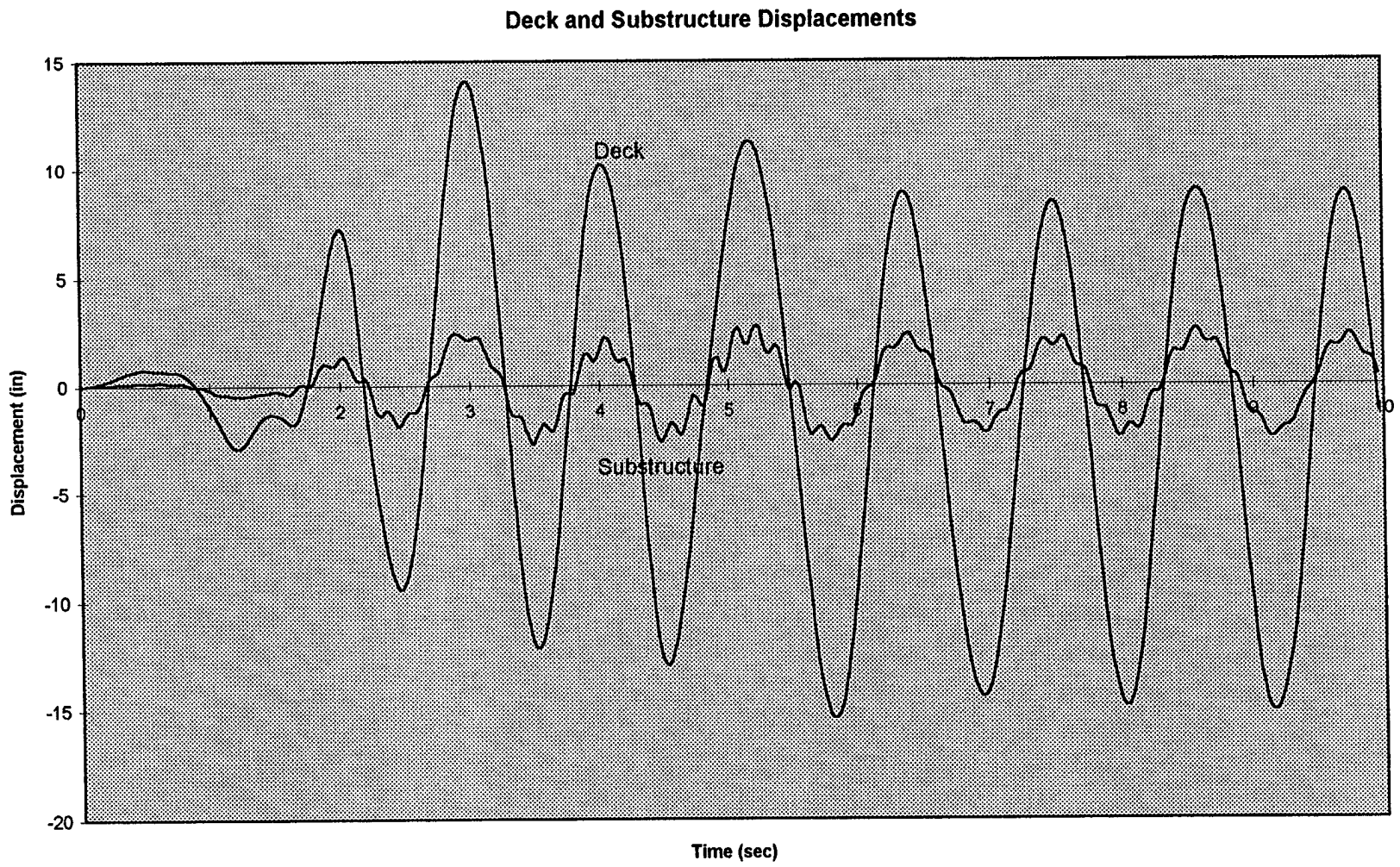

Figure 82. Pier with batter piles deck and substructure response at 0.9g.

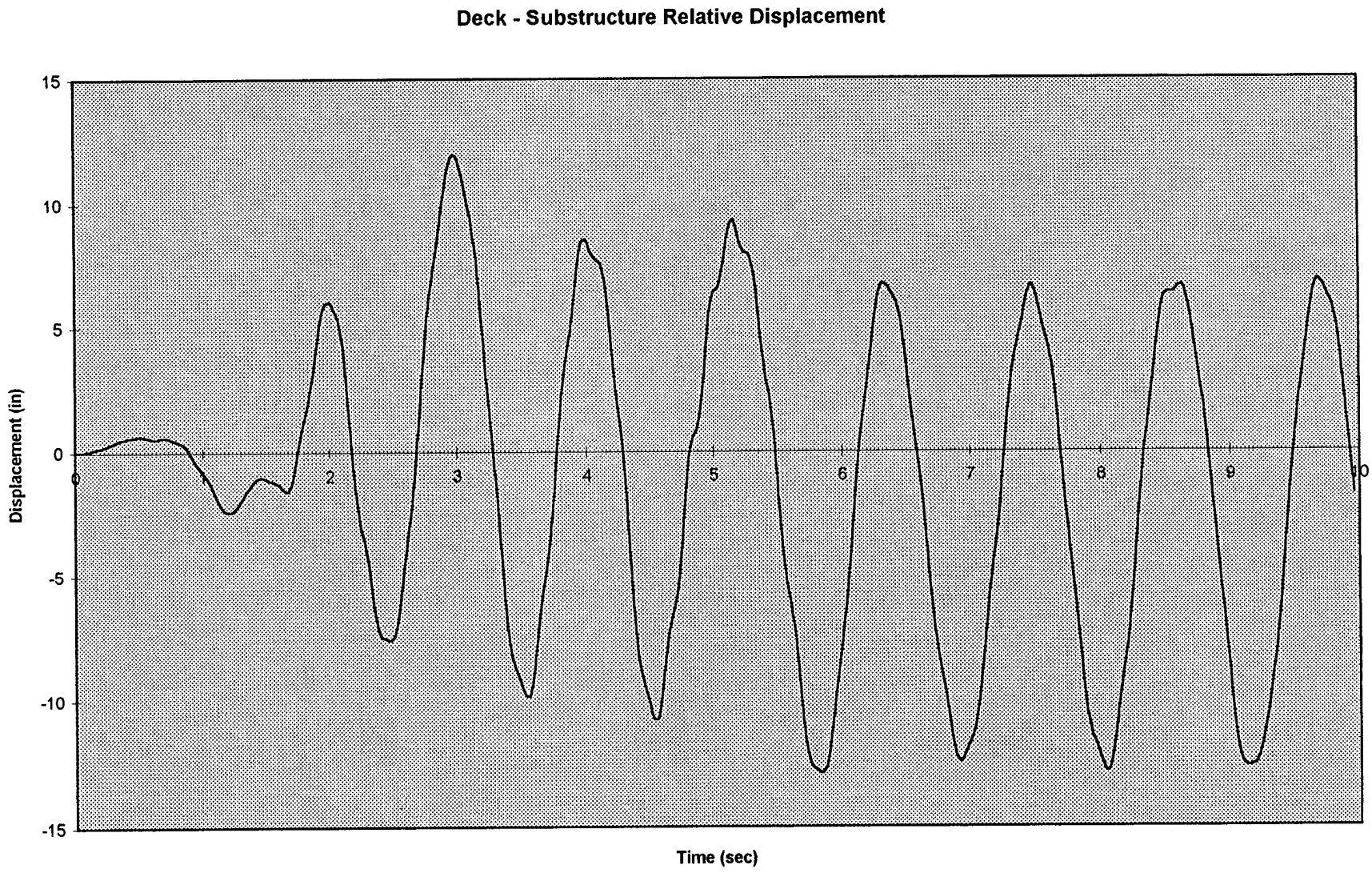

Figure 83. Pier with batter piles deck and substructure response at 0.9g.

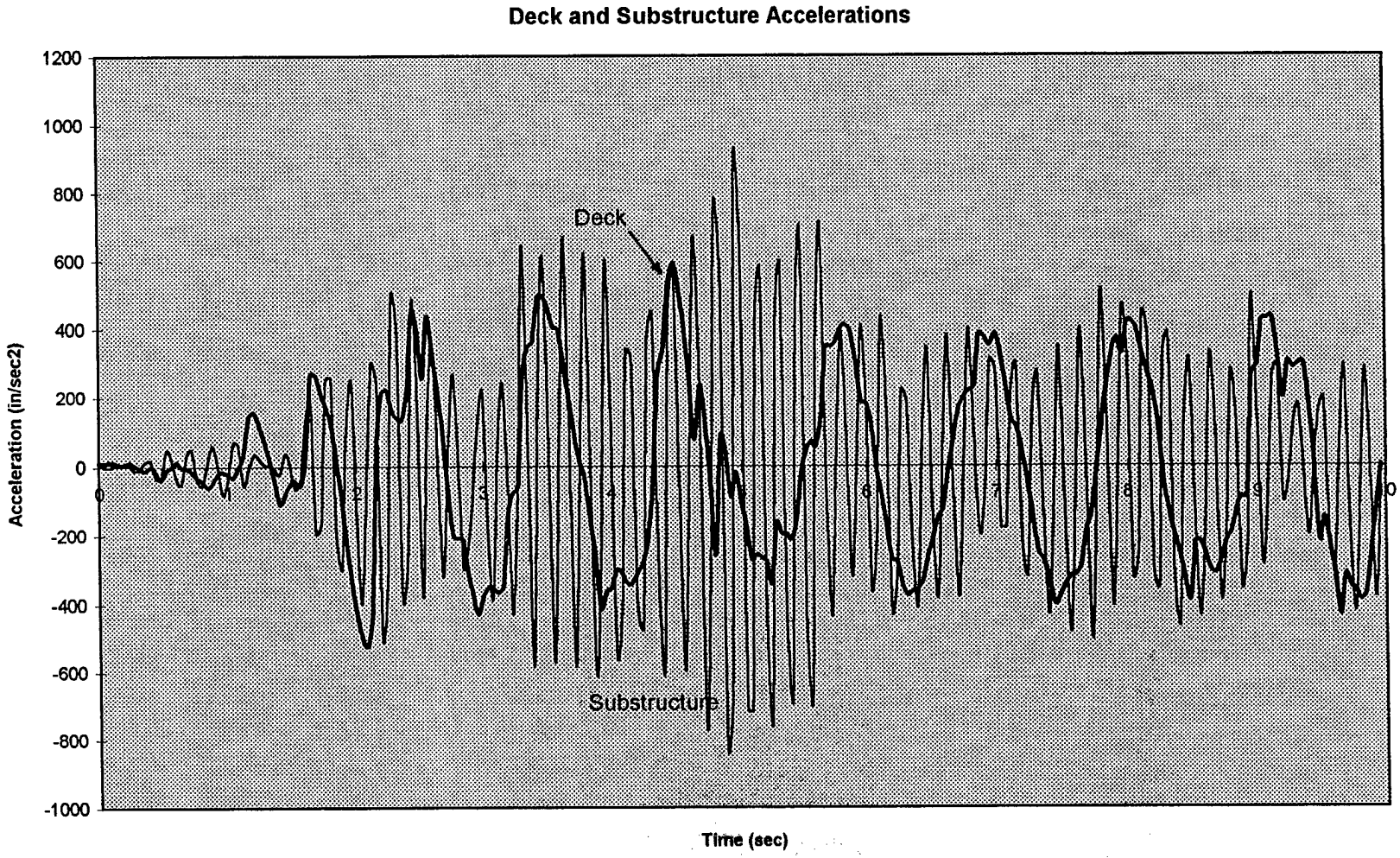

Figure 84. Pier with batter piles deck and substructure response at 0.9g.

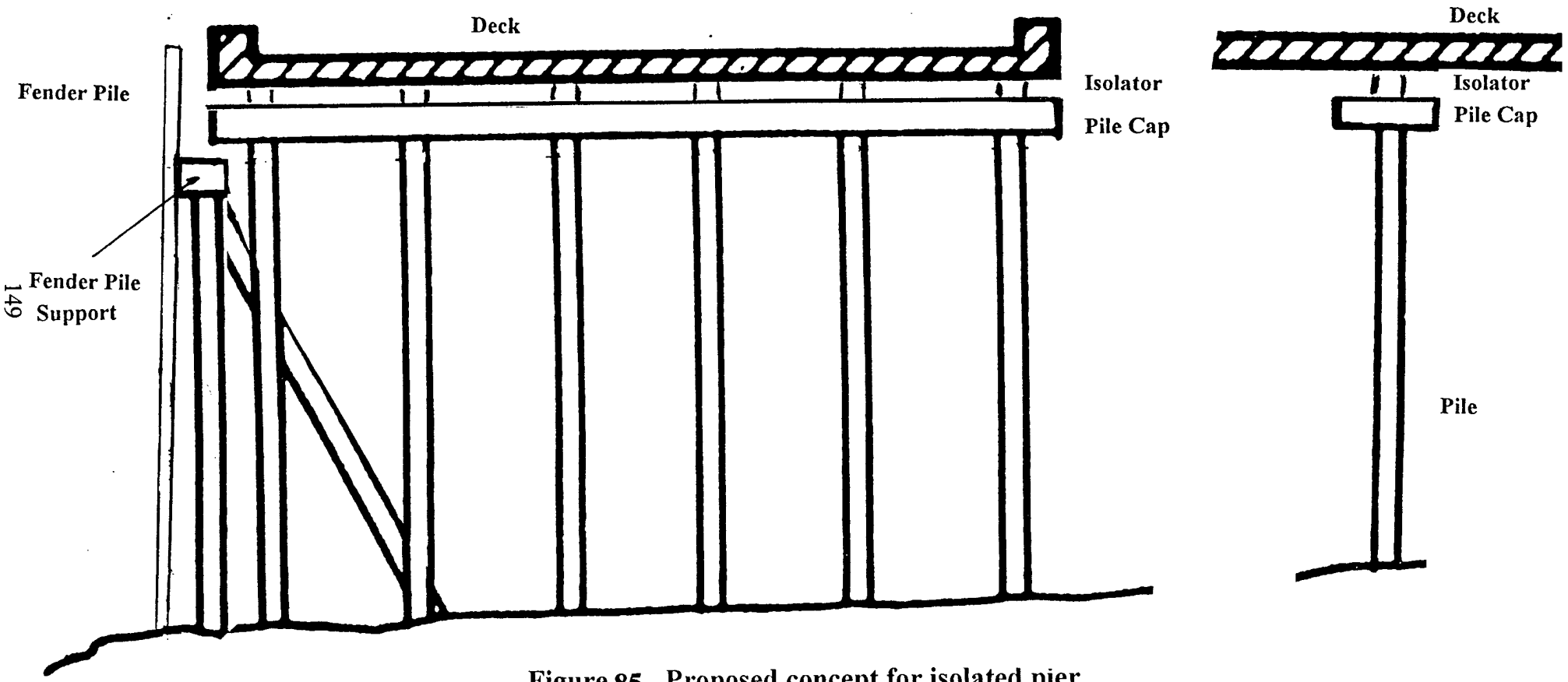

Figure 85. Proposed concept for isolated pier having separate fender lateral resistance system.

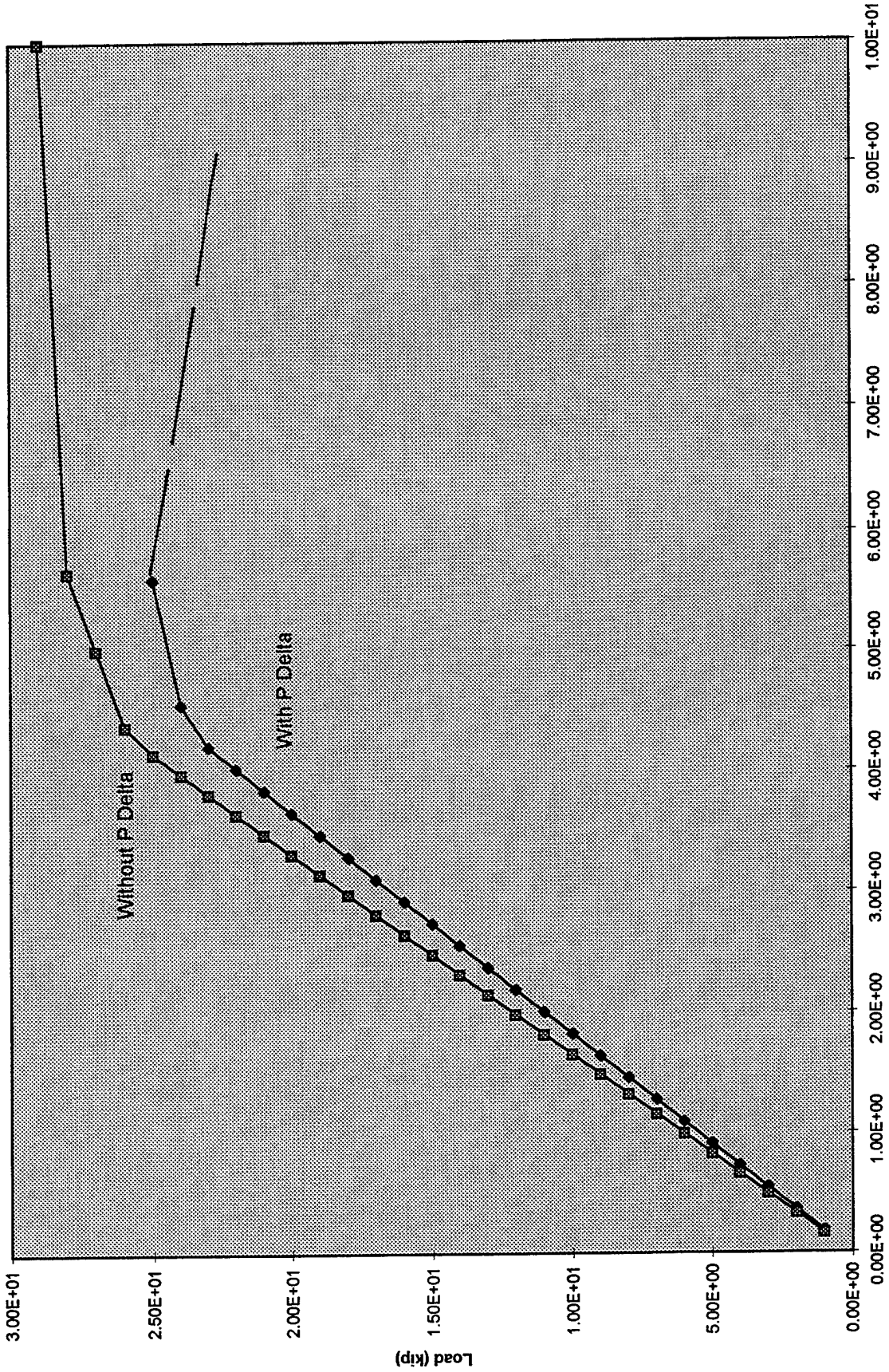

Figure 86 Influence of P - delta effect on pier in Figure 69.

APPENDIX

Actual Lateral Load Tests On Piles

And Comparison To

Calculated Results

API Equations and Lateral Load Tests On Piles

As engineers we are required to use the best available technology in design of structures. The technology presented in this report does that. It is important that we realize that response of structures in soil have the potential for high variability. This appendix will present results of studies conducted as part of this task which show the accuracy of current analytical procedures.

Sands

A sensitivity analysis was performed in which the parameters of friction angle and density used in the API sand equation were increased by 20 percent, Figure A-1. As can be seen the friction angle has a greater influence on the p-y curve. O'Niell and Murtcheson (1983) performed a series of sensitivity variations on a pile shown in Figure A-2. The deflection of the pile is influenced to a greater extent than the pile moments by variation in soil properties.

Lam and Cheang (1995) review soil - pile interaction. They note that the API equations for sand assumes the ultimate passive pressure and elastic stiffness increase linearly with depth. The suggest that this is valid for ultimate pressure, but overly stiff for elastic slope. The maximum shear modulus tends to be proportional to the square root of depth or confining pressure rather than depth directly. They note that under cyclic loading many researchers note a dynamic gapping effect which leads to softer pile response. They also suggest a pile diameter effect such that the API equations are too soft for larger diameter piles.

The accurate computation of lateral deflection is of significant interest. Actual lateral load tests on full scale piles were performed and reported by Morrison and Reese (1988). The lateral load test was performed on a 10.75-inch diameter steel pipe pile driven in to clay. The upper 10 feet were replaced with a compacted saturated SP sand. The soil had an average dry density of about 98.5 lbs/cu ft, a friction angle of 38 degrees. The buoyant weight was approximated from the dry density. The friction angle was determined from cone penetration test results. Figure A-3 shows the test pile section. . Strain gages were placed on the pile to measure bending moment. A polynomial function was fitted to the measured bending moments using the method of least squares. The polynomial was integrated twice to obtain the deflection and differentiated twice to obtain the soil resistance. Figure A-4 shows the p-y pile curves based on calculations from the test pile data based on these measurements.

A finite element analysis was performed of the basic pile loaded laterally by static horizontal force. The p-y curves based on the measured data shown in Figure A-4 were used to establish the properties of the soil springs. Figures A-5 and A-6 show the

computed pile deflection and bending moment in comparison with measured results. Agreement is excellent. The conclusion is that given the accurate p-y data upon which to establish the soil spring properties, the basic finite element model consisting of beam column elements representing the pile and bilinear springs representing the soil is capable of accurately predicting pile behavior.

O'Neill and Murtcheson (1983) report two case studies of piles in sand, the Mustang Ranch study and the Arkansas River study. Figure A-7 shows the Mustang River pile geometry and soil properties. Figure A-8 shows the comparison between the computed and the observed deflection of the pile at the measured location. Computed results in this case underestimate observed deflection. A sensitivity analysis was performed in which the stiffness and yield strength was varied individually. The stiffness of each of the soil elements was reduced by 10 percent; deflections at the reference point increased by 1.5 percent (peak values 1.40 to 1.42 inches). A 10 percent reduction was made in the yield strength of each soil element; a 7 percent increase was noted in the reference deflection (peak values 1.40 to 1.50 inches). Based on these observations a trial was run in which both the stiffness and the yield strength were reduced by 50 percent. deflections increased from 1.4 to 2.5 inches at the reference point at peak load or about 78 percent. To match the observed results a reduction in both yield strength and stiffness of 40 percent from the original values determined by the API equation is estimated.

Figure A-9 shows the geometry and the soil properties for Arkansas River study, Figure A-10 shows a comparison of computed and the observed deflection at the measured location. In both cases the calculated results were based on the p-y curves determined using the API equations for sand. Both studies show that the comparison to test data is only approximate and that in one case the calculated results under-predict the measured and in the other they over-predict the measured results.

Clays

A sensitivity analysis was performed in which the soil properties used in the API clay equation were increased by 20 percent. Figure A-11 shows the results; the pile response is sensitive to variations in cohesion.

Reese et al (1988) conducted full scale lateral load test on piles in clay. Figure A-12 through Figure A-16 give the soil properties of the site. Figure A-17 shows the computed p-y curves as a function of depth for the soil reaction in the clay. Figure A-18 shows the p-y curves computed using the API equations. The is qualitatively acceptable at a depth of 5 feet and greater. The actual curves based on the test data give lower yield strengths than the API equations predict at shallow depths less than 5 feet.

Reese (1996) reports on work by Kerisel (1965) in which piles were instrumented and tested in clay. A pile was selected for analysis. It had a length of about 20 feet with approximately 3 feet extending above grade. The pile was formed by 2 steel sheet-pile

sections welded together and had a moment of inertia of 306 inches^4. The soil was classified as a CH medium stiff clay with an undrained shear strength of about 18.5 psi, total unit weight of 114 lb/cuft. the pile was modeled using beam column elements and soil bilinear springs. Based on the soil properties py curves were calculated and used to define the soil spring stiffness and strength. A typical py curve is shown in Figure A-19a. Figure A-19b represents a first trial at representing the multi-line py curve by a bilinear equivalent system. This as seen by the results in Figure A-20 places too much emphasis on the high load aspect of the curve and misses capturing the initial stiffer low load response. Figure 19c captures the initial low load stiffness accurately and also captures the yielding. As seen in Figure A-20 the second calculation agrees more closely with observed test results. To accurately capture the response of the pile under loading it is necessary to define the py curves accurately over the range at which they will be loaded.

References

American Petroleum Institute (1994) Recommended Practice For Planning, Design and Constructing Fixed Offshore Platforms - Load and Resistance Factor Design, RP2A-LRFD, Washington DC, Approved April 1994

Kerisel, J. L. (1965) "Vertical and horizontal bearing capacity of deep foundations in clay" Bearing Capacity and Settlement of Foundations, Duke University, April 1965

Lam, Iganatius Po and Lino Cheang " Dynamic Soil - Pile Interaction Behavior In Submerged Sands" Proceedings ASCE Convention, San Diego 1995

Morrison Clark S. and Lymon C. Reese (1988) Miscellaneous Paper GL 88-1 "A Lateral-Load Test Of A Full-Scale Pile Group In Sand" University of Texas for USACE Waterways Experiment Station, Vicksburg MS Feb. 1988

O'Niell, M. W. and J. M. Murtcheson (1983) " An Evaluation Of P-y Relationships in Sands", PRAC 82-41-1, University of Houston, Research Report GT DF02-83

Reese, Lymon C., Dan Allen Brown and Shin-Tower Wang (1988) USACEWES Miscellaneous Paper GL 88-10 " Experimental Research Into The Behavior Of Piles And Pile Groups Subjected To Cyclic Lateral Loading" University of Texas for Waterways Experiment Station, Vicksburg, MS June 1988

Reese, Lymon C. (1996) Unpublished communication

Figure A-1. Sensitivity of API sand equation.

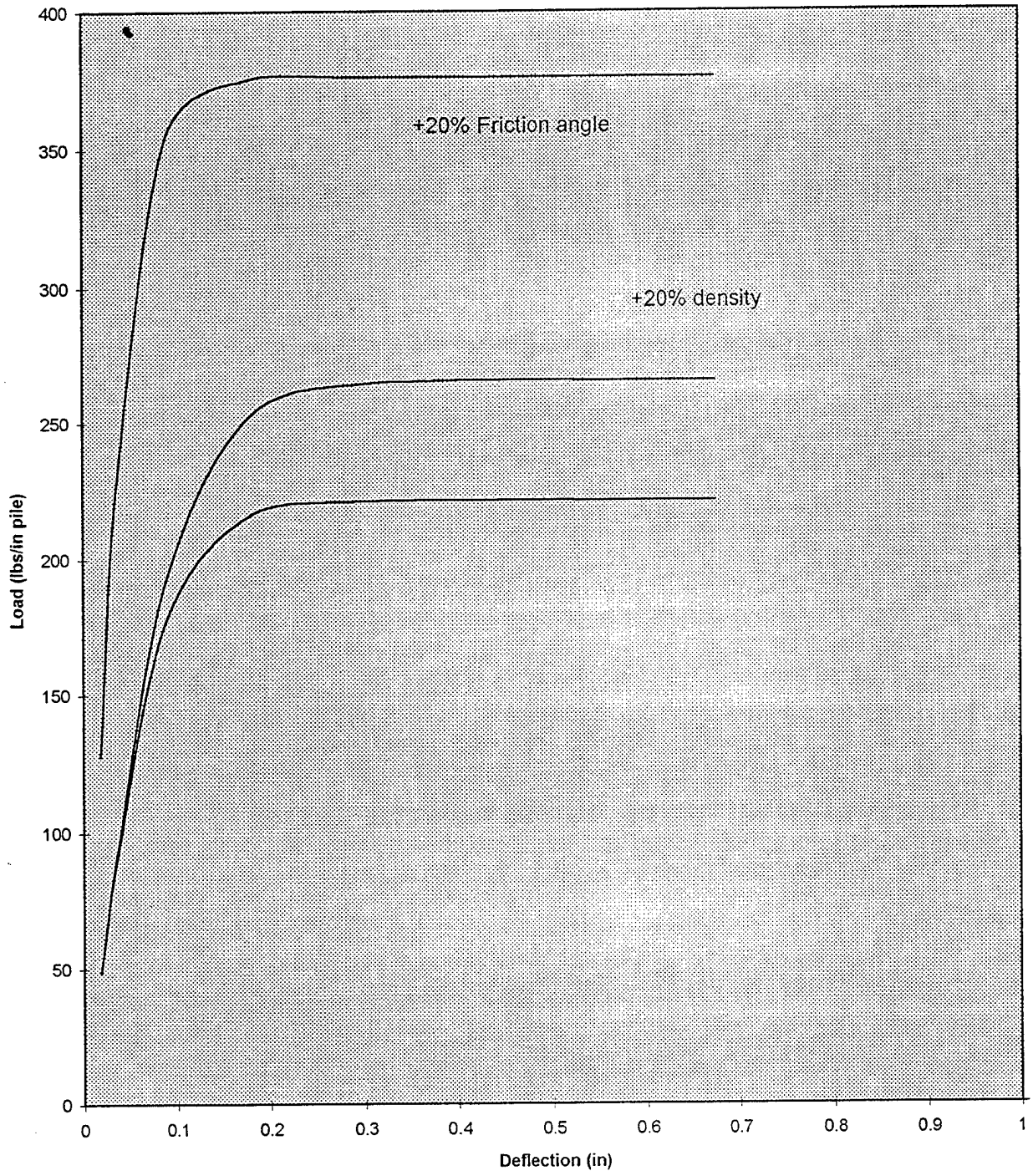

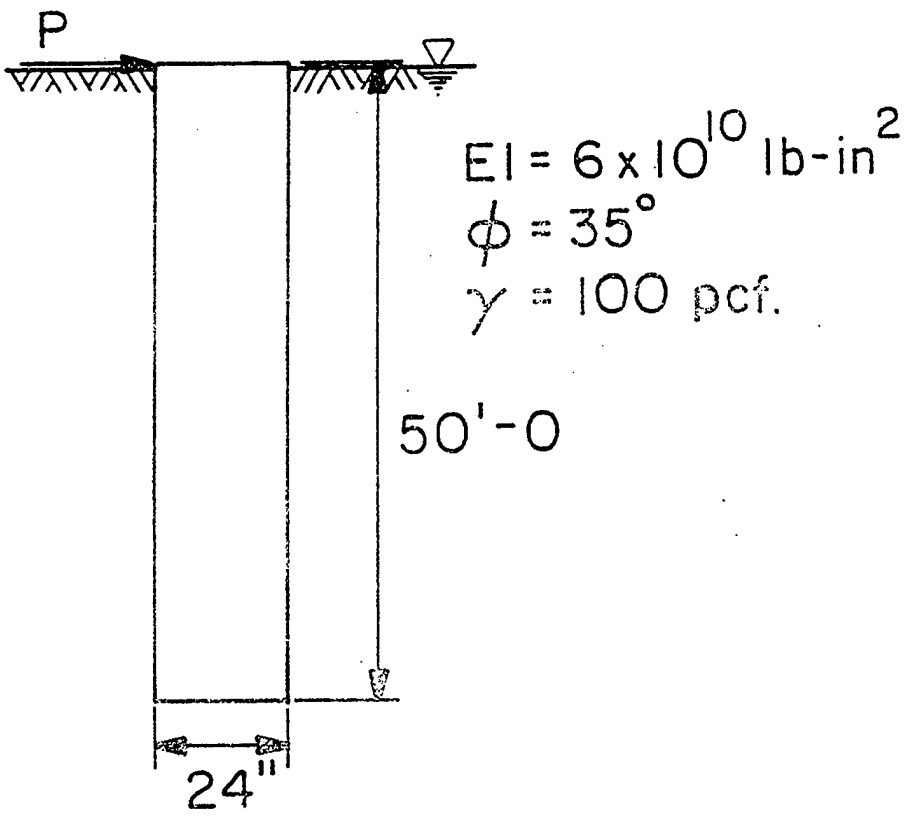

Case	ϕ	γ Lb/cu ft	k Lb/cu in	Variation
1	35	100	80	
2	31	100	80	-10% ϕ
3	39	100	80	+10% ϕ
4	35	90	80	-10% γ
5	35	110	80	+10% γ
6	35	100	60	-25% k
7	35	100	100	+25% k

Figure A-2 . Variation of pile response with soil properties. (After O'Neill and Murchison (1983))

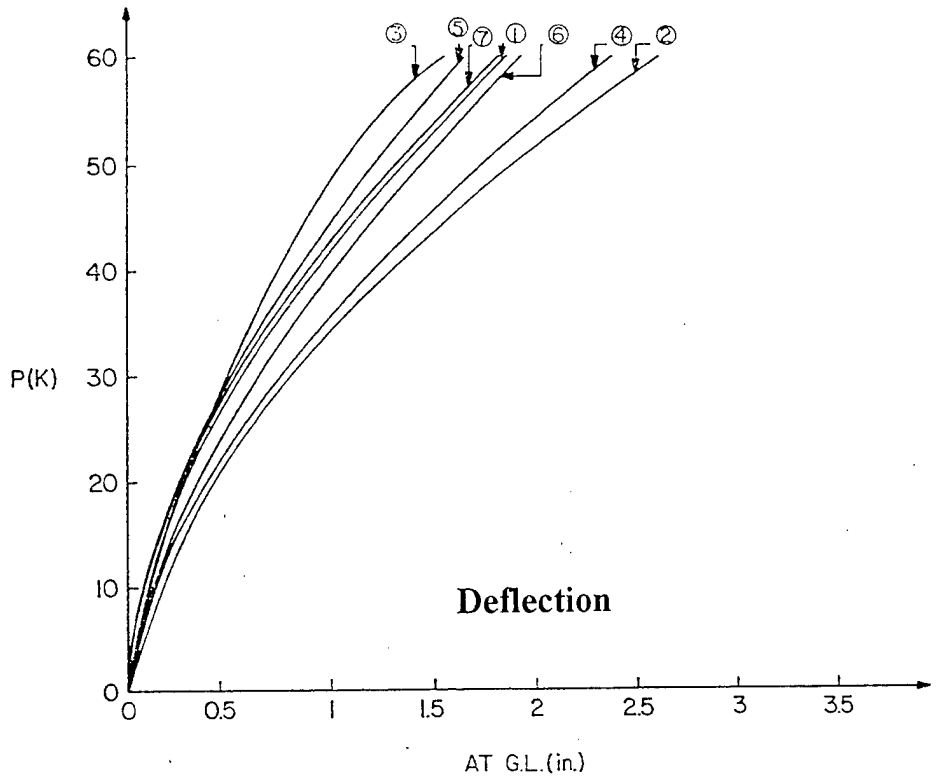

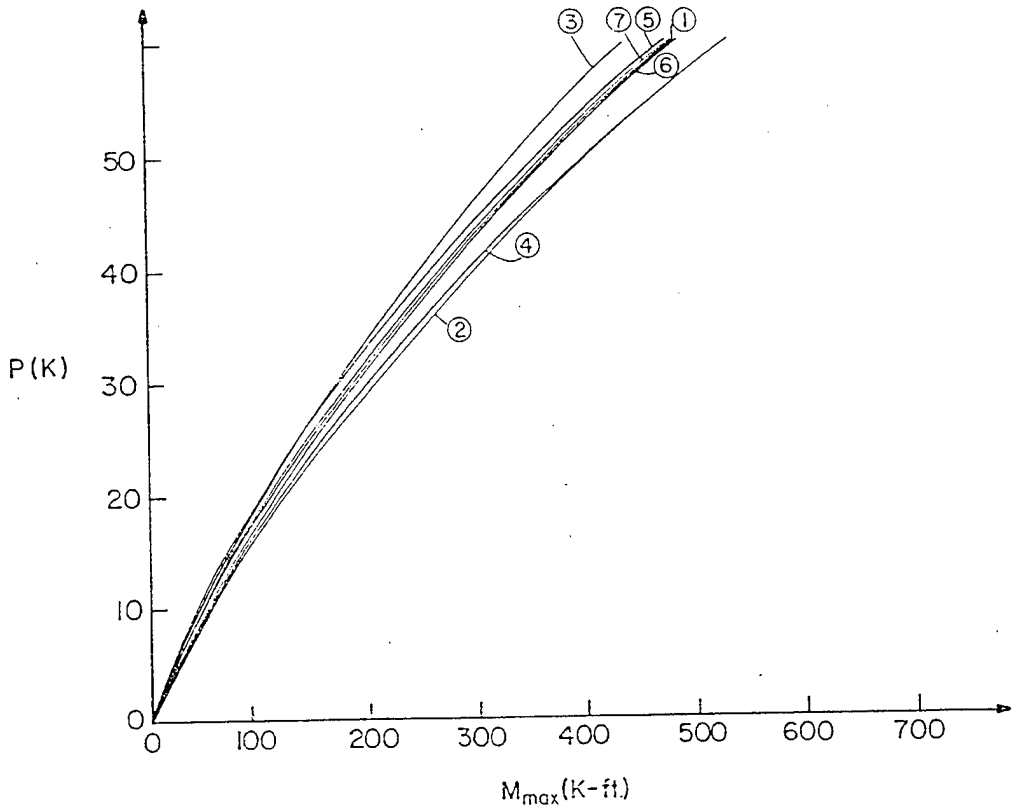

Figure A-2 . Continued

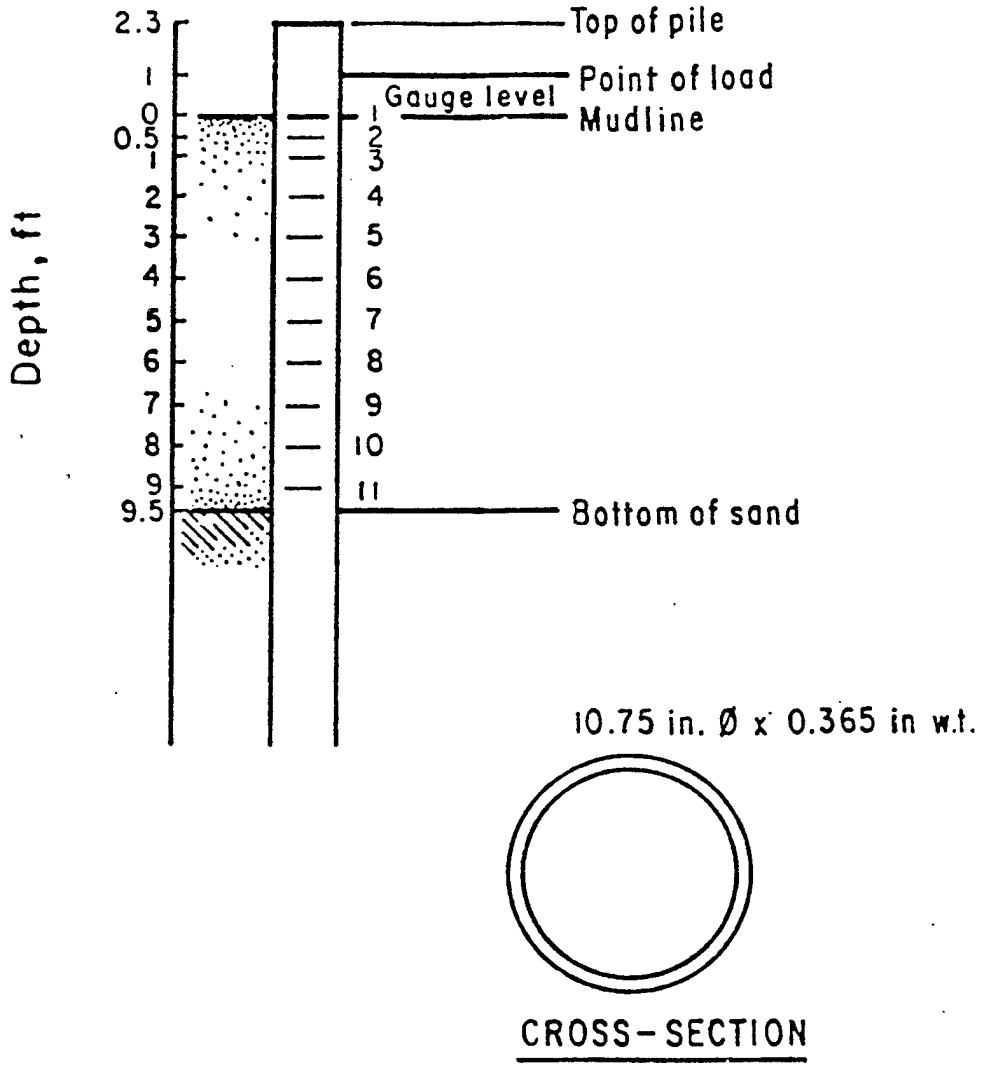

Figure A-3 . Test pile from Morrison and Reese (1988).

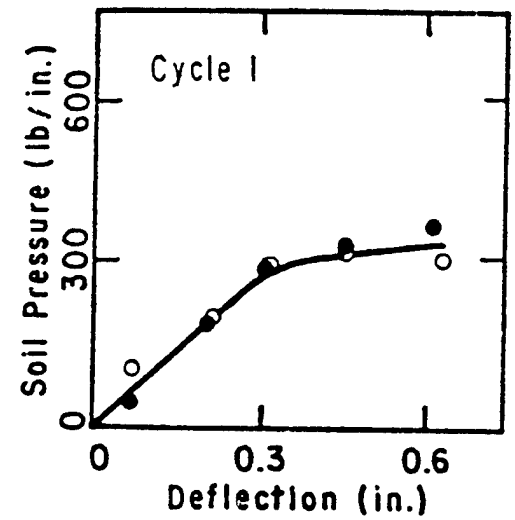

○ Compression Stroke
● Tension Stroke

Depth = 12 in.

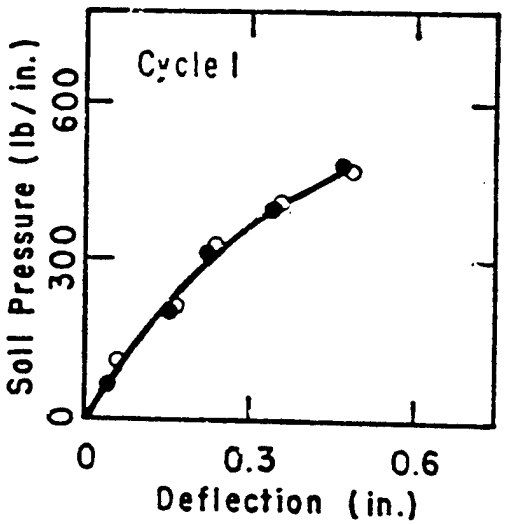

Depth = 24 in.

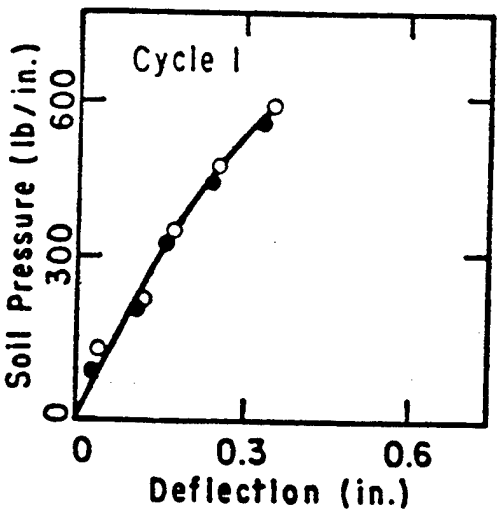

○ Compression Stroke
● Tension Stroke

Depth = 36 in.

Figure A-4 p-y curves from test data.

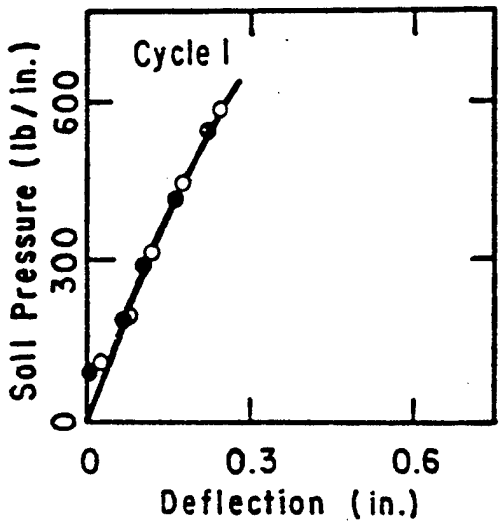

Depth = 48 in.

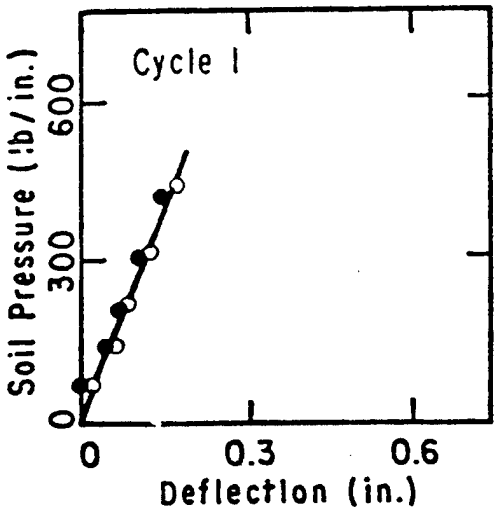

○ Compression Stroke
● Tension Stroke

Depth = 60 in.

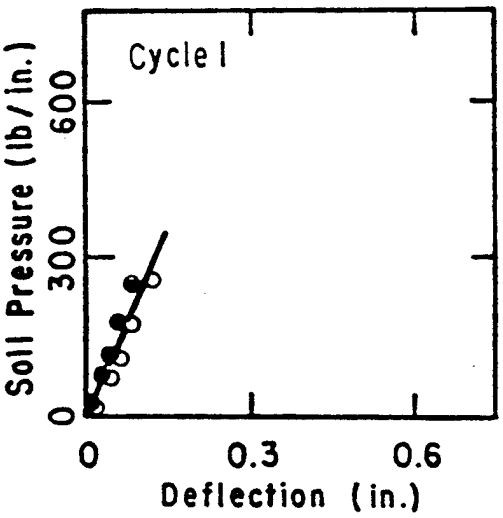

Depth = 72 in.

Figure A-4. Continued

Figure A-5 . Test pile from ref. WES GL88-1.

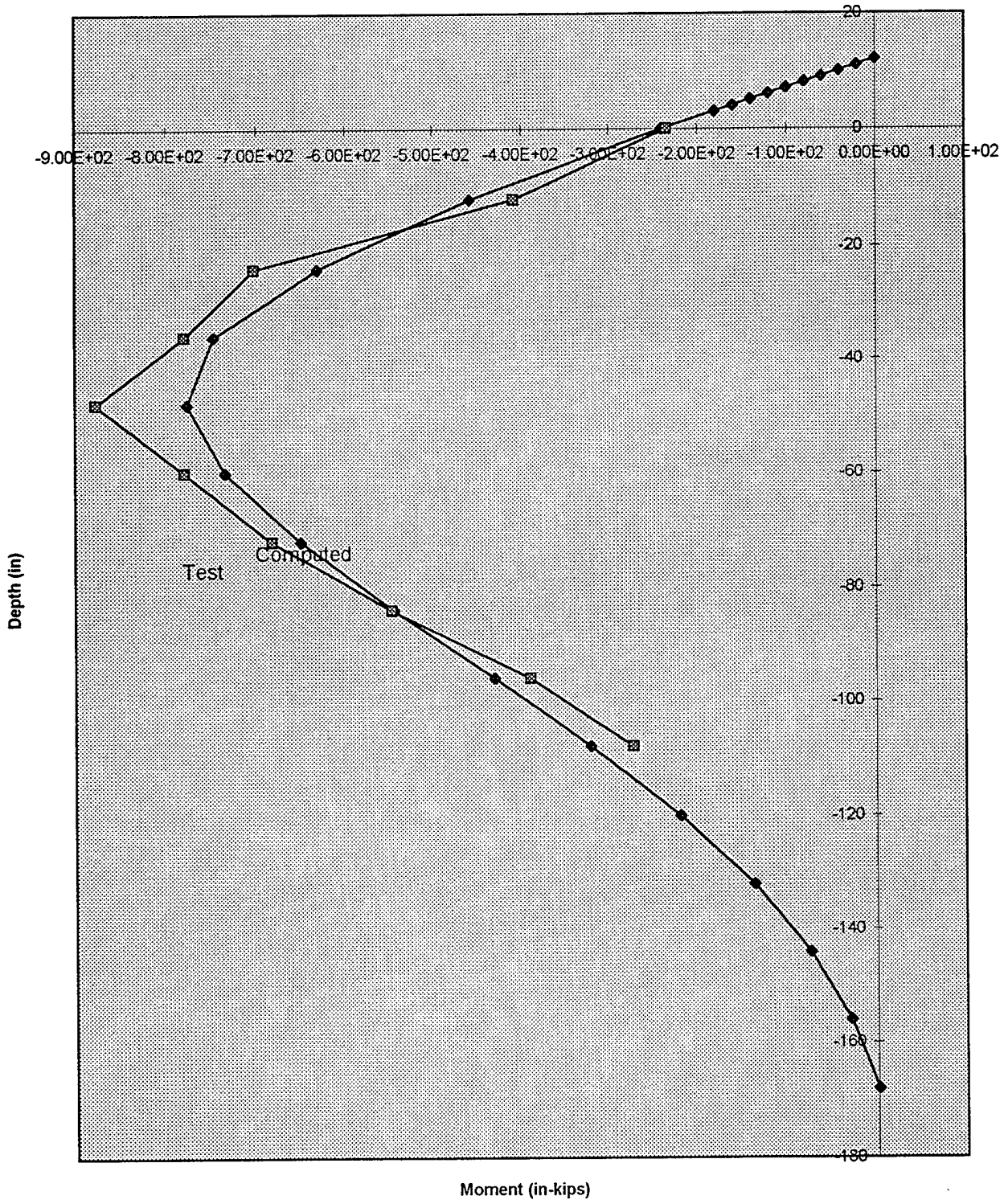

Figure A-6. Load - displacement for test pile, WES GL88-1.

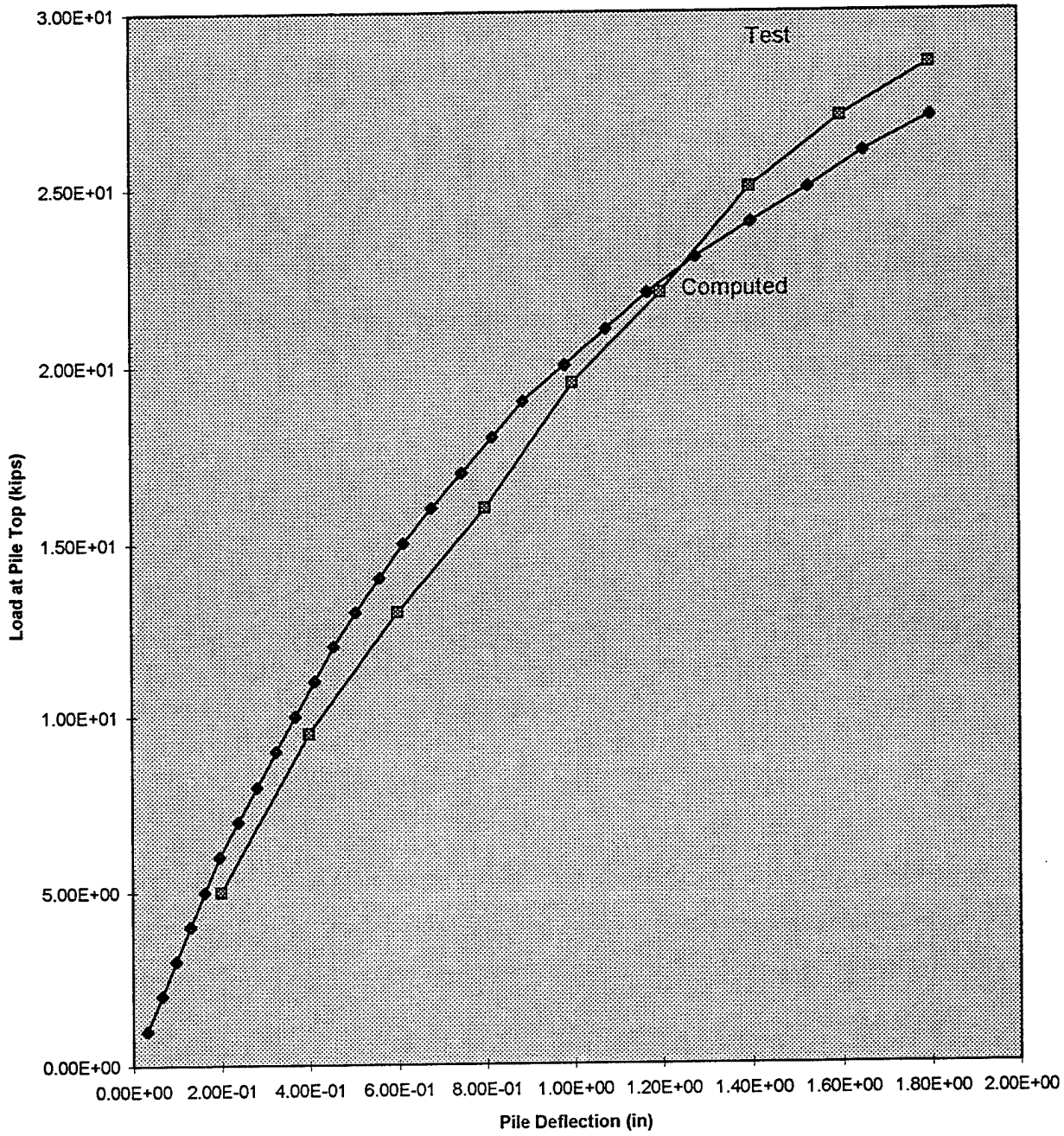

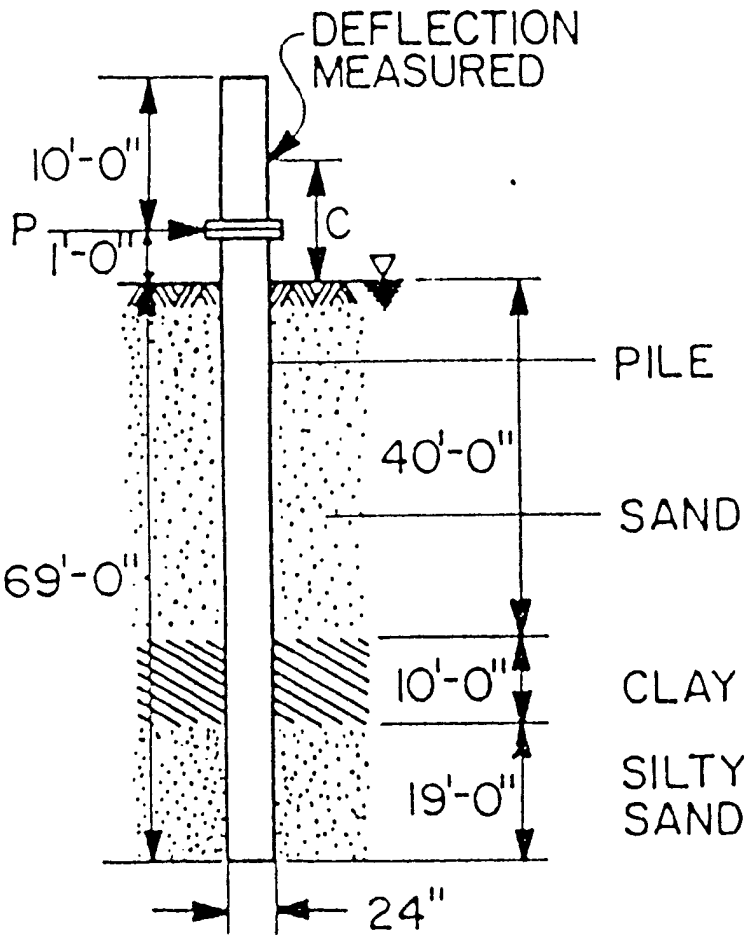

PILE 1 $EI = 5.867 \times 10^{10}$ lb in.^{2} c = 36 in.

PILE 2 $EI = 6.085 \times 10^{10}$ lb in.^{2} c = 19-5/16

Soil Properties

Depth	γ(pcf)	ϕ	Soil
2'-0"	118.0	36°	SM*
4-0	118.0	38	SM
6-0	118.0	38	SM
8-0	118.8	38	SM
10-0	118.8	39	SM
20-0	118.8	43	SM
69-0	122.5	45	SM

*Interpreted from soil tests.

Figure A-7 . Mustang Ranch test pile.

Figure A-8 . Mustang Island pile deflection.

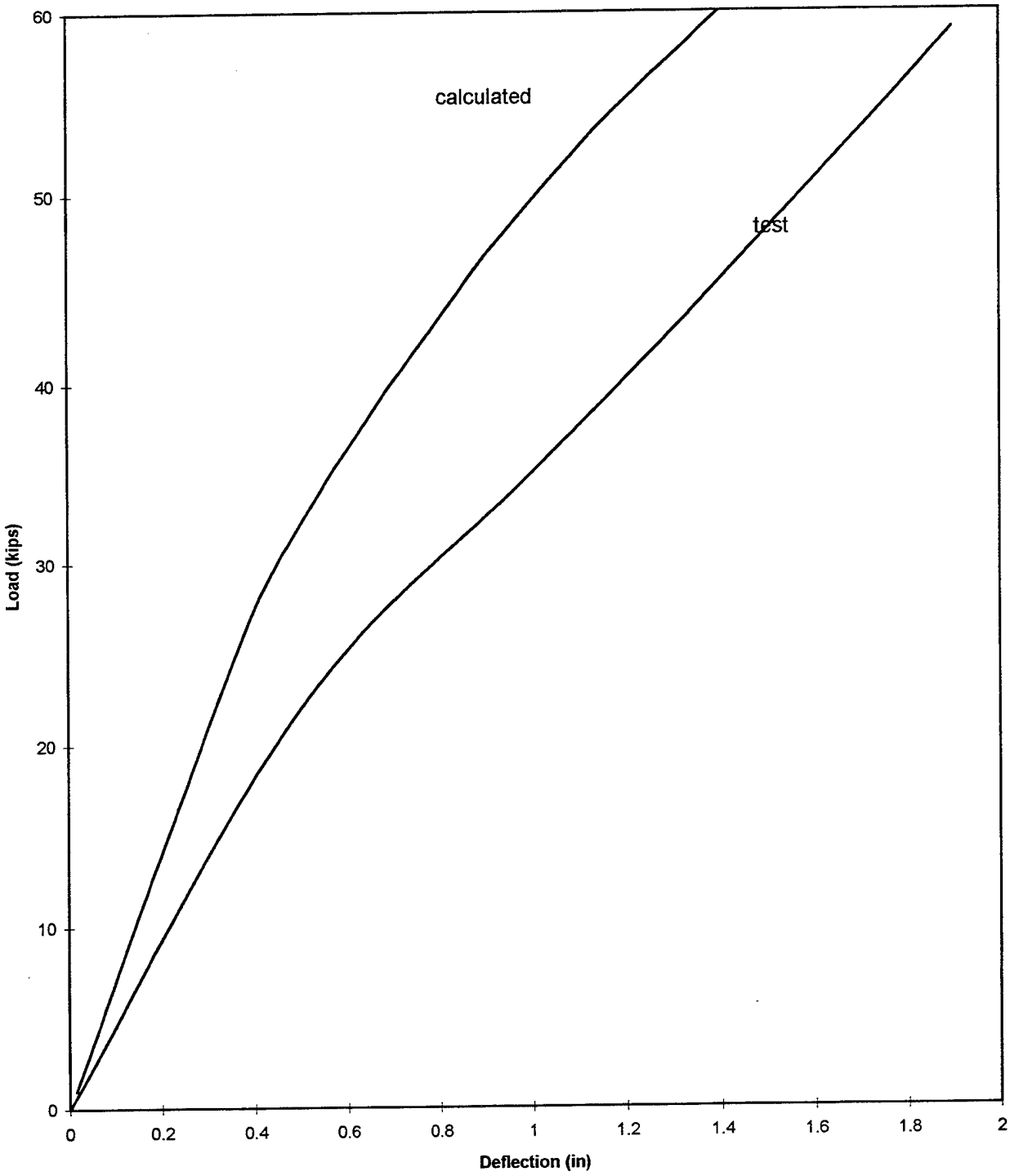

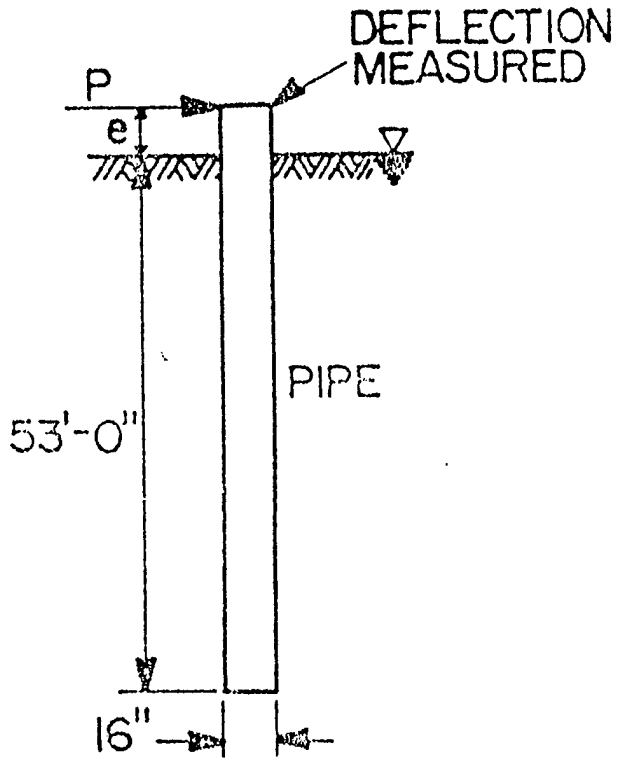

CYCLIC PILE 11A

$EI = 84 \times 10^9$ lb in.^{2}

L = 52'-0

b = 20 in. (square)

PILE 2 e = 1.2 in.

PILE 10 e = 4.2 in.

$EI = 24.4 \times 10^9$ lb in.^{2}

Soil Properties

Depth	γ(pcf)	ϕ	Soil
1'-4"	124	41°	SP
2-8	124	42	SP
4-0	124	42	SP
5-4	124	42	SP
6-8	124	42	SP
8-0	124	42	SP
9-4	124	43	SP
13-4	124	43	SP
53-0	124	43	SP-SM

Figure A-9 . Arkansas River test pile.

Figure A-10 . Arkansas River pile test.

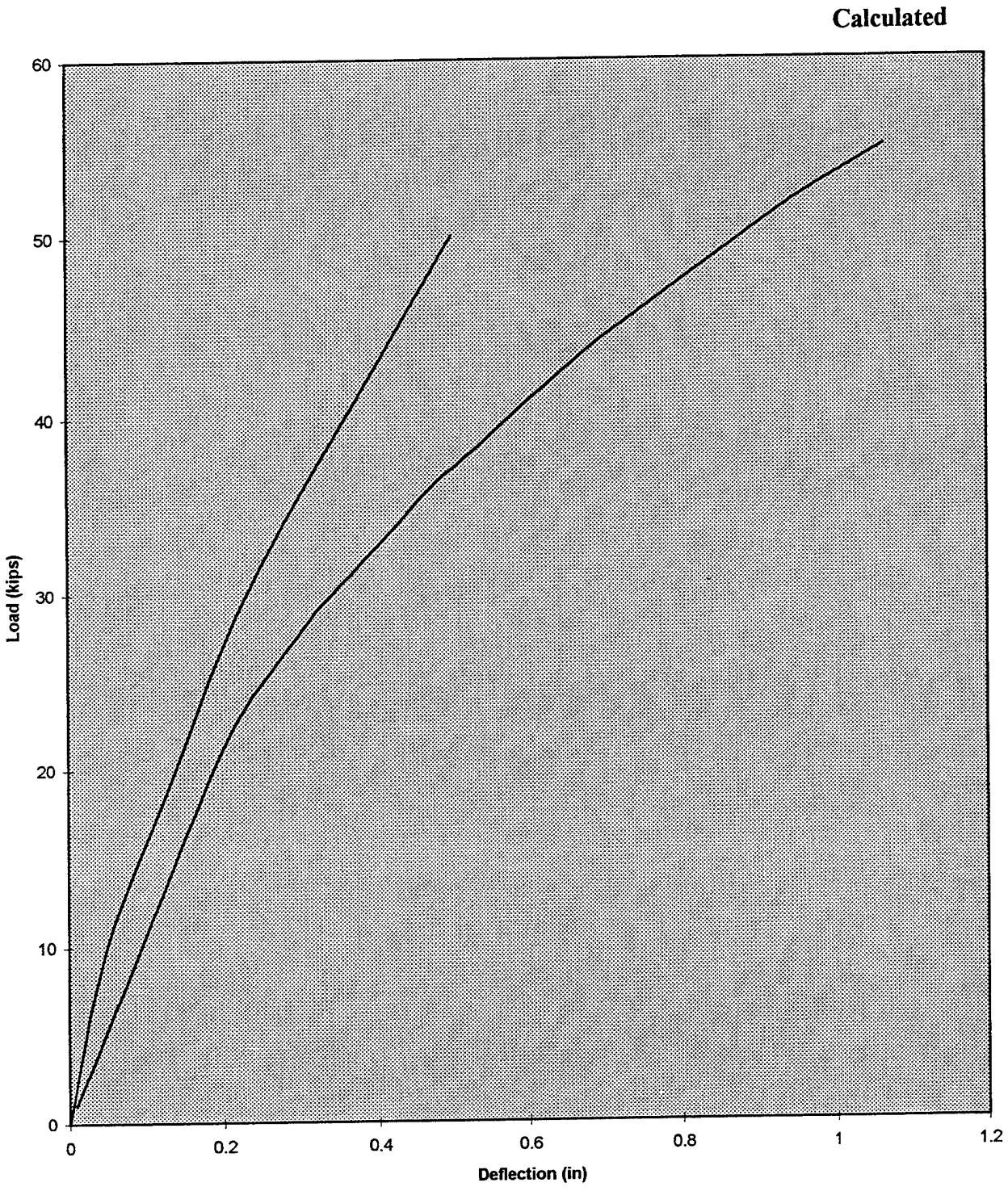

Figure A-11 . Sensitivity of API clay equation.

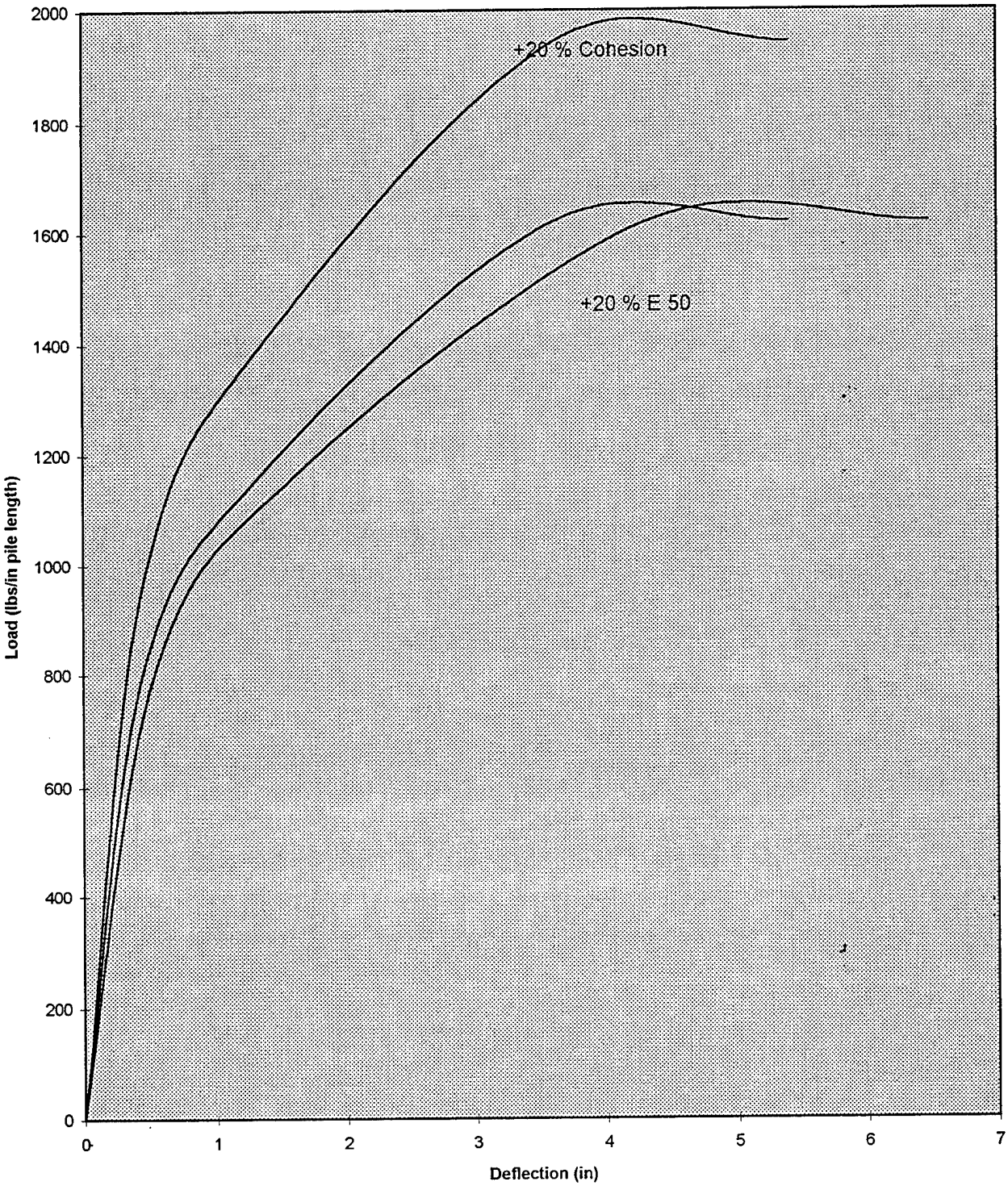

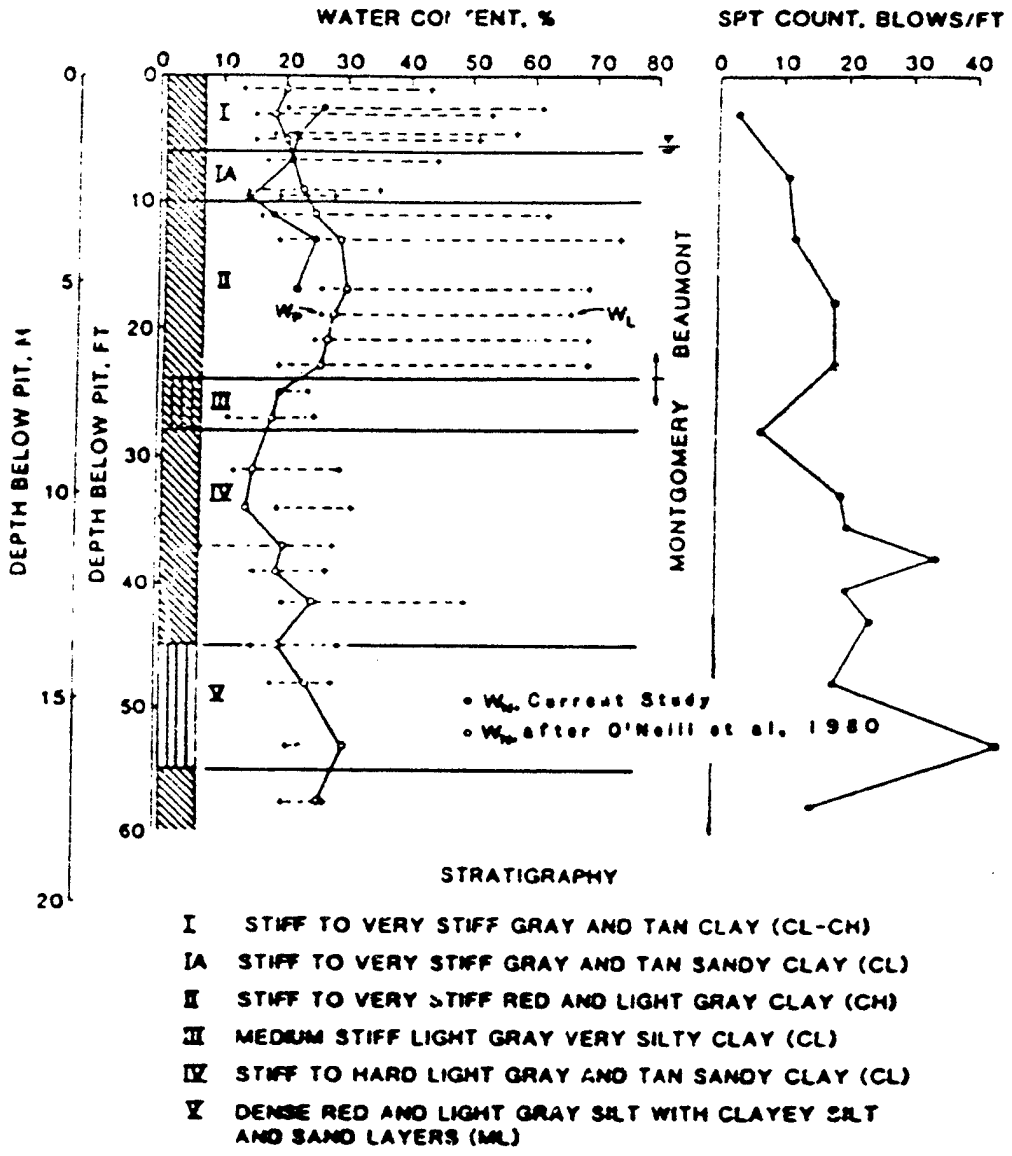

Figure A-12 . Cross section and boring log, clay site.

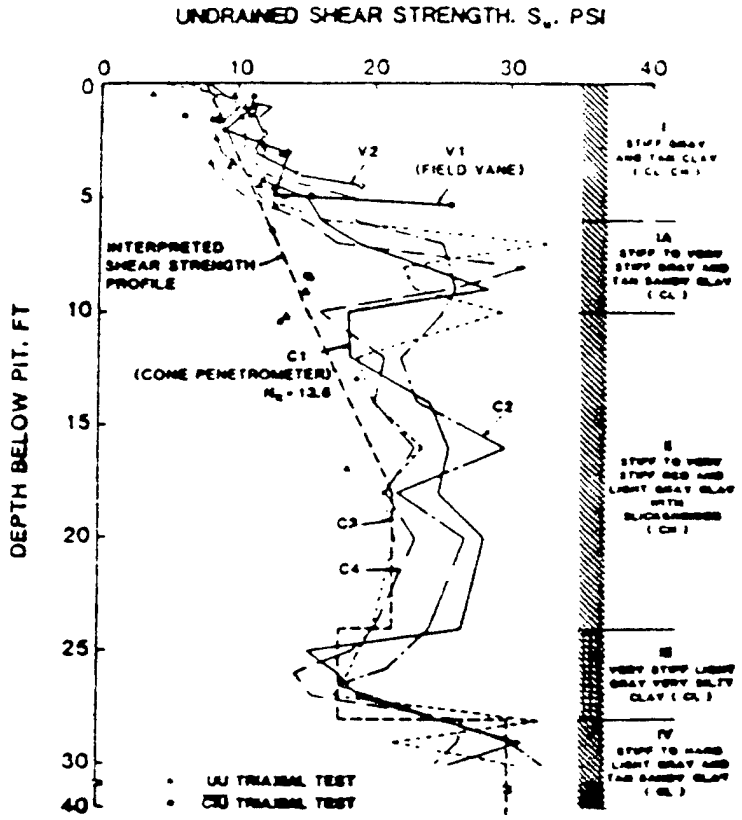

Figure A-13 . Undrained shear strength.

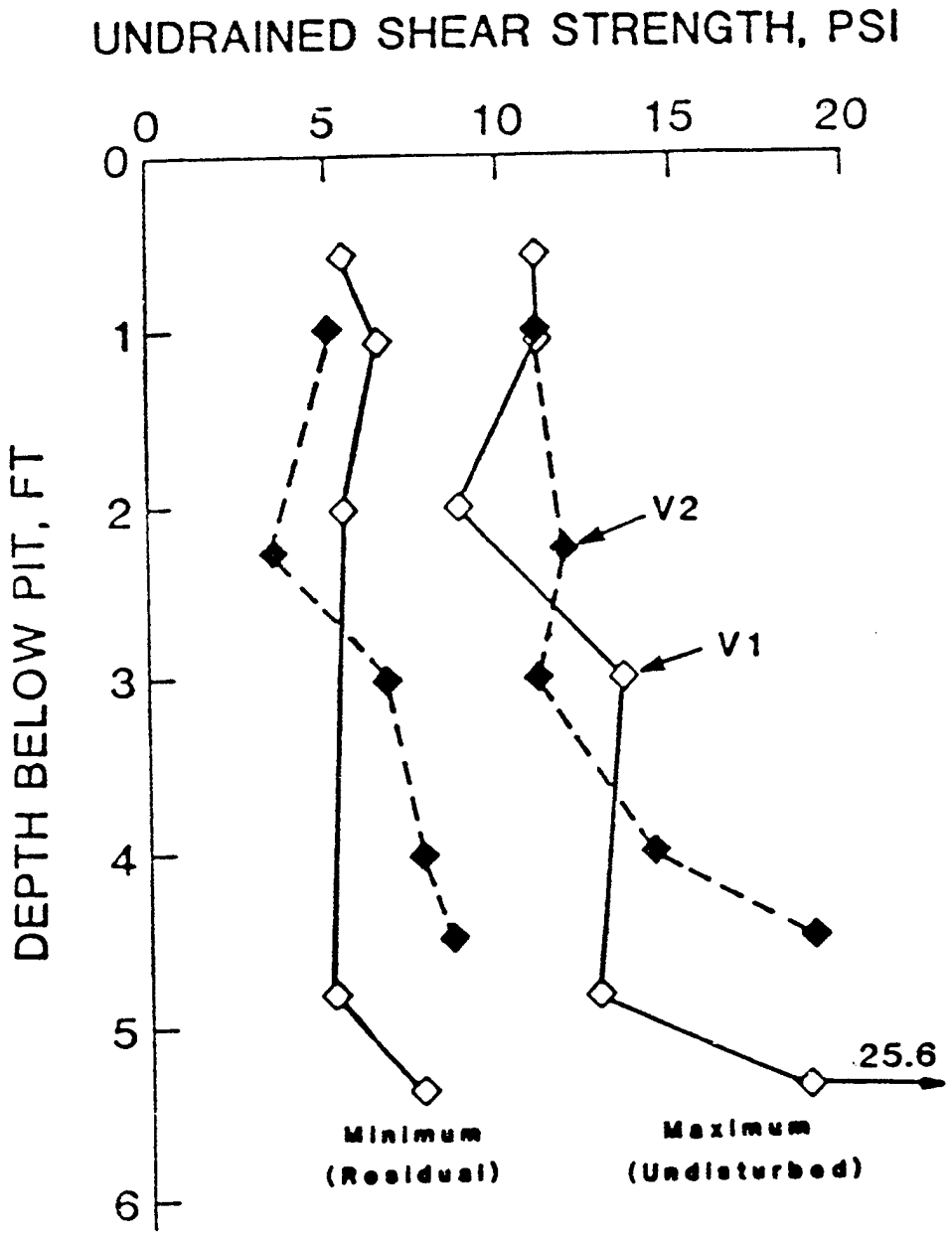

Figure A-14 . Near-surface undrained shear strength.

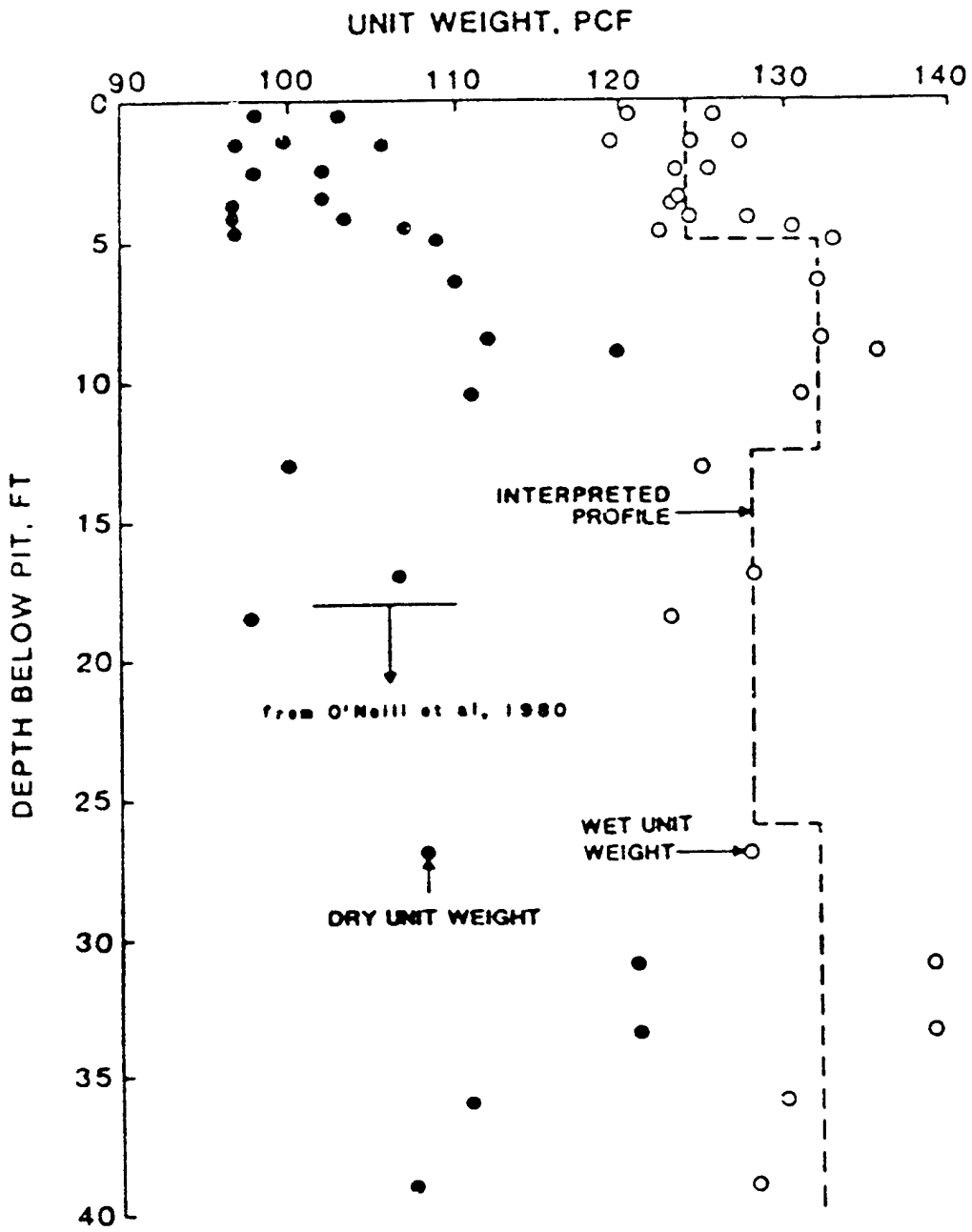

Figure A-15 . Unit weight as a function of depth.

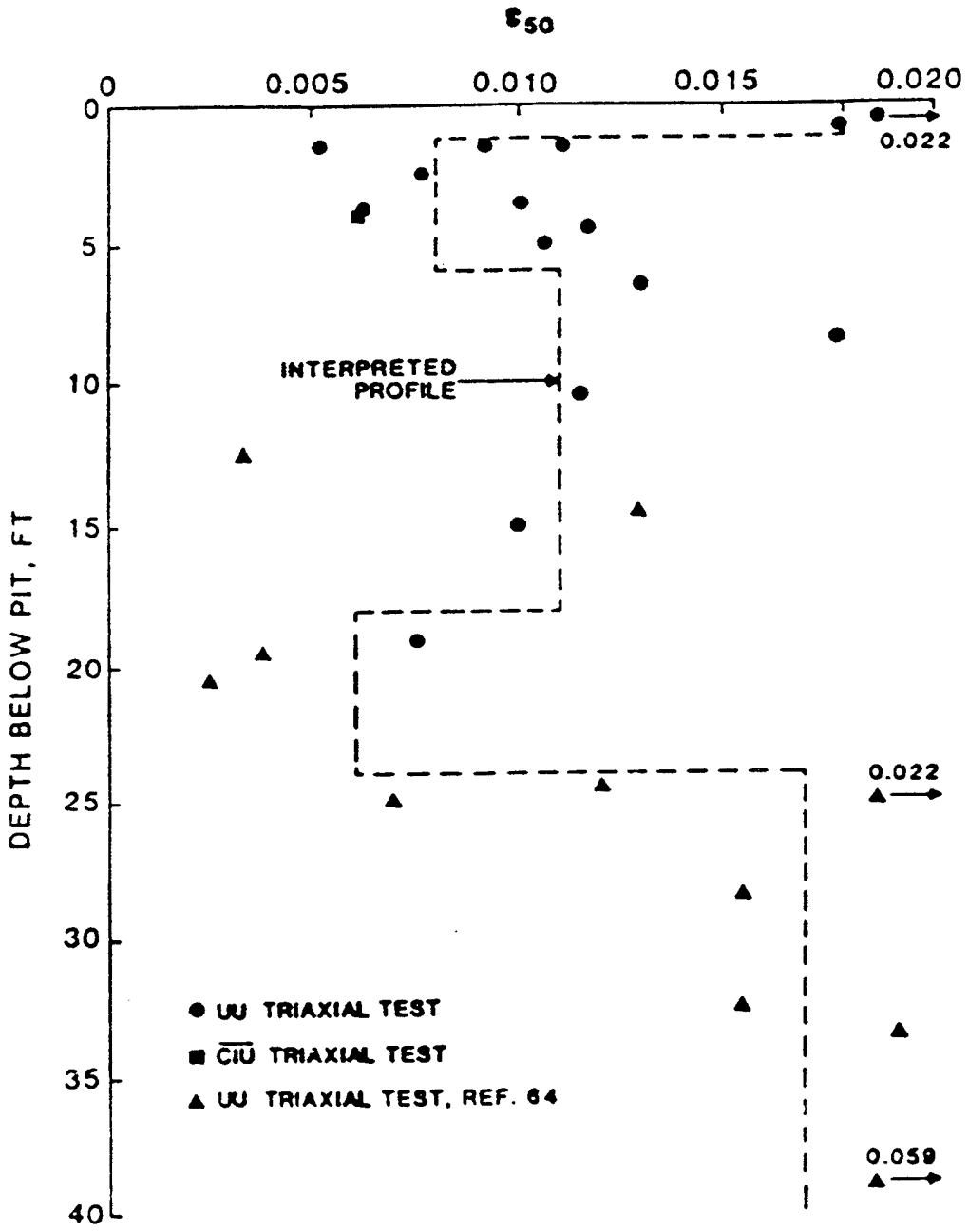

Figure A-16 . Strain ε_{50} as a function of depth.

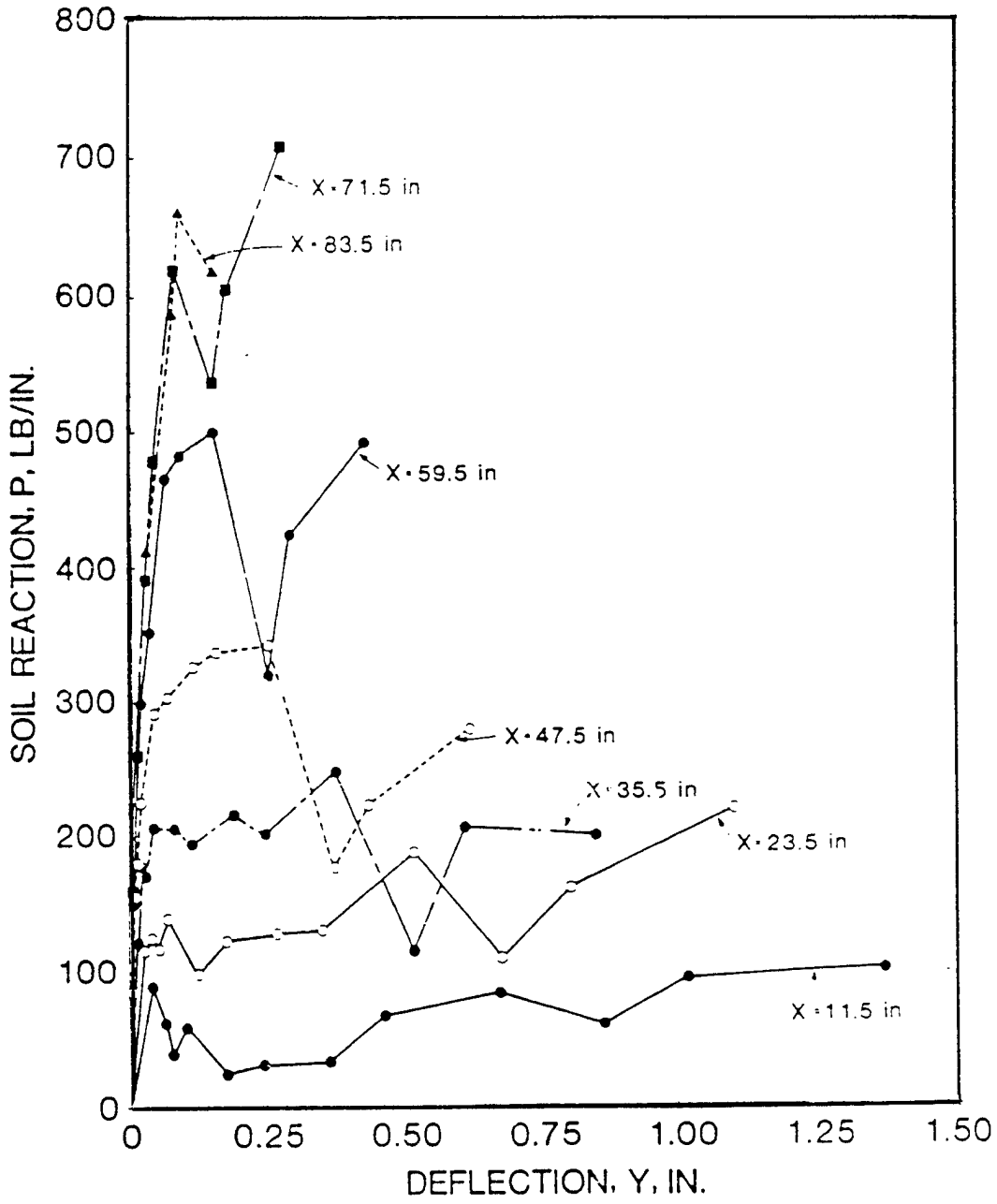

Figure A-17 . P-y curves based on test observations for pile in clay.

Figure A-18. Computed p-y curves from API equations for clay.

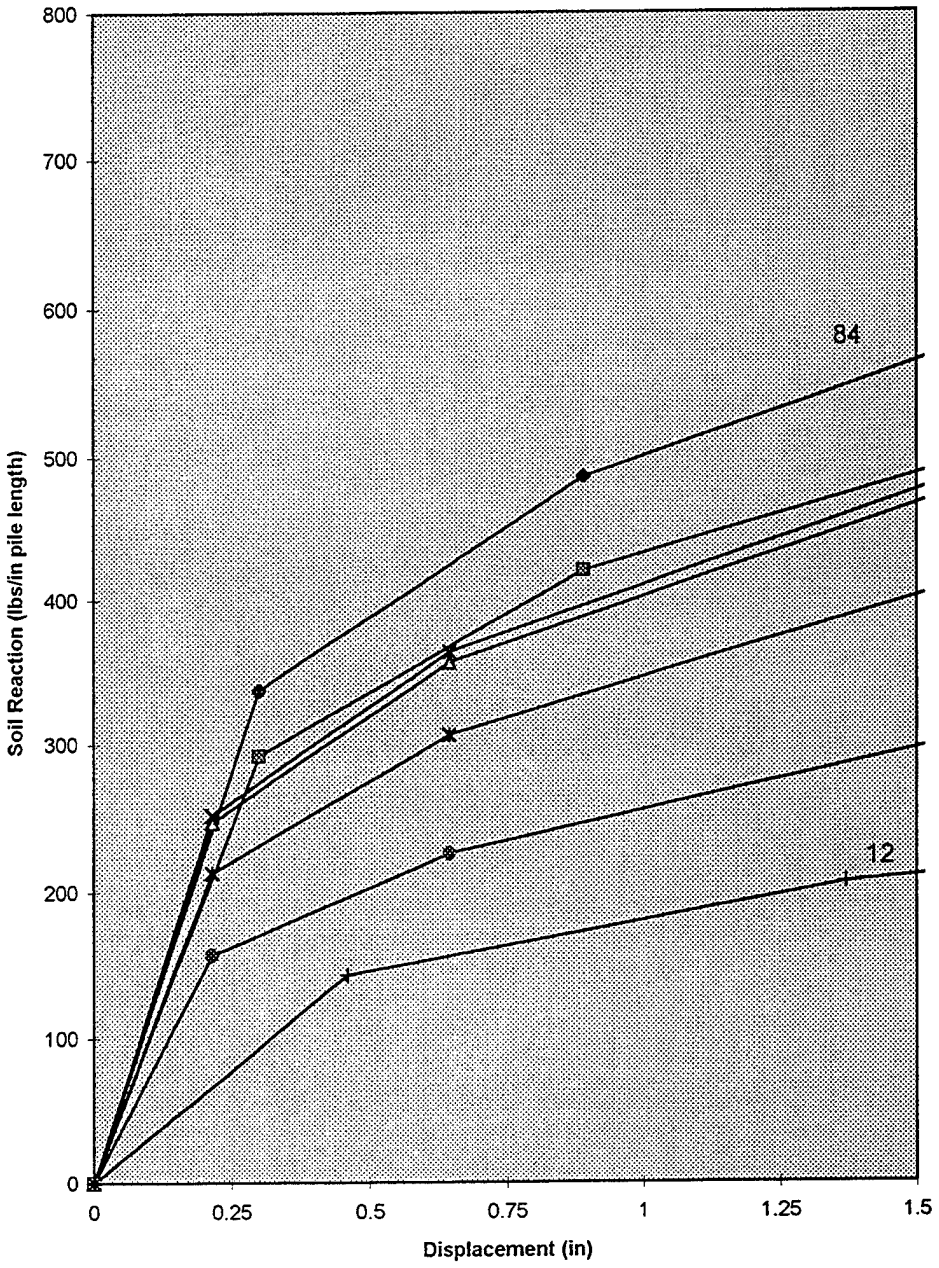

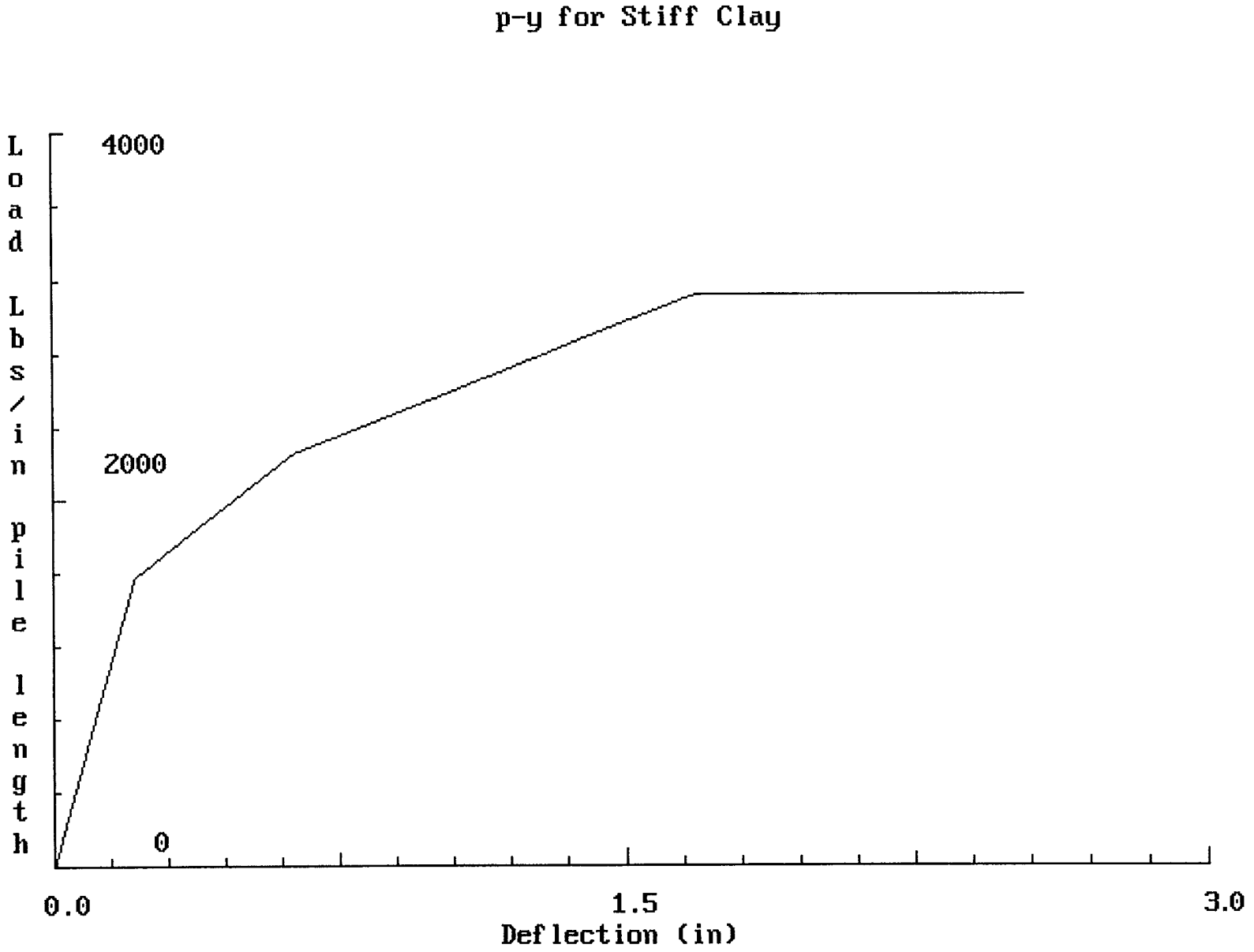

Figure A-19a. Py curve for clay.

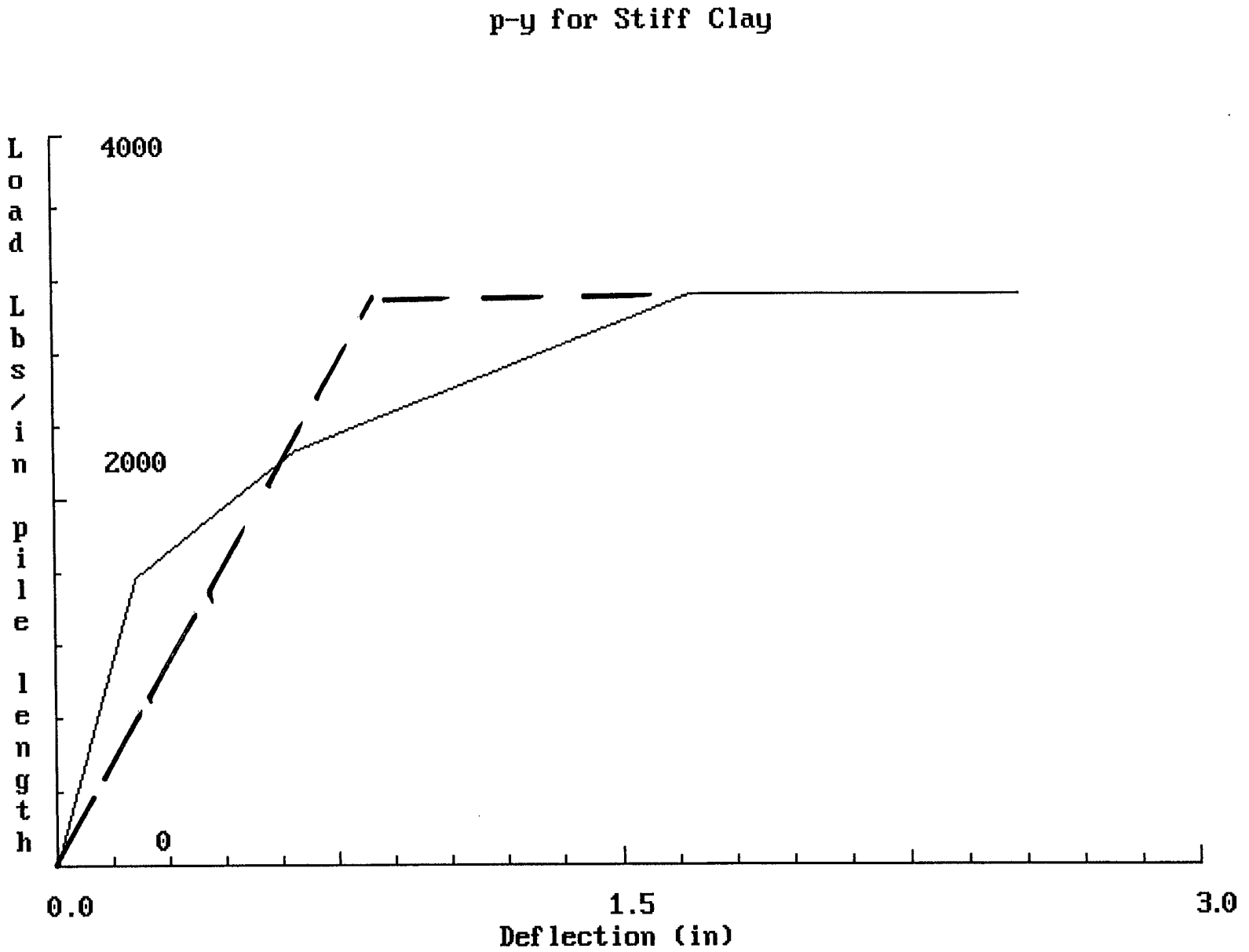

Figure A-19b. Py curve for clay, bilinear approximation #1.

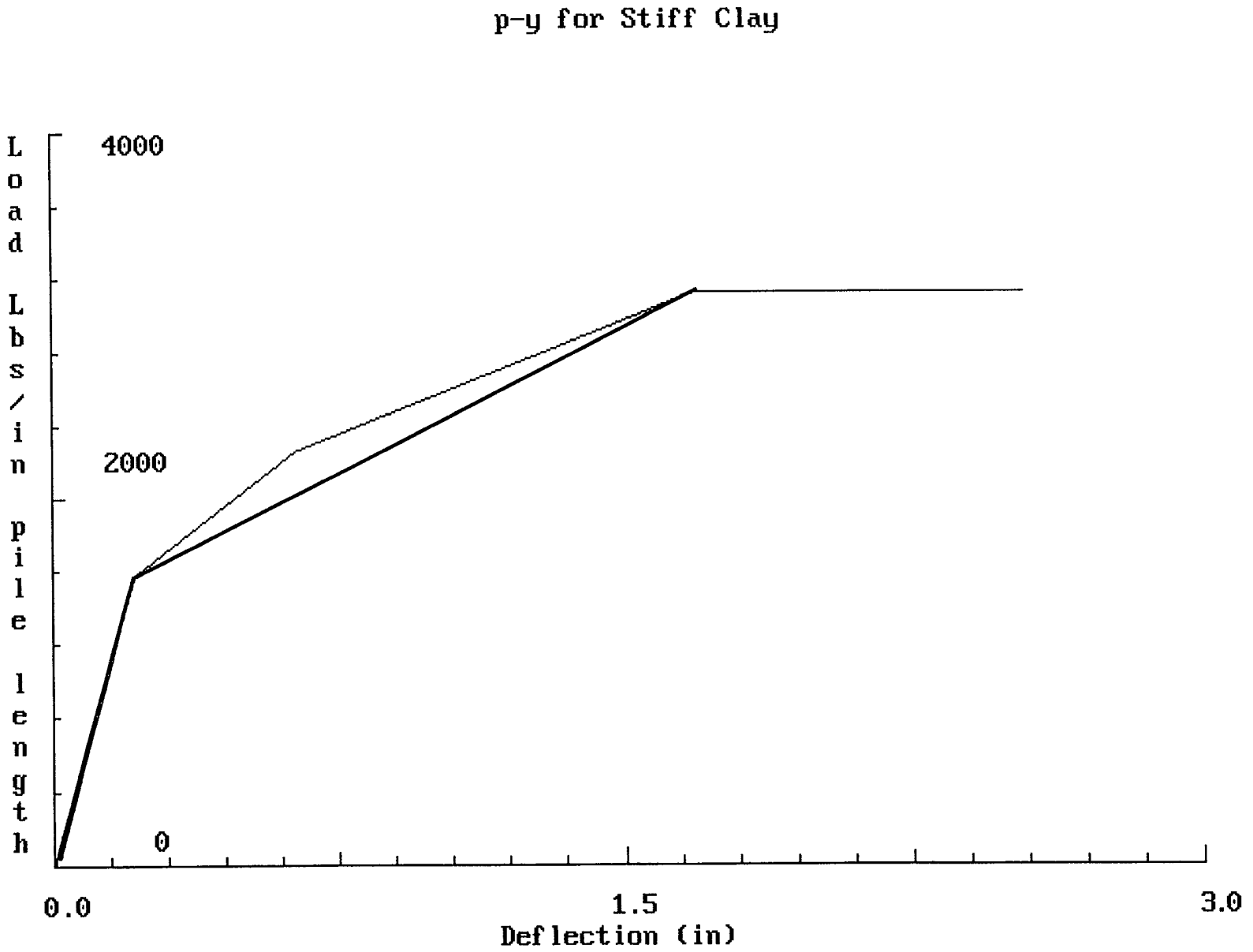

Figure A-19c. Py curve for clay, bilinear approximation #2.

Figure A-20. Bagnolet pile case 3.